

# **A SMART HOUSE ENERGY MANAGEMENT SYSTEM**

A Dissertation  
Presented to  
The Academic Faculty

by

Thamer Alquthami

In Partial Fulfillment  
of the Requirements for the Degree  
Doctor of Philosophy in the  
School of Electrical and Computer Engineering

Georgia Institute of Technology  
August 2015

Copyright © 2015 by Thamer Alquthami

# A SMART HOUSE ENERGY MANAGEMENT SYSTEM

Approved by:

Dr. A. P. Sakis Meliopoulos, Advisor  
School of Electrical and Computer  
Engineering  
*Georgia Institute of Technology*

Dr. Ying Zhang  
School of Electrical and Computer  
Engineering  
*Georgia Institute of Technology*

Dr. Ronald Gordon Harley  
School of Electrical and Computer  
Engineering  
*Georgia Institute of Technology*

Dr. Shabbir Ahmed  
School of Industrial and Systems  
Engineering  
*Georgia Institute of Technology*

Dr. Mayram Saeedifard  
School of Electrical and Computer  
Engineering  
*Georgia Institute of Technology*

Date Approved: [May 22, 2015]

*To my beloved parents Shaikah and Saad and my wife Abeer*

## ACKNOWLEDGEMENTS

I would never have been able to realize my dream and finish my dissertation without the guidance and profound support of countless people. The successful ending of my journey is deeply attributed to the people whom they have great impact on my life during my journey. Expressing my sincere thanks and gratitude to them is the least I can do.

First of all, I would like to thank my advisor Professor Sakis Meliopoulos. His leadership, unlimited support, and keen guidance during my studies have been of profound importance. It was a great honor for me to have him as an advisor. I am grateful to him for the many opportunities he offered me and the support he provided during studies, especially during difficult times. I would to express my appreciation to Professor Ronald Harley, Professor Maryam Saeedifard, Professor Ying Zhang, and Professor Shabbir Ahmed for serving on my Ph.D. committee members. Their support has guided me through the final steps of my dissertation. Also, my thanks are extended to GE Appliances for their support by providing actual data of most of regular house appliances.

I would like to extent my thanks to the Chair of Electrical and Computer Engineering Department and the Power Group members at King Abdulaziz University, Jeddah, Saudi Arabia for their constant support, especially Professor Ramzi Obaid. Without the financial support I received from by King Abdulaziz University, I would not be able to achieve my goal. So, many thanks are for their generous support.

Also, I would like to thank all my labmates. In particular, I would like to thank Yonghee Lee, Evangelos Polymeneas, Hussain Albinali, and Thibault Prevost (a visitor

engineer from RTE-France). The technical discussions we had have honed my technical understanding and expanded my knowledge. Further, I would like to extend my appreciation to every member of the Saudi Association Students at Georgia Tech. I will not forget the moments we spent together. I would like also to extend my thanks to my friends Abdullah Alotaibi, Omar Baamer, and Jaber Nyrabeah. The long distance between me and them did not hamper them to provide me with their constant support and encouragement.

Last but not least I would like to thank my family. My parents have started me in the right direction and have been supporting me ever since. My mother Shaikah has been a constant source of inspiration for me to have willpower and to achieve whatever I set my mind to do. My father Saad has inspired me for constant pursuing high valued goals in my life. So, my ultimate love, thanks, and appreciation are for them. Also, I would like to thank my wife Abeer for her understanding and love during my years for study. Her unlimited support and encouragement was what made this dissertation possible. I would like to thank my siblings, especially my brother Dr. Nader. He sacrificed ample things of his own life to help me realize my dream. He abounded a scholarship to pursue education overseas, took care of our parents during difficult times while I am away, and provided me with unlimited support to seize my goal. Further, I would like to thank my uncle Ataig for his support. His nice words kept resonating in my mind during my work.

The support of these people is of paramount importance during my journey. I have grown and become technically matured throughout the support of these people. My journey has been also supported by people whom I have crossed with during my years of study. Their support is also greatly appreciated.

# TABLE OF CONTENTS

	Page
ACKNOWLEDGEMENTS .....	iv
TABLE OF CONTENTS.....	vi
LIST OF FIGURES .....	x
LIST OF TABLES .....	xiii
LIST OF ABBREVIATIONS .....	xv
SUMMARY .....	xviii
1 INTRODUCTION.....	1
1.1 Smart Grid Technologies .....	1
1.2 Penetration Potential of House DERs and Appliances .....	1
1.3 Aging Power Grid Infrastructure.....	4
1.4 Research Motivation and Key Contributions.....	5
1.5 Dissertation Outline .....	6
2 LITERATURE SURVEY AND BACKGROUND INFORMATION.....	7
2.1 Introduction.....	7
2.2 Residential DERs and Smart Assets Impact on the Distribution System....	7
2.3 Current Status of Demand Response and Customer Satisfaction .....	9
2.4 Current House Energy Management Systems .....	12
2.5 Overview of Loads and Transformer Thermal Models .....	15
2.6 Summary.....	17
3 PROPOSED ADVANCED HOUSE INFRASTRUCTURE .....	19
3.1 Introduction.....	19
3.2 Advanced House Infrastructure Development .....	19
3.2.1 Description of the Advanced House Infrastructure.....	20
3.2.2 How Does the House Infrastructure Works? .....	21
3.3 Summary.....	22
4 HOUSE ENERGY MANAGEMENT SYSTEM OPTIMIZATION .....	23
4.1 Introduction.....	23
4.2 Mathematical Formulation of the House Optimization Problem.....	23
4.2.1 Minimization of Customer’s Total Energy Cost.....	24

4.2.2	House Peak Load Control .....	29
4.2.3	Electrothermal Model of the House .....	30
4.3	Summary .....	31
5	HOUSE SYSTEM COMPONENTS MODELING .....	32
5.1	Introduction.....	32
5.2	Object Orientation Modeling Approach .....	32
5.3	Description of Device Modeling .....	33
5.3.1	Modeling Procedure .....	33
5.3.2	Thermal Modeling .....	40
5.3.3	Smart House Energy Management System Devices .....	41
5.4	Electrothermal Model of a Single Phase Distribution Transformer .....	42
5.4.1	Electrical Model .....	43
5.4.2	Thermal Model.....	44
5.4.3	Mathematical Model of the Distribution Center-Tap Transformer.....	54
5.5	House DERs and Appliances Models.....	54
5.5.1	Thermal Model of the House .....	54
5.5.2	Electrothermal Air Conditioner Model.....	61
5.5.3	Electrothermal Refrigerator Model .....	64
5.5.4	Dishwasher Model.....	73
5.5.5	Variable Load Model.....	76
5.5.6	Roof-Top Solar Photovoltaic (PV) Model.....	78
5.5.7	Electrothermal Model of a Battery Energy Storage System (BESS) .....	78
5.5.8	Electric Vehicle (EV) Model .....	80
5.5.9	Power Electronics Converters Models .....	81
5.5.10	Miscellaneous Models .....	86
5.6	Summary .....	89
6	HOUSE DISTRIBUTED STATE ESTIMATION .....	91
6.1	Introduction.....	91
6.2	House DSE Description .....	91
6.3	House DSE Formulation.....	93
6.4	Summary.....	96
7	OPTIMIZATION PROBLEM SOLUTION METHOD.....	97
7.1	Introduction.....	97

7.2	Piecewise Linear Formulations .....	97
7.2.1	$\lambda$ -Formulation.....	97
7.2.2	Elimination of Bilinear Terms .....	99
7.3	Model Predictive Control.....	100
7.4	Summary.....	102
8	DEMONSTRATIVE CASE STUDIES: HOUSE MODEL SIMULATION RESULTS .....	104
8.1	Introduction.....	104
8.2	Transformer Model Case Study .....	104
8.2.1	System Description.....	104
8.2.2	Rise Time Characterization.....	109
8.2.3	Peak Loading.....	110
8.2.4	Extreme Loading .....	112
8.3	House Characteristics Case Studies .....	114
8.3.1	Description of the House Test System .....	114
8.3.2	House Simulation for Two different Days.....	119
8.3.3	House Insulation Improvement .....	123
8.4	Summary.....	126
9	DEMONSTRATIVE CASE STUDIES: SMART HOUSE ENERGY MANAGEMENT SYSTEM.....	127
9.1	Introduction.....	127
9.2	Description of House Test System .....	127
9.3	Simulation without the Smart House Energy Management System .....	128
9.4	House Operation with Minimization of Customer's Total Energy Cost .	130
9.5	House Operation with Peak Load Control.....	134
9.6	Summary.....	137
10	CONCLUSIONS, CONTRIBUTIONS, AND FUTURE RESEARCH DIRECTIONS.....	139
10.1	Conclusions.....	139
10.2	Contributions.....	143
10.3	Future Research Directions.....	144
Appendix A	Object Oriented Modeling .....	146
Appendix B	Single Phase Center-Tap Transformer Model .....	156



Appendix C	Thermal Model of a House .....	180
Appendix D	Electrothermal Air-Conditioner Model .....	187
Appendix E	Electrothermal Refrigerator Model .....	190
Appendix F	Dishwasher Mathematical Model.....	197
Appendix G	Variable Load Model.....	200
Appendix H	Solar Cell Mathematical Model .....	201
Appendix I	Electrothermal Lead-Acid Battery .....	203
Appendix J	Electric Vehicle Model.....	211
Appendix K	Averaged Model of DC-DC Boost Converter.....	214
Appendix L	Averaged Full Bridge Model of DC-AC Inverter .....	218
Appendix M	Averaged Model of DC-DC Buck-Boost Converter .....	221
Appendix N	Ambient Temperature Model.....	224
Appendix O	Thermostat Model .....	226
REFERENCES	.....	228

## LIST OF FIGURES

Figure 1. Distributed generation projection [3].....	2
Figure 2. The U.S. potential demand response (2019) [7].....	3
Figure 3. Projected EVs/PHEVs by 2030 [9]. ....	4
Figure 4. An actual house profile with EV charging [30]. ....	8
Figure 5. Classification of demand response programs [45]. ....	10
Figure 6. Actual and baseline thermostatically controlled load [48].....	12
Figure 7. Illustration of the proposed house advanced infrastructure. ....	21
Figure 8. Illustration of one smart house connected to a center-tap transformer.....	24
Figure 9. House DERs and appliances modeling procedure.....	34
Figure 10. Illustration of quadratic integration method.....	38
Figure 11. Electrothermal transformer model user interface in WinIGS program .....	43
Figure 12. Electrical circuit of the center-tap transformer.....	44
Figure 13. Single phase center-tap transformer temperature spots locations. ....	45
Figure 14. Segments of transformer primary winding, secondary winding, and core. ....	48
Figure 15. Thermal house model user interface in WinIGS program. ....	55
Figure 16. Thermal house model internal and external temperature spots locations. ....	57
Figure 17. House bedroom <sub>2</sub> RC thermal circuit.....	58
Figure 18. Electrothermal air conditioner model user interface in WinIGS program.....	62
Figure 19. Air conditioner electrical and thermal circuit model. ....	63
Figure 20. Top: Air conditioner actual heat rating (BR), Bottom: Coefficient of performance (COP) .....	64
Figure 21. Electrothermal refrigerator model user interface in WinIGS program.....	65
Figure 22. Electrical circuit model of the refrigerator.....	66
Figure 23. Refrigerator thermal circuit elements and temperature spots locations.....	69
Figure 24. Smart dishwasher model user interface in WinIGS program.....	74
Figure 25. Dishwasher power profile. ....	76
Figure 26. Variable load model user interface in WinIGS program. ....	77
Figure 27. Electric circuit of the variable load model. ....	77
Figure 28. Equivalent electrical circuit of the solar cell. ....	78
Figure 29. Circuit model of lead acid battery. ....	79

Figure 30. Lead acid battery model user interface window in the program. ....	80
Figure 31. Circuit model of lithium ion battery. ....	81
Figure 32. Lithium ion battery model user interface in WinIGS program. ....	81
Figure 33. Equivalent circuit model of a single phase dc-dc boost converter. ....	82
Figure 34. Average model of dc-dc boost converter user interface in WinIGS program. ....	82
Figure 35. Perturb and observe (P&O) algorithm. ....	83
Figure 36. Equivalent circuit model of the single phase full bridge DC-AC inverter.....	84
Figure 37. Average model of dc-ac inverter user interface in WinIGS program.....	84
Figure 38. Equivalent circuit model of a single phase dc-dc buck-boost Converter.....	85
Figure 39. Battery charger dc-dc buck-boost user interface in WinIGS program. ....	86
Figure 40. Equivalent thermal circuit diagram of ambient temperature.....	87
Figure 41. Ambient temperature model user interface in WinIGS program. ....	87
Figure 42. Equivalent circuit diagram of the thermostat. ....	88
Figure 43. Thermostat user interface in WinIGS program. ....	89
Figure 44. A general functional description of the house level DSE. ....	92
Figure 45. House state estimation procedure. ....	93
Figure 46. Piecewise linear approximation of (53) using $\lambda$ -formulation. ....	98
Figure 47. Illustration of the model predictive control concepts. ....	102
Figure 48. Transformer test system single line diagram.....	105
Figure 49. An example of ambient temperature condition. ....	105
Figure 50. Hourly load with 1.2 pu peak load connected to 10 kVA transformer. ....	106
Figure 51. 10 & 25 ABB kVA transformer temperatures waveforms.....	109
Figure 52. Power system at the system level in the house simulation. ....	114
Figure 53. House pole in the simulation. ....	115
Figure 54. House with appliances in the simulation.....	115
Figure 55. Data for July 1 <sup>st</sup> & 29 <sup>th</sup> , a) solar irradiance and b) ambient temperature.....	116
Figure 56. House data for July 1 <sup>st</sup> & 29 <sup>th</sup> , a) relative humidity and b) appliances load. ....	117
Figure 57. (a) House total load and (b) transformer hot spot temperature, for both July 1 <sup>st</sup> and 29 <sup>th</sup> .....	120
Figure 58. House dishwasher active and reactive power for both July 1 <sup>st</sup> and 29 <sup>th</sup> . ....	120
Figure 59. (a) House bedroom <sub>1</sub> temperature on July 1 <sup>st</sup> , (b) on July 29 <sup>th</sup> , and (c) house air conditioner control signal on July 1 <sup>st</sup> & 29 <sup>th</sup> .....	121

Figure 60. (a) Refrigerator fresh food compartment main temperature on July 1 <sup>st</sup> , (b) on July 29 <sup>th</sup> , and (c) refrigerator heat rate on July 1 <sup>st</sup> & 29 <sup>th</sup> .	122
Figure 61. (a) Refrigerator fresh food compartment main temperature on July 1 <sup>st</sup> , (b) on July 29 <sup>th</sup> , and (c) refrigerator heat rate on July 1 <sup>st</sup> & 29 <sup>th</sup> .	123
Figure 62. (a) House bedroom <sub>1</sub> temperature and (b) house air conditioner control signal, with insulation A on July 1 <sup>st</sup> .	125
Figure 63. (a) House bedroom <sub>1</sub> temperature and (b) house air conditioner control signal, with insulation B on July 1 <sup>st</sup> .	125
Figure 64. (a) House bedroom <sub>1</sub> temperature and (b) house air conditioner control signal, with insulation C on July 1 <sup>st</sup> .	126
Figure 65. Top: Transformer active power, Bottom: Transformer hot spot temperature with no management system.	128
Figure 66. Smart dishwasher active and reactive power characteristics with no management system.	129
Figure 67. EV battery characteristics with no management system.	130
Figure 68. House battery characteristics with no management system.	130
Figure 69. Top: Transformer active power, Bottom: Transformer hot spot temperature with cost minimization.	131
Figure 70. Smart dishwasher active and reactive power with cost minimization.	131
Figure 71. EV battery characteristics with cost minimization.	132
Figure 72. House battery characteristics with cost minimization.	133
Figure 73. Temperature at different locations of the house with cost minimization.	133
Figure 74. Top: Transformer active power, Bottom: Transformer hot spot temperature with peak load control.	134
Figure 75. Smart dishwasher active and reactive power with peak load control.	135
Figure 76. Electric vehicle characteristics with peak load control.	135
Figure 77. House battery characteristics with peak load control.	136
Figure 78. Temperature at different locations of the house with peak load control.	137
Figure 79. Series RLC circuit.	153
Figure 80. Capacitor voltage waveform.	154
Figure 81. Inductor current waveform.	155
Figure 82. Absolute error of the inductor current between the analytic solution and trapezoidal and quadratic integration methods [108].	155
Figure 83. Equivalent lead acid electric circuit model.	203
Figure 84. Equivalent electrical circuit of lithium ion battery.	211

## LIST OF TABLES

Table 1. Transformer thermal model thermal capacity. ....	48
Table 2. Transformer heat source. ....	49
Table 3. Center-tap transformer rated temperature at each temperature spot. ....	51
Table 4. Transformer empirical A & B values [111]. ....	53
Table 5. House thermal model rated temperature at each temperature spot. ....	58
Table 6. Thermal house model thermal capacitance connections. ....	60
Table 7. Electrothermal refrigerator thermal capacitance connections. ....	69
Table 8. Rated temperature at each temperature spot (°C). ....	72
Table 9. Dishwasher load levels. ....	74
Table 10. Case study transformer electrical impedance parameters. ....	105
Table 11. ABB transformer physical parameters (dimension and oil volume) [130]. ....	106
Table 12. Volume, mass density, specific heat, and heat capacity for each part of 10 kVA ABB transformer. ....	107
Table 13. Thermal circuit parameters results for ABB transformers. ....	107
Table 14. Transformer temperature waveforms approximate rise time in [min]. ....	110
Table 15. Aging calculation for 10 kVA transformer and for 24 hours with peak loading. ....	111
Table 16. Aging calculation for 10 kVA transformer and for 24 hours with extreme loading. ....	112
Table 17. Dishwasher input data. ....	117
Table 18. Refrigerator input data. ....	118
Table 19. Air conditioner model parameters. ....	118
Table 20. Thermostat control settings in July 1 <sup>st</sup> and 29 <sup>th</sup> . ....	118
Table 21. House roof-top data parameters. ....	119
Table 22. A (base) case, B case, and C case thermal conductances of the house. ....	124
Table 23. RLC circuit parameters. ....	153
Table 24. Transformer $T_{h1}$ conductances. ....	168
Table 25. Transformer $T_{h2}$ conductances. ....	169
Table 26. Transformer $T_{h3}$ conductances. ....	169
Table 27. Transformer $T_{L11}$ conductances. ....	170
Table 28. Transformer $T_{L12}$ conductances. ....	171

Table 29. Transformer $T_{L13}$ conductances. ....	172
Table 30. Transformer $T_{L21}$ conductances. ....	173
Table 31. Transformer $T_{L22}$ conductances. ....	173
Table 32. Transformer $T_{L23}$ conductances. ....	174
Table 33. Transformer $T_{CT}$ conductances. ....	175
Table 34. Transformer $T_{CB}$ conductances. ....	175
Table 35. Transformer $T_{CR}$ conductances. ....	176
Table 36. Transformer $T_{CL}$ conductances. ....	176
Table 37. Transformer $T_{TOT}$ conductances. ....	177
Table 38. Transformer $T_{BOT}$ conductances. ....	177
Table 39. Transformer $T_{ROT}$ conductances. ....	177
Table 40. Transformer $T_{LOT}$ conductances. ....	178
Table 41. Transformer $T_{CaseT}$ conductances. ....	178
Table 42. Transformer $T_{CaseB}$ conductances. ....	178
Table 43. Transformer $T_{CaseR}$ conductances. ....	178
Table 44. Transformer $T_{CaseL}$ conductances. ....	179
Table 45. House $T_{bed11}$ conductances. ....	184
Table 46. House $T_{bed21}$ conductances. ....	184
Table 47. House $T_{bath11}$ conductances. ....	184
Table 48. House $T_{bath21}$ conductances. ....	185
Table 49. House $T_{KI}$ conductances. ....	185
Table 50. House $T_{LI}$ conductances. ....	185
Table 51. House $T_E$ conductances. ....	185
Table 52. House $T_N$ conductances. ....	186
Table 53. House $T_W$ conductances. ....	186
Table 54. House $T_S$ conductances. ....	186
Table 55. House $T_{Top}$ conductances. ....	186
Table 56. Terminal voltage polynomial coefficients. ....	211
Table 57. Polynomails coefficients. ....	212

## LIST OF ABBREVIATIONS

DERs	Distributed Energy Resources
EV	Electric Vehicle
PHEV	Plug-In Hybrid Electric Vehicle
NE-ISO	New England – Independent System Operator
PV	Photovoltaic
EIA	Energy Information Administration
DR	Demand Response
FERC	Federal Energy Regulatory Committee
Micro-CHP	Mirco-Combined Heat and Power
DLC	Direct Load Control
EMS	Energy Management System
OPF	Optimal Power Flow
SE	State Estimation
DSE	Distributed State Estimation
EPRI	Electric Power Research Institute

TCLs	Thermostatically Controlled Loads
LP	Linear Programming
HVAC	Heating, Ventilating, and Air Conditioning
PSO	Particle Swarm Optimization
BPSO	Binary Particle Swarm Optimization
DP	Dynamic Programming
GA	Genetic Algorithm
IEDs	Intelligent Electronic Devices
HAN	Home Area Network
PCC	Point of Common Coupling
DAEs	Differential Algebraic Equations
AQCF	Algebraic Quadratic Companion Form
SCAQCF	State and Control Algebraic Quadratic Companion Form
LOIL	Loss of Insulation Life
OPS	Oil Preservation System
COP	Coefficient of Performance
BESS	Battery Energy Storage System



MPPT	Maximum Power Point Tracking
P&O	Perturb and Observe
IC	Incremental Conductance
SOC	State of Charge
MIQCP	Mixed Integer Quadratically Constraint Programming
PLA	Piecewise Linear Approximation
SOS2	Special Order Set 2
MPC	Model Predictive Control

## SUMMARY

Smart grid technologies have been in rapid growth over the last decade. Large portion of these technologies are experienced amalgamation with the power distribution infrastructure. Fast integration of these technologies can have a great impact on the power distribution system. There exist opportunities for residential energy resources and smart loads via increased controllability to provide house level benefits.

The impact of distributed energy resources (DERs), electric vehicles/plug-in hybrid electric vehicles (EVs/PHEVs), and smart appliances on the distribution grid has been studied from different aspects in the literature. The results of these studies suggest the following:

- a) the impact, generally, is beneficial in terms of environment, economy, and reliability; however, it can be more beneficial by implementing controls to maximize the beneficial impact and,
- b) in the absence of additional controls, a negative effect was identified regarding the service lifetime of power distribution system components, in particular distribution transformers.

This research presents a new class of a smart house energy management system that can provide management and control of a residential house electric energy without inconvenience to the residents of the house and without overloading the distribution infrastructure. In this research, the management system manages one house; however, the management system can provide control services to more than one residential house.

Furthermore, the system can provide energy management services for a commercial building, if it is appropriately sized.

The smart house energy management system that is presented in this dissertation deploys smart control strategies to maximize the beneficial effects that are associated with house energy resources and smart appliances. It can also lessen the unfavorable effect on the lifetime of distribution components. The management of the impact, whether favorable or not, requires properly designed control algorithms for the coordinated use of smart devices and intelligent control of charging cycles of EV/PHEV battery, house battery, and other resources in the house.

The implementation of these controls requires an infrastructure that exploits advanced smart grid technologies. This infrastructure continuously monitors the house power system operation, determines the real-time model of the house, computes better operating strategies over a planning period of time, and enables control of house resources. In other words, the smart house energy management system manages the house energy resources, such as EV/PHEV and smart loads, in a way that the power infrastructure components are not overloaded beyond permissible limits, thus avoiding unnecessary loss of service lifetime.

The smart house energy management system provides benefits for the good of utility and customer. In case of variable electricity rates, the management system can reduce the customer's total energy cost. The benefits can be also extended to provide ancillary services to the utility such as control of peak load and reactive power support—assuming that this is worked out under a certain mutually beneficial arrangement between the utility and customer.

This research resulted in a novel smart house energy management system that can optimize and control the operation of a house. This is achieved without inconvenience to the customer and overloading the infrastructure. The work describes the following contributions: 1) the development of an advanced house infrastructure that can provide real-time management of the house, 2) the formulation of the house optimization model in a way that benefits both the utility and customer, without inconvenience to the customer and without overloading the distribution transformer, 3) the development of physically based and detailed electrothermal model of a center-tap distribution transformer, and 4) the development of physically based and detailed electrothermal models of various house energy resources and controllable/non-controllable appliances including batteries, dishwasher, refrigerator, and air conditioner.

# 1 INTRODUCTION

This dissertation presents a new smart house energy management system that provides smart control functions to optimally schedule house DERs and smart appliances. This Chapter introduces current smart grid technologies and discusses penetration potential of these technologies at a residential house level. Also, this Chapter presents the research motivation, key contributions, and outlines the remainder of this dissertation.

## 1.1 Smart Grid Technologies

In recent decades, the modernization of the electrical grid has attracted the attention of world leaders, power and energy entities, and policy makers. Particularly, the act of 2007 has amplified the need to accelerate the ongoing effort by power utilities, system operators, and other stockholders to meet smart grid goals [1]. As a result, a growing number of new smart grid technologies, such as DERs, EVs/PHEVs, smart appliances, and advanced measurement and sensing meters have seen amalgamation with the existing power grid. Consequently, the market share of these advanced technologies has been dramatically increased. Statistics about the market share of these technologies are presented in the next section.

## 1.2 Penetration Potential of House DERs and Appliances

In terms of DER penetration, the New England Independent System Operator (NE-ISO) expected that DERs will provide approximately 2.855 GW by 2021; 800 MW

of the total estimate was forecasted to be supplied by solar photovoltaic (PV) [2]. In a house/building level [3], the U.S. Energy Information Administration (EIA) projected that house/building solar PV is expected to generate 25 GW in the year 2040 as illustrated in Figure 1. Other types of energy distributed generations installation projections, sorted by generation technology, are shown in Figure 1.

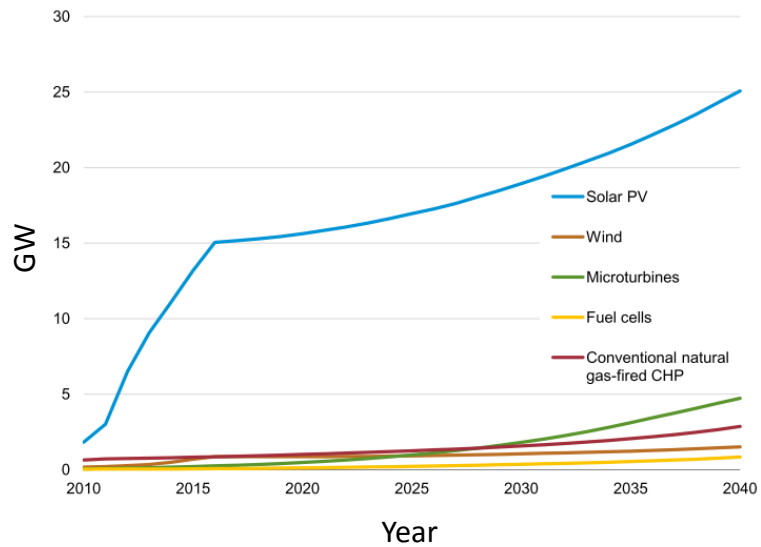


**Figure 1. Distributed generation projection [3].**

One of the important cornerstones of the future power grid is the house [4]. Smart grid technologies related to a house have been in rapid development and the market share of these technologies is expected to further increase. In a worldwide scale, market analysts expected that the market value of smart appliances reach over 26.1 billion U.S. dollars in 2019 [5]. In an optimistic study [6], it was estimated that Demand Response (DR) enabled house appliances could generate as high as \$59 billion in the U.S. by 2019. Furthermore, benefits related to DR could get up to \$16 billion reducing the need for new generation power plants [6]. Deployment of smart grid technologies, such as smart

appliances with smart control, can deliver full range of benefits, particularly benefits related to end user.

Realizing the potential of DR, the Federal Energy Regulatory Commission (FERC) has provided an assessment of the U.S. national demand response potential [7]. One of the conclusions is that, by the time the report was written, the majority of demand response comes from large commercial and industrial customers, primarily through interruptible tariffs and capacity and demand bidding programs. However, the residential class was found to represent the most untapped potential for demand response. In particular, 10% was approximately the maximum potential of residential peak load reduction by the year 2019, if full customer participation is achieved as illustrated in Figure 2. This 10% is equivalent to 100 GW. As a result, residential demand was specifically stressed for more careful and thorough analysis [8]. In fact, it was asserted that achieving smart grid technical goals will not fully realized without capturing benefits associated with the house [4]. With current technology advancement in communication, information technology, automation, and computing power, demand response applications can be extended to engage individual customers.

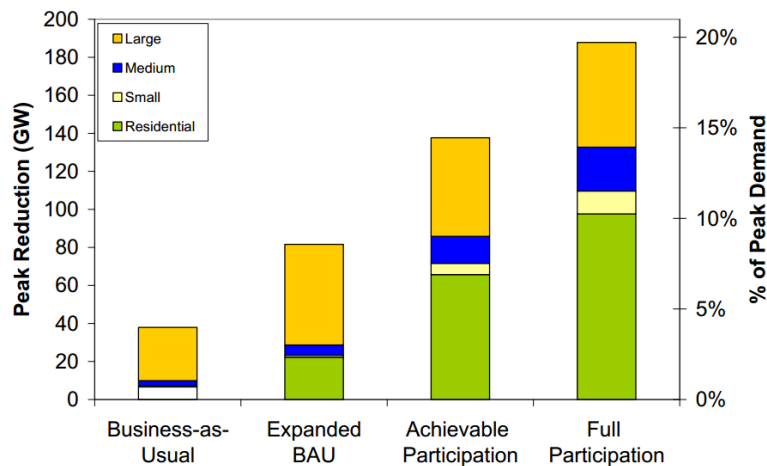


Figure 2. The U.S. potential demand response (2019) [7].

Due to environmental and sustainable energy advantages of EVs/PHEVs compared with conventional transportation means that depend on fossil fuel, the penetration of EVs/PHEVs and other green technology based vehicles is anticipated will grow significantly in the worldwide market. In the U.S., the projected market portion of EVs/PHEVs was nearly 4.5% of the national fleet by 2030 as illustrated in Figure 3. Higher EVs/PHEVs penetration scenarios were also depicted in Figure 3 [9]. Although these projections might be quite high, these statistical projections were supported by other studies [10, 11]. These smart grid technologies are integrated with an already aging power distribution infrastructure. This aging power infrastructure is discussed next.

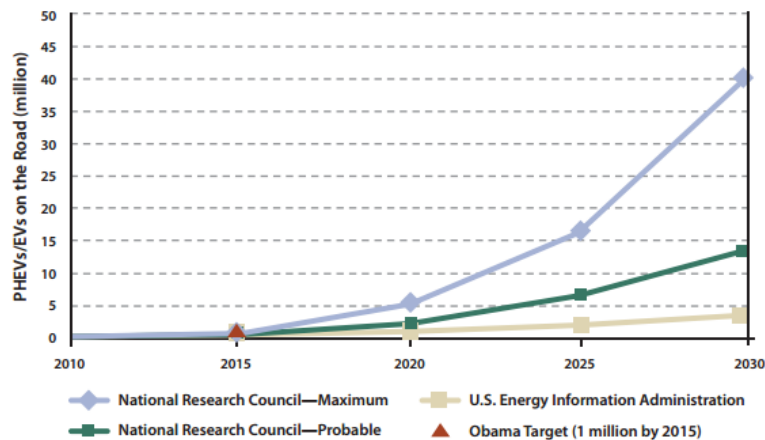


Figure 3. Projected EVs/PHEVs by 2030 [9].

### 1.3 Aging Power Grid Infrastructure

In most developed countries, large parts of existing electrical grid infrastructure can be dated back to the 1960s. A recent survey of over 400 U.S. electric utilities revealed that the top pressing issue facing utilities is old infrastructure [12]. One of the important components of any power distribution system is distribution transformers. Maintaining these transformers represent a significant cost of electric utility total annual investment.



According to FERC, distribution transformers can account for about 9-20% of total distribution capital spending in a year [13]. Despite the fact that larger transformer had become more efficient, smaller distribution transformers had in general declined [14].

Large penetration potential of House DERs and appliance with aging distribution infrastructure pose significant challenges for power grid utilities. The question becomes how utilities can manage smooth integration of advanced smart grid technologies without adding more stress on existing electric power infrastructure. The answer of this question is framed in the following section.

#### **1.4 Research Motivation and Key Contributions**

The objective of the research is to develop a smart house energy management system that controls and optimizes the operation of a house. The integration of DERs, smart appliances, and EV are expected to have an impact on the distribution electric grid. In particular, the proliferation of EV is expected to tax existing infrastructure of the distribution system and its reliability in supplying customers. In contrast, present day end users have resources (DERs and smart appliances) that are expected to alleviate the burden on the infrastructure, if appropriately used. Therefore, the goal of this research is to develop a smart house energy management system that makes use of available resources at the house level and perform optimization functions that benefit both the utility and customer. The management system works without inconvenience to the customer and without overloading the distribution transformer, which elongate the lifetime cycle of the transformer.

To achieve this goal, a novel house infrastructure was designed. Major components of the infrastructure were developed. The mathematical formulation of the house optimization model was developed in way that provides benefits for the power utility provider and end customer, without incurring any inconvenience to the customer and without overloading/overheating the transformer. Also, house level DSE was mathematically formulated. To perform optimization and estimation, models of important appliances and DERs at the house including distribution transformer were needed. Accordingly, new electrothermal model of a center-tap transformer was developed. Furthermore, house energy resources and loads, whether controllable or not, electrothermal models were developed.

## **1.5 Dissertation Outline**

In the following Chapters, the specifics of the smart house energy management system are provided. Specifically, the dissertation is divided as follows: Chapter 2 introduces existing literature review and important background information related to the research topic. The advanced house infrastructure is described in Chapter 3. In Chapter 4, the house optimization model is presented. Then, the modeling methodology used to develop various devices is discussed in Chapter 5. Chapter 6 describes the house distributed state estimation. In Chapter 7, the solution methodology used to solve the problem is discussed. In Chapter 8, demonstrative examples of the house models including the distribution transformer are presented. Also, demonstrative case studies of the house energy management system are presented in Chapter 9. Finally, Chapter 10 summarizes research conclusions, contributions, and directions for research future.

## **2 LITERATURE SURVEY AND BACKGROUND INFORMATION**

### **2.1 Introduction**

This chapter provides literature review and background information related to the research topic. Firstly, a literature review on the impact of integrating distributed generation resources and smart appliances on the power distribution grid is provided. Then, current residential demand response programs and their satisfactory level of customer comfort are discussed. After that, a background overview of existing research in house energy management system topic is provided. The last section provides a discussion about existing residential loads and transformer thermal models.

### **2.2 Residential DERs and Smart Assets Impact on the Distribution System**

The deregulations of the electric power system and customers desire for a reliable, economic, and clean energy have increased the interests in DERs. Previous penetration potential and market share statistics that are presented in Chapter 1 are an indication that the proliferation and integration of distributed generation resources, smart appliances, and EVs/PHEVs will take place in a large part in the residential sector. This integration is expected to have an impact on the power distribution system.

In the literature, the impact of DERs, smart appliances, and EVs/PHEVs was found that the impact is generally expected to be beneficial for the grid [9, 15-24]. Yet, electric utilities express also a growing concern about several issues including voltage stability, system protection, issues related to PV variability, and the possibility for overloading/overheating power distribution apparatus and their service lifetime [24-28].

On the assets service lifetime in particular, the impact of integrating EVs/PHEVs on distribution system components, such as distribution transformers and local circuits, was discussed and analyzed in many research projects. To characterize the impact of EVs integration on the distribution grid, Uriate and Hebner performed a study on 735 homes with 100 EVs that were randomly placed [29]. They did a system simulation over 24 hours and concluded that utilities should express worry regarding possible overloading conditions. This is, in particular, true with fast adaptation of EVs on a single distribution feeder. The study also expressed further concern regarding the state of health of the distribution transformer insulation, specifically during peak days of the year. Ureh, in [30], adopted more random loads from EVs/PHEVs without careful planning and found that this strategy may expose the already aging electrical infrastructure to become susceptible for overloading conditions. Ureh also found that the load resulting from an EV can be as large as four times that of a regular-sized house load. Figure 4 is an illustration of an actual load of a house with 3.7 kW EV charging between 1-6:30 am.

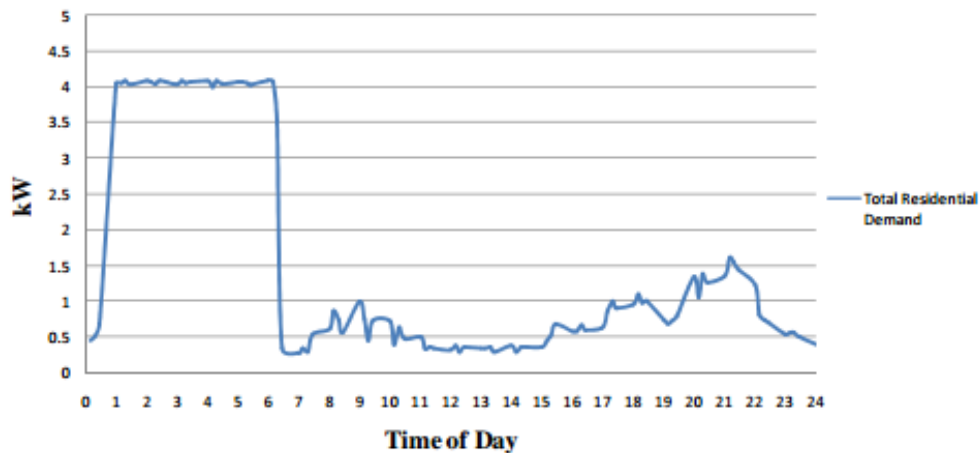


Figure 4. An actual house profile with EV charging [30].

Fast and uncoordinated charging of EVs posed a greater threat to the distribution transformer lifetime service as concluded in [31-33]. This is, particularly, true with high EV power consumption. To avoid that, Masoum *et al.* proposed a smart and coordinated EVs charging approach [34]. However, coordinated control approach might fail to work well with a large cluster of EVs/PHEVs. On another research, Shafiee *et al.* investigated the impact of EV on the distribution grid and verified that the peak load is also a big concern, especially in the winter season [35]. To avoid these adversary impact, Trovao in [36] showed that a comprehensive control strategy of EVs/PHEVs is necessary. Due to the uncertainty nature of EVs/PHEVs, Papadopoulos *et al.* used a probabilistic approach and found that the distribution transformer that was responsible of serving 96 customers, was in fact overloaded [37]. In an attempt to propose a solution, authors of [8, 38] suggested to install solar PV to counterpart the increment load. Solar power however is an intermittent resource. So, this might not be a solution. A small scale micro combined heat and power (micro-CHP) was also suggested to be installed in the house [39]. But, this solution requires infrastructure modification of the house.

Due to the expected proliferation of controllable appliances in the house, DR is foreseen to offer a better solution and can potentially improve the reliability of the power system operation [40, 41]. A brief review regarding current DR practices and customers approval from these programs is discussed next.

### **2.3 Current Status of Demand Response and Customer Satisfaction**

For decades, DR has been implemented in the form of direct-load control (DLC) of end user loads, which permits the power utility provider to interrupt electricity to large size commercial or industrial loads. Because of the large potential of DR, it was

recognized by FERC as one of top three important initiatives [42]. With current technology advancement in communication, automation, and computing power, DR applications can be extended to engage individual customers in a smart approach. However, the effect would be reduced without using proper residential load models and appropriate controls [43, 44]. This section focuses on DR programs that are related to residential customers. DR programs are employed by electric utility supplier to make use of the available energy in a more efficient way without the need for more infrastructure installation. An excellent classification of DR programs is shown in Figure 5.

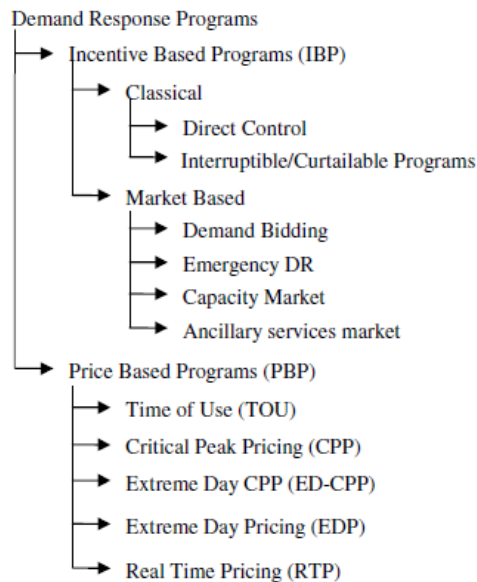


**Figure 5. Classification of demand response programs [45].**

DLC and load-interruptible programs occur where the electricity supplier, in usual cases, provides incentive to participated consumers in a form of bill credit or discount rate. An example of a conventional DLC is to cycle off the air conditioner of half of the consumers periodically for 15 minutes and then on for 15 minutes; or to cycle the water heater off for three hours and then on for three hours [46]. Heffner and Goldman performed a case study to analyze feedback impact on customers energy consumptions

[47]. This study involved residential customers' participation. In the study, the utility provided the participants feedback about their energy consumption, which included the time-of-use information and some tips of how to shift electricity usage from peak time to off-peak period. The study concluded that over the three months test period, participants' shifted their power demand from peak to off-peak period.

With the advent of electricity markets, special DR programs were introduced, where participants are rewarded money based on the amount of curtailed load during critical times. When electricity tariff is dynamics, price based programs were also introduced; the main goal here is to flatten the demand curve by offering high price during peak time and lower price during off-peak time. Chassin and DeSteele performed a field case study to analyze the impact of communicating the variable price to the customer on the peak load. The study results were presented in [48, 49]. With a two-way communication system, DR performance using controllable devices was tested. The controllable devices were five water pumps, two diesel generators, micro turbine, and 112 residential participants. Two capacity constraints for a virtual feeder connecting all participants were considered in the study. However, results for the 500 kW feeder constraint period are only presented. Each controllable device was managed by a price signal that was sent through the internet and updated every five minutes. In Figure 6, the results of the 500 kW constraint case are shown. It is shown that not only peak was shifted, but also it was reduced for the aggregated residential thermostatic loads.

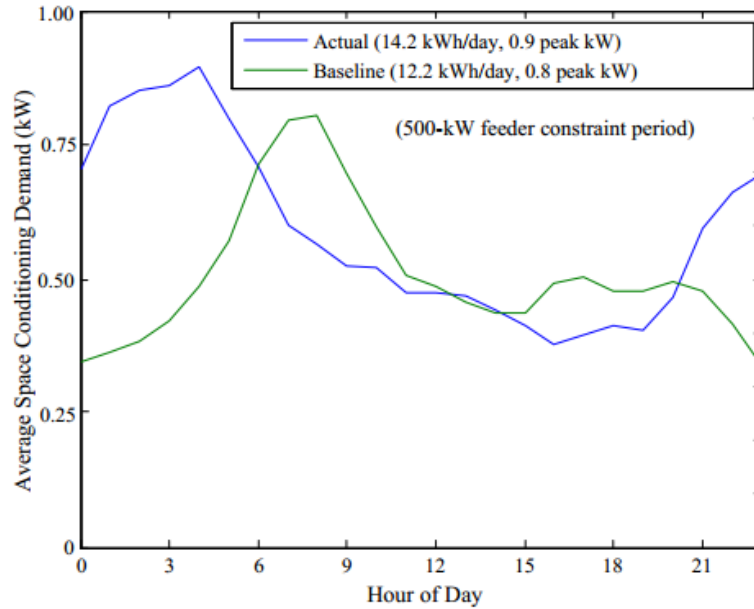


**Figure 6. Actual and baseline thermostatically controlled load [48].**

Other classifications of DR programs were provided in [50, 51]. However, these programs require consumers' participation. Further, these programs introduce full or little demand interruption in a time when it might be needed by the customer. The current DR programs, generally, underscore the comfort of end user. To consider end user comfort, several solutions were proposed. These solutions are discussed in the following section.

## 2.4 Current House Energy Management Systems

In the power utility control center, lays one of the most critical components that is the energy management system (EMS). It is used by system operators to monitor and control the power system. Critical applications are performed by EMS such as state estimation (SE) and optimal power flow (OPF). Basically, data coming from the field, though SCADA system, are used usually to perform SE. Results of the estimation are used to optimize the operation of the system (OPF) and other functions needed for the operation of the power system. The increase integration of renewable resources, storage



systems, EVs/PHEVs and smart appliances in the distribution system have urged toward EMS modernization. One of the proposed solutions is the distributed EMS.

Extensive literature exists on the topic of optimal scheduling and control of a house appliances and energy resources (EVs/PHEVs, energy storage, PV rooftops and other possible resources). To alleviate the negative effects of integrating EV, two main approaches were identified in the literature; these are the use of battery energy storage systems (BESS) and load management. To evaluate the former approach, Mardira *et al.* investigated the impact of residential BESS on the aggregated power demand profile with the presence of many residential roof-tops solar PV [52]. They concluded that the average and peak aggregated power demand was reduced. The contribution of the battery storage systems on residential and commercial load was analyzed in [53]. It was found that the battery storage systems assisted in shifting and smoothing the peak demand.

The second main approach to lessen the undesirable impact of EVs on the distribution power grid is to provide load management for house loads. One main method for managing house load is DLC approach [54-58]. Electric Power Research Institute (EPRI) has identified three classes of DLC schemes to assess the economic and technical performance; those are traditional DLC, enhanced DLC, and coordinated end-user switching [54]. Ruiz *et al.* adopted traditional DLC and created a framework to control domestic appliances including thermostatically controlled loads (TCLs) using linear programming (LP) [55]. In a similar approach, Sheble *et al.* designed a profit based DLC using LP [56]. Ning in [58] used DLC of heating, ventilating, and air-conditioning (HVAC) system to provide load balancing service. To reduce the load scheduling problem complexity, Abras *et al.* in [59] adopted a multi-agent paradigm to schedule

smart appliances. Multi-agent approach was found to, perfectly, be suited for spatially distributed loads. Similarly, Mohsenian *et al.* used the same approach to establish an interaction between end users themselves instead of user-utility relation using two-way communication infrastructure; they used game theory to solve the scheduling problem [60, 61]. Similarly, Suhara *et al.* [62] developed a control box to share energy between participants and make use of the available energy consumption to perform future load demand prediction.

Computational intelligence methods were also used to schedule the house appliances. fuzzy logic, neural network and intelligent look-up tables were implemented to create a house energy management system, where fuzzy logic was assumed to produce inputs rules and neural network was assumed to direct these inputs to proper outputs [63, 64]. To maximize benefits associated with house energy management system, a coordinated scheduling approach was proposed using particle swarm optimization (PSO) to schedule residents appliances [65]. Gudi *et al.* [66] used a binary particle swarm optimization (BPSO) to optimize the operation of household appliances. To know the current condition of the grid, Moholkar in [67] developed a fuzzy inference system; where rule based system was implemented to control residential smart appliances. Antunes *et al.* used genetic algorithm (GA) to select appropriate control actions [68].

Deterministic approaches were used too. In [69], Ikegami *et al.* developed optimal operation scheduling module for domestic appliances using mixed integer linear programming (MILP) algorithm. Using the same optimization algorithm, Esser *et al.* in [70] studied the impact of price signals on a household power demand. They modeled major residential appliances to minimize energy cost and maximize resident comfort by

rescheduling domestic appliances. Tischer and Verbic used dynamic programming (DP) instead to get more robust results [71]. Followed by Change *et al.* proposed a coordinated DP to achieve real-time power balancing [72]. Then they proposed a new methodology to decentralize the proposed coordination scheme [73]. Daniel *et al.* in [74] used Markov Chain to model electricity price and energy usage. They used online learning application to identify customer behavior and then scheduled domestic appliances to minimize discomfort and overall cost. In [75], based on the projection of the electricity price, residential appliances were scheduled. On the other hand, an algorithm was proposed to schedule the operation of domestic appliances based on inputs from end-users (user preference) [76, 77]. Similarly, Bozchalui *et al.* [78] developed a system that optimizes the operation of residential assets with automated decision making in real-time based on the customer preference and with minimum discomfort level. In a similar way, Molderink *et al.* [79, 80] adopted three levels method with local prediction to manage domestic appliances with minimum level of customer discomfort. Smart HVAC controls with advanced functionalities incorporating minimum customer discomfort were introduced and presented in [81-83]. In case of stand-alone house, Yamauchi *et al.* designed a new energy management system that works well when the house is disconnected from the main power grid [84]. To perform load management, appliances models are required. Next, literature review about existing models is presented.

## **2.5 Overview of Loads and Transformer Thermal Models**

This section provides discussion regarding existing distribution transformer and house appliances models. Any house energy management system requires accurate models of house appliances for better decision making. To determine whether or not a

distribution transformer is overheated or when the air conditioner should be turned on or off, the thermal behavior of the model (transformer, house, refrigerator ...) should be considered. Although there are many research were done to model phenomenon associated with a house such as solar irradiance [85], house occupant's behavior [86], and heat gains by occupants [87], few efforts were made to model heat relationships of domestic appliances.

To bridge that gap, Park *et al.* developed a generic thermal model for electrical appliances suitable for house appliances [88]. Then, they proposed a methodology to estimate the model thermal parameters [89]. For TCLs, a general model of electric-heating was presented by Bompard *et al.* in [90] to analyze the impact of resistive heating loads aggregation. In [91], Costanzo *et al.* used gray-box methodology to model refrigeration system that is suitable for residential application, which was then implemented to predict the system power consumption. Also, Costanzo *et al.* proposed a method to estimate the thermal parameter of a TCL using maximum likelihood estimation algorithm. In [82], Thomas *et al.* presented a simplified thermal model of HVAC that can be used to optimize air conditioner operation. Similarly, Tashtoush *et al.* developed a detailed thermal model to quantify energy losses in all different parts of HVAC [92]. To achieve that purpose, they developed a thermal model for each part of HVAC zones including heating coil, cooling, humidifier, fan, ductwork, and mixing box. Also, Shunsuke *et al.* developed a thermal model for heat pump and HVAC, which then were considered parts of a microgrid simulation [93]. Talyor *et al.* developed simplified thermal models for most of house appliances [94].

Few work discussed the development of a thermal model of center-tap distributed transformer that is connected to residential house. In [24, 95], a thermal model of a center-tap transformer with nine hot spots was presented. Authors used the model to perform an assessment of the impact of EV/PHEVs on the distribution power grid infrastructure. Additionally, an estimation methodology was presented to compute the thermal circuit parameters. On a large scale transformers (power transformers), several thermal models were presented in the literature. For example, a simple model was developed by IEEE transformer committee [96]. Also, Susa *et al.* developed a thermal model for power transformer considering temperature spots for the core, winding, and oil tank [97-99]. In addition, Susa *et al.* presented an empirical data based methodology to estimate thermal model parameters. Similarly, Swift *et al.* presented an equivalent thermal model for power transformer to determine hot spot temperature [100, 101]. In [102], Qingquan *et al.* presented results of a comparison between the previous three models. The comparison was based on computer simulation. Another simplified thermal model was developed and suggested to be used to approximate temperature inside transformer [103]. Moreover, genetic algorithm (GA) was also implemented to obtain a good estimation of the thermal circuit parameters.

## **2.6 Summary**

Literature review and background information related to the research topic were presented. The proliferation of EV is expected to tax existing distribution infrastructure and can potentially reduce the distribution transformer service lifetime. However, this unfavorable impact can be managed.

Two approaches were presented in the literature to lessen this unfavorable impact, 1) the use of battery energy systems and 2) house loads management through DR solutions. It was found that battery storage systems, whether house battery bank or EV battery, can potentially alleviate the problem. It was also concluded that management and control of the house appliances can lessen the problem and further can provide other services to the utility. Combination of both approaches however in a comprehensive one is not implemented yet.

Current house energy management systems ignore full customer convenience. Furthermore, they did not consider the management of a house without overloading the infrastructure. Without careful monitoring of the distribution transformer loading condition, the service lifetime could be significantly impacted. Also, most of current house energy management systems used simplified models of house appliances. Furthermore, some of these energy management systems did not consider thermal model of house loads. Lack of effective and proper models may result into inaccurate outcomes. Therefore, a better solution is imperative to exist specially with current advanced technologies in the power system field. This research provides a new energy management system for a house without incurring any discomfort to the customer and without overloading the distribution transformer; thus elongates the service lifetime. To design an effective house energy management system, an advanced infrastructure is necessary. This infrastructure is discussed in the next Chapter.

## **3 PROPOSED ADVANCED HOUSE INFRASTRUCTURE**

### **3.1 Introduction**

This Chapter provides discussion regarding the advanced house infrastructure. The smart house energy management system uses a novel infrastructure that exploits state-of-the-art technologies such as distributed state estimation (DSE), smart appliances, advanced communications, electrothermal models of important components, and advanced optimization models. The main advantage of this energy management system is that it enables real-time management and control of the house that is monitored with all components that are connected to the house (i.e. distribution transformer and house appliances). The management system works without changing the life style of the customer. In particular, the physical system considered in this research consists of a distribution transformer, service drop, and one residential house. The house includes DERs and several controllable/non-controllable appliances.

The key components of the advanced house infrastructure are: house DERs and appliances models, house DSE, and advanced optimization models. In this Chapter, the advanced house infrastructure is described. Further, discussion regarding the key components of the infrastructure and how this infrastructure works are provided.

### **3.2 Advanced House Infrastructure Development**

This section introduces the infrastructure that is required for the proposed house management system. This new infrastructure was designed to optimize the power operation of the house according to selected objectives, provide assistance to the grid operations via ancillary services (if needed), ensure the customer convenience, and

elongate the service lifetime of distribution devices, in particular the distribution transformer, because it is the most volatile device in the system. The key points of the overall new approach are the following:

- a) coordinated integration and operation of house DERs, battery storage system, EV, and appliances without overloading/overheating the distribution transformer and
- b) no inconvenience to the customers, i.e. no life style changes of the customer.

Next section provides description of the advanced house infrastructure.

### ***3.2.1 Description of the Advanced House Infrastructure***

The new approach assumes that the monitored house is equipped with some DERs such as roof-top solar PV, energy storage system, and controllable/non-controllable appliances. The advantages of implementing this new approach are many. The major one is that it enables for real-time management and control of all the different components that are connected to the house that the customer/utility owned. Therefore, the burden of integrating new loads, such as EV, is lessened and further increases more integration of renewable generation resources at the distribution system. Furthermore, it enables the implementation of different optimization functions for the operation of the house to extract the maximum benefits to both utility and customer. All these are without incurring any inconvenience to the end-user and without overloading/overheating the distribution transformer. An illustration of the house infrastructure components is shown in Figure 7.

The advanced house infrastructure consists of the following major parts: a) physically based models of every component in the house system including the distribution transformer and house DERs and appliances, b) communication



infrastructure, c) house distributed state estimation, d) advanced optimization models, and e) house parameters (loads and weather conditions) forecasting.

However, the following major parts of the advanced infrastructure are discussed in this dissertation:

- a) physically based models of the house devices,
- b) house distributed state estimation, and
- c) advanced optimization.

Next, a discussion regarding how the advanced infrastructure works is provided.

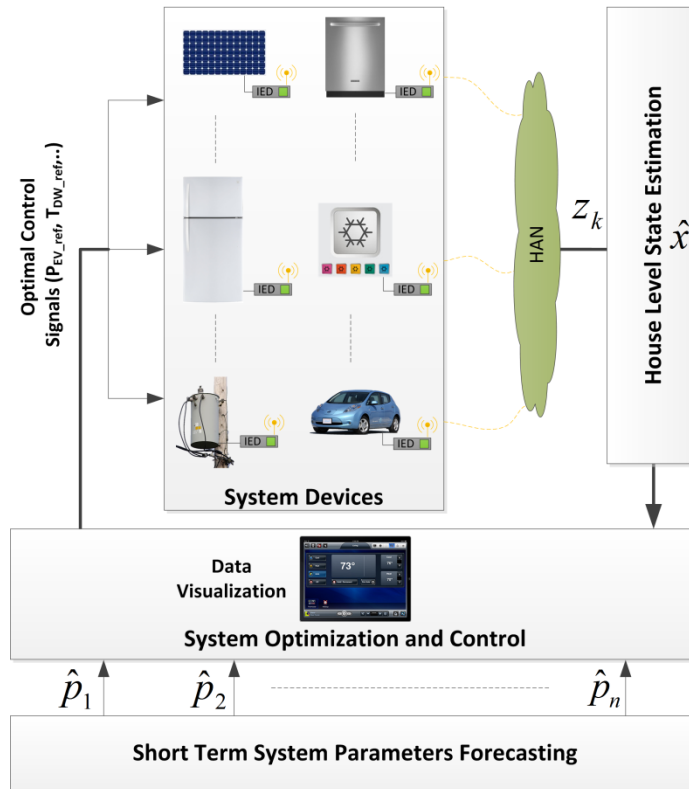


Figure 7. Illustration of the proposed house advanced infrastructure.

### 3.2.2 How Does the House Infrastructure Works?

The advanced house infrastructure works as follows: measurements, GPS synchronized or non-GPS synchronized, from various power components in the house

system are collected. Distribution transformer, house DERs, and house appliances measurements can be collected by IEDs, for example: a universal metering device [104], and then transmitted to the house DES by Home Area Network (HAN). These measurements are sent to the house DSE to perform estimation of the house states. The outcome of the state estimation is a reliable and validated real-time model of the entire house including the distribution transformer. This validated model of the house is then used by the smart house energy management system to perform optimization.

An important function of the smart house energy management system is optimization. Results of the optimization model are basically in the form of scheduling control signals of the house DERs and smart appliances. These control signals could be, for example, EV and battery bank charging/discharging, open/close smart switches, smart dishwasher operation. Besides the real-time model of the house that is provided by the DSE, the optimization model requires data, such as solar irradiance and outside temperature, for the entire planning horizon, which are forecasted.

### **3.3 Summary**

An advanced house infrastructure that can provide real-time energy management of house components including distribution transformer is discussed. A description of the infrastructure operation is provided. The following Chapters present discussion of major parts of the advanced infrastructure: (a) optimization, (b) house devices models, and (c) house DSE.

## **4 HOUSE ENERGY MANAGEMENT SYSTEM OPTIMIZATION**

### **4.1 Introduction**

This Chapter presents the house optimization model. The smart house energy management system provides benefits by solving a particular optimization problem for the good of utility and customer. For example, in case of variable electricity rates, it can optimize the cost of electricity by utilizing the capabilities of house resources. Also, the smart house energy management system can provide control of peak load if the utility requests – assuming that this service is provided for a fee or some economic arrangement. In case of need by the utility, the smart house energy management system can provide information of how much voltage control it can provide. The optimization results are in the form of control signals transmitted by the smart house energy management system to each controllable component in the house. In this research, it is assumed that the smart house energy management system provides controls to one house that is fed by one distribution transformer as illustrated in Figure 8. However, the management system with its optimization functionality can provide management for more than one house as this a quit usual configuration. In this Chapter, the mathematical formulation of the house optimization model with two different objectives is presented. These two objectives are: (a) minimization of the customer’s total energy cost and (b) peak load control.

### **4.2 Mathematical Formulation of the House Optimization Problem**

The smart house energy management system provides benefits for both the utility and customer by solving a particular optimization problem. As mentioned earlier, there



$$\min_{\{\mathbf{x}^k, \mathbf{u}^k\}_{k=1}^N} \sum_{k=1}^N C^k \operatorname{Re}\{\tilde{V}_{pcc}^k (\tilde{I}_{pcc}^k)^*\}, \quad (1)$$

where  $\tilde{V}_{pcc}^k$  and  $\tilde{I}_{pcc}^k$  are the voltage and current states at the point of common coupling (PCC),  $C^k$  is the electricity variable price, and  $k$  is the time interval of planning horizon and equals  $1, 2, \dots, N$ .

The model objective function is subject to

$$g(\mathbf{x}^k, \mathbf{u}^k, \hat{p}^k) = 0, \forall k. \quad (2)$$

Constraint (2) represents the electrothermal house model at each time interval  $k$ , and vectors  $\mathbf{x}^k$ ,  $\mathbf{u}^k$ , and  $\hat{p}^k$  represent state variables, control variables, and forecasted parameters of the house model, respectively. The electrothermal model of the house consists of all house DERs, house appliances, whether controllable or not, and the distribution transformer. The synthesis procedure of the electrothermal house model is explained later in this Chapter.

To represent the operational voltage constraints at every node in the house and current capacity limit constraints for each device that is part of the house system at each time interval  $k$  in the planning horizon, the following two limits are considered

$$\underline{V}^k \leq |\tilde{V}^k| \leq \overline{V}^k, \forall k, \quad (3)$$

$$\underline{I}^k \leq |\tilde{I}^k| \leq \overline{I}^k, \forall k, \quad (4)$$

where  $\tilde{V}^k$  is the voltage state variable and  $\underline{V}^k$  &  $\overline{V}^k$  are minimum and maximum voltage magnitude limits at every node in the house system.  $\tilde{I}^k$  is the current through variables and  $\underline{I}^k$  &  $\overline{I}^k$  are minimum and maximum current magnitude limits for every device in the

house model. It should be noted that  $\tilde{V}^k$  &  $\tilde{I}^k$  are states in the house electrothermal model.

To maintain the refrigerator temperature inside the fresh food compartment within permissible bounds and also ensure that temperature is according to the customer setting at each time interval  $k$  of the future planning period, the next limit is enforced

$$\underline{T_{ref}^k} \leq T_{ref}^k \leq \overline{T_{ref}^k}, \forall k, \quad (5)$$

where  $T_{ref}^k$  is the temperature state inside the refrigerator, which is part of the electrothermal model of the refrigerator, and  $\underline{T_{ref}^k}$  &  $\overline{T_{ref}^k}$  are the minimum and maximum temperature bounds for the temperature in the fresh food compartment.

To ensure that the customer convenience is met by maintaining the temperature inside the house within the set bounds at each time interval  $k$  of the planning period, the following limits is considered

$$\underline{T_{house}^k} \leq T_{house}^k \leq \overline{T_{house}^k}, \forall k, \quad (6)$$

where  $T_{house}^k$  is the monitored temperature state inside the house, which is part of the thermal model of the house, and  $\underline{T_{house}^k}$  &  $\overline{T_{house}^k}$  are the minimum and maximum temperature bounds of the temperature inside the house.

Two control variables are considered for each one of the refrigerator and the air conditioner electrothermal models. The refrigerator basically is turned on/off to maintain the temperature inside it within permissible limits. Similarly, the air conditioner is turned on/off to maintain the monitored temperature inside the house within set limits. These control variables are given by

$$0 \leq u_s^k \leq 1, \quad u_s^k \in \{0,1\}, \forall k, s = \{refrigerator, air\ conditioner\}. \quad (7)$$

To ensure that the hot spot temperature inside the distribution transformer is not exceeding the maximum permissible temperature limit at every time interval  $k$  of the planning window horizon, the following inequality is considered

$$T_{hotSpot}^k \leq HST_{permissible}, \forall k, \quad (8)$$

where  $T_{hotSpot}^k$  is the hot spot temperature state, which is part of the electrothermal model of the distribution transformer that is also part of the entire electrothermal model of the house represented by (2).  $HST_{permissible}$  is the maximum allowed limit of the hot spot temperature of the transformer.

To model the maximum and minimum charging/discharging power of each one of the electrothermal models of the house battery bank and EV battery, the following limits are enforced

$$\underline{P_{batt}^k} \leq P_{batt}^k \leq \overline{P_{batt}^k}, \forall k, \quad (9)$$

$$\underline{P_{EV}^k} \leq P_{EV}^k \leq \overline{P_{EV}^k}, \forall k, \quad (10)$$

where  $P_{batt}^k$  &  $P_{EV}^k$  are the charging/discharging power at every time interval  $k$  for the house battery bank and EV battery, respectively. Note that  $P_{batt}^k$  is part of the house battery charger model and the minimum and maximum charging/discharging power are  $\underline{P_{batt}^k}$  and  $\overline{P_{batt}^k}$ , respectively. Similarly,  $P_{EV}^k$  is part of the EV charger model and the minimum and maximum charging/discharging power are  $\underline{P_{EV}^k}$  and  $\overline{P_{EV}^k}$ , respectively.

To be able to control the dishwasher operation, which consists of several cycles, the set of constraints given by (11)-(17) are considered. In particular, the time limit of every

cycle  $i$  during the operation of the dishwasher is modeled by enforcing the following constraint

$$\underline{T}_i \leq \sum_{k=1}^N u_{dw,i}^k \leq \overline{T}_i, \forall i, \quad (11)$$

where  $u_{dw,i}^k \in \{0,1\}$  is the dishwasher control variable for every cycle at every time interval  $k$  of the planning period.  $\underline{T}_i$  and  $\overline{T}_i$  are the minimum and maximum number time slots for every cycle. Note that  $u_{dw,i}^k$  is part of the electrothermal model of the house.

To model the cycle operation, which is assumed to work without interruption, and enforce the sequential process of all dishwasher cycles, the following three inequalities (12)-(14) are introduced

$$u_{dw,i}^k + s_i^k \leq 1, s_i^k \in \{0,1\}, \forall i, k, \quad (12)$$

$$u_{dw,i}^{k-1} - u_{dw,i}^k - s_i^k \leq 0, \forall i, \forall k = 2,3,\dots,N, \quad (13)$$

$$s_i^{k-1} - s_i^k \leq 0, \forall i, \forall k = 2,3,\dots,N, \quad (14)$$

where  $s_i^k \in \{0,1\}$  is an additional slack variable at every time interval  $k$  of the planning horizon. Note that  $s_i^k$  is part of the electrothermal model of the house.

To guarantee that there is no delay between the cycles themselves during the dishwasher operation, the following equality constraint is considered

$$s_{i-1}^k - u_{dw,i}^k - s_i^k = 0, \forall k, \forall i = 2,3,\dots,n, \quad (15)$$

To ensure that the dishwasher cycles work within the customer allowed time (customer setting), the following inequality is introduced

$$u_{dw,i}^k \leq T_{preference,i}^k, \forall i, k, \quad (16)$$



where  $T_{preference,i}^k$  characterizes the customer time preference interval at every time interval  $k$  of the planning period.

To make sure that every cycle during the dishwasher operation meets the energy requirement, the following equality constraint is imposed

$$\sum_{k=1}^N u_{dw,i}^k P_{dw,i}^k = E_i, \forall i, \quad (17)$$

where  $P_{dw,i}^k$  and  $E_i$  are the power and energy profiles for every cycle at every time interval  $k$  of the future planning horizon.

The house model states and controls initials are given by the following

$$\mathbf{x}_0 = \mathbf{x}(t_0), \mathbf{u}_0 = \mathbf{u}(t_0), \mathbf{x}(\alpha) = \mathbf{p}, \quad (18)$$

where  $\mathbf{x}_0$  and  $\mathbf{u}_0$  are the vectors represent the house model states and control initial values, respectively.  $\mathbf{x}(\alpha)$  is the vector represents the house states values at  $\alpha$ . This concludes the optimization model with the objective is to minimize the customer's total energy cost. Next is the mathematical formulation of the optimization model of the house with peak load control.

#### 4.2.2 House Peak Load Control

Another objective function that the smart house energy management system can provide is to control the house peak load over a planning period of time. This function becomes much more desirable in areas served by vertically regulated utilities. The goal here is to minimize the peak load of the house system over a day subject to meeting the customer convenience and observing every component ratings and constraints. The objective mathematical formulation of the problem is given by

$$\min_{\{x^k, u^k\}_{k=1}^N} X, \quad (19)$$

where  $X$  is the peak load of the house and therefore

$$X > \text{Re}\{\tilde{V}_{pcc}^k (\tilde{I}_{pcc}^k)^*\}, \forall k, \quad (20)$$

where  $\tilde{V}_{pcc}^k$  and  $\tilde{I}_{pcc}^k$  are the voltage and current states at the point of common coupling (PCC) and  $k$  is the time interval of the planning horizon and equals  $1, 2, \dots, N$ . This objective function is subject to limits and constraints given by (2)-(18). One major equality constraint is the electrothermal model of the house, which is represented by (2). The construction method of that constraint is presented in the next section.

#### 4.2.3 *Electrothermal Model of the House*

The equality constraint given by (2) represents the electrothermal model of the house including the distribution transformer. This constraint is derived as follows: every device model in the house including the distribution transformer, refrigerator, air conditioner, thermal model of the house, etc..., is described by a set of mathematical equations and then cast into one standard form represented by the following

$$\tilde{\mathbf{I}}^k = f(\mathbf{x}^k, \mathbf{u}^k, \hat{\mathbf{p}}^k), \forall k, \quad (21)$$

where the vector  $\tilde{\mathbf{I}}^k$  is given by  $[\tilde{\mathbf{I}}^k; \mathbf{0}]$ . The vector  $\tilde{\mathbf{I}}^k$  represents the through variables of a device at each time interval  $k$  of the planning period of time and vectors  $\mathbf{x}^k$ ,  $\mathbf{u}^k$ , and  $\hat{\mathbf{p}}^k$  represent external and internal state variables, control variables, and forecasted parameters of that device, respectively. Then, the electrothermal house model is constructed by applying Kirchhoff's current law (KCL) at each node of the house as follows

$$g(\mathbf{x}^k, \mathbf{u}^k, \hat{\mathbf{p}}^k) = \begin{cases} \sum_{I \in i} \tilde{\mathbf{I}}^k = 0 \text{ for all nodes} \\ \text{Internal equations of all devices} \end{cases}. \quad (22)$$

### 4.3 Summary

In this Chapter, the mathematical formulation of the house optimization model is presented. Although the smart house energy management system can provide several functions, only two different objectives are considered. Firstly, the formulation of the problem with the minimization of the customer's total energy cost is presented. Then, the formulation of the problem with house peak load control is discussed. Part of both formulations is the equality constraint represented by (2). The methodology that was adopted to construct this equality is also presented. To be able to construct the electrothermal model of the house, a mathematical model for every device in the house including the distribution transformer was developed. Discussion regarding the development of the mathematical model for every component in the house including DERs, appliances, and distribution transformer before it becomes in a standard syntax given by (21) is presented in the next Chapter.

## **5 HOUSE SYSTEM COMPONENTS MODELING**

### **5.1 Introduction**

One of the keys to have a successful house energy management system is to have accurate models for the distribution transformer and various house components including DERs and domestic appliances. There are several approaches in the literature that can be used to designing systems and developing models. However, physically-based modeling with object orientation approach is one of the most desired approaches, because it is based on how the system lays out in the physical world. In this approach, the physical component is represented by a detailed, yet well understood, abstract mathematical model. This mathematical model is then used to simulate the physical component and further develop various applications. In this Chapter, the modeling technique that was used to model the distribution transformer and various components of the house is presented. Additionally, the Quadratic Integration method that was used to integrate the model is discussed. Finally, new electrothermal models for important components of the house including the distribution transformer and important appliances are also presented.

### **5.2 Object Orientation Modeling Approach**

The object orientation approach is generally used to designing a device, application, or system by applying the object oriented paradigm and visual modeling throughout the development life cycles. The advantages of this approach are many; some are listed below:

- provides a unified syntax to all various house components, associates controls, and facilitates advanced applications such as state estimation, protection, and optimization,
- simplifies communication between various parts of the device, application, system in an efficient and reliable manner without loss of any information,
- facilitates and simplifies the integration of a new device, application, or system with already existing components (Plug and Play concept), and
- this generalization enables standardization for utilizing and exchanging a device model among applications. Thus, advanced smart grid applications can be easily implemented.

Next, discussion regarding the modeling procedure that was used in this research starting from extracting the mathematical model until casting the model in a standard syntax is presented.

### **5.3 Description of Device Modeling**

#### ***5.3.1 Modeling Procedure***

Every device in the house including the distribution transformer goes through a number of steps before it is cast in one unified syntax (standard) form. The modeling procedure that was used to model various devices that are part of the smart house energy management system is illustrated in Figure 9. This procedure is explained as follows,

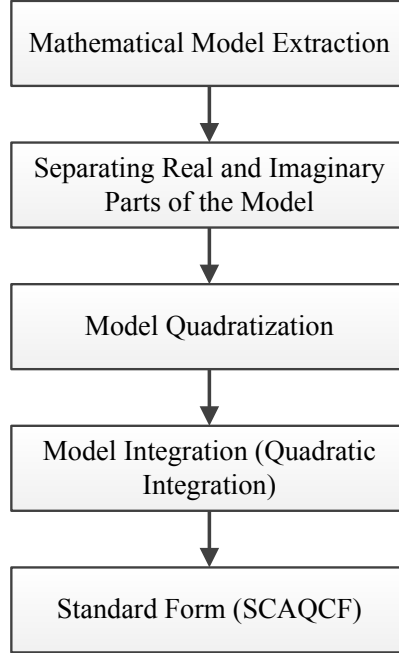


**Figure 9. House DERs and appliances modeling procedure.**

### **1. Mathematical Model Extraction:**

An abstract mathematical model of any device that is part of the smart house energy management system is derived based how the physical device is in the physical world. This model is formulated as a set of linear and nonlinear differential algebraic equations (DAEs) and algebraic equations in terms of device state and control variables. Device states could be external or internal states. Examples of external states are voltages at the device terminals. Examples of internal states are state of charge of the house battery bank, actual rating of the air conditioner, and temperature inside the house. The differential equations part of the derived mathematical model is then cast in a simple compact form as follows

$$A_1 \begin{bmatrix} i(t) \\ 0 \end{bmatrix} + A_2 \frac{d}{dt} \begin{bmatrix} i(t) \\ 0 \end{bmatrix} = B_1 x(t) + B_2 \frac{dx(t)}{dt}, \quad (23)$$

whereas the algebraic equations of the model are cast in the following form

$$\begin{bmatrix} i(t) \\ 0 \end{bmatrix} = B_3 x(t) + \begin{bmatrix} x(t)^T F_{eq1} x(t) \\ x(t)^T F_{eq2} x(t) \\ \vdots \end{bmatrix} + K_{eq}, \quad (24)$$

where

$$\begin{bmatrix} i(t) \\ 0 \end{bmatrix} = \begin{bmatrix} i_1(t) \\ i_2(t) \\ \vdots \\ 0 \\ 0 \\ \vdots \end{bmatrix}, \quad x(t) = \begin{bmatrix} x_1(t) \\ x_2(t) \\ \vdots \\ \vdots \end{bmatrix},$$

$i(t)$ : Vector defining the through variable of the model.

$x(t)$ : Vector defining the external and internal state variables of the model.

$A_1$ : Identity matrix of the differential equations defining the linear part of the through variables with appropriate dimension.

$A_2$ : Matrix defining the coefficients of the differential equations part of the through variables with appropriate dimension.

$B_1$ : Matrix defining the linear part of the differential equations with appropriate dimension.

$B_2$ : Matrix defining the coefficients of the differential part with appropriate dimension.

$B_3$ : Matrix defining the linear part of the algebraic equations with appropriate dimension.

$F_{eq}$ : Matrix defining the quadratic part of the algebraic equations with appropriate dimension.

$K_{eq}$ : Vector defining the constant part of the algebraic equations.

## 2. Separation of Real and Imaginary Parts:

In this step, the model is separated into real and imaginary parts. Basically, voltages and currents phasors are expressed with their Cartesian coordinates ( $\tilde{V} = V_r + jV_i$  &  $\tilde{I} = I_r + jI_i$ ). These complex equations are separated into two real equations.

### **3. Model Quadratzation:**

The mathematical model, described previously, is then quadratized. Simply, any nonlinear equation that is above degree two is reduced to degree not higher than two. In addition, nonlinear functions, for example exponential function or logarithmic function, need to be quadratized. This can be done by applying Maclaurin series expansion to the function and then reduce the higher order terms to two. The reduction from high order into not more than two can be achieved by introducing slack variables, as necessary. Several examples of function or system quadratization can be found in [105-107].

### **4. Quadratic Integration:**

The resulting quadratic differential and algebraic system are then integrated using state-of-the-art integration method, the Quadratic Integration method [108]. For a system of equations, whether linear or nonlinear, especially for stiff systems when power electronics with IGBTs switches or induction machines are part of the model, the quadratic integration method has exhibited superiority over other integration methods such as Trapezoidal method [107-109]. Some of the advantages of this integration method are:

- absolutely stable numerical integration method,
- free of numerical oscillation,
- fourth order method. Solution is achieved with high numerical accuracy and precision, and
- fast convergence with low number of iteration.

The quadratic method is formulated based on three point collocation method; and it is used to convert the system of equations into a set of algebraic linear or quadratic



equations. The concept of the quadratic integration method is illustrated in Figure 10. It is unlike the Trapezoidal integration method, where the system model states are assumed to vary linearly throughout the time step, the quadratic integration method is assumed that within every integration time step ( $h$ ), the system states variables vary quadratically. In principle, within every integration time step of length  $h$ , which is defined by an interval  $[\tau - h, \tau]$ , the two end points  $x[\tau - h]$  and  $x[\tau]$ , and the midpoint  $x_m$ , is defined by the following equation ( $x_m = x[\tau - h / 2]$ ), can define a quadratic function in the interval  $[\tau - h, \tau]$ . This function is then integrated in the time interval  $[\tau - h, \tau]$  resulting in a set of algebraic equations for this integration step. The solution of the quadratic system of equations is obtained via Newton's method. Note that the resulting algebraic equations are either linear or quadratic.

To show the difference between the quadratic and trapezoidal integration methods, a case study of a series RLC circuit was modeled and simulated. Results of this case including the difference between these two integration methods are reported in Appendix A.

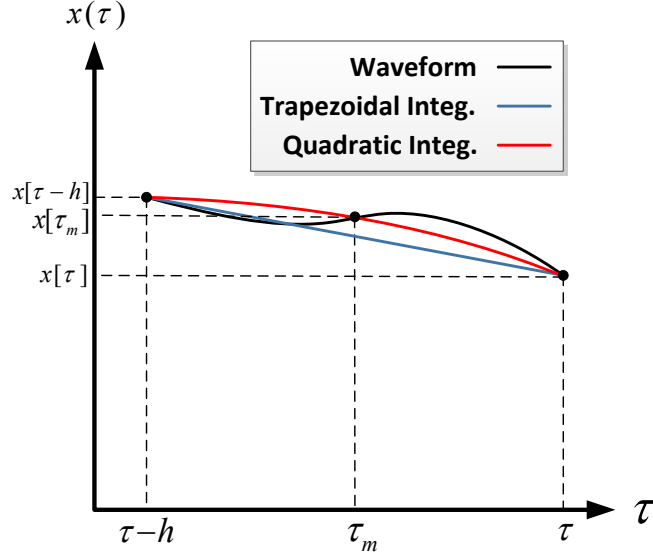


Figure 10. Illustration of quadratic integration method

## 5. State and Control Algebraic Quadratic Companion Form (SCAQCF)

In the last step, the state and control variables are separated and then formed according to the State and Control Algebraic Quadratic Companion Form (SCAQCF) given by (25) in a matrix notation and (26) in a detailed notation. The main advantage of the SCAQCF model is that this formulation gives a generalized and an abstract model for any component of the house including the distribution transformer, which is independent of any device type. It is also suitable for implementation of object oriented algorithms for any application. More details concerning the extraction of the final model in SCAQCF format is provided in Appendix A.

- SCAQCF in a matrix format

$$i(x, u) = Y_{eqx}x + [x^T F_{eqx}x] + Y_{equ}u + [u^T F_{equ}u] + [x^T F_{eqxu}u] - B_{eq}, \quad (25)$$

- SCAQCF in detailed format

$$\begin{aligned}
& \begin{bmatrix} \tilde{I}(t) \\ 0 \\ \tilde{I}(t_m) \\ 0 \end{bmatrix} = \\
& Y_{eq_x} \begin{bmatrix} \tilde{V}(t) \\ Y(t) \\ \tilde{V}(t_m) \\ Y(t_m) \end{bmatrix} + \begin{bmatrix} [\tilde{V}^T(t) & Y^T(t) & \tilde{V}^T(t_m) & Y^T(t_m)] & F_{eq_x_1} \\ \vdots \\ [\tilde{V}^T(t) & Y^T(t) & \tilde{V}^T(t_m) & Y^T(t_m)] & F_{eq_x_n} \end{bmatrix} \begin{bmatrix} \tilde{V}(t) \\ Y(t) \\ \tilde{V}(t_m) \\ Y(t_m) \end{bmatrix} + \\
& Y_{eq_u} \begin{bmatrix} \tilde{U}(t) \\ \tilde{U}(t_m) \end{bmatrix} + \begin{bmatrix} [\tilde{U}^T(t) & \tilde{U}^T(t_m)] & F_{eq_u_1} \\ \vdots \\ [\tilde{U}^T(t) & \tilde{U}^T(t_m)] & F_{eq_u_n} \end{bmatrix} \begin{bmatrix} \tilde{U}(t) \\ \tilde{U}(t_m) \end{bmatrix} + \\
& \begin{bmatrix} [\tilde{V}^T(t) & Y^T(t) & \tilde{V}^T(t_m) & Y^T(t_m)] & F_{eq_xu_1} \\ \vdots \\ [\tilde{V}^T(t) & Y^T(t) & \tilde{V}^T(t_m) & Y^T(t_m)] & F_{eq_xu_n} \end{bmatrix} \begin{bmatrix} \tilde{U}(t) \\ \tilde{U}(t_m) \end{bmatrix} - B_{eq}.
\end{aligned} \tag{26}$$

where

$x$ : the external and internal states at time  $t$  and time  $t_m$ .

$u$ : the control variables at time  $t$  and time  $t_m$ .

$Y_{eqx}$ : matrix defining the linear part of device state variables.

$F_{eqx}$ : matrix defining the nonlinear part of device state variables.

$Y_{equ}$ : matrix defining the linear part of device control variables.

$F_{equ}$ : matrix defining the nonlinear part of device control variables.

$F_{eqxu}$ : matrix defining the nonlinear part of device state control variables.

$B_{eq}$ : vector defining the constant part of device model.

$t_m$ : a middle point in the integration time step  $h$ .

### 5.3.2 Thermal Modeling

To determine whether or not, for example, the transformer is overheated or when the air conditioner should be turned on/off, the thermal behavior of the model (transformer, house, refrigerator and other devices) should be modeled. Using the analogy between thermal – electrical physical laws, the thermodynamics of any thermal device can be modeled by

$$T(t) = \dot{Q}(t)R_{th}, \quad (27)$$

$$\dot{Q}(t) = C_{th} \frac{dT(t)}{dt}, \quad (28)$$

$$\dot{Q}(t) = C_{th} \frac{dT(t)}{dt} + G_{th}\Delta T(t), \quad (29)$$

where  $T$  is spot temperature in [ $^{\circ}\text{C}$ ],  $\dot{Q}$  is heat flow rate in [Btu/h],  $C_{th}$  is thermal capacitance in [Btu/ $^{\circ}\text{C}$ ], and  $G_{th}$  is thermal conductance in [Btu/ $^{\circ}\text{C}\cdot\text{h}$ ]. The computation of the thermal parameters in any thermal device is presented next.

#### 5.3.2.1 Thermal Parameters Computation

In this section, the computation methodology that was used to estimate the thermal parameters, thermal conductance and capacitance, is discussed.

##### 1) Computation of Thermal Conductance ( $G_{th}$ )

In principle, the heat at each temperature spot is experienced a thermal resistance as it propagates to other temperature spots. The reciprocal of that thermal resistance is the thermal conductance, which is defined as the quantity of heat transmitted between two temperature spots. Thermal conductance parameters are estimated considering rated

parameters of the device such as rated current and rated temperature. Basically, steady state equations of the device model are used to estimate the numerical values of the thermal conductance between temperature spots. The reason for this approach is the fact that for devices, such as transformers, the manufacturer provides the steady state operating temperatures under full loading conditions. This information is then used to estimate the thermal conductances. In some cases, the number of thermal conductances is larger than the number of the device model equations. In this case, each thermal conductance is represented by a percent of a collective main thermal conductance. Next, the thermal capacitance computation is discussed.

## 2) Computation of Thermal Capacitance ( $C_{th}$ )

The thermal capacitance or heat capacity is defined as the amount of the heat energy required to raise the temperature by one unit. It is a function of the volume, mass density, and specific heat of the matter as given by

$$C_{th} = Vol \rho C_p, \quad (30)$$

where

$Vol$  is the volume in [ $m^3$ ],

$\rho$  is the mass density [ $kg/m^3$ ],

$C_p$  is specific heat [ $Btu/kg.^{\circ}C$ ],

Note that, the procedure of computing both thermal conductance and capacitance are performed automatically.

### 5.3.3 *Smart House Energy Management System Devices*

The following devices were considered part of the smart house energy management system: electrothermal model of the distribution transformer, electrothermal model of the

house, smart dishwasher, electrothermal model of a refrigerator, and electrothermal model of an air conditioner. Other house loads, such as lighting, cloth washer, and dryer, were modeled as a time variable load. Distributed energy resources, such as roof-top solar PV, residential battery bank, and EV that is modeled as lithium ion battery, were also considered. Averaged models of battery charger, DC-DC boost converter, DC-AC inverter, and all associated control circuits, such as thermostat control and maximum power point tracking control, were also considered. It should be noted that these devices can be connected together in different configuration as they exist in the physical house. This facilitates modeling different houses with different arrangements. In this research, the model domain is the quasi-dynamic domain. In this domain, the slow moving behaviors such as house temperature and battery state of charge are captured. On the other hand, electromagnetic transient phenomena are not of interest and thus not considered. Next, the models of the distribution transformer, house DERs, and house appliances are presented.

#### **5.4 Electrothermal Model of a Single Phase Distribution Transformer**

The distribution transformer is one of the most important devices in the electrothermal model of the house. And it is the most volatile equipment in the overall house system. Typical residential distribution transformer is a single phase, two winding transformer with secondary center-tapped; and usually is connected to one or several house(s) through a service drop. The service drop is, in most cases, overhead wires that are connected from power provider pole, where the transformer usually is, to a residential house. These distribution transformers are usually rated 7.2/(0.12-0.240) kV with power

ratings up to 50 kVA. Depending on the application, special configuration of the distribution transformer can exist. It is a usual practice to use a pole mounted transformer in case if the power is provided to a residential customer. Normal voltage rating of these types of transformers is 110-140 V phase to neutral and 210-240 V two phases. Figure 11 shows the distribution transformer interface window in WinIGS program. In the following sections, the electrothermal model of the transformer is described.

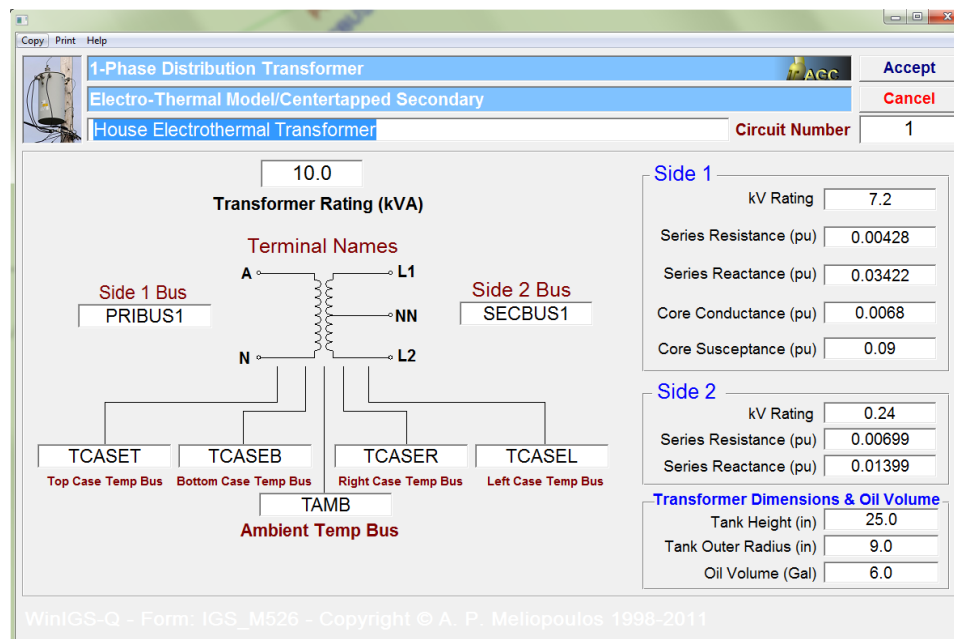


Figure 11. Electrothermal transformer model user interface in WinIGS program

#### 5.4.1 Electrical Model

The electrical model is used to compute the center-tap transformer electrical currents for a specific electric load demand. In this research, a standard electrical model of a single phase distribution transformer with a center-tap at the secondary winding was considered. This model can adapt various voltages and power ratings. The electrical model circuit is illustrated in Figure 12. This center-tap distribution transformer was implemented to provide a low voltage to a residential house via a service drop.

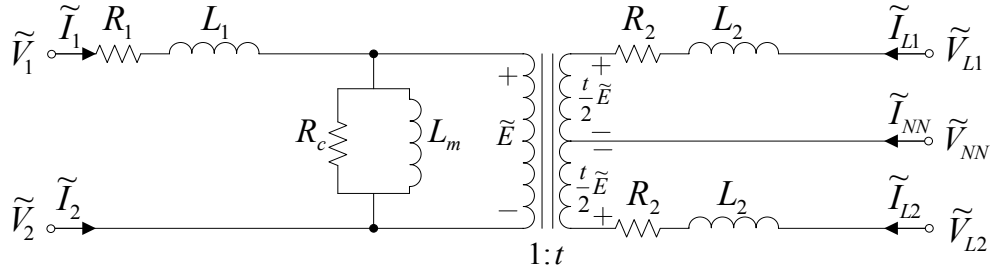


Figure 12. Electrical circuit of the center-tap transformer.

#### 5.4.2 Thermal Model

Transformer's overall insulation life expectancy and overloading capabilities depend on several factors. However, it is determined primarily by the hot spot temperature in the transformer. It is, therefore, essential to predict thermal loading of the transformer during normal loadings and, in particular, during abnormal (overloading) conditions. Furthermore, the improved knowledge of transformer thermal characteristics can predict the expected service lifetime of distribution transformer insulation. This can indicate whether the transformer is properly sized for a particular application or not. Therefore, this improved realization can

- a) allow the enhancement of transformer operation, and
- b) provide better load management optimization decisions.

In this section, the development of a new thermal model is discussed.

Although there are thermal models of the transformer in the literature, it is concluded that a new model is needed as concluded in 2.5 and 2.6. Most of these existing models were mainly modeled and developed for power transformers applications and were lacking accuracy in terms of temperature spots number. In this research, a new and detailed thermal model of a single phase center-tap distribution transformer was developed. This model enables better monitoring of the gradient temperatures and thus



accurate estimation of the hot spot temperature and loss of insulation life. The process of developing the thermal model is explained below.

#### 5.4.2.1 Temperature Spots Definition

The first step of developing a thermal model of a center-tap distribution transformer is to define and select a number of temperature spots and to determine their locations. For a better monitoring of rapid temperature change and to be able to locate the hot spot temperature inside a center-tap transformer with high accuracy, a total of 21 temperature spots were selected. The location of each one of these temperature spots is illustrated in Figure 13. The reference temperature of the thermal model is the ambient temperature. External temperature spots of the transformer electrothermal model (transformer case temperature spots) were designed to have external connections to an ambient temperature spot that is connected to a reference temperature model.

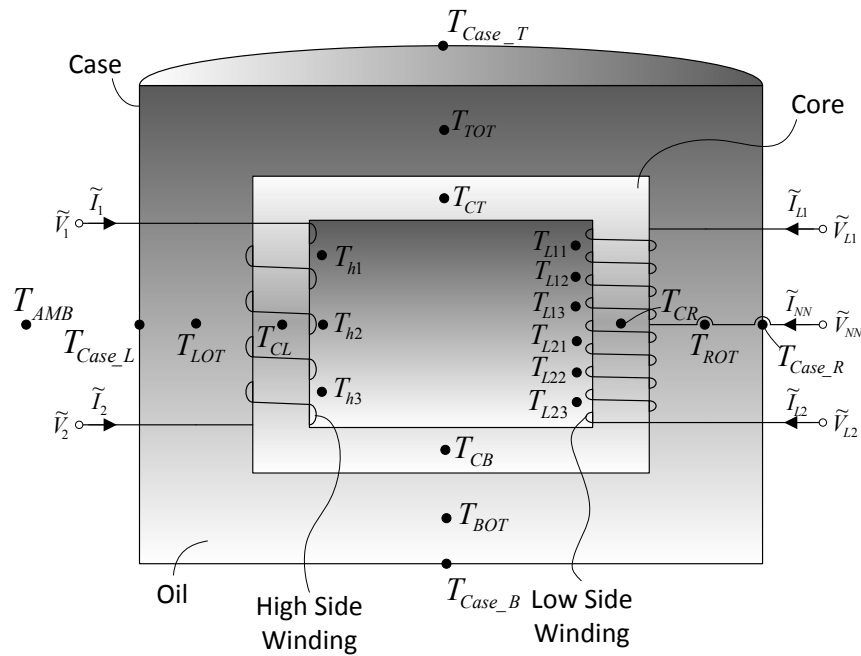


Figure 13. Single phase center-tap transformer temperature spots locations.

Each temperature spot is briefly explained as the following:

- **Primary Winding Temperature Spots:**

The transformer primary winding was divided into three segments as illustrated in Figure 14. Each one of these segments was assumed to have a temperature spot located in the middle of the segment. In total, there are three temperature spots as the following,

$T_{h1}$ : High-side temperature spot for segment one in [ $^{\circ}\text{C}$ ].

$T_{h2}$ : High-side temperature spot for segment two in [ $^{\circ}\text{C}$ ].

$T_{h3}$ : High-side temperature spot for segment three in [ $^{\circ}\text{C}$ ].

- **Secondary Winding Temperature Spots:**

The transformer secondary winding was segmented into two main parts as the following:

1) Secondary winding part between phase  $L_1$  and  $NN$ .

2) Secondary winding part between phase  $L_2$  and  $NN$ .

Each one of these parts was divided into three segments as illustrated in Figure 14, where each segment was assumed to have a temperature spot located in the middle of the segment. In total, there are six temperature spots as the following,

$T_{L11}$ : Low-side temperature spot for part one segment one in [ $^{\circ}\text{C}$ ].

$T_{L12}$ : Low-side temperature spot for part one segment two in [ $^{\circ}\text{C}$ ].

$T_{L13}$ : Low-side temperature spot for part one segment three in [ $^{\circ}\text{C}$ ].

$T_{L21}$ : Low-side temperature spot for part two segment one in [ $^{\circ}\text{C}$ ].

$T_{L22}$ : Low-side temperature spot for part two segment two in [ $^{\circ}\text{C}$ ].

$T_{L23}$ : Low-side temperature spot for part two segment three in [ $^{\circ}\text{C}$ ].

- **Transformer Core Temperature Spots:**

The core of the transformer was divided into four regions as illustrated in Figure 14, where each one was assumed to have a temperature spot located in the middle of the region. In total, there are four temperature spots as the following,

$T_{CT}$ : Core-Top temperature spot for region one in [ $^{\circ}\text{C}$ ].

$T_{CB}$ : Core-Bottom temperature spot for region two in [ $^{\circ}\text{C}$ ].

$T_{CR}$ : Core-Right temperature spot for region three in [ $^{\circ}\text{C}$ ].

$T_{CL}$ : Core-Left temperature spot for region four in [ $^{\circ}\text{C}$ ].

- **Transformer Oil Tank Temperature Spots:**

The transformer oil tank was divided into four sub-spaces, where each one was assumed to have a temperature spot. In total, there are four temperature spots as the following,

$T_{TOT}$ : Top of the Oil temperature spot for region one in [ $^{\circ}\text{C}$ ].

$T_{BOT}$ : Bottom of the Oil temperature spot for region two in [ $^{\circ}\text{C}$ ].

$T_{ROT}$ : Right of the Oil temperature spot for region three in [ $^{\circ}\text{C}$ ].

$T_{LOT}$ : Left of the Oil temperature spot for region four in [ $^{\circ}\text{C}$ ].

- **Transformer Case Temperature Spots:**

The transformer case was divided into four segments, where each one was assumed to have a temperature spot. In total, there are four temperature spots as the following,

$T_{caseT}$ : Case-Top temperature spot for region one in [ $^{\circ}\text{C}$ ].

$T_{caseB}$ : Case-Bottom temperature spot for region two in [ $^{\circ}\text{C}$ ].

$T_{caseR}$ : Case-Right temperature spot for region three in [ $^{\circ}\text{C}$ ].

$T_{caseL}$ : Case-Left temperature spot for region four in [ $^{\circ}\text{C}$ ].

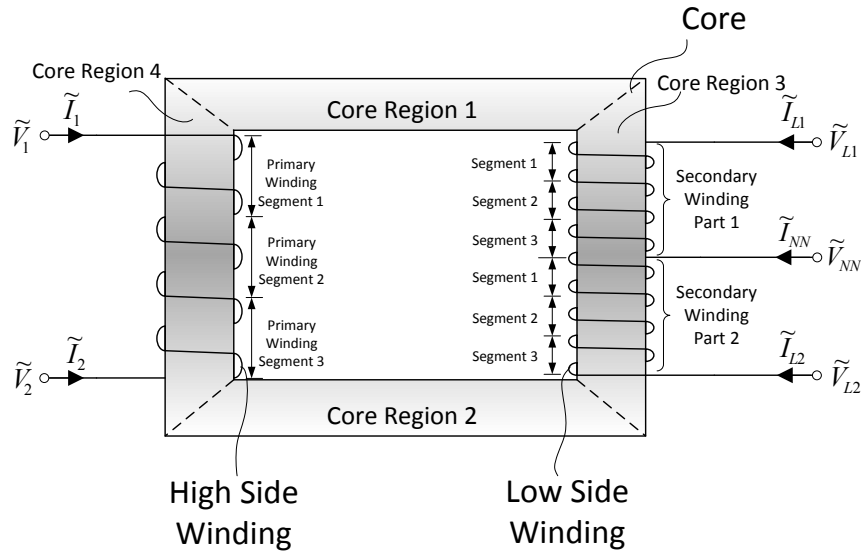


**Figure 14. Segments of transformer primary winding, secondary winding, and core.**

#### 5.4.2.2 Thermal Parameters Selection

The first thermal element is the thermal conductance ( $G_{th}$ ). For every selected temperature spot in the transformer thermal model, it was assumed that there are 21 thermal conductances connected to it. Additionally, it was also assumed that there is a thermal capacitance ( $C_{th}$ ) for every selected temperature spot in the model. The thermal capacitance was assumed to be connected between the corresponding temperature spot and a specific temperature spot that is near to it. The connections of these thermal capacitances are provided in Table 1. The third thermal element is the heat source. There were 13 heat sources assumed in the model. Location of these heat sources are provided in Table 2.

**Table 1. Transformer thermal model thermal capacity.**

Thermal Capacitance ( $C_{th}$ )	Spot 1	Spot 2
$C_{h1}$	$T_{h1}$	$T_{CT}$

$C_{h2}$	$T_{h2}$	$T_{CL}$
$C_{h3}$	$T_{h3}$	$T_{CB}$
$C_{L11}$	$T_{L11}$	$T_{CT}$
$C_{L12}$	$T_{L12}$	$T_{CR}$
$C_{L13}$	$T_{L13}$	$T_{CR}$
$C_{L21}$	$T_{L21}$	$T_{CR}$
$C_{L22}$	$T_{L22}$	$T_{CR}$
$C_{L23}$	$T_{L23}$	$T_{CB}$
$C_{CT}$	$T_{CT}$	$T_{TOT}$
$C_{CB}$	$T_{CB}$	$T_{BOT}$
$C_{CR}$	$T_{CR}$	$T_{ROT}$
$C_{CL}$	$T_{CL}$	$T_{LOT}$
$C_{TOT}$	$T_{TOT}$	$T_{Case\_T}$
$C_{BOT}$	$T_{BOT}$	$T_{Case\_B}$
$C_{ROT}$	$T_{ROT}$	$T_{Case\_R}$
$C_{LOT}$	$T_{LOT}$	$T_{Case\_L}$
$C_{CaseT}$	$T_{CaseT}$	$T_{AMB}$
$C_{CaseB}$	$T_{CaseB}$	$T_{AMB}$
$C_{CaseR}$	$T_{CaseR}$	$T_{AMB}$
$C_{CaseL}$	$T_{CaseL}$	$T_{AMB}$

**Table 2. Transformer heat source.**

Heat Source ( $\dot{Q}$ )	Spot
$\dot{Q}_{h1}$	$T_{h1}$

$\dot{Q}_{h2}$	$T_{h2}$
$\dot{Q}_{h3}$	$T_{h3}$
$\dot{Q}_{L11}$	$T_{L11}$
$\dot{Q}_{L12}$	$T_{L12}$
$\dot{Q}_{L13}$	$T_{L13}$
$\dot{Q}_{L21}$	$T_{L21}$
$\dot{Q}_{L22}$	$T_{L22}$
$\dot{Q}_{L23}$	$T_{L23}$
$\dot{Q}_{CT}$	$T_{CT}$
$\dot{Q}_{CB}$	$T_{CB}$
$\dot{Q}_{CR}$	$T_{CR}$
$\dot{Q}_{CL}$	$T_{CL}$

5.4.2.2.1 Computation of the Transformer Model Thermal Parameters

**1) Transformer Thermal Conductance ( $G_{th}$ )**

For estimating the transformer thermal conductances, manufacturer data of steady state temperatures at various points of the transformer under full loading conditions were utilized. Note that these temperatures can be also measured in the laboratory. Transformer model rated temperatures at every temperature spot are provided in Table 3. These rated temperatures are used with steady state equations of the transformer model to estimate the transformer thermal conductances. There is a very large number of thermal conductances in the transformer model. To estimate them all, each thermal conductance was represented by a percent of a main thermal conductance. This reduced the number of

thermal conductance into only 21, which can be estimated easily. Then, all other thermal conductances can be calculated using the assumed percentage provided in Appendix B.

**Table 3. Center-tap transformer rated temperature at each temperature spot.**

Temperature Spot	Rated Temp [°C]
$T_{h1}$	103
$T_{h2}$	95
$T_{h3}$	91
$T_{L11}$	105
$T_{L12}$	100
$T_{L13}$	95
$T_{L21}$	94
$T_{L22}$	93
$T_{L23}$	92
$T_{CT}$	94
$T_{CB}$	88
$T_{CR}$	92
$T_{CL}$	90
$T_{TOT}$	80
$T_{BOT}$	70
$T_{ROT}$	77
$T_{LOT}$	73
$T_{caseT}$	65
$T_{caseB}$	55

$T_{caseR}$	62
$T_{caseL}$	59
$T_{AMB}$	40

## 2) Transformer Thermal Capacitance ( $C_{th}$ )

Each thermal capacitance in the transformer model was computed by (29). The volume of the space surrounding a temperature spot in the transformer, however, can be computed by

$$Vol = \pi r^2 h, \quad (31)$$

where

$r$  is radius of the tank [in], and

$h$  is the height of the tank [in].

In particular, the following assumptions were made when the volume of each part of the transformer was computed:

- Inner radius of the transformer was assumed 96% of the outer radius.
- A number of inches were subtracted of the transformer height due to bushing as necessary. Some manufacture provides exact height without bushing.
- Each winding side volume was assumed to be 2% of the resulted transformer volume (core and windings volume).

### 5.4.2.3 Transformer Loss of Insulation Life (LOIL)

The degradation of the transformer insulation life attributes to three different factors: moisture, oxygen, and temperature [24, 96]. Each one of these factors contributes separately to the degree of the transformer insulation degradation; therefore, they must be



controlled independently. The contamination of the transformer oil resulted from either moisture or oxygen can be controlled by the transformer Oil-Preservation System [OPS].

Thus, moisture and oxygen were excluded from the analysis provided in this research; and the transformer was assumed to be well dried and oxygen free. It was only assumed that the temperature factor was the only factor considered in the loss of insulation life (LOIL) of the transformer computation procedure.

LOIL during time interval  $t$  can be explained by the equivalent total life hours consumed divided by the predefined normal insulation life, which is usually given in hours. Thus, LOIL can be computed using the following equation [96, 110]

$$LOIL = \exp\left(-\left(A + \frac{B}{T_{HotSpot}}\right)\right)h, \quad (32)$$

where

$T_{HotSpot}$ : Hot spot temperature at time  $t$  in [ $^{\circ}K$ ],

$t$ : time period in [ $h$ ],

$A$  &  $B$ : Empirical constants depending on the design of the transformer. Numerical values of  $A$  &  $B$  are summarized in Table 4.

**Table 4. Transformer empirical A & B values [111].**

Constant	65 °C Insulation System	55 °C Insulation System
A	-11.269	-11.968
B	6328.8	6328.8

### ***5.4.3 Mathematical Model of the Distribution Center-Tap Transformer***

Using the selected thermal parameters, the thermal circuit of the distribution center-tap distribution was developed. The detailed electrothermal model of a center-tap distribution transformer is provided in Appendix B.

## **5.5 House DERs and Appliances Models**

Physically based models of major house DERs and appliances were developed. A description of each one of these models including DERs and appliance (controllable/non-controllable) is briefly discussed. Note that the discussion in this section is focused on providing description regarding a residential smart house. However, the house model can be used to represent a commercial building, if properly sized.

### ***5.5.1 Thermal Model of the House***

A thermal model of a single story house with two bedrooms and two bathrooms was developed. The layout of the house is illustrated on Figure 15. The model provides an estimation of all selected temperature spots inside the house. These temperatures impact the operation of thermal loads that are connected to the house such as the refrigerator and air conditioner.

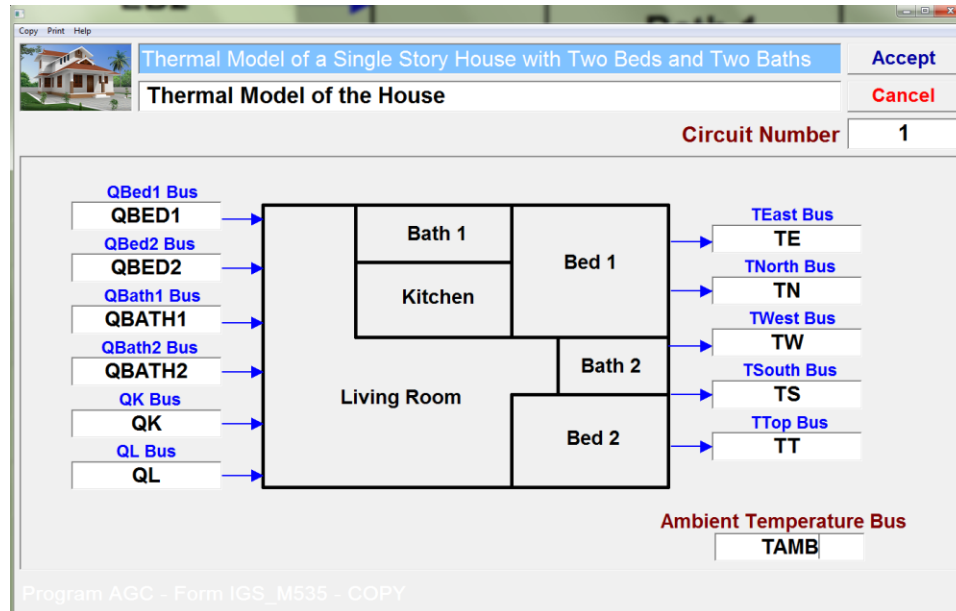


Figure 15. Thermal house model user interface in WinIGS program.

#### 5.5.1.1 Definition of the House Thermal Model Parameters

An approximately 1200 ft<sup>2</sup> single story house with two bedrooms and two bathrooms was considered. The house was simplified to have six main spaces as the following: two bedrooms, two bathrooms, kitchen, and living room. Extra spaces, such as closets and storages, were merged with their associated space. The thermal parameters of the house are defined as the following:

##### 1) *Temperature Spots Selection*

To monitor gradient temperatures of the thermal model of the house, several temperature spots were selected. Precisely, 17 temperature spots were selected. Location of each one of these temperature spots is illustrated in Figure 16. Specifically, every space was assigned two temperature spots; a main temperature spot and an internal wall temperature spot. To capture the temperature outside the house walls, every cardinal direction including the top direction of the house was assigned a temperature spot. The

reference temperature of the thermal model is the ambient temperature. The external temperature spots of the thermal model of the house (external temperature spots) were designed to have connections to an ambient temperature spot that is connected to a reference temperature model. The definition of each of the spot temperature is given next.

- **Bedroom One Spots (Bed1):**

$T_{Bed1}$ : Bedroom 1 temperature spot in [ $^{\circ}$ C].

$T_{Bed1-I}$ : Bedroom 1 internal wall temperature spot in [ $^{\circ}$ C].

- **Bedroom Two Spots (Bed2):**

$T_{Bed2}$ : Bedroom 2 temperature spot in [ $^{\circ}$ C].

$T_{Bed2-I}$ : Bedroom 2 internal wall temperature spot in [ $^{\circ}$ C].

- **Bathroom One Spots (Bath1):**

$T_{Bath1}$ : Bathroom 1 temperature spot in [ $^{\circ}$ C].

$T_{Bath1-I}$ : Bathroom 1 internal wall temperature spot in [ $^{\circ}$ C].

- **Bathroom Two Spots (Bath2):**

$T_{Bath2}$ : Bathroom 2 temperature spot in [ $^{\circ}$ C].

$T_{Bath2-I}$ : Bathroom 2 internal wall temperature spot in [ $^{\circ}$ C].

- **Kitchen Spots (K):**

$T_K$ : Kitchen temperature spot in [ $^{\circ}$ C].

$T_{K-I}$ : Kitchen internal wall temperature spot in [ $^{\circ}$ C].

- **Living Room Spots (L):**

$T_L$ : Living room temperature spot in [ $^{\circ}$ C].

$T_{L-I}$ : Living room internal wall temperature spot in [ $^{\circ}$ C].

- **House External Spots (L):**

$T_E$ : East temperature spot in [ $^{\circ}\text{C}$ ].

$T_N$ : North temperature spot in [ $^{\circ}\text{C}$ ].

$T_W$ : West temperature spot in [ $^{\circ}\text{C}$ ].

$T_S$ : South temperature spot in [ $^{\circ}\text{C}$ ].

$T_{Top}$ : Top of the house temperature spot in [ $^{\circ}\text{C}$ ].

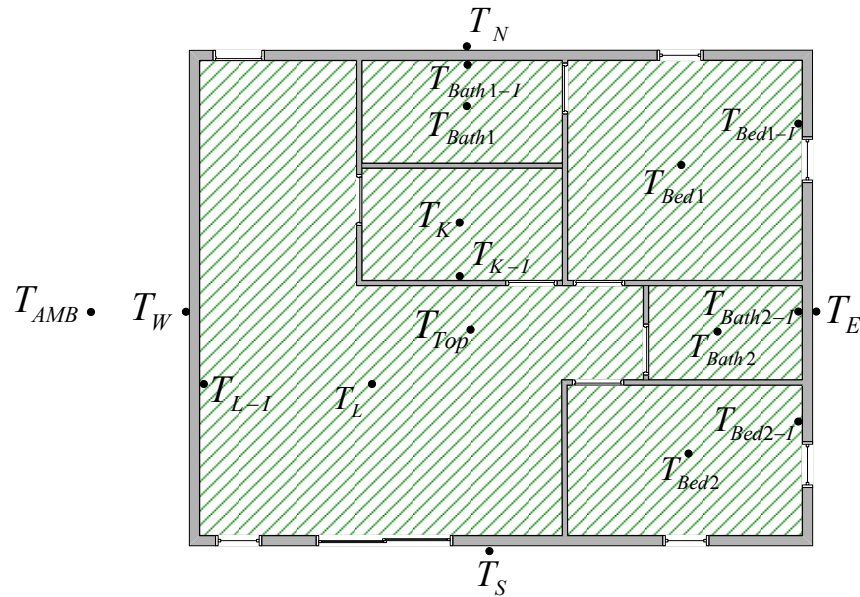
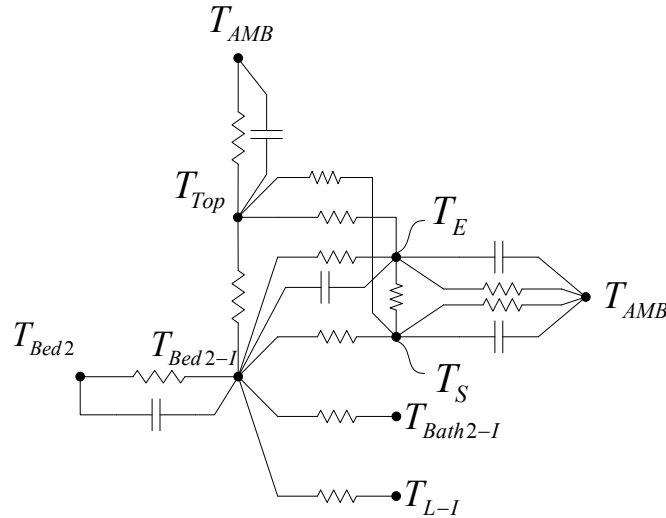


Figure 16. Thermal house model internal and external temperature spots locations.

## 2) Thermal Conductance:

For every temperature spot in the model, there is one or several thermal conductances were connected to it. In the thermal model, it was assumed that the main space spot has a thermal conductance connected to the internal wall temperature spot. The internal wall temperature spot was assumed to have thermal conductances with all its direct connected temperature spots such as external wall, top, and other spaces. Also, it was assumed that there was a thermal conductance between every internal temperature

spot and its direct neighboring temperature spots. To illustrate this, thermal RC circuit for bedroom<sub>2</sub> is shown in Figure 17. The same was also applied for other spaces.



**Figure 17. House bedroom<sub>2</sub> RC thermal circuit.**

Thermal conductance circuit parameters were computed considering the house rated temperatures as provided in Table 5. To estimate the model thermal conductances, steady state equations of the thermal model of the house with rated temperature were used. Because there is large number of thermal conductances in the model, each thermal conductance was represented by a percent of a main thermal conductance. As a result, the number of thermal conductances was reduced. Then, all other thermal conductances can be calculated using the assumed percentage provided in Appendix C.

**Table 5. House thermal model rated temperature at each temperature spot.**

Temperature Spot	Rated Temp [°C]
$T_{bed1}$	15
$T_{bed1-I}$	16
$T_{bed2}$	15

$T_{bed2-1}$	16
$T_{Bath1}$	17
$T_{Bath1-1}$	18
$T_{Bath2}$	17
$T_{Bath2-1}$	18
$T_K$	16
$T_{K-1}$	18
$T_L$	15.5
$T_{L-1}$	16.5
$T_E$	48
$T_N$	48
$T_W$	48
$T_S$	48
$T_{Top}$	48
$T_{AMB}$	50

### 3) Thermal Capacitance:

Connections of each thermal capacitance are provided in Table 6. The thermal capacity for every space in the house is computed considering the sum of every element heat capacity inside that particular space. For example, bedroom<sub>1</sub> thermal capacity is computed by

$$C_{Bed1} = C_{woodenBed} + C_{dresser} + C_{Glass} + \dots \quad (33)$$

Below is a summary of the assumed thermal capacitances:

$C_{Bed1}$ : The sum of the heat capacity of every element inside bedroom one in [Btu/°C].

$C_{Bed1\_I}$ : The heat capacity of the wall for bedroom one in [Btu/°C].

$C_{Bed2}$ : The sum of the heat capacity of every element inside bedroom two in [Btu/°C].

$C_{Bed2\_I}$ : The heat capacity of the wall for bedroom two in [Btu/°C].

$C_{Bath1}$ : The sum of the heat capacity of every element inside bathroom one in [Btu/°C].

$C_{Bath1\_I}$ : The heat capacity of the wall for bathroom one in [Btu/°C].

$C_{Bath2}$ : The sum of the heat capacity of every element inside bathroom two in [Btu/°C].

$C_{Bath2\_I}$ : The heat capacity of the wall for bathroom two in [Btu/°C].

$C_K$ : The sum of the heat capacity of every element inside the kitchen in [Btu/°C].

$C_{K\_I}$ : The heat capacity of the wall for kitchen in [Btu/°C].

$C_L$ : The sum of the heat capacity of every element inside the living room in [Btu/°C].

$C_{L\_I}$ : The heat capacity of the wall for living room in [Btu/°C].

$C_E$ : East side spot heat capacity in [Btu/°C].

$C_N$ : North side spot heat capacity in [Btu/°C].

$C_W$ : West side spot heat capacity in [Btu/°C].

$C_S$ : South side spot heat capacity in [Btu/°C].

$C_{Top}$ : Top side spot heat capacity in [Btu/°C].

**Table 6. Thermal house model thermal capacitance connections.**

Thermal Capacitance ( $C_{th}$ )	Spot 1	Spot 2
$C_{Bed1}$	$T_{bed1}$	$T_{bed1-I}$
$C_{Bed1-I}$	$T_{bed1-I}$	$T_E$
$C_{Bed2}$	$T_{bed2}$	$T_{bed2-I}$
$C_{Bed2-I}$	$T_{bed2-I}$	$T_S$
$C_{Bath1}$	$T_{Bath1}$	$T_{Bath1-I}$



$C_{Bath1-I}$	$T_{Bath1-I}$	$T_N$
$C_{Bath2}$	$T_{Bath2}$	$T_{Bath2-I}$
$C_{Bath2-I}$	$T_{Bath2-I}$	$T_E$
$C_K$	$T_K$	$T_{K-I}$
$C_{K-I}$	$T_{K-I}$	$T_{Top}$
$C_L$	$T_L$	$T_{L-I}$
$C_{L-I}$	$T_{L-I}$	$T_W$
$C_E$	$T_E$	$T_{AMB}$
$C_N$	$T_N$	$T_{AMB}$
$C_W$	$T_W$	$T_{AMB}$
$C_S$	$T_S$	$T_{AMB}$
$C_{Top}$	$T_{Top}$	$T_{AMB}$

### 5.5.1.2 Thermal House Mathematical Model

The thermal circuit of the house was assumed to have 44 thermal conductances, 17 heat capacities, and 6 heat sources. The first order differential equation given by (29) was used to derive the thermal model of the house. The model equations for the thermal house model are provided in a compact form in Appendix C. The house thermal model provides interfacing capabilities with models that inject thermal loads such as air conditioner and refrigerator. The air conditioner model is discussed next.

### 5.5.2 Electrothermal Air Conditioner Model

An electrothermal model of an air conditioner house load was developed. The model was assumed to inject heat (cooling) to the house through six output ducts. The

model window in WinIGS program is shown in Figure 18. Typical air conditioner load voltage is line to line with voltage ranges between 210-240 V.

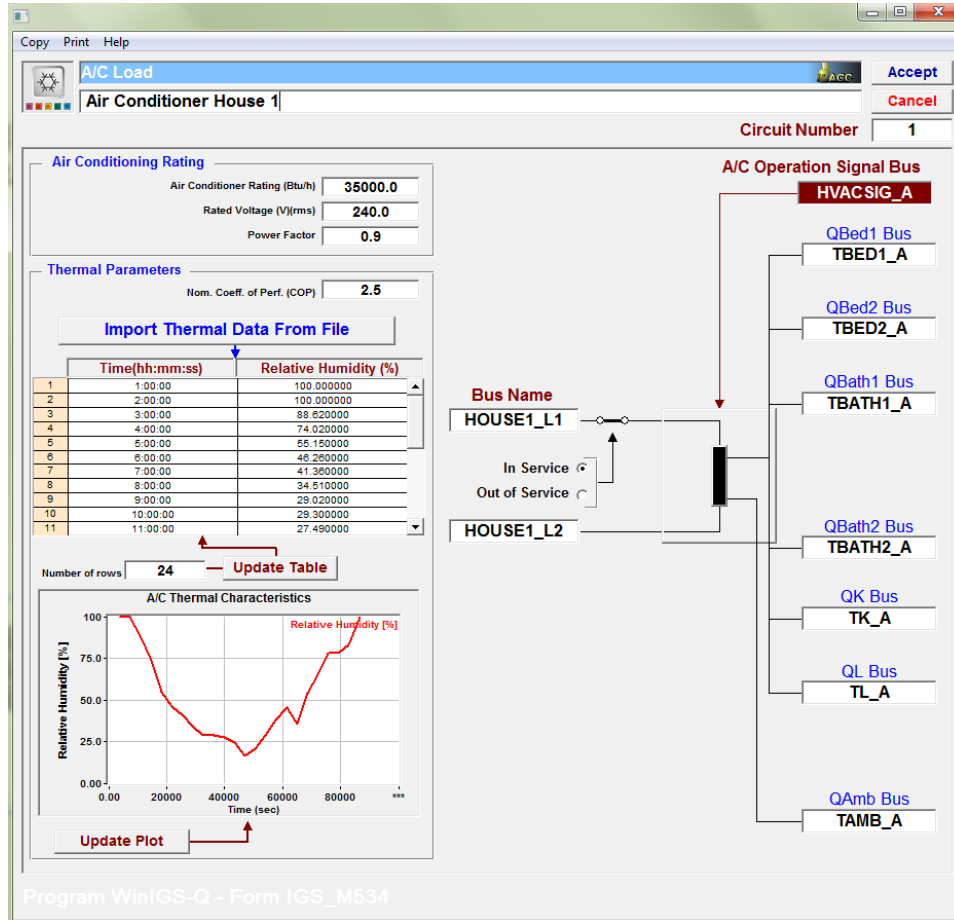


**Figure 18. Electrothermal air conditioner model user interface in WinIGS program**

Electrical and thermal circuits of the electrothermal air conditioner are illustrated by Figure 19. Output power, shown in the top part of Figure 19, is a function of actual air conditioner (BR) rating and coefficient of performance (COP).

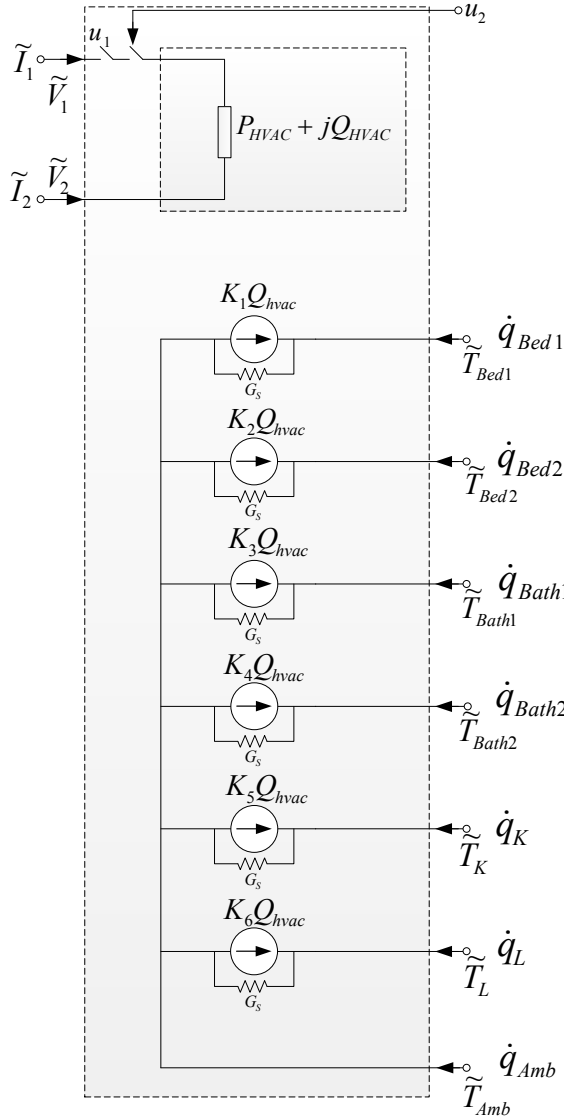


**Figure 19. Air conditioner electrical and thermal circuit model.**

As shown in Figure 19, the air conditioner model generates heat, denoted by  $\dot{Q}_{hvac}$ , and injects this heat to the house via six ducts. Each one of these ducts was designed to provide cooling according to specific amount of  $\dot{Q}_{hvac}$  as follows:  $k_1 = 22.5\%$ ,  $k_2 = 22.5\%$ ,  $k_3 = 7.5\%$ ,  $k_4 = 7.5\%$ ,  $k_5 = 15\%$ , and  $k_6 = 25\%$ .

The heat (cooling) generated by the air conditioner model is a function of nominal size of the air conditioner, ambient temperature, relative humidity, and COP. The model

was developed with a control signal terminal that sets to receive on/off control signal command ( $u_2$ ) from the thermostat control model to control the operation of the model. It should be noted that BR and COP were assumed to vary over time based on the ambient temperature. Typical BR and COP characteristics are illustrated in Figure 20. Basically, the air conditioner actual heat rating changes based on the ambient temperature. As the temperature drops, the actual heat rating increases. Similarly, the air conditioner COP improves when the temperature cools down as shown in bottom part of Figure 20. The mathematical model of the electrothermal air conditioner is provided in Appendix D.

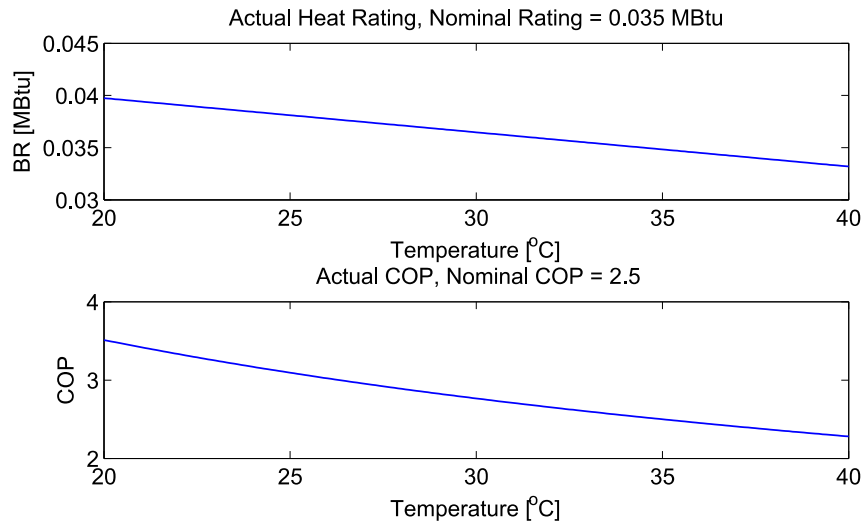


**Figure 20. Top: Air conditioner actual heat rating (BR), Bottom: Coefficient of performance (COP)**

### 5.5.3 *Electrothermal Refrigerator Model*

The second appliance that injects heat to the house is the refrigerator. In this section, a physically based electrothermal model of a top-mounted refrigerator with two compartments, fresh food and freezer, is discussed. The model was connected to the kitchen main temperature spot, assuming that the refrigerator is in the kitchen inside the house. However, the refrigerator can be placed in a different location. Typical voltage

connection is line to neutral with voltage ranges approximately from 110 V to 140 V. The refrigerator model interface window in WinIGS program is illustrated in Figure 21. The mathematical equations of the model are provided in a compact form in Appendix E. Details about the model are provided in the following sections.

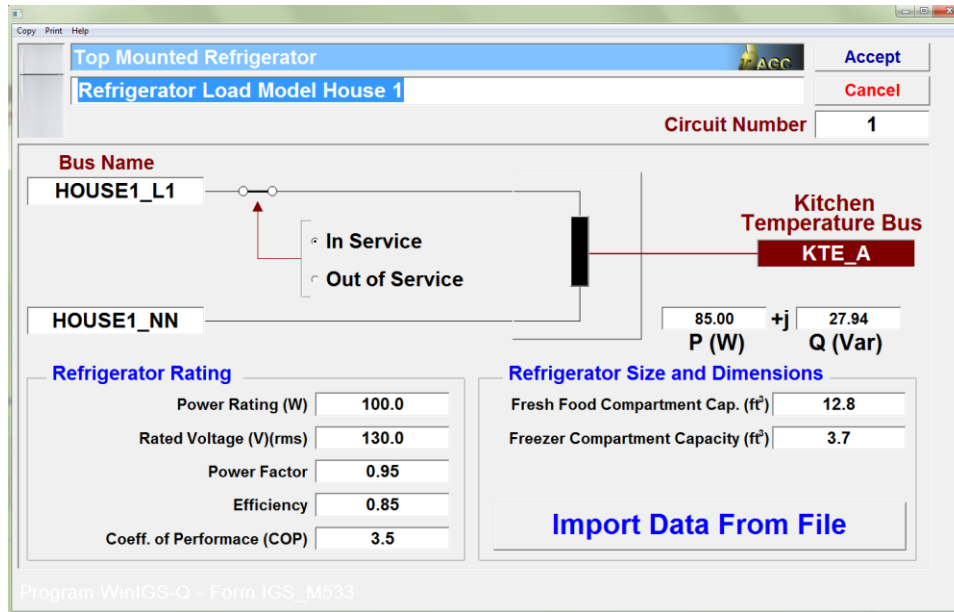


Figure 21. Electrothermal refrigerator model user interface in WinIGS program

### 5.5.3.1 Refrigerator Electrical Model

The electrical load is computed according to the refrigerator specified rated power, approximated efficiency, and coefficient of performance (COP). This information can be found on the manufacturer datasheet. The electrical circuit model of the refrigerator is illustrated in Figure 22.

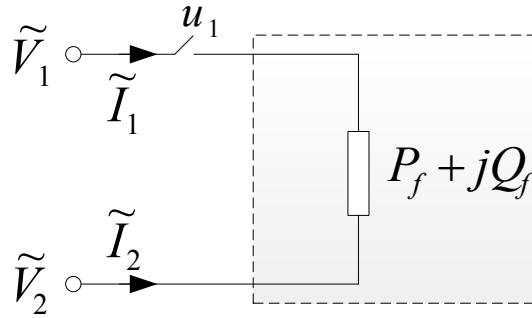


Figure 22. Electrical circuit model of the refrigerator

### 5.5.3.1 Refrigerator Thermal Model

The electrothermal model of the refrigerator provides an estimation of all temperature spots in the refrigerator. The thermal parameters of the refrigerator are defined as the following:

#### 5.5.3.1.1 Refrigerator Thermal Parameters

##### 1) *Temperature Spots:*

To monitor gradient temperatures of the refrigerator model, seven temperature spots were selected. Figure 23 shows the location of each one of these temperature spots. Specifically, the fresh food compartment of the refrigerator was assigned a spot; and the freezer compartment was also assigned a spot. Due to the temperature difference between the internal and external wall of each one of the compartments, two temperature spots were selected for each of the internal and external walls. These selected temperature spots are listed as the following,

$T_{ff}$ : Fresh food compartment main temperature spot in [ $^{\circ}\text{C}$ ].

$T_{friw}$ : Fresh food compartment internal wall temperature spot in [ $^{\circ}\text{C}$ ].

$T_{frew}$ : Fresh food compartment external wall temperature spot in [ $^{\circ}\text{C}$ ].

$T_{fz}$ : Freezer compartment temperature spot in [ $^{\circ}\text{C}$ ].

$T_{fziw}$ : Freezer compartment internal wall temperature spot in [ $^{\circ}\text{C}$ ].

$T_{fzew}$ : Freezer compartment external wall temperature spot in [ $^{\circ}\text{C}$ ].

$T_k$ : Kitchen temperature spot in [ $^{\circ}\text{C}$ ].

## 2) **Thermal Conductance:**

It was assumed that for every temperature spot in the refrigerator, there one or several thermal conductances were connected to it. Below is a summary of the assumed thermal conductances,

$G_{ff}$ : Thermal conductance between the fresh food compartment mass and the fresh food compartment internal wall in [ $\text{Btu}/^{\circ}\text{C h}$ ].

$G_{fz}$ : Thermal conductance between the freezer compartment mass and the freezer compartment internal wall in [ $\text{Btu}/^{\circ}\text{C h}$ ].

$G_{fziw-fziw}$ : Thermal conductance between the fresh food compartment internal wall and the freezer compartment internal wall mass in [ $\text{Btu}/^{\circ}\text{C h}$ ].

$G_{fziw-frew}$ : Thermal conductance of the fresh food compartment wall in [ $\text{Btu}/^{\circ}\text{C h}$ ].

$G_{fziw-fzew}$ : Thermal conductance of the freezer compartment wall in [ $\text{Btu}/^{\circ}\text{C h}$ ].

$G_{frew-fzew}$ : Thermal conductance of the fresh food and freezer compartments external walls in [ $\text{Btu}/^{\circ}\text{C h}$ ].

$G_{frew-K}$ : Thermal conductance between the fresh food compartment external wall and the Kitchen air mass in [ $\text{Btu}/^{\circ}\text{C h}$ ].

$G_{fzew-K}$ : Thermal conductance between the freezer compartment external wall and the Kitchen air mass in [Btu/°C h].

### **3) Thermal Capacity:**

It was assumed that there is a thermal capacitance associates with each one of fresh food compartment and freezer compartment. The thermal capacitance is connected between the corresponding spot and a specific reference as provided in Table 7. Below is a summary of the assumed thermal capacitances,

$C_{fr}$ : The sum of the heat capacity of every element inside the fresh food compartment in [Btu/°C].

$C_{friw}$ : Heat capacity of internal door mass in the fresh food compartment in [Btu/°C].

$C_{frew}$ : Heat capacity of external door mass in the fresh food compartment in [Btu/°C].

$C_{fz}$ : The sum of the heat capacity of every element inside the freezer compartment in [Btu/°C]

$C_{fziw}$ : Heat capacity of internal door mass in the freezer compartment in [Btu/°C].

$C_{fzew}$ : Heat capacity of external door mass in the freezer compartment in [Btu/°C].

### **4) Heat Sources:**

There is one main heat source  $\dot{Q}_r$  provides cooling to both the fresh food and freezer compartments as shown in Figure 23. Injected heat to the fresh food compartment was assumed to be ( $k_1 = 60\%$ ) of the total generated heat by the main heat source. Also, injected heat to the freezer compartment was assumed to the rest, ( $k_2 = 40\%$ ), of the total generated heat by the main heat source of the refrigerator.



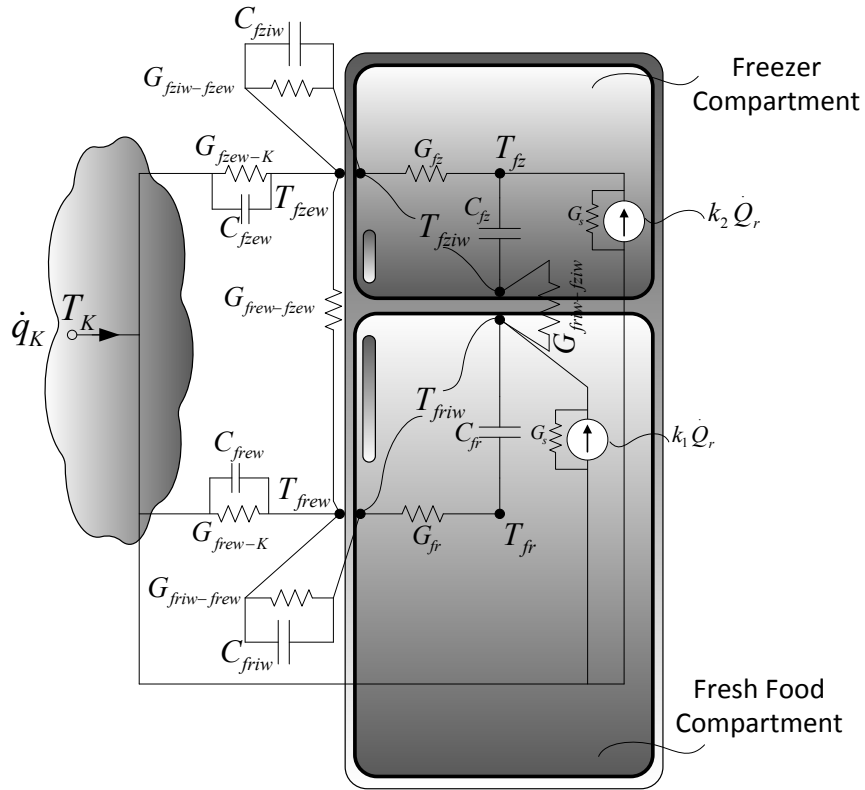


Figure 23. Refrigerator thermal circuit elements and temperature spots locations

Table 7. Electrothermal refrigerator thermal capacitance connections

Thermal Capacitance ( $C_{th}$ )	Spot 1	Spot 2
$C_{fr}$	$T_{fr}$	$T_{friw}$
$C_{friw}$	$T_{friw}$	$T_{frew}$
$C_{frew}$	$T_{frew}$	$T_{K1r}$
$C_{fz}$	$T_{fz}$	$T_{fziw}$
$C_{fziw}$	$T_{fziw}$	$T_{fzew}$
$C_{fzew}$	$T_{fzew}$	$T_{K1r}$

5.5.3.1.2 Computation of Thermal Quantities

Methods used to compute the refrigerator model thermal capacitance and thermal conductance are presented as follows:

**1. Thermal Capacitance ( $C_{th}$ )**

The compartment main thermal capacity was computed considering the sum of each element heat capacity inside that compartment (34), including cool air, various types of vegetables, fruits, meats, dairy products, candy, nuts, fluid... etc. In total, there are 94 elements considered in each one of the refrigerator compartments.

$$C_{fr} = C_{fr0} + C_{fr1} + \dots + C_{fri} , \quad (34)$$

The heat capacity of every element inside the compartment, fresh food or freezer, is a function of element mass and specific heat (35). Data regarding every element mass and specific heat can be found in reference books such as [112, 113].

$$C_{th} = m C_p, \quad (35)$$

where  $m$  is the mass of the element in [kg] and  $C_p$  is the element specific heat in [Btu/kg. °C].

When all heat capacities are computed, their volumes can be then calculated by

$$Vol = m/\rho, \quad (36)$$

where  $Vol$  is the volume of the element in [m<sup>3</sup>] and  $\rho$  is the mass density of the element [kg/m<sup>3</sup>].

**Air Heat Capacity**

Air is assumed to fill the volume of the refrigerator less the sum of the elements volumes. To compute air heat capacity, the following equation is used

$$C_{th} = Vol \rho C_p. \quad (37)$$

### **Door Opening and Mass Change**

There are two other factors that were assumed to impact the compartment thermal capacity, when the compartment's door is opened and when the mass inside the compartment is experienced some changes. In case of door opening, the duration of time while the door is opened is assumed to be enough for the entire cold air to escape and get replaced with air that has the kitchen temperature. In addition, the volume that was occupied by cold air is the same as kitchen temperature air, unless if there is an internal mass change. To account for that, the temperature inside the compartment is reinitialized. For example, if the fresh food compartment door is opened, the new initialized temperature value is computed using the following equation

$$T_{fr}^{new} - T_{friw} = \frac{C_{fr}(T_{fr} - T_{friw}) + C_{fr-door}(T_K - T_{friw})}{C_{fr} + C_{fr-door}}, \quad (38)$$

where  $C_{fr-door}$  is the heat capacity of the air mass with kitchen temperature.

In case of the compartment mass changes, thermal capacities for elements that experience mass change become different and should be recomputed. For example, if the water mass is increased by 5% in the fresh food compartment, the heat capacity of water has to change. The extra mass is assumed to have a kitchen temperature. As a result, the temperature at the main spot inside the compartment has to be reinitialized and the sum of the all elements heat capacities,  $C_{fr}$ , should be updated. The new initialized temperature value is computed as the following

$$T_{fr}^{new} - T_{friw} = \frac{C_{fr}(T_{fr} - T_{friw}) + \Delta C_{fr1}(T_K - T_{friw})}{C_{fr} + \Delta C_{fr1}}, \quad (39)$$

where  $\Delta C_{fr1}$  is the thermal capacity due to the extra mass element change.

Note that these changes are incorporated in the model in real-time. Although equations (34),(38), and (39) are expressed for fresh food compartment, these equations were also implemented for freezer compartment with related values.

## 2. Thermal Conductance ( $G_{th}$ ):

Thermal conductance parameters were computed considering the refrigerator rated data including rated temperatures as provided in Table 8. Also, it was assumed that the thermal conductance between internal walls of the compartments is 0.02 of the freezer door thermal conductance. In addition, the thermal conductance between the compartments external walls was assumed to be 100 times the thermal conductance between kitchen air mass temperature and fresh food compartment external temperature. To compute these conductances, steady state equations of the model that is given by (E.1)-(E.11) were used.

**Table 8. Rated temperature at each temperature spot (°C).**

Temperature Spot	Rated Temperature [°C]
$T_{fr}$	2.0
$T_{friw}$	5.0
$T_{frew}$	28.0
$T_{fz}$	-5.0
$T_{fziw}$	0.0
$T_{fzew}$	28

$T_{KI}$	33.0
----------	------

#### 5.5.4 Dishwasher Model

A dishwasher load is mathematically modeled as a constant active and reactive power. Based on the dishwasher efficiency and rated power, the output power is computed. Typical model connection is line to neutral. Also, typical voltage is 110-140 V. Figure 24 shows the dishwasher model interface window in WinIGS program. There are two factors were assumed to impact dishwasher power consumption: load level inside the dishwasher and dishwasher power profile for every cycle. The model equations of the dishwasher are provided in a compact form in Appendix F.

##### 5.5.4.1 Dishwasher Load Level

Three different load levels were assumed to represent the dishwasher internal loading. These are high, medium, and light, which corresponds to 100%, 75%, and 50% of the dishwasher power profile. These three load levels are summarized in Table 9. It should be noted that when the load level is set for a particular operation, the load for that operation cycles are fixed and cannot be changed until the end of the operation.

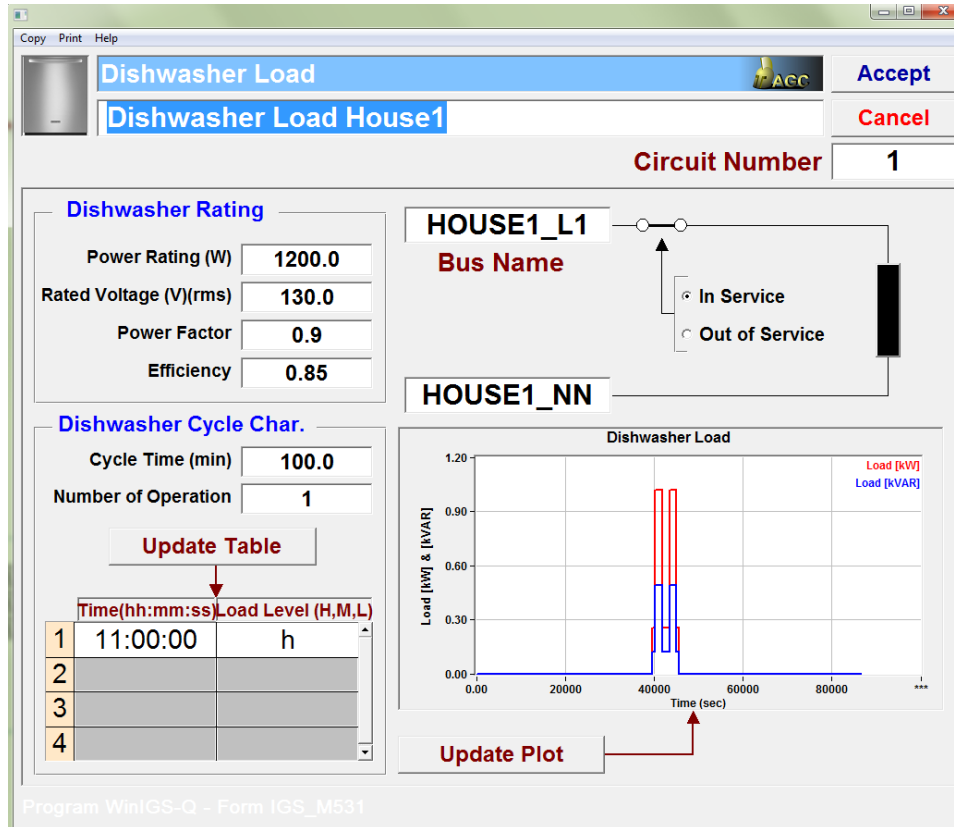


Figure 24. Smart dishwasher model user interface in WinIGS program.

Table 9. Dishwasher load levels.

Load	Load Level in % of the Dishwasher Power Profile
High	100
Medium	75
Light	50

#### 5.5.4.2 Dishwasher Power Profile

The dishwasher operation can be modeled assuming different power profiles [114, 115]. Fixed power over the operation cycle profile is also widely used. To reflect more realistic energy consumption, a detailed power profile was considered. For every dishwasher operation, it was assumed that there are five different cycles as the following:

pre-wash, main wash, rinse, rinse and heat, and drying cycles. The duration of time for every cycle varies depending on the dishwasher. However, the overall duration of time for one dishwasher operation is usually ranged between 60 - 200 minutes. Brief technical explanation of each one of these stages is provided next:

**1. Pre-wash:**

In the pre-wash cycle, water is pumped and sprayed to loosen particles stuck on dishes, utensils, pans, and other stuff inside the dishwasher. Water sprayed is not heated up and usually regular in temperature. The water is then pumped out to prepare the dishwasher for the next cycle.

**2. Main wash:**

After the pre-wash cycle, fresh water is sprayed and mixed with the detergent. The water used in this cycle is heated up to become 125 - 140 °F (50 – 70 °C). When the cycle is over, the water is pumped out.

**3. Rinse:**

With a cold water, the inside dishwasher is sprayed to clean the residuals from the previous cycle.

**4. Rinse and heat:**

In this stage, water is sprayed again. Rinse aid soap could be mixed with sprayed water. Water temperature is increased up to about 140 °F (70 °C). By the end of the cycle, hot water is pumped out.

**5. Dry:**

After pumping all the water in the previous cycle, a heating element positioned on the bottom of the dishwasher is used to provide more heat and dry the left of water and kills bacteria.

The power profile and time duration for every cycle are presented in Figure 25.

The y-axis is in percentage of the dishwasher rated power.

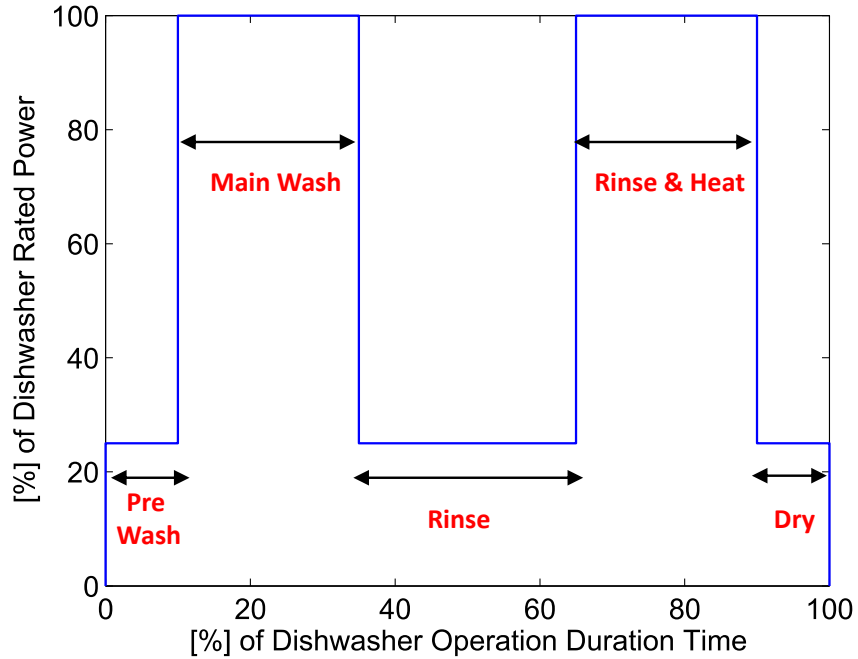


Figure 25. Dishwasher power profile.

### 5.5.5 Variable Load Model

To account for other house appliances, such as washer, dryer, and water heater, a time varying load was developed. The variable load is modeled mathematically as a specified constant active and reactive power for every time period. The model can also adopt different voltage ratings. Figure 26 illustrates the variable load model window in the program in WinIGS program. The basic electrical circuit is illustrated in Figure 27. The mathematical model in a compact form is provided in Appendix G.



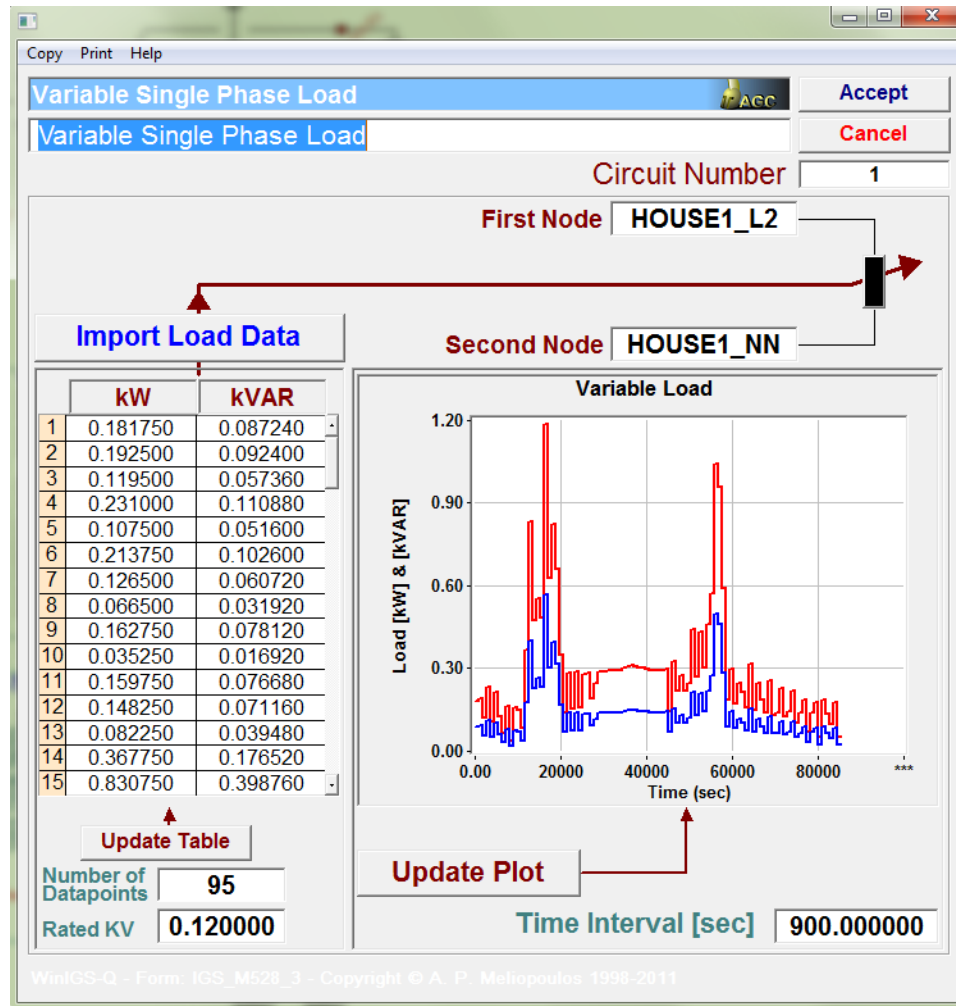


Figure 26. Variable load model user interface in WinIGS program.

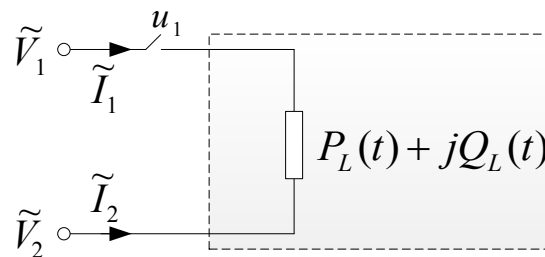


Figure 27. Electric circuit of the variable load model.

### 5.5.6 Roof-Top Solar Photovoltaic (PV) Model

A physically based model of a PV array with solar cell (single diode) was developed. The solar cell model is based on [116]. The model is dependent on the environment conditions, i.e. temperature and solar irradiance. Figure 28 shows the equivalent electrical circuit of a single diode solar cell. The mathematical model of the PV solar cell is provided in a compact form in Appendix H.

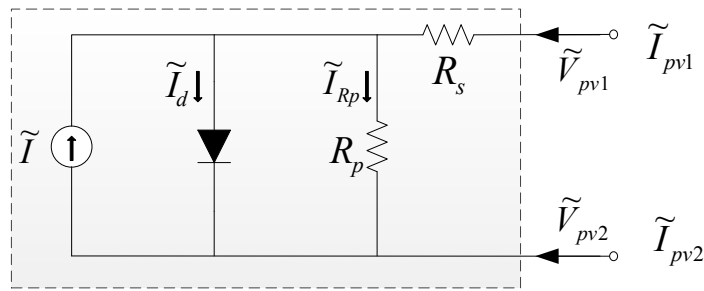


Figure 28. Equivalent electrical circuit of the solar cell.

Data regarding solar array characteristics are usually provided by the solar manufacturer except series and parallel resistances. To compute them, an algorithm was used to find the optimized values of the both resistances that is based on [116].

### 5.5.7 Electrothermal Model of a Battery Energy Storage System (BESS)

Battery based, energy storage system was modeled as part of the smart house energy management system. There are several types of battery technologies that could be used for energy storage. However, the mostly and widely used type for solar PV and house application is lead acid battery technology because it is economically attractive, easily maintained, and can last for a long time. Several dynamic models of a lead acid battery are already developed and exist in the literature. The mathematical model of lead

acid battery was extracted from [117-119]. Then, an electrothermal, third order, and physically based model was developed. The model accounts for the following:

- The model is dynamic and built mainly for lead acid batteries.
- Surrounding and internal battery temperature variation was considered.
- Internal gassing current was modeled.
- Battery self-discharging characteristic was neglected.

The battery circuit model is shown in Figure 29. Figure 30 illustrates the battery of lead acid type model window in the program in WinIGS program. Two switches were considered to control the operation of the model. The first switch is to determine the status of the battery, standby or connected. And the second switch is used to govern the battery's mode of operation, charging or discharging. The mathematical model in a compact form for every mode of operation is provided in Appendix I.

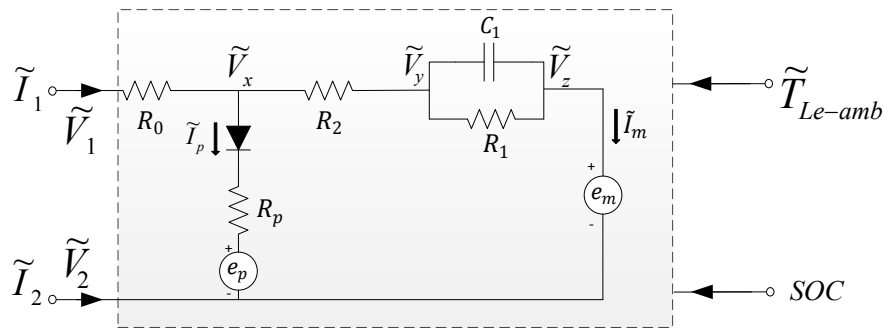


**Figure 29. Circuit model of lead acid battery.**

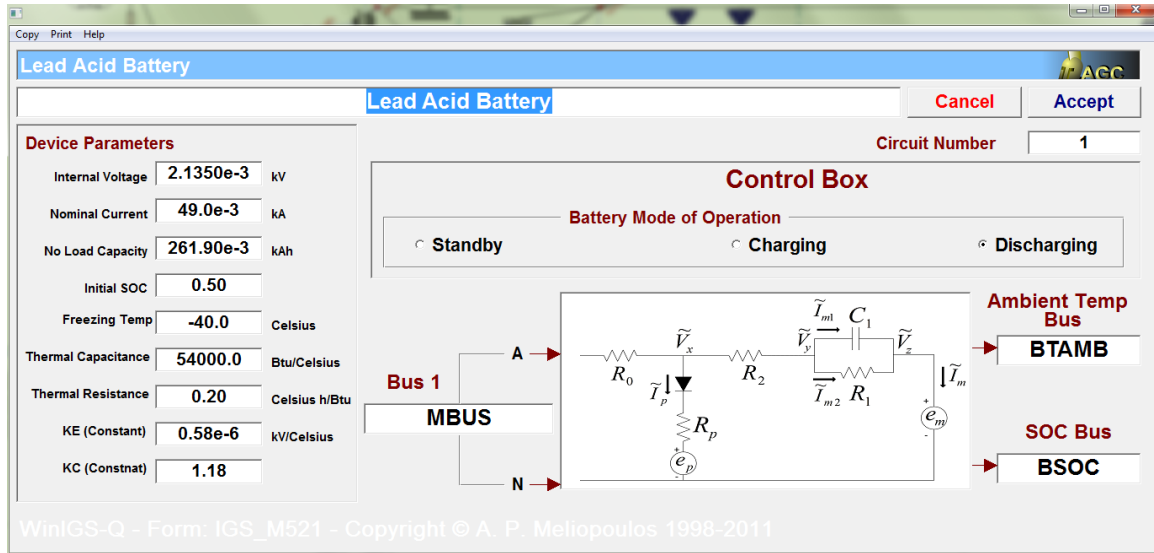


Figure 30. Lead acid battery model user interface window in the program.

### 5.5.8 Electric Vehicle (EV) Model

A physically based electrothermal model of EV battery was developed. In particular, the EV is modeled as lithium ion battery with appropriate size [120]. The model accounts for the following,

- The model is in the quasi-dynamic domain and was developed to model mainly lithium ion batteries.
- Surrounding and internal battery temperature variation was considered.
- Battery self-discharging characteristic was neglected.

The circuit model of the lithium ion battery is shown in Figure 31. The lithium ion battery model window in the program in WinIGS program is illustrated in Figure 32. There is one control switch added to the mode to identify the status of the battery, standby or connected. The mathematical model of the electrothermal lithium ion battery cast in a compact form is provided in Appendix J.

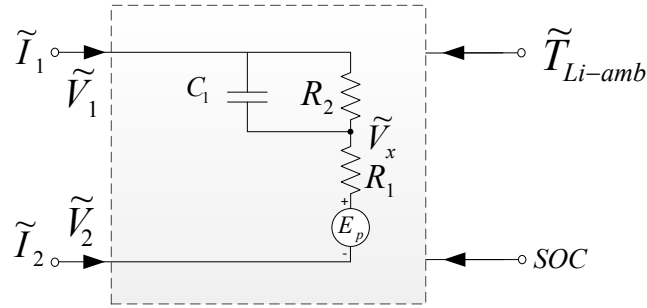


Figure 31. Circuit model of lithium ion battery.

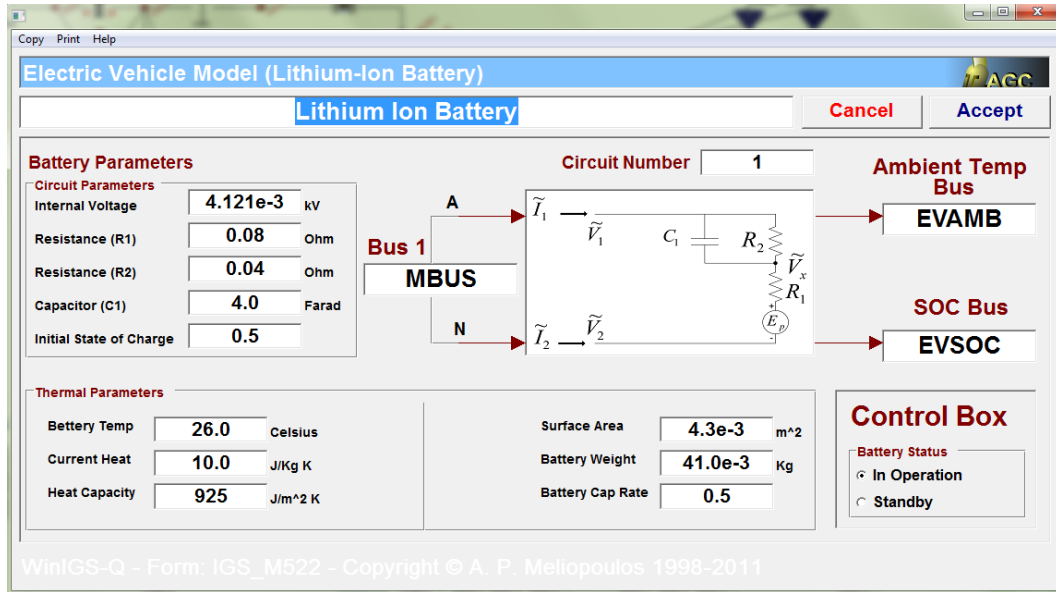


Figure 32. Lithium ion battery model user interface in WinIGS program.

### 5.5.9 Power Electronics Converters Models

The house system was contracted by power electronics converters. Averaged domain was adopted when converters were modeled. Next, discussion regarding every converter model considered in this research is provided.

#### 5.5.9.1 Single Phase Averaged DC-DC Boost Converter Model

Boost converters are used to regulate the input voltage, such as the house solar PV array voltage, which is an unregulated dc voltage. The output is a stepped up and

regulated dc voltage by the duty ratio,  $D$ . Typical switching frequency used is 60 kHz. The circuit diagram of the dc-dc boost is shown in Figure 33. The model was developed in WinIGS program and the window of the model is illustrated in Figure 34.

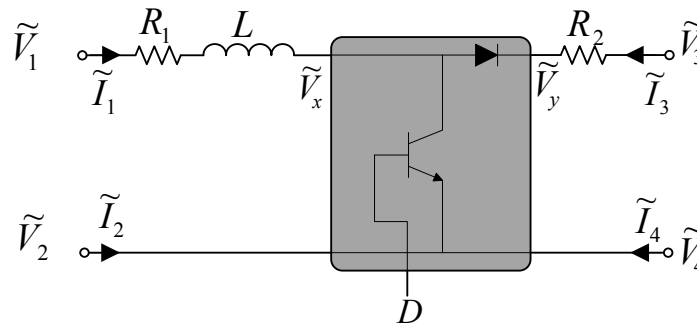


Figure 33. Equivalent circuit model of a single phase dc-dc boost converter.

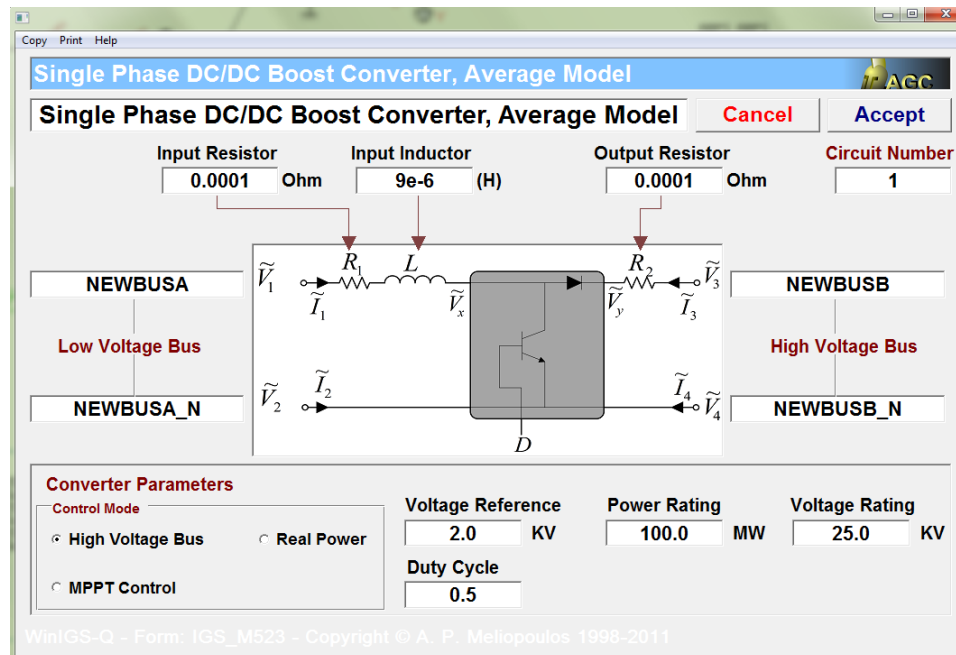
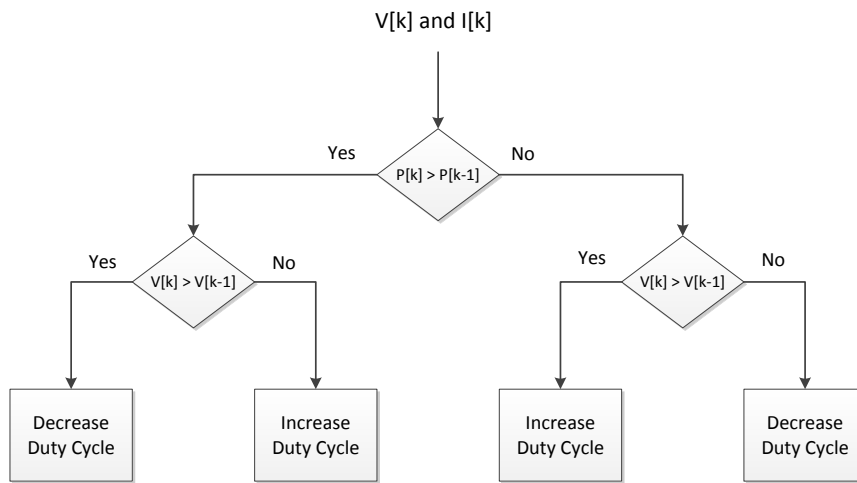


Figure 34. Average model of dc-dc boost converter user interface in WinIGS program.

The model was designed to work with three control schemes as the following:

- 1) **DC voltage control:** This control maintains a constant dc output voltage.
- 2) **Real power control:** This control maintains a constant real output power.

3) **Maximum power point tracking (MPPT) control:** This control was also developed to extract maximum power out of solar PV. This control basically regulates the converter duty cycle ( $D$ ) to maintain a constant dc output voltage. There are several MPPT algorithms such as perturb and observe (P&O), incremental conductance (IC), fuzzy logic, current sweep [121]. However, perturb and observe (P&O) algorithm was implemented. A schematic diagram of (P&O) is illustrated in Figure 35. The algorithm exploits the relation between the output power and the voltage of PV to determine whether increasing or decreasing the duty cycle. The compact model that describes the averaged single phase dc-dc boost converter in the frequency domain and with every control scheme is given in Appendix K.



**Figure 35. Perturb and observe (P&O) algorithm.**

### 5.5.9.2 Single Phase Full Bridge DC-AC Inverter Model

Inverters are used to convert input dc current or voltage to ac current or voltage waveform, which is controlled by the modulation index,  $M$ . The circuit diagram of a

single phase dc-ac inverter is shown in Figure 36. The model was developed in WinIGS program. The user interface window is shown in Figure 36.

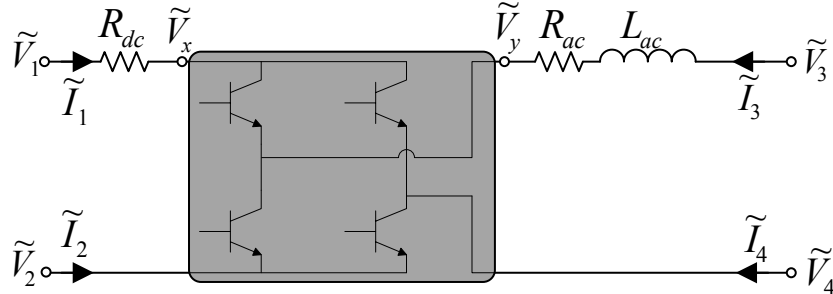


Figure 36. Equivalent circuit model of the single phase full bridge DC-AC inverter.

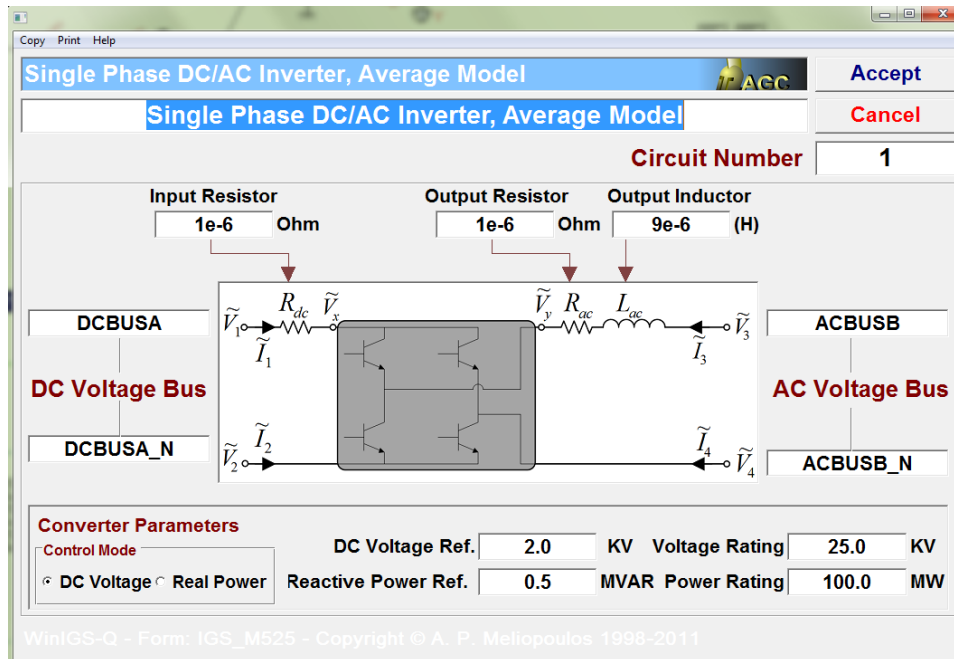


Figure 37. Average model of dc-ac inverter user interface in WinIGS program.

The model is equipped with two controls as the following:

- 1) **VQ Control**: This control maintains an input dc voltage equals to a dc reference voltage and constant reactive power equals to an imaginary power reference.



2) **PQ Control:** This control maintains a constant real and imaginary power equal to a specified real and imaginary power references.

The mathematical model with every control is provided in Appendix L.

### 5.5.9.3 Battery Charger Model

The battery charger was modeled as a single phase dc-dc buck-boost converter. These types of converters are used to step up or down the input dc voltage. Stepping up the input voltage can be achieved by using the boost converter. On the other hand, stepping down the input voltage can be done by using the buck converter. The output voltage is controlled by the duty ratio,  $D$ . The circuit diagram of the buck-boost converter is shown in Figure 38. The model was developed in WinIGS program and the window of the model is illustrated in Figure 39. One of the main functions of the battery charger is to monitor the state of charge (SOC) of the battery that it monitors and ensures that the charge inside the battery does not exceed the minimum and maximum charge limits, which are set by the user.

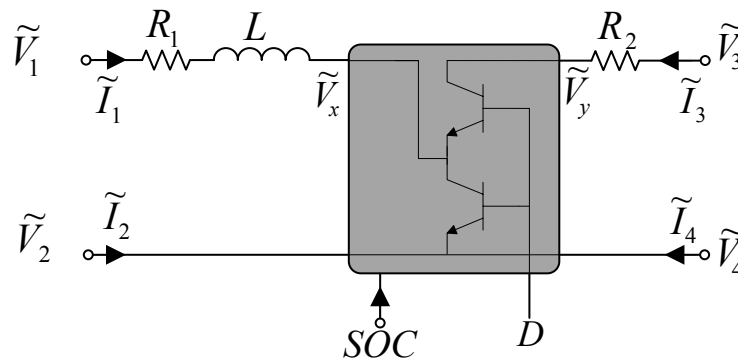


Figure 38. Equivalent circuit model of a single phase dc-dc buck-boost Converter.

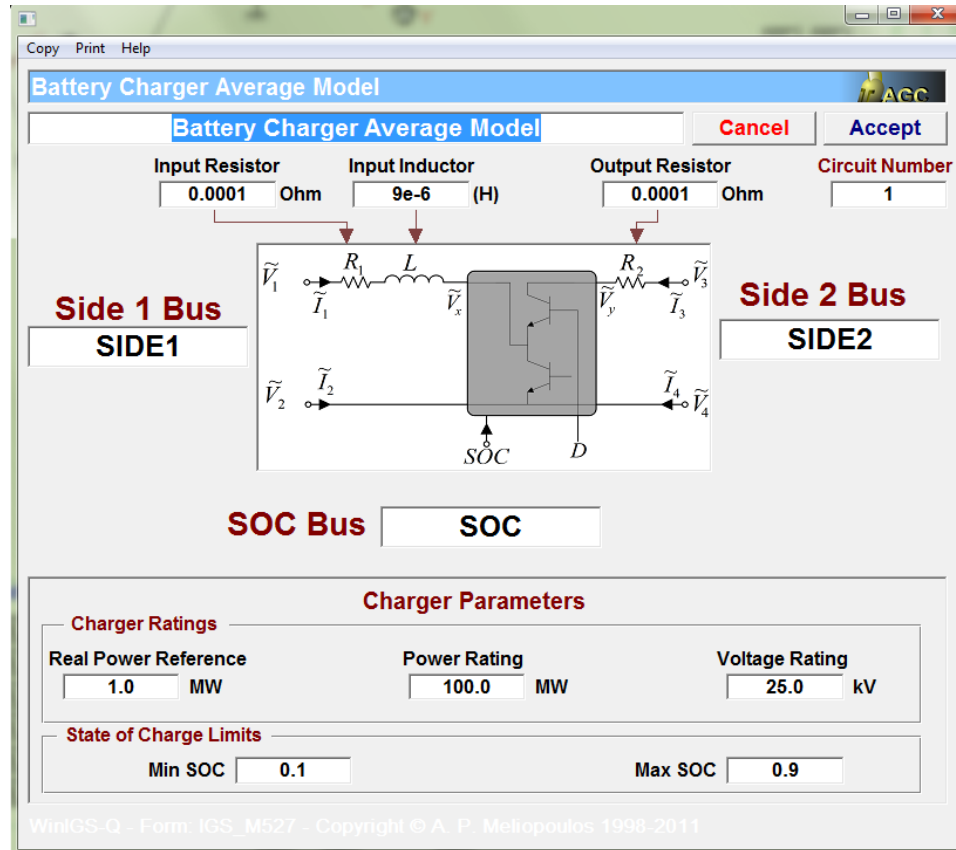


Figure 39. Battery charger dc-dc buck-boost user interface in WinIGS program.

The mathematical model of the buck-boost converter is provided in Appendix M.

The model is equipped with two different controls as the following:

- 1) **DC Voltage Control:** This control maintains an input dc voltage equals to dc reference voltage.
- 2) **Real Power Control:** This control maintains a constant real power equals to a specified real power reference.

#### 5.5.10 Miscellaneous Models

Other devices that are not part of the previous sections, such as reference temperature and thermostat controller, are discussed in this section.

### 5.5.10.1 Ambient Temperature Model

The electrothermal model of the house consists of several electrothermal devices such as the distribution transformer and air conditioner. These electrothermal devices need to be connected to a reference temperature, in most cases, it is the ambient temperature. The circuit model of the ambient temperature model is shown in Figure 40. The user interface window of this model in WinIGS program is illustrated in Figure 41.

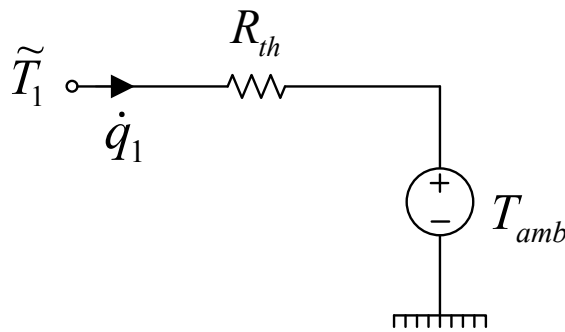


Figure 40. Equivalent thermal circuit diagram of ambient temperature.

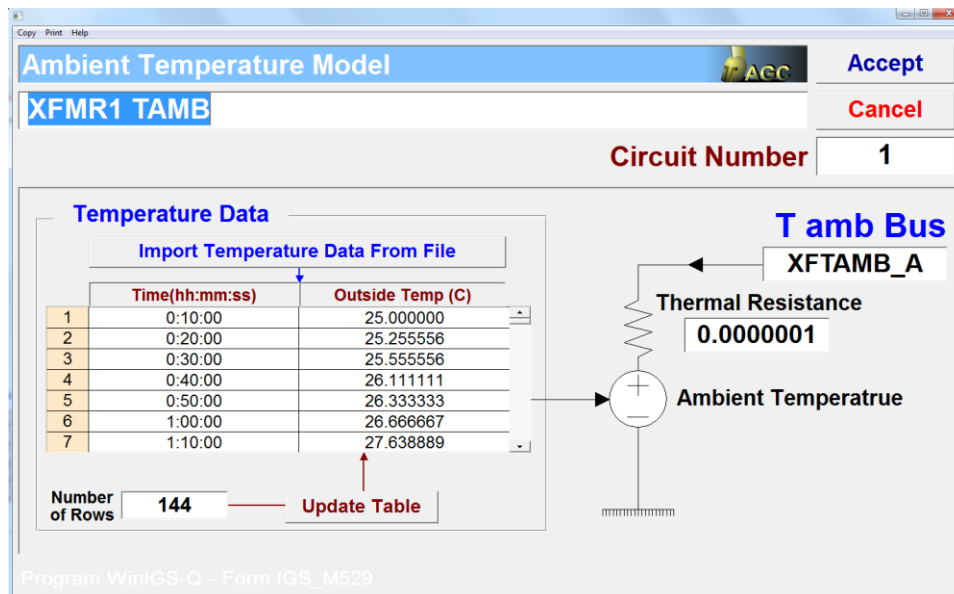


Figure 41. Ambient temperature model user interface in WinIGS program.

Most of electrothermal devices in the house are connected to several ambient temperature models. For example, external temperature spots of the distribution transformer (Case Spots) are connected ambient temperature model. Similarly, the external temperature spots of the thermal house model are connected to another ambient temperature model. Note that both ambient temperature models are not necessary having the same temperatures. For example, if the EV is inside a garage, where the temperature inside the garage is controlled, then the reference temperature of the EV is different than the reference temperature of the distribution transformer. The model equations in compact form are provided in Appendix N.

#### 5.5.10.2 Thermostat Controller

The thermostat controller monitors a temperature spot that is connected to it. It compares that temperature with the customer preference temperature setting. Based on the results, a control signal is sent to the air conditioner to turn it on or off. The model accepts several temperature settings at different times. The equivalent circuit diagram is illustrated in Figure 42. The user interface window in WinIGS program is shown in Figure 43. The model equations in the frequency domain are provided in Appendix O.

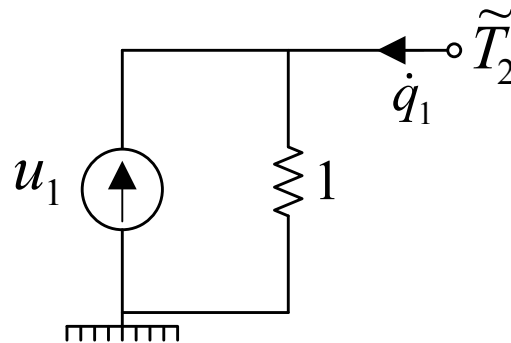


Figure 42. Equivalent circuit diagram of the thermostat.

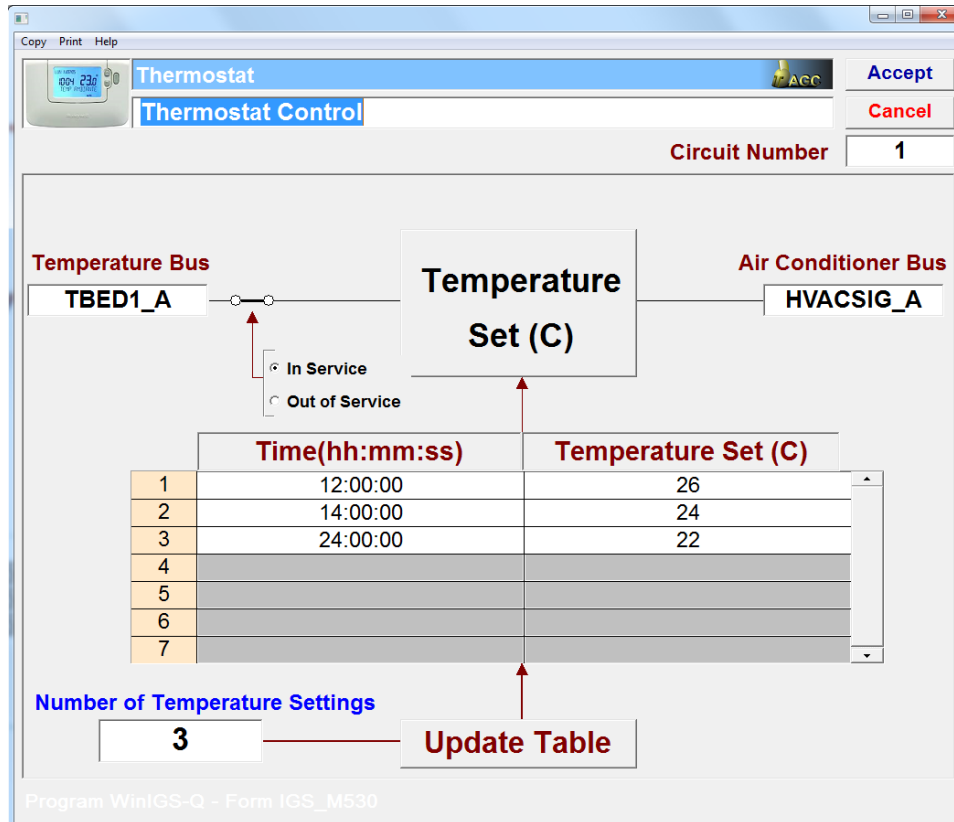


Figure 43. Thermostat user interface in WinIGS program.

## 5.6 Summary

To obtain accurate estimation of the house states, accurate models of house energy resources and appliances are important. The modeling methodology that was used to model distribution transformer and various house, energy resource, battery energy storages, and appliances is presented in this Chapter. A physically based and object oriented modeling approach was used to model various components of the electrothermal model of the house. A novel and detailed electrothermal model of a center-tap transformer was developed. The model is able to provide measurements for 21 temperature spots. Also, other electrothermal models of important DERs and appliances were presented.

A thermal model of a single story house with six rooms was developed. This model has the capability to be interfaced with appliances that inject thermal loads such as air conditioner and refrigerator. An electrothermal model of an air conditioner is assumed to provide the house with cooling only is presented in this Chapter. The air conditioner cools the house through six ducts; each one was connected to a room in the house. A detailed electrothermal model of a top-mounted refrigerator with two compartments was developed. The model is connected to the main kitchen temperature spot, assuming that the refrigerator is in the kitchen. Furthermore, a dishwasher with five cycles was developed. The power consumption of the dishwasher was assumed to be impacted by the level of internal loading of the dishwasher and the cycle power profile. The rest of the house appliances were modeled as time variable active and reactive power. Two types of batteries, lead-acid and lithium-ion, electrothermal models were developed. An average model of a battery charger is also presented. Required power electronics converters and necessary controls, such as thermostat controller and MPPT, were also developed. In the next Chapter, the third major component of the advanced house infrastructure that is the house distributed state estimation is discussed.

## 6 HOUSE DISTRIBUTED STATE ESTIMATION

### 6.1 Introduction

The next major component of the advanced house infrastructure is house DSE. Firstly, a general description regarding the house DSE is discussed. Additionally, various house DSE functions are explained. Secondly, the house DSE mathematical formulation is presented.

### 6.2 House DSE Description

A house DSE is discussed in this section. The house DSE is performed at the house level by utilizing local real-time measurements and data that are obtained from the house. These data are obtained by local metering devices that monitor the house, which are then sent to DSE. The house DSE is set to receive various measurements and fit the received data into an accurate model.

A general illustration of the house DSE is shown in Figure 44. House measurements are obtained by various metering devices at the house level. These measurements are compared with the house model values, which is obtained from the electrothermal model of the house. The outcome is the residual errors. To perform state estimation, a standard least squares algorithm is used. This algorithm is used to minimize the sum of the errors squared and provide the best estimate of the house external and internal states. If the results of the estimation process are not satisfactory, this might be an indication of the presence of bad data. Statistical hypothesis testing methods can be used, which are based on the chi-square test, to check the presence of bad data. If bad

data are present, they can be identified based on their normalized residual values; and can be removed from the measurement set. This process is repeated as necessary. Otherwise, the best estimates of the house external and internal states are calculated and can be used as an input for numerous applications. In this research, the outcome of house state estimation is utilized by the smart house energy management system to provide optimization.

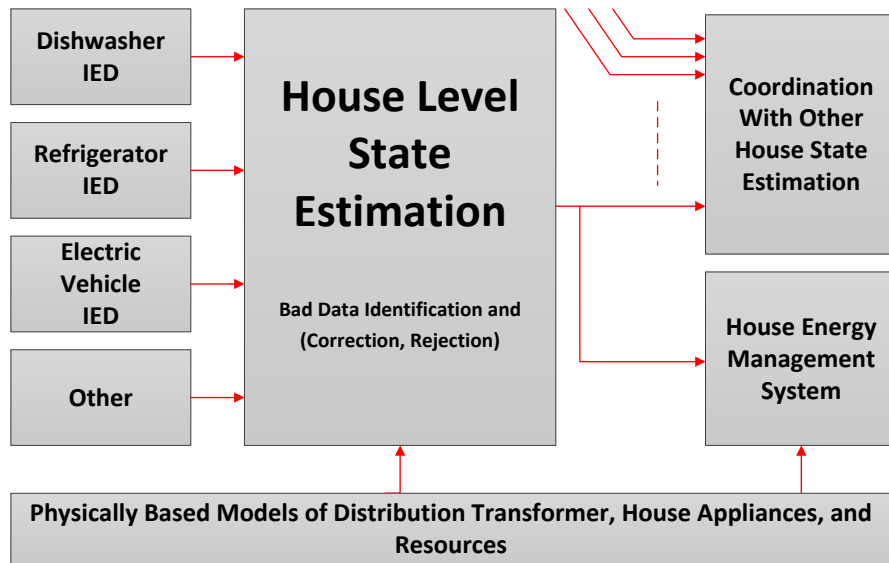


**Figure 44. A general functional description of the house level DSE.**

The scheme explained before results in monitoring the house in real-time [122-125]. The outcome of the house DSE are a collection of external and internal states of all components states that are connected to the house. External states include phasor voltages. On the other hand, internal states are algebraic or dynamic states which exist inside the device. Examples of internal states are various temperature spots inside the house and EV battery SOC. Measurements will also include the control variables of controllable devices such as dishwasher operation time and converter controllers. The mathematical formulation of the DSE is discussed in the next section.



### 6.3 House DSE Formulation

In this section, the formulation of the house DSE is provided. Mathematically, the house DSE consists of: Devices, State Set, Measurements Set, State Estimation Algorithm, Detection and Identification of Bad Data and Error Analysis. The process of the estimation is illustrated in Figure 45.

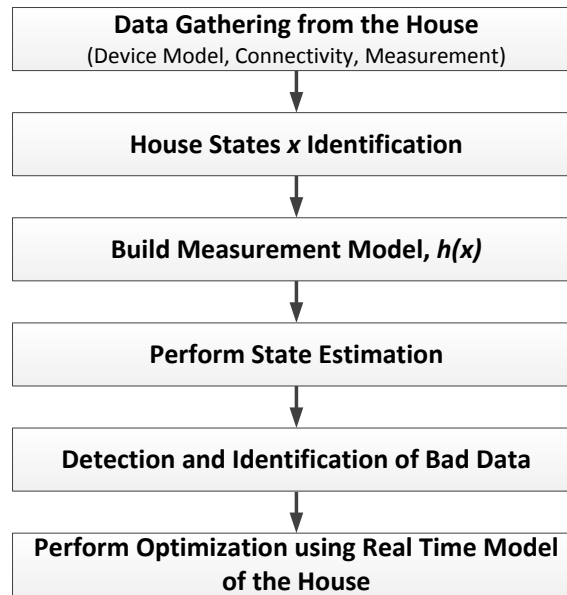


Figure 45. House state estimation procedure.

#### 1) Double Phase Device Model

Due to single phase loads, feeders, system imbalances, and asymmetries are common in the distribution circuits. To capture this, the house devices have to be modeled on a single phase using the physical model of each device.

#### 2) State Set

The state set is defined as the set of the voltage phasors of every node of the house that describes the operating conditions. For every node  $i$  of the house, the following electrical states can be defined as

$$\tilde{V}_i = [\tilde{V}_{i,L1} \quad \tilde{V}_{i,L2} \quad \tilde{V}_{i,NN}]^T. \quad (40)$$

### 3) Object Oriented Measurements

The measurements, synchronized or non-synchronized, are expressed as a linear and nonlinear functions in terms of the states of order at most quadratic. The object oriented generic form of the measurement is as follows

$$z_k = c_k + \sum_i a_{k,i} x_i + \sum_{i,j} b_{k,i,j} x_i x_j + \eta_k, \quad (41)$$

where  $z_k$  is the measured value,  $c_k$  is the constant term,  $a_{k,i}$  are the linear coefficients,  $b_{k,i}$  are the nonlinear coefficients, and  $\eta_k$  is the error term.

### 4) State Estimation Algorithm

The state estimation algorithm is solved using least square approach, where the objective is to estimate the states  $\mathbf{x}$ . Therefore, the problem is formulated as follows

$$\min J(x) = \eta^T W \eta, \quad (42)$$

where  $\eta = z - h(x)$ , and  $W$  is a diagonal matrix whose non-zero entries are equal to the inverse of the variance of the measurement errors given by

$$W = \text{diag} \left[ \frac{1}{\sigma_v^2} \right]. \quad (43)$$

Then, the below iterative algorithm is used to obtain the best estimate of the house states

$$\hat{x}^{j+1} = \hat{x}^j + (H^T W H)^{-1} H^T W (z_a - h(\hat{x}^j)), \quad (44)$$

where  $\hat{x}$  refers to the best estimate of the state vector and  $H$  is the Jacobian matrix of the measurement equations. At each time step of the estimation, the contributions of each measurement to the information matrix  $H^T W H$  and the vector  $H^T W (h(x^y) - z)$  must be computed.

### 5) State Estimation Accuracy Quantification

Chi-square test is used to quantify the accuracy of the estimator and the estimation confidence. Given the number of measurements  $m$  and the number of states  $n$ , the degrees of freedom can be calculated as  $v=m-n$ . Calculating the value  $\zeta$  of the objective function, the estimation confidence level is given by the probability

$$Pr[\chi^2 \geq \zeta] = 1.0 - Pr[\chi^2 \leq \zeta] = 1.0 - Pr(\zeta, v). \quad (45)$$

For an acceptable confidence level, the accuracy of the solution is computed via the covariance matrix as follows

$$C_x = E[(\hat{x} - \bar{x})(\hat{x} - \bar{x})^T], \quad (46)$$

where  $\bar{x}$  denotes the true state value and  $\hat{x}$  the estimated value, and computed as

$$C_x = (H^T W H)^{-1}. \quad (47)$$

Once the information matrix of the solution has been computed, the standard deviation of a component of the solution vector is given by

$$\sigma_{x_i} = \sqrt{C_x(i, i)}, \quad (48)$$

where  $C_x(i, i)$  is the  $i^{th}$  diagonal entry of the  $C_x$ .

The estimates of the measurements can also be computed as

$$\hat{b} = h(\hat{x}, \hat{y}), \quad (49)$$

which covariance matrix is proved to be,

$$Cov(\hat{b}) = H(H^T W H)^{-1} H^T. \quad (50)$$

In the end, the house DSE provides real-time model of the house. The estimated states of the house model are used to do optimization.

## 6.4 Summary

In this Chapter, the house DSE is discussed. A general description of the house state estimation is also provided. A house state estimation is set to perform estimation on data and measurements that are gathered by metering devices at the house. The estimator uses a least squares algorithm to perform house state estimation. Further, the mathematical model of the house DSE is formulated and presented. The formulation includes device modeling, state set, measurements object orientation, numerical solution, and bad data identification. The outcome of the estimation is a real-time model of the house that is set to be used by the smart house energy management system to perform optimization.

## 7 OPTIMIZATION PROBLEM SOLUTION METHOD

### 7.1 Introduction

Due to the quadratization process that was implemented when modeling distribution transformer, house DERs, and appliances, the electrothermal model of the house is a large set of quadratic equality and inequality constraints. Therefore, the house optimization model is a Mixed Integer Quadratically Constrained Programming (MIQCP) problem. In this Chapter, piecewise linear approximation technique is discussed. This technique was used to approximate the quadratic terms in the optimization model. To provide optimal control variables that yield optimal house states trajectory, model predictive control was utilized. This advanced control is explained in this Chapter.

### 7.2 Piecewise Linear Formulations

To solve the optimization problem, PLA techniques are used to linearize quadratic functions that exist in the optimization model [126, 127]. It should be noted that PLA applies on separable functions. Some examples of separable functions are

$$f_1(x) + f_2(y) + f_3(z) = x^2 + \frac{1}{y} - 2z + z^2. \quad (51)$$

Also, the following examples are non-separable functions

$$f_1(x) + f_2(x, y) = x^2 + xy + 2y. \quad (52)$$

#### 7.2.1 $\lambda$ -Formulation

There are several techniques of linear approximation; one of these techniques is  $\lambda$ -formulation [126]. To illustrate this method, a simple example is considered. Consider a

simple function with only one quadratic term to be approximated. This function is given by

$$f(x) = x^2, \quad (53)$$

and  $x$  is a continuous variable bounded by

$$0 \leq x \leq 2.5 \quad (54)$$

The curve of the function given by (53) within the bound 0-2.5 is shown in black in Figure 46. This curve is divided into three pieces that are approximated with straight lines; each one of these pieces is bounded by two breakpoints. These lines are represented by linear equations. This approximation can be expressed mathematically in different forms; one of these forms is the  $\lambda$ -formulation, which is described below.

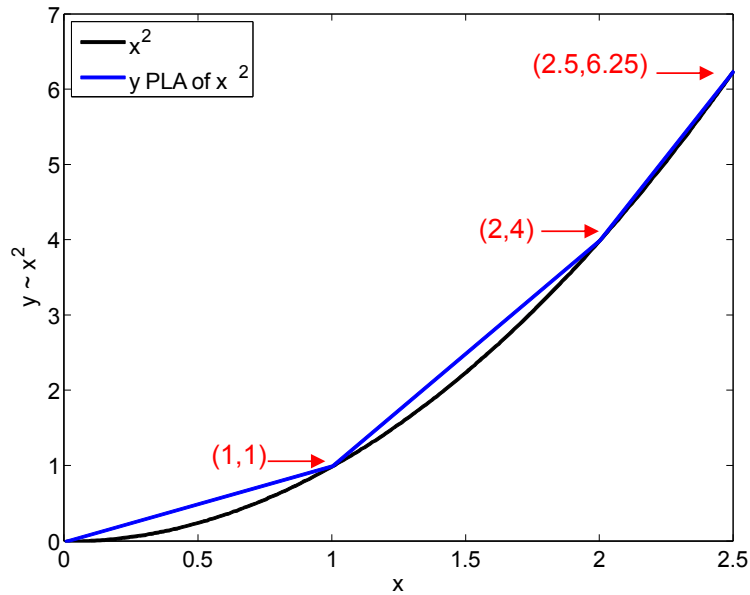


**Figure 46. Piecewise linear approximation of (53) using  $\lambda$ -formulation.**

Let  $x_1 = 0$ ,  $x_2 = 1$ ,  $x_3 = 2$ , and  $x_4 = 2.5$  denote four selected breakpoints along the  $x$ -axis in Figure 46. Let  $f(x_1) = 0$ ,  $f(x_2) = 1$ ,  $f(x_3) = 4$ , and  $f(x_4) = 6.25$  denote to the corresponding function values that are shown in Figure 46. So, any point  $x$  between two

breakpoints is the weighted sum of these two breakpoints. Now, consider  $\lambda_1, \lambda_2, \lambda_3,$  and  $\lambda_4$  are nonnegative weights and their sum equals 1. Then, (53) can be approximated by

$$x = 0 \lambda_1 + 1 \lambda_2 + 2 \lambda_3 + 2.5 \lambda_4, \quad (55)$$

$$y = 0 \lambda_1 + 1 \lambda_2 + 4 \lambda_3 + 6.25 \lambda_4, \quad (56)$$

$$\lambda_1 + \lambda_2 + \lambda_3 + \lambda_4 = 1, \quad \lambda_i \geq 0. \quad (57)$$

Also, it should be noted that at most two adjacent  $\lambda_i$  can be nonzero. This condition together with the last constraint form a special order set of type 2 (SOS2). Therefore, any quadratic term in the form of (53) in the house optimization model is replaced by a slack term, for example  $y$ . Also, three equality constraints represented by (55)-(57) are added to the house optimization model.

### 7.2.2 Elimination of Bilinear Terms

The electrothermal model of the house represented by (2) contains two types of quadratic terms,  $f_1(x) = x^2$  and  $f_2(x,y) = xy$ . The former is a single variable squared term and it is a separable function can be approximated using  $\lambda$ -formulation. But, the latter is a bilinear term that is non-separable function. This section presents a method to approximate a function with a bilinear term. Consider two variables  $x$  and  $y$ ; and the product of them is given by

$$f(x, y) = xy, \quad (58)$$

where  $x$  and  $y$  are continuous variables and bounded by

$$x_{lb} \leq x \leq x_{ub}, \quad (59)$$

$$y_{lb} \leq y \leq y_{ub}. \quad (60)$$

The non-separable function  $f(x,y)$  given by (58) can be converted into a separable form by introducing two new slack variables  $g_1$  and  $g_2$ , which are defined as

$$g_1 = \frac{1}{2}(x + y), \quad (61)$$

$$g_2 = \frac{1}{2}(x - y). \quad (62)$$

Now, the bilinear term  $xy$  can be replaced by an equivalent separable function

$$f(x, y) = g_1^2 - g_2^2, \quad (63)$$

which can be easily approximated using the method explained in the previous section.

The additional two slack variables  $g_1$  and  $g_2$  are bounded by

$$\frac{1}{2}(x_{lb} + y_{lb}) \leq g_1 \leq \frac{1}{2}(x_{ub} + y_{ub}), \quad (64)$$

$$\frac{1}{2}(x_{lb} - y_{ub}) \leq g_2 \leq \frac{1}{2}(x_{ub} - y_{lb}). \quad (65)$$

Therefore, for any bilinear term in the house optimization model, two slack variables represented by (61) and (62) are added to the model. Further, the bilinear term is replaced by (63); and each single quadratic variable can be approximated using  $\lambda$ -formulation as explained before. In addition, the new slack variables are bounded by (64) and (65). Next, model predictive control is discussed.

### 7.3 Model Predictive Control

The optimization model of the house is formulated to provide optimal control over a future horizon (planning period). Model predictive control (MPC) is an advanced method to control the future behavior of a dynamical system to achieve specific objective and meeting the dynamical system constraints [128, 129]. The goal of implementing the MPC is to compute the future trajectory of the house control variables that optimize the



future states of the house. To illustrate the concept, major parts of MPC are explained below.

### ***1. The House Optimization Model***

It is the model that MPC uses to predict future evolution of the house states in order to optimize the control variables. The optimization model not only covers the current time, but also during the future course of the house states. The detailed formulation of the house optimization model is presented in 3.1.

### ***2. Moving Horizon Window***

It is from  $n$  to  $n + N$ , which is denoted by 2 in Figure 47 (a). Note that the length of this horizon window is kept during the entire process. When the horizon window moves to the next step, shown in Figure 47 (b), the moving horizon window becomes from  $n+1$  to  $n+N+1$ . The length of the horizon window could be for example an hour, two hours, or even a day.

### ***3. Planning Horizon***

The planning horizon of MPC dictates how far we wish the future of the house states to be predicted. It is equal to the length of the moving horizon window,  $N$ ; and it is represented by 3 in Figure 47 (a).

### ***4. Receding Horizon Control***

One of the outcomes of the optimization problem solution at every step is the control variables at the current and future time steps i.e. complete trajectory of the control variables. It is only the first control variable vector at the current time is implemented and

the moving horizon window is moved one step. This procedure is performed until the end of the planning period.

To summarize, the general scheme of MPC works as the following: 1) Initial values are obtained from the state estimation, 2) Solve the optimization problem for the entire planning horizon, 3) Only implement the first controls at the current time step and ignore the future controls, 4) move the window horizon one step, and 5) Back to 2.

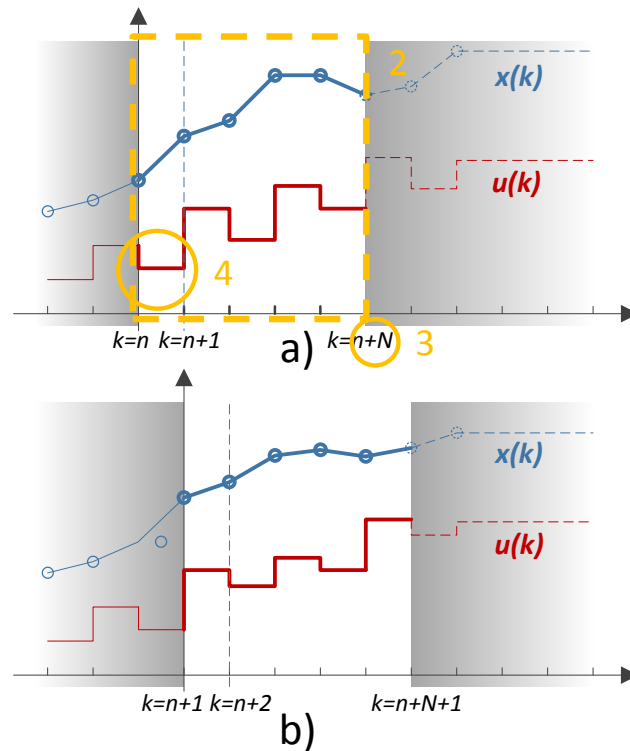


Figure 47. Illustration of the model predictive control concepts.

## 7.4 Summary

In this Chapter, the methods that were used when developing the optimization problem are presented. The  $\lambda$ -formulation that was used to approximate a single quadratic variable is explained in this Chapter. Also, the elimination procedure of any

bilinear term that exists in the house optimization model is discussed in this Chapter. Moreover, model predictive control that was utilized to provide optimal control variables to yield optimal house states trajectory over a planning horizon window is explained in this Chapter. The overall optimization model has around 15552 variables before the relaxation. After the relaxation, the model has 55872 variables. It should be noted that the number of total variables is impacted by the total number of planning horizon. For example, the previous number of variables is with 10 minutes time step for one day. With 5 minutes time step, the total number of variables will double. Average execution time for the problem with 10 minutes time step for a day was found to be around 5 minutes and 46 seconds on a laptop that has the following characteristics: Windows 7 with Intel i7, 2.8 GHz, and 4 GB installed memory. With more advanced computers, the execution time would be reduced. The following Chapters present demonstrative case studies about the house components models and the smart house energy management system.

# **8 DEMONSTRATIVE CASE STUDIES: HOUSE MODEL**

## **SIMULATION RESULTS**

### **8.1 Introduction**

This Chapter provides demonstrative examples for house system simulation results and examination of component performance such as distribution transformer, house DERs, and house appliances. Note that all the models for the house components are already presented in Chapter 5. The first section presents results for the electrothermal model of distribution transformer. This example provides characterization of the model response rise time. It presents also the computation results of the transformer loss of insulation life for two different loading conditions: normal and extreme. The second section presents results for several house simulations. In these simulations, the house consists of transformer, DERs, and appliances. These simulations are: 1) two simulations for the house operation under different loading and environmental conditions and 2) a simulation for the house operation with regular and improved house wall insulation.

### **8.2 Transformer Model Case Study**

#### ***8.2.1 System Description***

A 13.8 kV system was developed to test the electrothermal center-tap distribution transformer model. The test system consists of mainly slack generator, power transformers, transmission line, distribution substation (13.8 kV), overhead distribution line, and the electrothermal distribution transformer as illustrated in Figure 48. The

secondary winding of the transformer is connected to a variable load. The transformer external case temperature spots are connected to an ambient temperature model, which is considered the reference temperature for the thermal model. Parameters related to the electrothermal distribution transformer are presented next.

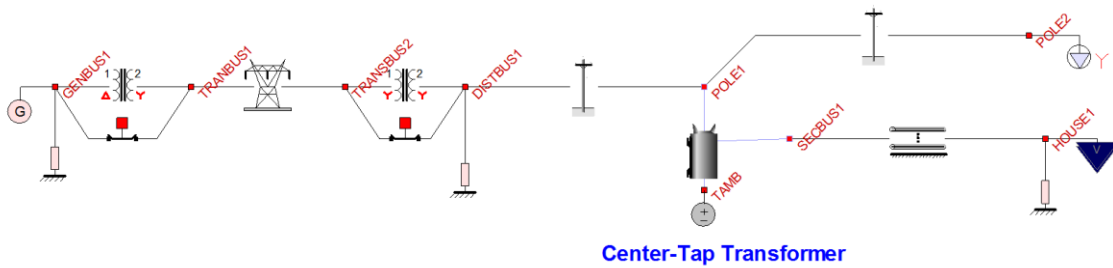


**Figure 48. Transformer test system single line diagram.**

The electrical circuit parameters for a 10 kVA distribution transformer are provided in Table 10. Temperature data for the City of Atlanta for August 08, 2013 are illustrated in Figure 49. Peak temperature was about 31 °C and occurred at 2 to 5 pm.

**Table 10. Case study transformer electrical impedance parameters.**

$Z_1$ [pu]	0.00428+j0.03422
$Z_{L1}, Z_{L2}$ [pu]	0.00699+j 0.01399
$Y_m$ [pu]	0.0068+j 0.09

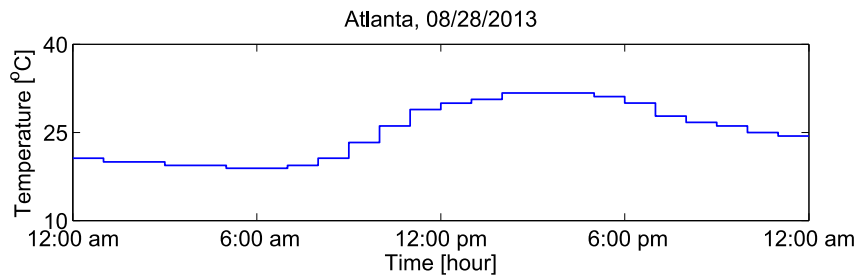


**Figure 49. An example of ambient temperature condition.**

The daily load profile is shown in Figure 50. During the 16<sup>th</sup> hour of that day, the transformer experienced a peak load equals 1.2 pu.

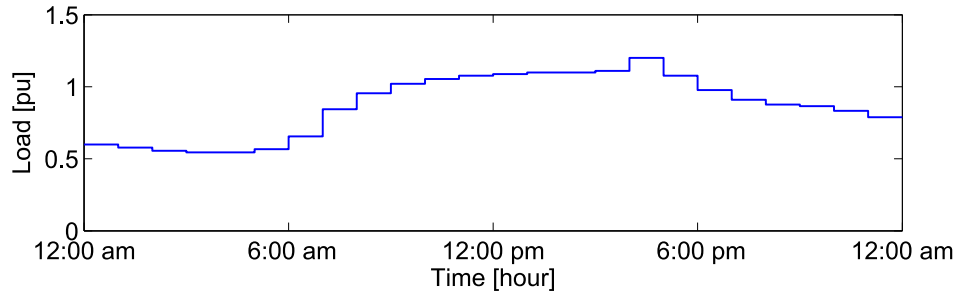


**Figure 50. Hourly load with 1.2 pu peak load connected to 10 kVA transformer.**

To compute the transformer various thermal capacities, the volume of every transformer part, such as tank and case, was computed. The computation of the transformer model parameters is based on the transformer physical dimensions and volumetric quantity of oil data; such data can be found in the transformer manufacture data sheet. In this case study, physical data for a 10 and 25 kVA ABB transformers were used. These data are summarized in Table 11.

**Table 11. ABB transformer physical parameters (dimension and oil volume) [130].**

	10 kVA	25 kVA
<b>Height <math>h</math> [in]</b>	22.0	24.2
<b>Radius <math>r</math> [in]</b>	8.27	9.0
<b>Oil Volume [U.S. Gal]</b>	5.8	7.92

Given the height and radius data, the transformer overall volume including the transformer case volume was computed. The case volume was computed using the transformer inner and outer radius. This case volume was subtracted from the transformer volume. Next, the oil volume was subtracted from the transformer volume resulting in an

approximation of the transformer less oil volume, representing the total volume for transformer core and windings. Then, each one of the transformer windings volume was assumed to be 2% of total core and winding volume. Table 12 summarizes the volume, mass density, specific heat, and heat capacity for each part of 10 kVA ABB transformer.

**Table 12. Volume, mass density, specific heat, and heat capacity for each part of 10 kVA ABB transformer.**

	Vol [m <sup>3</sup> ]	( $\rho$ )[kg/m <sup>3</sup> ]	$C_p$ [J/kg.°C]	$C_{th}$ [Btu/°C]
<b>Primary Winding</b>	0.00098865	(Copper) 8930	385	$C_h = 3399.01$
<b>Secondary Winding</b>	0.00098865	(Copper) 8930	385	$C_L = 3399.01$
<b>Transformer Core</b>	0.047455628	(Iron) 7874	450	$C_{core} = 168150$
<b>Transformer Oil Tank</b>	0.02195537	(Mineral Oil) 800	1860	$C_{oil} = 32669.6$
<b>Transformer Case</b>	0.00607296	(Steel) 7874	450	$C_{case} = 21518.3$

Finally, the thermal capacities were divided by the total number of temperature spots assigned to each part of the transformer. The computation for 10 & 25 ABB kVA transformer thermal circuit values was performed and the results are shown in Table 13.

**Table 13. Thermal circuit parameters results for ABB transformers.**

Thermal Capacity [Btu/°C]	10 kVA	25 kVA
$C_{h1}, C_{h2}, C_{h3}$	1133.019609	1453.1590
$C_{L11}, C_{L12}, C_{L13}, C_{L21}, C_{L22}, C_{L23}$	566.5098	726.57953
$C_{CT}, C_{CB}, C_{CR}, C_{CL}$	42037.382166	53915.221

$C_{TOT}, C_{BOT}, C_{ROT}, C_{LOT}$	8167.400615	11011.90910
$C_{CaseT}, C_{CaseB}, C_{CaseR}, C_{CaseL}$	5379.584307	7008.34387
$G_{h1}$	0.9392	2.34804
$G_{h2}$	4.9646	12.41160
$G_{h3}$	9.2251	23.06277
$G_{L11}$	1.3173	3.29348
$G_{L12}$	5.1539	12.88472
$G_{L13}$	15.9001	39.75033
$G_{L21}$	6.6761	16.69016
$G_{L22}$	12.7690	31.92241
$G_{L23}$	13.8044	34.51093
$G_{CT}$	114.4823	286.20563
$G_{CB}$	342.9088	857.27202
$G_{CR}$	411.6648	1029.16195
$G_{CL}$	638.6320	1596.57994
$G_{TOT}$	93.6341	234.08525
$G_{BOT}$	557.5581	1393.89515
$G_{ROT}$	235.7097	589.27419
$G_{LOT}$	608.0865	1520.21629
$G_{CaseT}$	179.2948	448.2369
$G_{CaseB}$	1091.0020	2727.505025
$G_{CaseR}$	264.8116	662.0288
$G_{CaseL}$	487.5559	1218.8897



Three cases were simulated to test the electrothermal transformer model: a) rise time of the transformer waveforms, b) normal loading, and c) extreme loading.

### 8.2.2 Rise Time Characterization

The objective of this case is to analyze the rise time of temperature waveforms for the transformer model. This case was simulated with one second time step. Results are reported for two different transformer ratings 10 and 25 kVA for three different manufacturers ABB, Power Partners, and Cooper Power Systems. For 10 and 25 kVA ABB transformers, temperature waveforms at  $T_{h2}$ ,  $T_{L12}$ ,  $T_{CB}$ ,  $T_{TOT}$ , and  $T_{CaseR}$  spots are shown in Figure 51 (a) & (b), respectively. The simulation was performed as follows: no load was considered in the beginning of the simulation. By the end of the first half hour, full load equals 100% of the transformer rating was connected to the transformer secondary side. The reference temperature during the simulation was fixed at 40 °C.

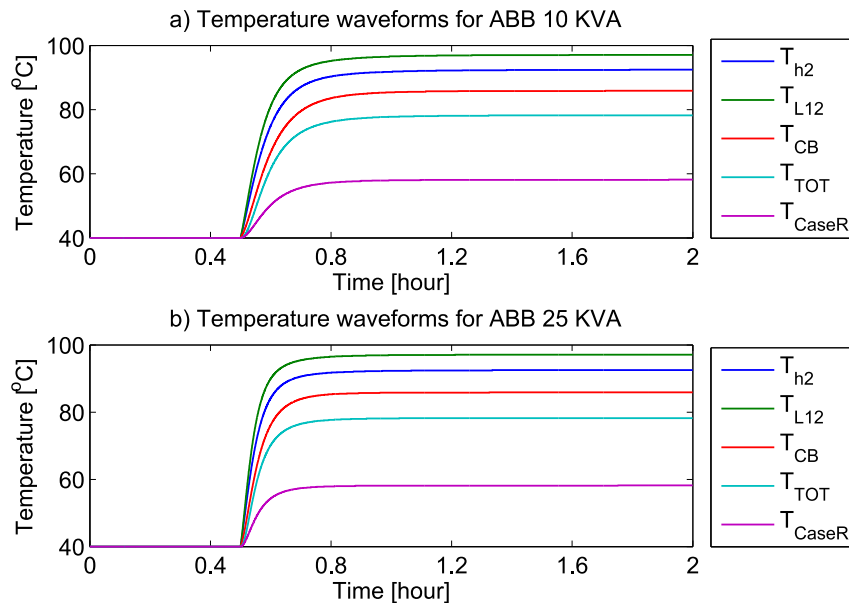


Figure 51. 10 & 25 ABB kVA transformer temperatures waveforms.

Approximate rise times are reported in Table 14 for three different manufactures ABB, Power Partners, and Cooper Power Systems with 10 and 25 kVA ratings. Physical data used to estimate the rise time were taken from the manufacture data sheet [130, 131].

**Table 14. Transformer temperature waveforms approximate rise time in [min].**

<b>Manufacture</b>	<b>10 kVA</b>	<b>25 kVA</b>
<b>ABB</b>	20.45	19.3
<b>Cooper Power Systems</b>	21.55	20.4
<b>Power Partners Inc.</b>	22.15	17.72

The rise time of temperature signals depends on transformer manufacture specification and transformer rating. According to Table 14, the parameters indicate that the thermal time constants are in the order of 15 to 25 minutes. This means that there is plenty of time for the smart house energy management system to schedule the use of electricity and avoid overloading the transformer.

### **8.2.3 Peak Loading**

The objective of this case is to compute LOIL for a transformer with normal peak load that is comparable to the transformer rating over a day. Temperature data presented in Figure 49 were used for the temperature reference model. Hourly load data that are shown in Figure 50 were connected to the secondary winding of 10 kVA transformer. LOIL and cumulative LOIL results are reported in Table 15. The hot spot temperature and location (spot name) are provided, too. The computations were based on aging rate constant equals 14580 and normal insulation life equals 150000. The expected transformer loss of insulation life during the 16<sup>th</sup> hour (peak load) was 0.0016173 %. The

expected LOIL of the transformer under study during the entire day was found equals 0.004 %.

**Table 15. Aging calculation for 10 kVA transformer and for 24 hours with peak loading.**

<b>Time</b>	<b>Load (pu)</b>	<b>Amb. Temp. (°C)</b>	<b>Hot Spot Temp (°C)</b>	<b>Spot Name</b>	<b>LOIL (%)</b>	<b>Cumulative LOIL (%)</b>
0:00:00	0.599	20.611	42.785	L11	0.00000017	0.00000017
1:00:00	0.577	20.000	40.576	L11	0.00000012	0.00000029
2:00:00	0.555	20.000	39.038	L11	0.00000010	0.00000039
3:00:00	0.544	19.389	37.680	L11	0.00000008	0.00000047
4:00:00	0.544	19.389	37.678	L11	0.00000008	0.00000055
5:00:00	0.566	18.889	38.684	L11	0.00000009	0.00000064
6:00:00	0.655	18.889	45.397	L11	0.00000025	0.00000088
7:00:00	0.844	19.389	63.448	L11	0.00000287	0.00000376
8:00:00	0.955	20.611	77.083	L11	0.00001552	0.00001928
9:00:00	1.021	23.278	87.868	L11	0.00005386	0.00007314
10:00:00	1.054	26.111	94.967	L11	0.00011739	0.00019053
11:00:00	1.077	28.889	100.798	L11	0.00021773	0.00040827
12:00:00	1.088	30.000	103.394	L11	0.00028490	0.00069317
13:00:00	1.099	30.611	105.504	L11	0.00035352	0.00104669
14:00:00	1.099	31.722	106.616	L11	0.00039574	0.00144244
15:00:00	1.11	31.722	108.128	L11	0.00046083	0.00190327
16:00:00	1.2	31.722	121.067	L11	0.00161726	0.00352052
17:00:00	1.077	31.111	103.043	L11	0.00027480	0.00379532
18:00:00	0.977	30.000	89.145	L11	0.00006211	0.00385743
19:00:00	0.91	27.778	79.057	L11	0.00001960	0.00387704

20:00:00	0.877	26.722	74.332	L11	0.00001116	0.00388820
21:00:00	0.866	26.111	72.527	L11	0.00000897	0.00389717
22:00:00	0.832	25.000	67.834	L11	0.00000502	0.00390218
23:00:00	0.788	24.389	62.801	L11	0.00000264	0.00390483

#### 8.2.4 Extreme Loading

In this case, the objective is to compute LOIL for a transformer with extreme peak load. During the 16<sup>th</sup> hour of the daily load presented in the previous section, the transformer experienced a load equals 1.4 pu. LOIL and cumulative LOIL results are reported in Table 16. The hot spot temperature and location (spot name) are provided, too. The computations were based on aging rate constant equals 14580 and normal insulation life equals 150000. The expected transformer LOIL during the 16<sup>th</sup> hour (peak load) was 0.02679 %. The expected LOIL of the transformer under study during the entire day was found equals 0.029 %.

**Table 16. Aging calculation for 10 kVA transformer and for 24 hours with extreme loading.**

Time	Load (pu)	Amb. Temp. (°C)	Hot Spot Temp (°C)	Spot Name	LOIL (%)	Cumulative LOIL (%)
0:00:00	0.599	20.611	42.784	L11	0.000000169	0.000000169
1:00:00	0.577	20.000	40.575	L11	0.000000122	0.000000291
2:00:00	0.555	20.000	39.037	L11	0.000000097	0.000000388
3:00:00	0.544	19.389	37.678	L11	0.000000079	0.000000467
4:00:00	0.544	19.389	37.678	L11	0.000000079	0.000000546
5:00:00	0.566	18.889	38.684	L11	0.000000092	0.000000638
6:00:00	0.655	18.889	45.398	L11	0.000000247	0.000000885
7:00:00	0.844	19.389	63.447	L11	0.000002873	0.000003757

8:00:00	0.955	20.611	77.083	L11	0.000015523	0.000019281
9:00:00	1.021	23.278	87.868	L11	0.000053860	0.000073140
10:00:00	1.054	26.111	94.967	L11	0.000117384	0.000190524
11:00:00	1.077	28.889	100.797	L11	0.000217716	0.000408240
12:00:00	1.088	30.000	103.394	L11	0.000284908	0.000693148
13:00:00	1.099	30.611	105.503	L11	0.000353506	0.001046654
14:00:00	1.099	31.722	106.615	L11	0.000395718	0.001442371
15:00:00	1.11	31.722	108.127	L11	0.000460785	0.001903157
16:00:00	1.4	31.722	153.443	L11	0.026797767	0.028700923
17:00:00	1.077	31.111	103.078	L11	0.000275797	0.028976720
18:00:00	0.977	30.000	89.147	L11	0.000062115	0.029038836
19:00:00	0.91	27.778	79.057	L11	0.000019605	0.029058440
20:00:00	0.877	26.722	74.331	L11	0.000011163	0.029069603
21:00:00	0.866	26.111	72.527	L11	0.000008967	0.029078570
22:00:00	0.832	25.000	67.834	L11	0.000005017	0.029083587
23:00:00	0.788	24.389	62.801	L11	0.000002643	0.029086230

Data that are provided in Table 15 and Table 16 indicate that the transformer LOIL can experience substantial increase whenever there is high load. Thus, with appropriate management and control of the house controllable components, the service lifetime of the transformer can be extended. Moreover, the outcome of the transformer LOIL computation can show if this specific transformer is appropriately sized for a particular application or not.

### 8.3 House Characteristics Case Studies

In this section, two case studies are presented to show the operational characteristics of the house. The house consists of all models that are presented in Chapter 5. To show the response of the house during different loading and environmental conditions, two different days with different loading and ambient conditions were simulated. The second case shows the house operation results when the house wall insulation was improved. First, a description of the house test system is discussed.

#### 8.3.1 Description of the House Test System

A test case system with house DERs, EV, and house appliances was developed. The system consists of a 13.8 kV slack generator, 13.8/115 kV delta-why power transformer, transmission line, 115/13.8 kV why-why power transformer, and a distribution network consists of two poles as shown in Figure 52. The electrothermal model of the house is connected to the system via pole 1.

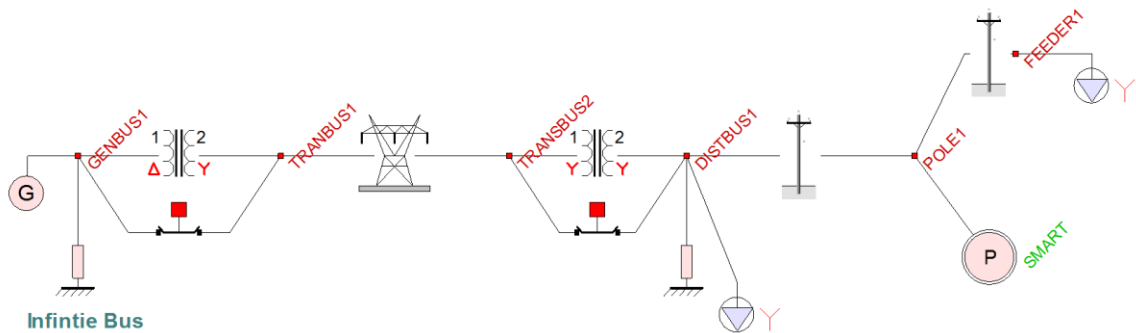


Figure 52. Power system at the system level in the house simulation.

The house model, which represents the physical house under consideration, is shown in Figure 53. A single phase electrothermal transformer rated 10 kVA 7.2/0.24 kV is used to connect the house with the power grid. EV and house battery are located outside of the house; a reference temperature model is connected to each one of them.

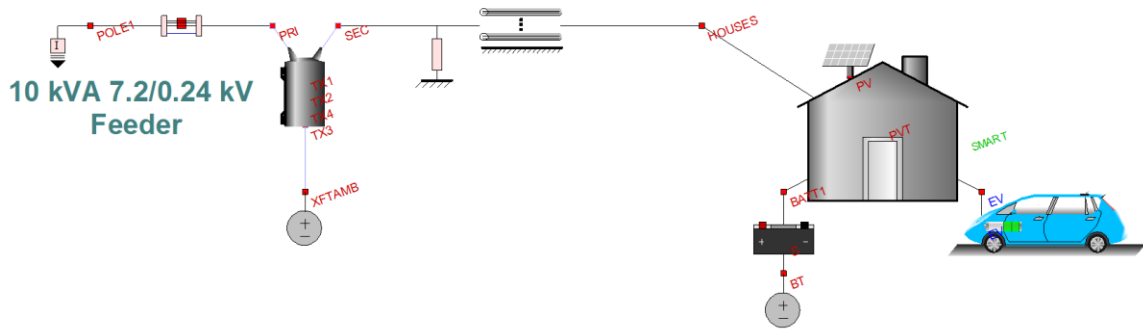


Figure 53. House pole in the simulation.

The details of the house are shown in Figure 54. The house has solar PV, battery bank (lead acid), EV battery (lithium ion), and appliances including air conditioner, refrigerator, dishwasher, dryer, washer, water heater, and other. The house, additionally, includes power electronics converters, associates controls, and the thermostat, which is connected to bedroom<sub>1</sub> temperature spot as shown in Figure 54.

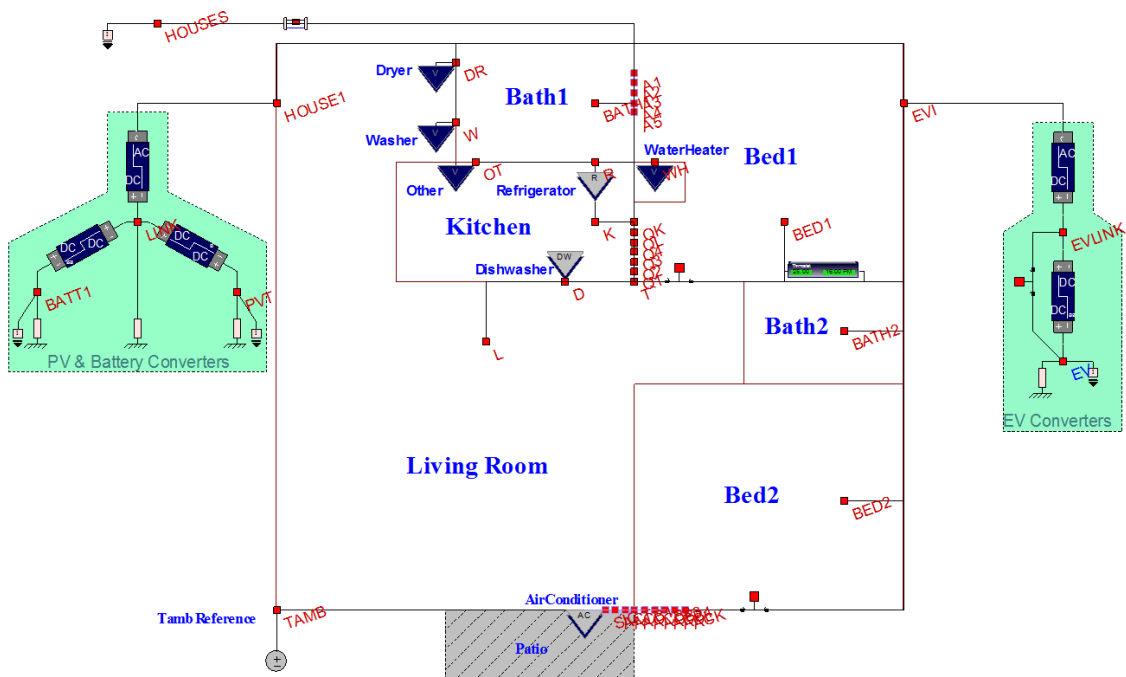
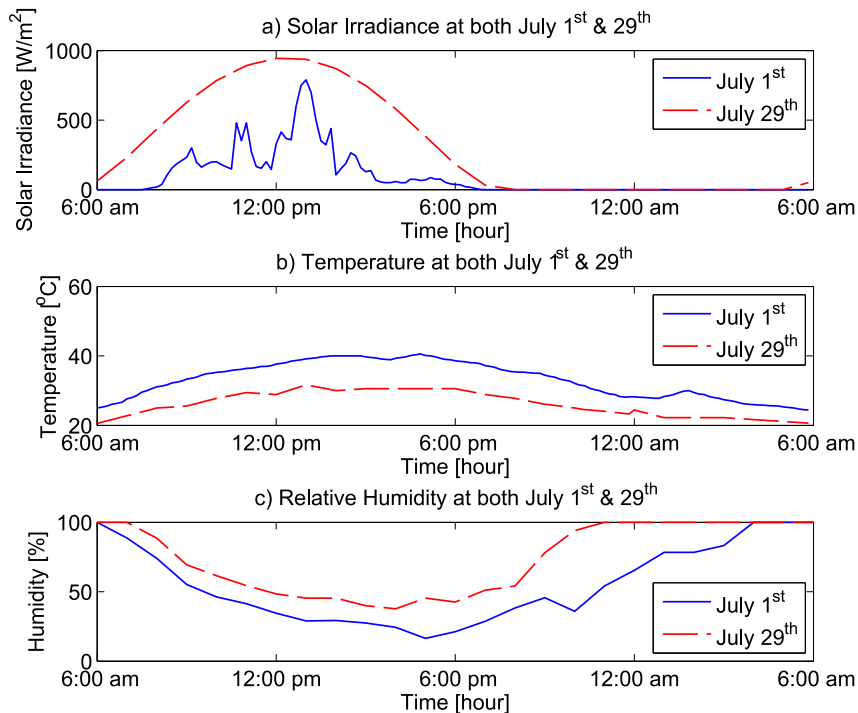


Figure 54. House with appliances in the simulation.

Actual environmental conditions and appliances loading data for a single story house were used. The house is located in in Glasgow, Kentucky US. These data include solar irradiance data, ambient temperature, relative humidity, and appliances loading condition. They are for July 1<sup>st</sup> and 29<sup>th</sup> of 2012 and presented from 6:00 am for 24 hours.

Solar irradiance, ambient temperature, and relative humidity data for July 1<sup>st</sup> and 29<sup>th</sup> are presented in Figure 55. The data are presented every 10 minutes. Solar irradiance data are presented in Figure 55 (a). In July 29<sup>th</sup>, the solar PV can supply power to the house that is greater than the solar PV power in July 1<sup>st</sup>. In Figure 55 (b), the ambient temperatures of the house for both days are shown. The peak temperature was about 40 °C at 04:50 pm in July 1<sup>st</sup>. Similarly, the peak temperature was 31.6 °C in July 29<sup>th</sup> at 01:00 pm. Relative humidity data for both days are presented in Figure 55 (c).



**Figure 55. Data for July 1<sup>st</sup> & 29<sup>th</sup>, a) solar irradiance and b) ambient temperature.**



The house appliances including washer, dryer, water heater, and range were represented by an aggregated several time variable active and reactive power load model. The aggregated data for these appliances for July 1<sup>st</sup> and 29<sup>th</sup> are illustrated in Figure 56 (a) and (b), respectively.

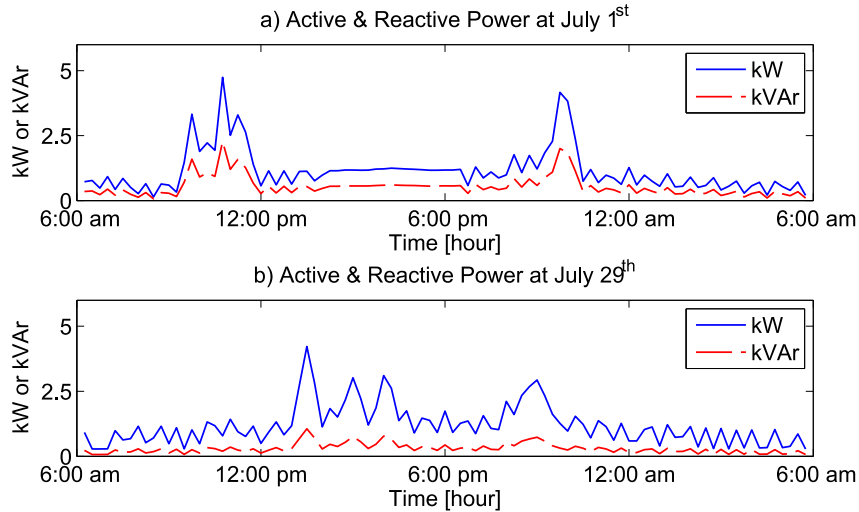


**Figure 56. House data for July 1<sup>st</sup> & 29<sup>th</sup>, a) relative humidity and b) appliances load.**

Dishwasher electrical parameters are provided in Table 17. The smart dishwasher was set to operate one time at 5:00 pm with high internal loading in July 1<sup>st</sup>. Similarly, it was set to operate one time at 11:30 pm with high internal loading in July 29<sup>th</sup>. Both dishwasher operations time duration was assumed to equal 100 minutes.

**Table 17. Dishwasher input data.**

$P_{dvrated} = 1200 \text{ W}$	$V_{rms} = 130 \text{ V}$	$Efficiency = 0.85$
$Pf = 0.9$	$Total \ Time \ Duration \ Per \ One \ Operation = 100 \ min$	$Connection \ L1-NN$

Refrigerator model parameters are provided in Table 18. The refrigerator food and freezer compartments capacity are:  $12.8 \text{ ft}^3$  and  $3.7 \text{ ft}^3$ . The temperature set for the refrigerator for both days, July 1<sup>st</sup> and 29<sup>th</sup>, was 2.5 with 1 °C deadband. The refrigerator

was assumed to be half full during the entire July 1<sup>st</sup> day. But, in July 29<sup>th</sup>, the refrigerator was assumed to experience several internal heat capacity changes due to opening the refrigerator door and internal load changes. In particular, there was a large heat capacity change at 06:00 pm.

**Table 18. Refrigerator input data.**

<i>Prefrated = 100 W</i>	<i>Vrms = 130 V</i>	<i>Efficiency = 0.85</i>
<i>Pf = 0.95</i>	<i>COP = 3.5</i>	<i>L1-NN</i>

An air conditioner with six ducts was also considered. Model parameters are provided in Table 19. The air conditioner operation was controlled by a thermostat controller with temperature reference that are varies based on the resident desires. The thermostat controller, in this case, monitored the main bedroom<sub>1</sub> temperature with a deadband equals 1 °C. Table 20 presents the thermostat settings for both July 1<sup>st</sup> and 29<sup>th</sup>.

**Table 19. Air conditioner model parameters.**

<i>Heat Rate = 35 kBtu</i>	<i>Vrms = 230 V</i>	<i>Nominal COP = 2.5</i>
<i>Pf = 0.85</i>	<i>Thermostat Controlled</i>	<i>Connection L1-L2</i>

**Table 20. Thermostat control settings in July 1<sup>st</sup> and 29<sup>th</sup>.**

	<b>Time</b>	<i>06:00:00 am</i>	<i>06:00:00 pm</i>	<i>08:00:00 pm</i>	<i>10:00:00 pm</i>
<b>Temperature Setting (°C)</b>	<b>July 1<sup>st</sup></b>	26	24	22	22
	<b>July 29<sup>th</sup></b>	29	24	24	21

House roof-top solar PV was sized as follows, 6 panels with 60 cells in each panel. Characteristics for every panel are provided in Table 21. Perturb and Observe MPPT algorithm was used.

**Table 21. House roof-top data parameters.**

<i>Rated Power = 0.26 kW/panel</i>	<i>Voc = 38.3 V</i>	<i>Isc = 9.09 A</i>
<i>Rs = 0.4 Ω</i>	<i>Rp = 850 Ω</i>	<i>P&amp;O MPPT Algorithm</i>

For both days July 1<sup>st</sup> and 29<sup>th</sup>, EV battery was rated 24 kWh with 3.3 kW maximum charging/discharging. To avoid deep charging/discharging, the minimum and maximum SOC limits were 0.1 and 0.9. In addition, EV was assumed to be connected to the house at 6:00 pm. Residential battery bank was also included. The battery bank was rated 2.4 kWh with rated 0.3 kW charging/discharging. Minimum and maximum SOC were 0.1 and 0.9. Power electronics converters were used with typical parameters. Simulation case studies that are presented in this Chapter were performed with 10 seconds time step. Next, simulation results for house normal operation are presented for July 1<sup>st</sup> and 29<sup>th</sup>.

### **8.3.2 House Simulation for Two different Days**

This section presents the simulation results of the house normal operation when it was simulated for two different days, July 1<sup>st</sup> and 29<sup>th</sup> of 2012. The total house load is depicted in Figure 57 (a). The peak loads were 12.4 kW and 9.82 kW for July 1<sup>st</sup> and 29<sup>th</sup>, respectively. A higher load was observed during July 1<sup>st</sup>. This was due to several factors; one of these factors was frequent operation of the house air conditioner. This frequent operation of the air conditioner was due mainly to the high ambient temperature at that day as shown in Figure 55 (b). The transformer hot spot temperature waveforms for both days are shown in Figure 57 (b). The peak transformer hot spot temperatures were 127 °C and 80.2 °C for July 1<sup>st</sup> and 29<sup>th</sup>, respectively. Due to large energy consumption and high

ambient temperature in July 1<sup>st</sup>, the distribution transformer hot spot temperature most of the day was higher than in July 29<sup>th</sup>.

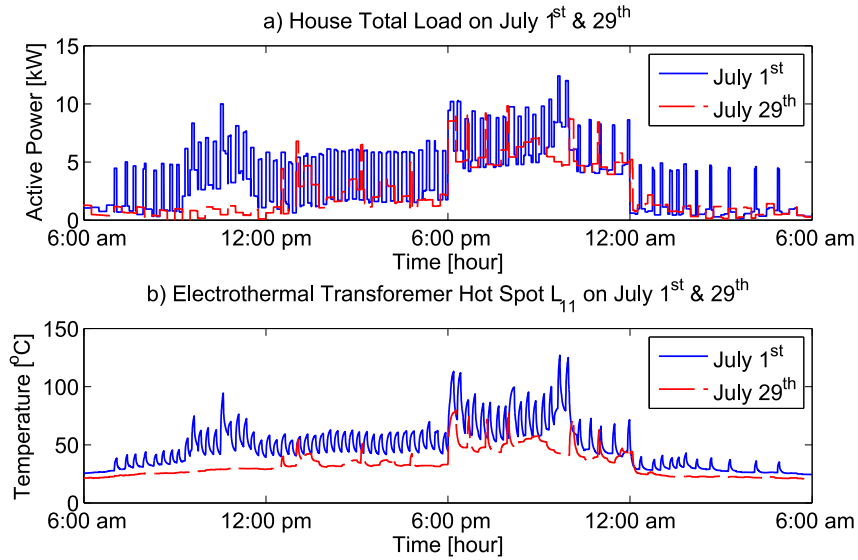


**Figure 57. (a) House total load and (b) transformer hot spot temperature, for both July 1<sup>st</sup> and 29<sup>th</sup>.**

The house dishwasher active and reactive power for July 1<sup>st</sup> and 29<sup>th</sup> are shown in Figure 58 (a) and (b), respectively. In both days, the dishwasher operated at the exact set time by the customer.

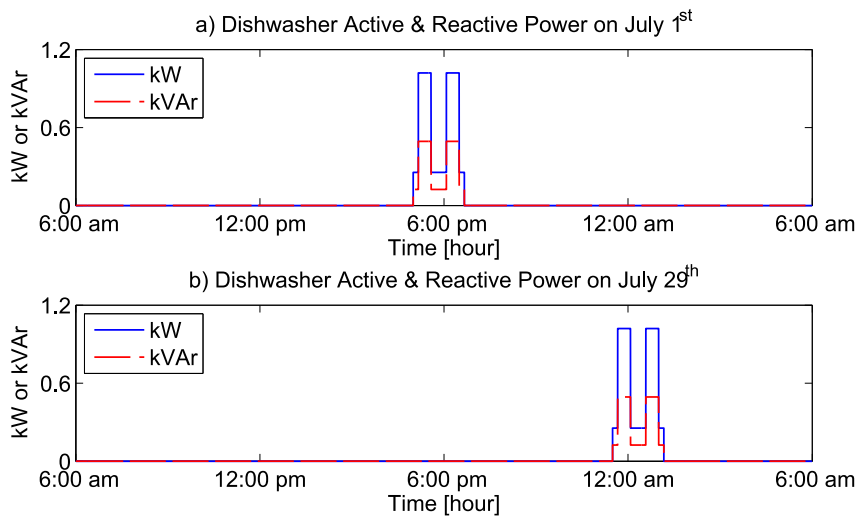


**Figure 58. House dishwasher active and reactive power for both July 1<sup>st</sup> and 29<sup>th</sup>.**

Bedroom<sub>1</sub> temperature, thermostat setting, and the house air conditioner control waveforms for July 1<sup>st</sup> and 29<sup>th</sup> are shown in Figure 59. In July 1<sup>st</sup>, the temperature in bedroom<sub>1</sub> was maintained within the set temperature as shown in Figure 59 (a). Similarly, in July 29<sup>th</sup>, bedroom<sub>1</sub> temperature was maintained within the set temperature as shown in Figure 59 (b). The thermostat was connected to bedroom<sub>1</sub>. It monitored the temperature inside bedroom<sub>1</sub> and sent on/off signal to the air conditioner. The air conditioner received a command signal from the thermostat to turn on/off. The control signals of the house air conditioner for July 1<sup>st</sup> and 29<sup>th</sup> are shown in Figure 59 (c).

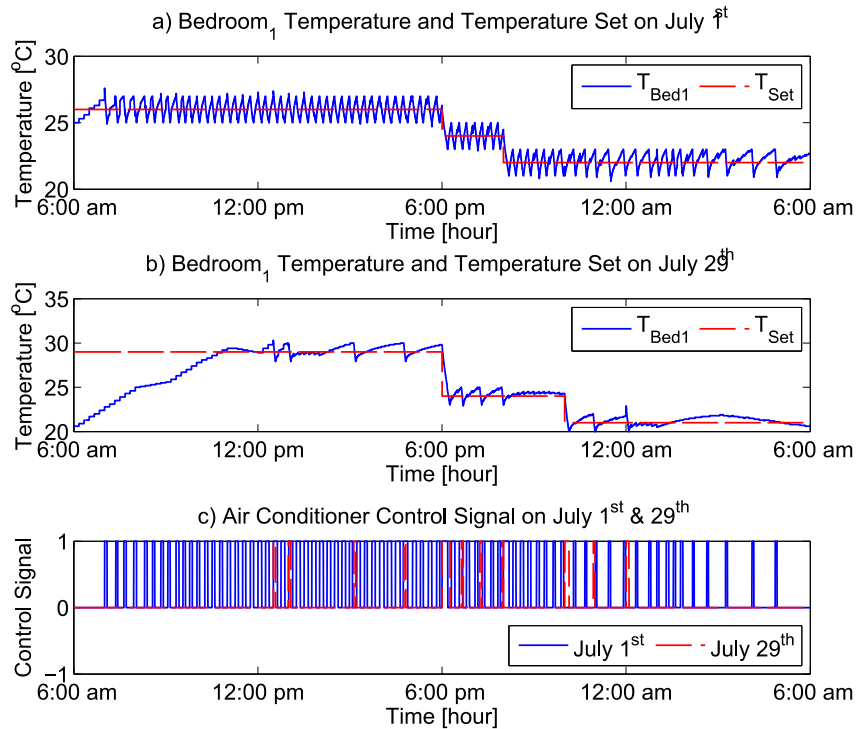


**Figure 59. (a) House bedroom<sub>1</sub> temperature on July 1<sup>st</sup>, (b) on July 29<sup>th</sup>, and (c) house air conditioner control signal on July 1<sup>st</sup> & 29<sup>th</sup>.**

The house refrigerator waveforms in July 1<sup>st</sup> and 29<sup>th</sup> are shown in Figure 60. In Figure 60 (a) and (b), the fresh food compartment main temperature is shown for July 1<sup>st</sup> and 29<sup>th</sup>, respectively. The temperature inside the fresh food compartment was monitored

by a thermostat that was set at 2.5 °C with 1 °C deadband. Due to internal heat capacity changes around 6:00 pm, the temperature inside the fresh food in July 29<sup>th</sup> was reinitialized as shown in Figure 60 (b). As a result, the compartment heat capacity was recomputed. The heat rate responses of the refrigerator for July 1<sup>st</sup> and 29<sup>th</sup> are shown in Figure 60 (c). When the temperature exceeded the upper set limit, the refrigerator's electric motor turned on to cool the refrigerator.

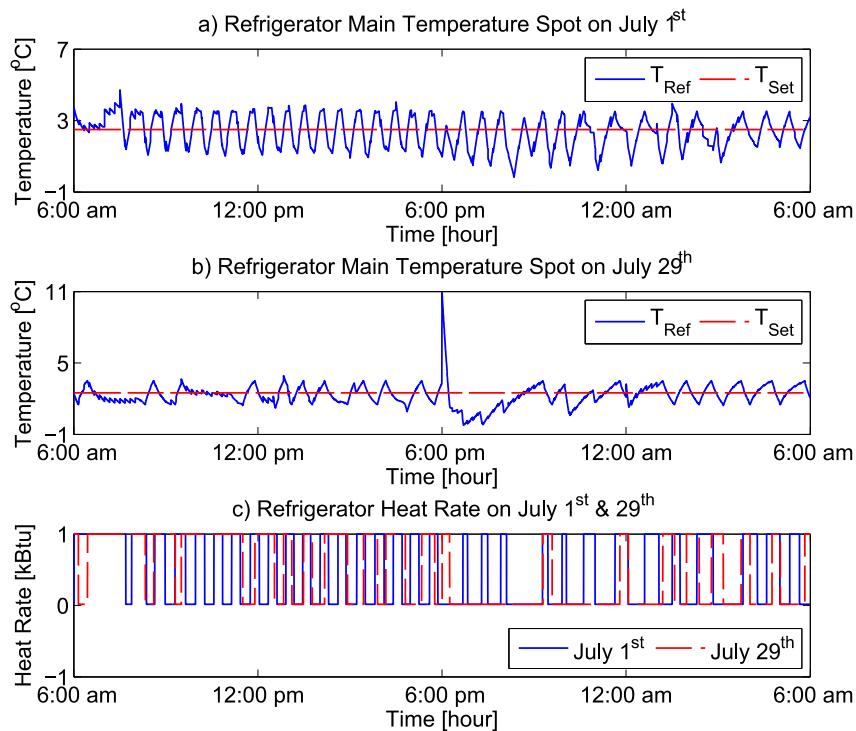


**Figure 60. (a) Refrigerator fresh food compartment main temperature on July 1<sup>st</sup>, (b) on July 29<sup>th</sup>, and (c) refrigerator heat rate on July 1<sup>st</sup> & 29<sup>th</sup>.**

Similarly, Figure 61 shows the house refrigerator waveforms during two hours of the days, July 1<sup>st</sup> and 29<sup>th</sup>. The waveforms are shown from 5:00 pm to 7:00 pm. The refrigerator main temperature at the main spot on July 1<sup>st</sup> is shown in Figure 61 (a). In Figure 61 (b), the refrigerator temperature on July 29<sup>th</sup> is shown. In Figure 61 (c), the heat rate waveforms for both days July 1<sup>st</sup> and 29<sup>th</sup> are shown.

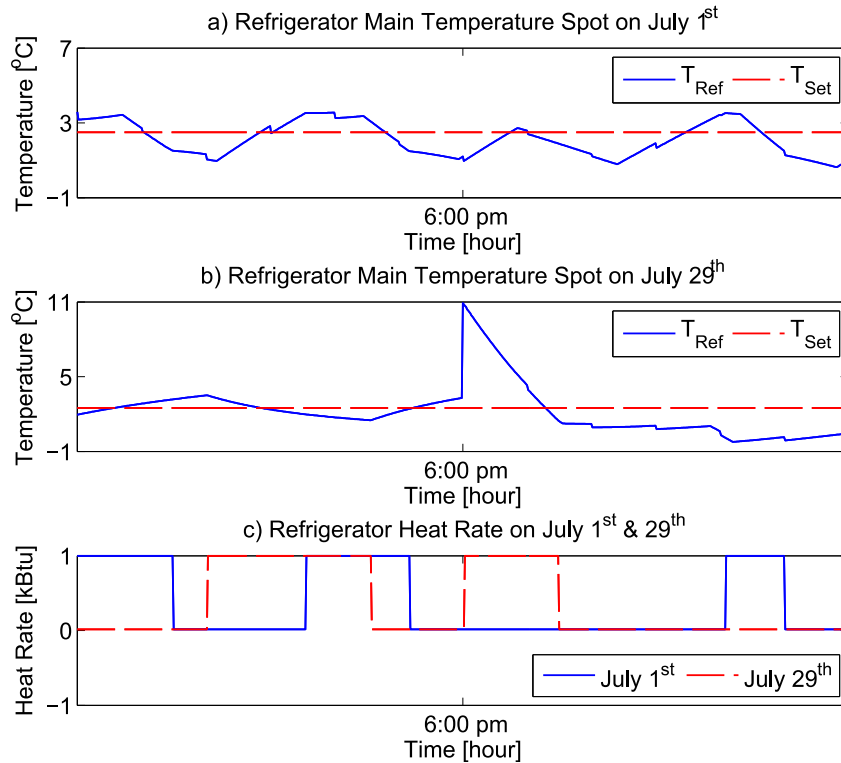


**Figure 61. (a) Refrigerator fresh food compartment main temperature on July 1<sup>st</sup>, (b) on July 29<sup>th</sup>, and (c) refrigerator heat rate on July 1<sup>st</sup> & 29<sup>th</sup>.**

### 8.3.3 House Insulation Improvement

This case presents the simulation results of the house for July 1<sup>st</sup> only, but with two different house walls insulations. The house data for July 1<sup>st</sup> provided in section 8.3.1 regarding solar irradiance, ambient temperature, relative humidity, and appliances loads were considered in this case. In this case, the house walls insulation was changed by considering different thermal conductivities of the walls. Table 22 presents thermal conductance parameters for three different insulation cases, A (base), B, and C.

**Table 22. A (base) case, B case, and C case thermal conductances of the house.**

<b>Thermal Conductance (<math>G_{th}</math>) [Btu/°C.h]</b>	<b>Case A (Base)</b>	<b>Case B</b>	<b>Case C</b>
$G_{bed1}$	7.8750	7.8750	4.5
$G_{bed2}$	7.8750	7.8750	4.5
$G_{bath1}$	2.6250	2.6250	1.5
$G_{bath2}$	2.6250	2.6250	1.5
$G_K$	2.6250	2.6250	1.5
$G_L$	8.7500	8.7500	4.5
$G_{bed1-I}$	0.6674	0.5595	0.198
$G_{bed2-I}$	0.7159	0.5932	0.205
$G_{bath1-I}$	0.5074	0.4013	0.126
$G_{bath2-I}$	0.6031	0.4640	0.128
$G_{K-I}$	2.8292	2.2117	0.704
$G_{L-I}$	0.5394	0.4557	0.148
$G_{house-E}$	14.1032	14.0661	8.027
$G_{house-N}$	12.1745	12.3211	7.144
$G_{house-W}$	3.8617	3.7578	2.269
$G_{house-S}$	9.0683	9.0158	5.387
$G_{house-Top}$	17.9142	17.6113	9.926

Bedroom<sub>1</sub> temperature and house air conditioner control signal are shown in Figure 62 with insulation A parameters. Also, bedroom<sub>1</sub> temperature and house air conditioner control signal with insulation B and C parameters are shown in Figure 63 and Figure 64, respectively. The insulation parameters for C case are better than B; and the insulation parameters for B case are better than the base case. The temperature inside



bedroom<sub>1</sub> was monitored by a thermostat based on one temperature profile setting. Based on Figure 62 and Figure 63, the air conditioner did not operate quite frequently the house insulation was improved. Similarly the air conditioner in case C did turn on fewer times than in case B as illustrated in Figure 63 and Figure 64.

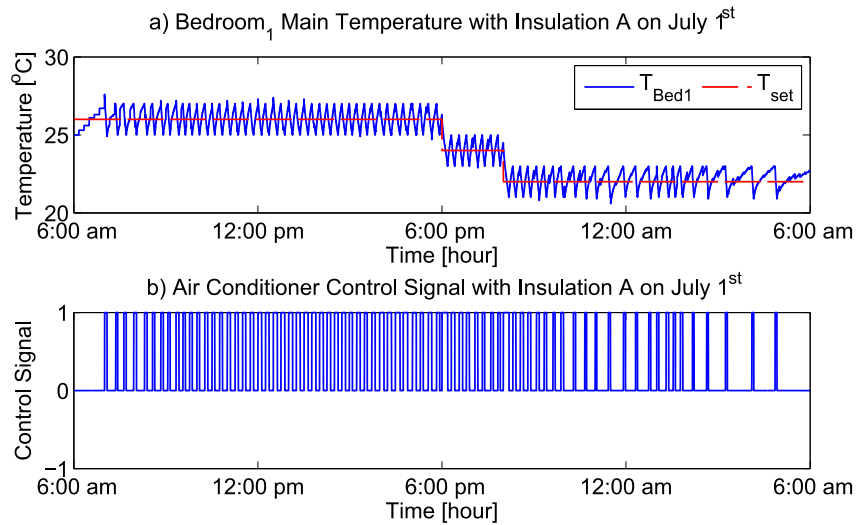


**Figure 62. (a) House bedroom<sub>1</sub> temperature and (b) house air conditioner control signal, with insulation A on July 1<sup>st</sup>.**

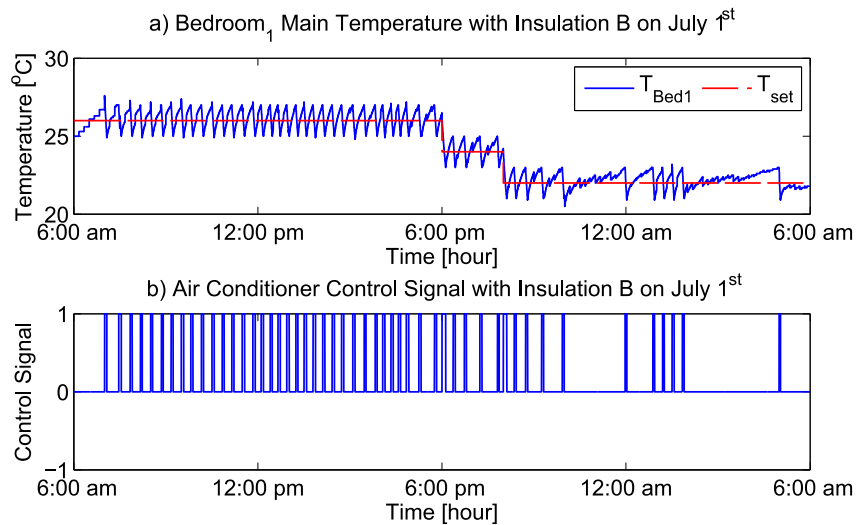


**Figure 63. (a) House bedroom<sub>1</sub> temperature and (b) house air conditioner control signal, with insulation B on July 1<sup>st</sup>.**

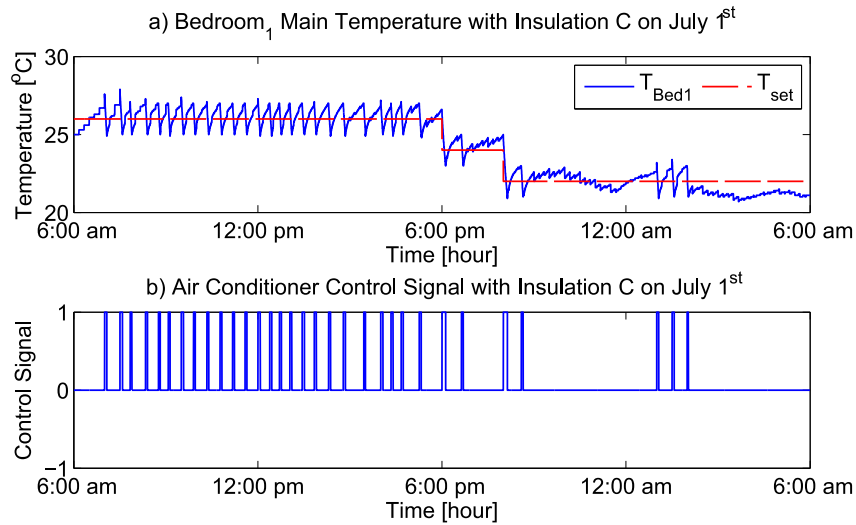


**Figure 64. (a) House bedroom<sub>1</sub> temperature and (b) house air conditioner control signal, with insulation C on July 1<sup>st</sup>.**

#### 8.4 Summary

This Chapter presents several demonstrative simulation results for distribution transformer, house DERs and house appliances models. Transformer rise time temperature waveforms and transformer LOIL simulation results are presented. Also, simulation results for the house operation for different two days that are characterized by different environmental loading conditions are presented. In addition, in this Chapter, a simulation of the house operation with regular and improved house wall insulation was performed and the results were compared.

# **9 DEMONSTRATIVE CASE STUDIES: SMART HOUSE ENERGY MANAGEMENT SYSTEM**

## **9.1 Introduction**

The smart house energy management system is demonstrated through two examples. A description of the house test system is provided. All necessary data and related information that are required to perform the case studies are also presented. Then, a demonstrative case study of the system without the smart house energy management system is presented. After that, a demonstrative case study of the smart house energy management system with the objective to minimize the residential customer's total energy cost over a day is presented. The last section presents another demonstrative example of the smart house when the objective of the optimization model is to provide peak load control of the customer over a day.

## **9.2 Description of House Test System**

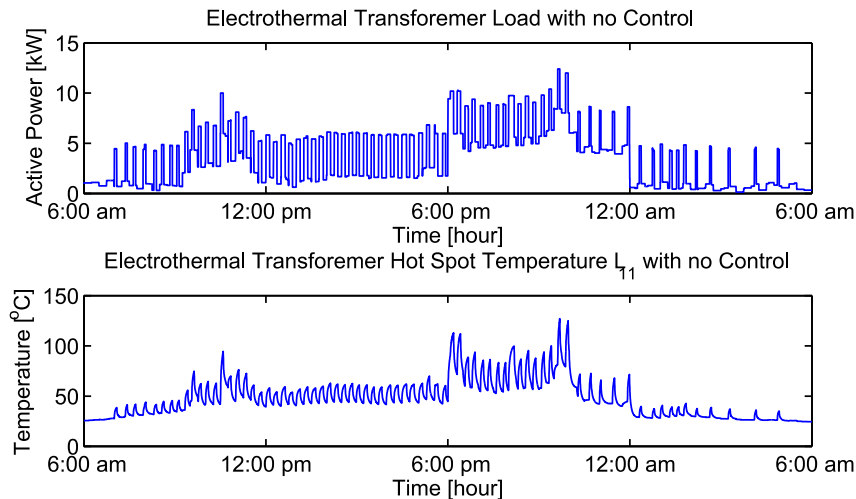
The house test system that is presented in section 8.3.1 is reused in this Chapter. Actual data for a single story house were utilized. Data reported in section 8.3.1 for July 1<sup>st</sup>, which include solar irradiance data, ambient temperature, relative humidity, and appliances loading condition were considered. Provided data in section 8.3.1 regarding house components for July 1<sup>st</sup> were also considered. These data are for dishwasher, refrigerator, air conditioner, thermostat setting, solar PV, EV, and house battery bank.

The smart house energy management system was assumed to provide management and control for the. In this case study, three devices were assumed to be

controllable: 1) smart dishwasher, 2) electric vehicle battery, and 3) house battery bank. The control, however, must not violate any of the system constraints, customer convenience, or overloading the transformer beyond the allowed limit. It should be noted that the customer indicated that the dishwasher must be ready by 9:00 pm, house bedroom<sub>1</sub> main temperature should be maintained according the temperature set provided in Table 20, and EV battery must be fully charged by 6:00 am.

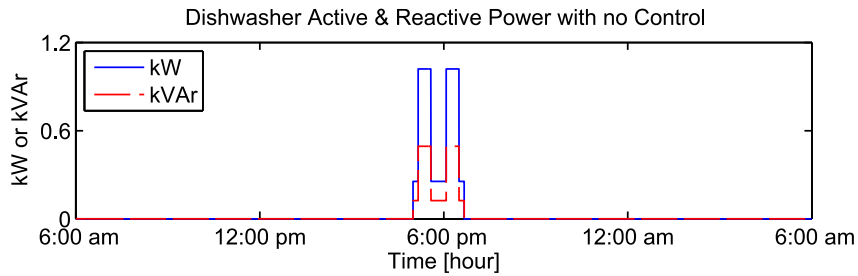
### 9.3 Simulation without the Smart House Energy Management System

The distribution transformer active power without implementing any control strategy is presented in the top of Figure 65. The house load was peaked to 12.4 kW at 09:37 pm, which was higher than the transformer rating. Two temperature peaks were observed as shown in the bottom of Figure 65. These are 113 °C at 6:11 pm and 127 °C at 09:41 pm. These peaks exceeded the permissible temperature (105 °C). The increase in the temperature may increase the deterioration of the transformer insulation life.



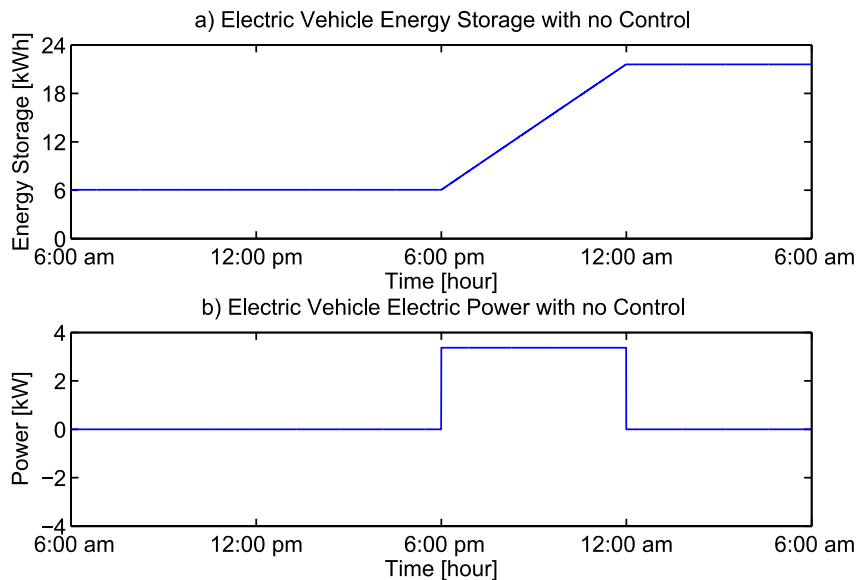
**Figure 65. Top: Transformer active power, Bottom: Transformer hot spot temperature with no management system.**

Figure 66 shows the dishwasher characteristics during the simulation including active and reactive power when the house is not controlled by the smart management system. The dishwasher started at the scheduled time, at 5:00 pm and ended after 100 minutes as shown in Figure 66.



**Figure 66. Smart dishwasher active and reactive power characteristics with no management system.**

The second controllable device is EV. It was assumed that the EV battery has one fourth of its rated capacity when it was connected to the house. The EV was originally scheduled to start charging as soon as it is connected to the house power, i.e. at 06:00 pm. The energy storage and charging/discharging power of the EV battery are presented in Figure 67 (a) and (b). The EV battery started charging with maximum charging power (3.3 kW) at 6:00 pm.



**Figure 67. EV battery characteristics with no management system.**

Similarly, the house battery was assumed to have 10% of its rated capacity at the starting of the simulation at 6:00 am. Normal charging/discharging scenario was used. The battery bank was charged to full capacity during the day; and provided the house with power during the night. The battery bank energy storage and charging/discharging power are shown in Figure 68 (a) and (b).

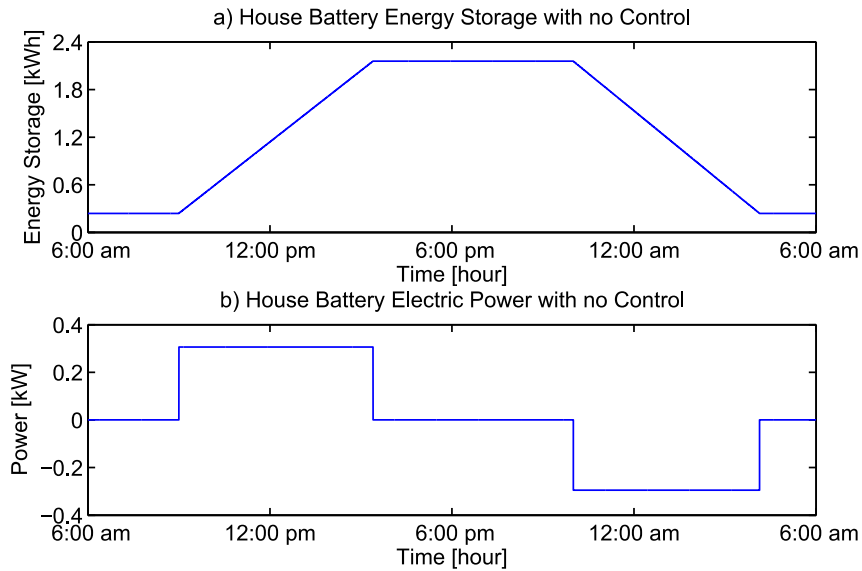
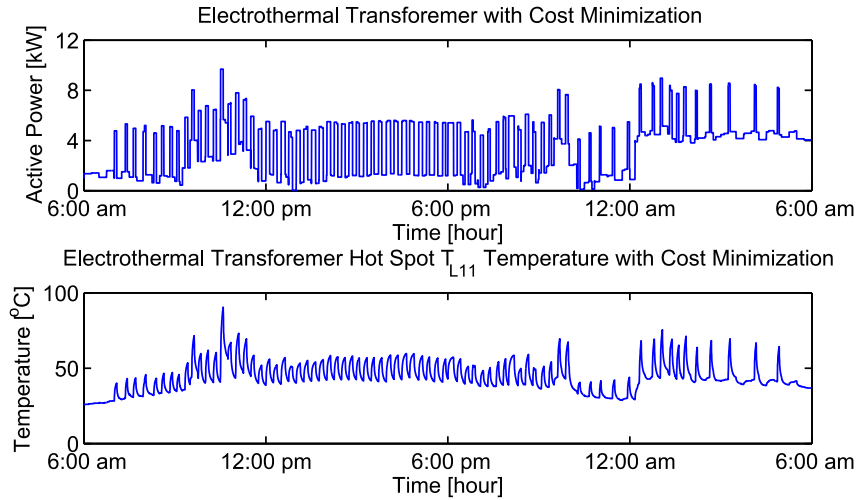


**Figure 68. House battery characteristics with no management system.**

#### **9.4 House Operation with Minimization of Customer's Total Energy Cost**

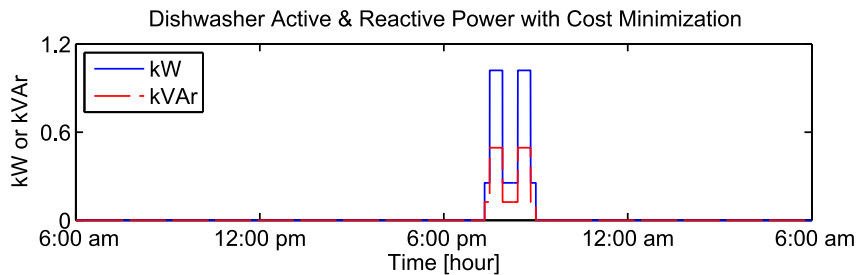
The section presents the simulation results of the system under study when the smart house energy management system is used. The objective of the house optimization model is to minimize the customer's total energy cost over one day. The optimization was performed every ten minutes for 24 hours. GUROBI program, the academic version 5.6.3 was used to solve the optimization problem [132]. The program implemented branch and bound algorithm and took about 4 minutes to solve the problems. The

distribution transformer active power is presented in the top of Figure 69. The peak transformer power was 9.69 kW, which is below the maximum allowed limit (10.0 kW) around 10:30 am. In the bottom of Figure 69 presents the transformer  $L_{11}$  hot spot temperature. The maximum temperature was 90.8 °C at 10:35 am, which is less than the temperature permissible limit.



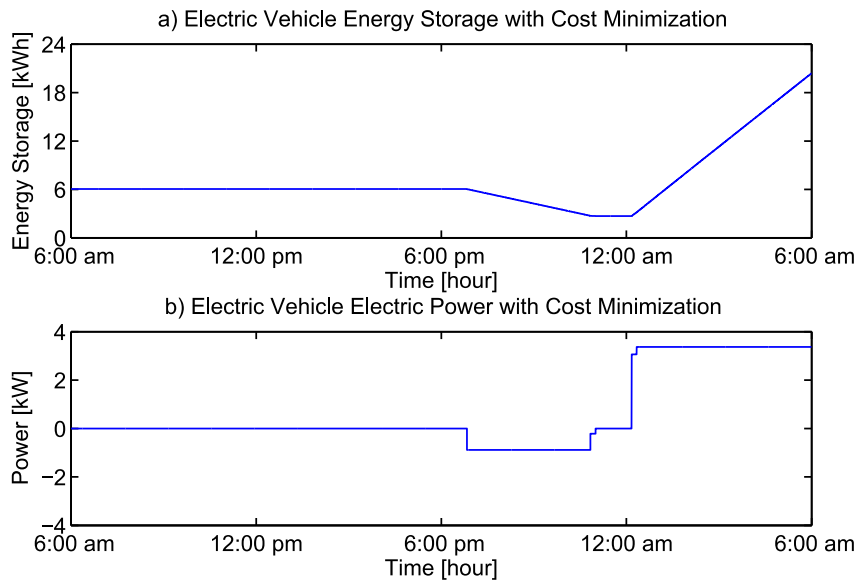
**Figure 69. Top: Transformer active power, Bottom: Transformer hot spot temperature with cost minimization.**

Figure 70 shows the dishwasher active and reactive power. It is shown that dishwasher operation was shifted and rescheduled to start at 7:20 pm. Also, it is shown that the dishwasher worked without interruption.



**Figure 70. Smart dishwasher active and reactive power with cost minimization.**

EV battery charging was originally scheduled to start as soon as it is connected to the house. However, with the smart house energy management system, EV charging/discharging time was intelligently rescheduled. The energy storage and rescheduled charging/discharging power of the EV battery are presented in Figure 71. By the deadline time, 6:00 am, the EV battery was charged up-to the maximum limit. Similarly, the management system used the house battery bank to reduce the cost over that day by rescheduling charging/discharging power as shown in Figure 72. It met the deadline with half the battery capacity was available to be used the next day.



**Figure 71. EV battery characteristics with cost minimization.**



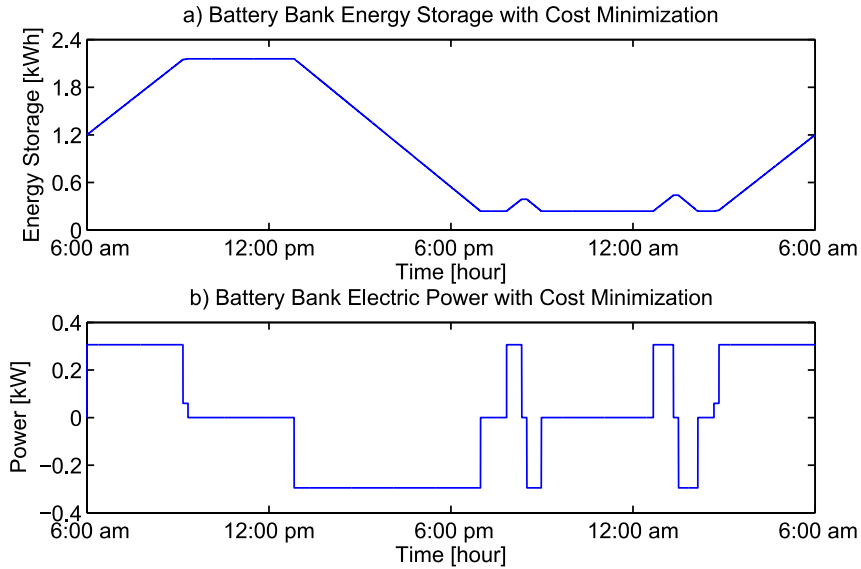


**Figure 72. House battery characteristics with cost minimization.**

The thermostat controller monitored bedroom<sub>1</sub> temperature during the day; and it provided a control signal to control the operation of the air conditioner. Bedroom<sub>1</sub> temperature and thermostat setting are shown in Figure 73 (a). Similarly, the refrigerator main compartment temperature and the refrigerator set temperature are shown in Figure 73 (b).

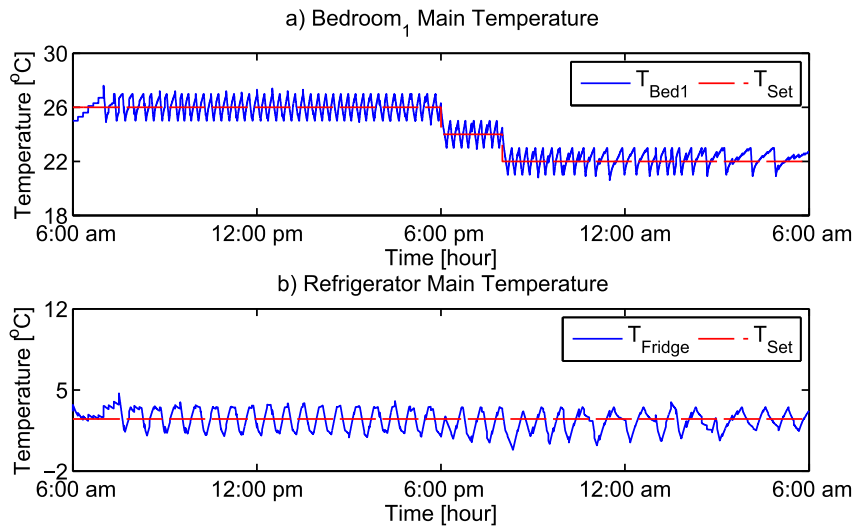
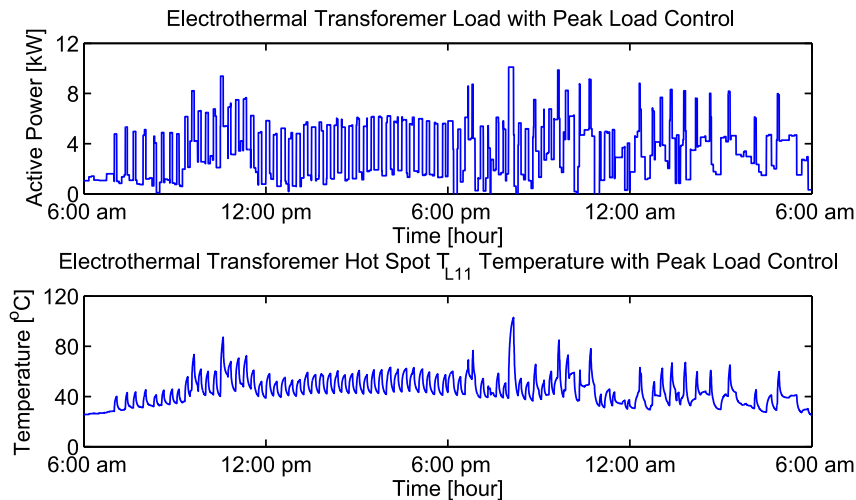


**Figure 73. Temperature at different locations of the house with cost minimization.**

The customer's total energy cost, for that day with the cost considered, was reduced by around 15%. Moreover, the peak demand and transformer hot temperature were reduced by 21.8% and 28.5%, respectively.

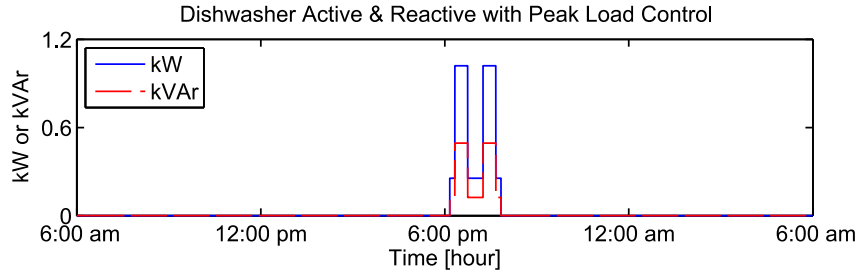
## 9.5 House Operation with Peak Load Control

This section presents the optimization results of the system under study when the smart house energy management system is used to provide peak load control over the planning period, a day. The optimization was performed every ten minutes for 24 hours using GUROBI program, the academic version 5.6.3 [132]. The distribution transformer active power is presented in the upper part of Figure 74. The peak transformer power was to 9.9 kW below the maximum allowed limit (10.0 kW) around 08:05 pm. The bottom part of Figure 74 presents the transformer  $L_{11}$  hot spot temperature. The maximum temperature was 103 °C at 08:10 pm.



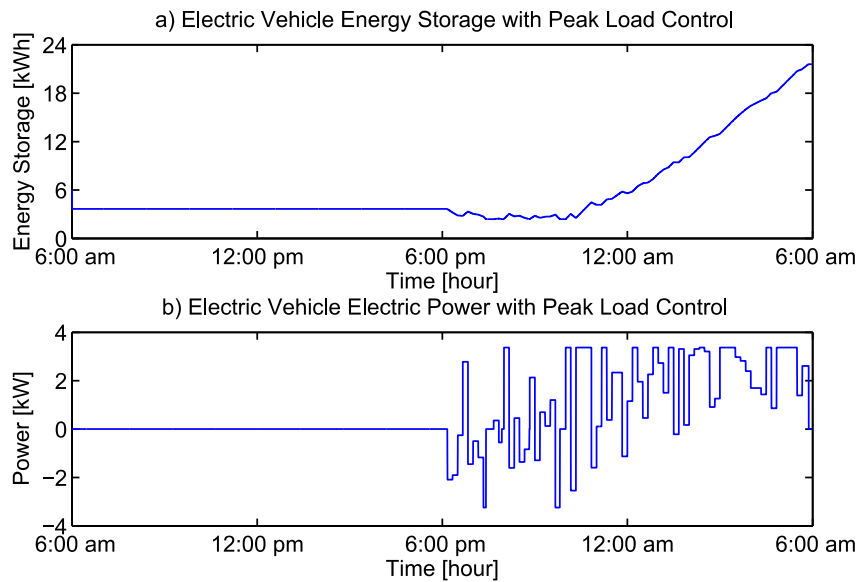
**Figure 74. Top: Transformer active power, Bottom: Transformer hot spot temperature with peak load control.**

Figure 75 shows the active and reactive power of the dishwasher. It is shown that the dishwasher was shifted to start at 6:10 pm; and it worked without interruption.



**Figure 75. Smart dishwasher active and reactive power with peak load control.**

The EV battery charging was originally scheduled to start as soon as it is connected to the house power circuit. But, with the smart house energy management system, the EV charging/discharging capabilities were used to levelize the peak load over the day. The energy storage and charging/discharging power of the EV battery are presented in Figure 76. By the deadline time, 6:00 am, the car battery was charged up-to the maximum limit, 90% of the rated capacity as shown in Figure 76 (a).



**Figure 76. Electric vehicle characteristics with peak load control.**

Similarly, the management system used the battery bank capability to levelize the house peak load by rescheduling charging/discharging power of the battery as shown in Figure 77. At the end of the day, the house battery had about 50% of its capacity.

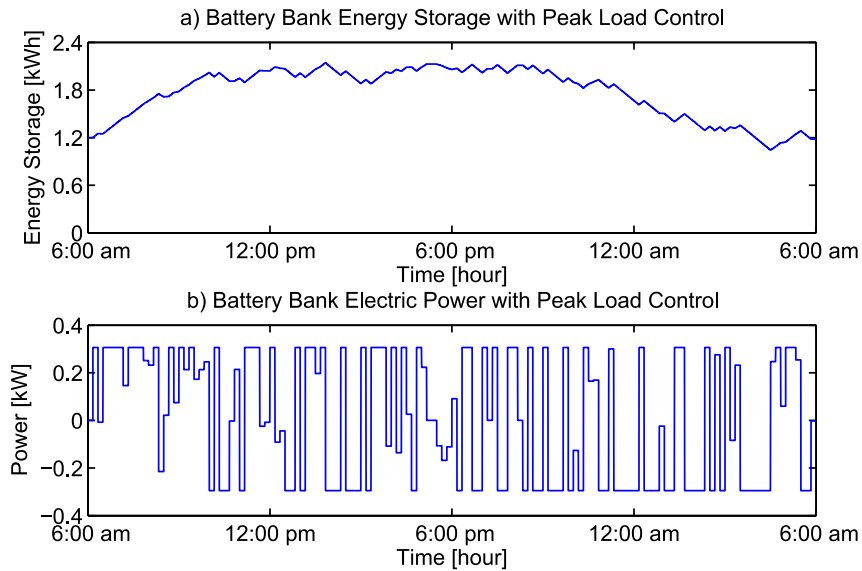


**Figure 77. House battery characteristics with peak load control.**

During this case, bedroom<sub>1</sub> temperature was maintained according to the customer setting temperature as shown in Figure 78 (a). Similarly, the refrigerator temperature was also maintained around the set temperature as shown in Figure 78 (b).

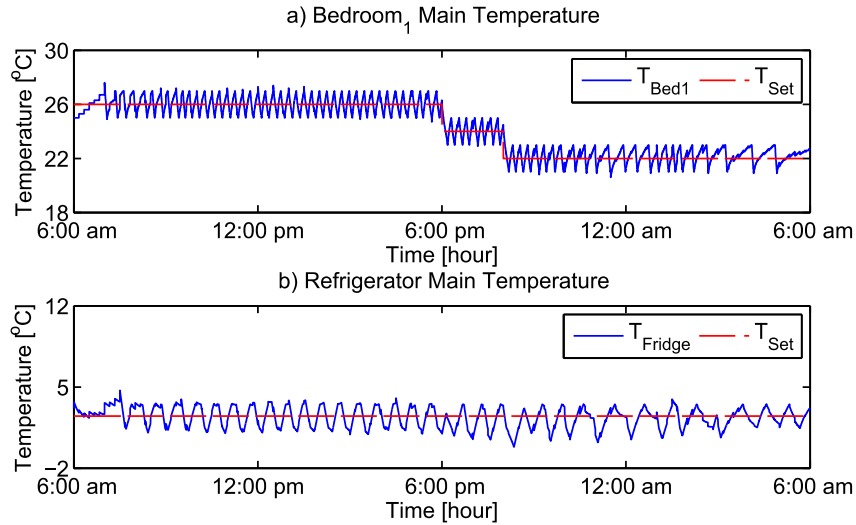


**Figure 78. Temperature at different locations of the house with peak load control.**

Over the planning period, the management system provided a house peak load control. The peak load was reduced by around 20%. Also, the peak transformer hot temperature was reduced by 18.9%.

## 9.6 Summary

In this Chapter, two examples are presented to demonstrate the smart house energy management system. Required data and information related to the house are provided in the first section. Then, a demonstrative case study of the system is presented to show the operation of the house without the smart house energy management system. This is followed by two examples when the smart house energy management system is used. First, a demonstrative case study of the smart house energy management system is presented to minimize the residential customer's total energy cost over the planning horizon. After that, a second demonstrative example of the smart house energy

management system is presented to provide peak load control of the customer over the planning horizon.

# 10 CONCLUSIONS, CONTRIBUTIONS, AND FUTURE RESEARCH DIRECTIONS

## 10.1 Conclusions

Large penetration of DERs and EVs/PHEVs on the power distribution grid is expected to take place in the near future. In addition, massive deployment of smart appliances is expected. Due to the expected penetration of EVs/PHEVs in particular, more stress is expected to occur on the power distribution system components. Nevertheless, the unfavorable impacts on the system can be averted with appropriate management and control of end user's resources including battery energy storages and smart appliances. Furthermore, smart utilization of these resources can alleviate the power distribution stresses and increase the reliability of the delivery system. This can be achieved by providing further important ancillary services such as control of peak load or reactive power support.

Toward that goal, a smart house energy management system was developed. The smart house energy management system can provide smart controls to the house controllable devices in order to mitigate unfavorable impacts resulting from integrating new loads, such as EV, and facilitate more integration of clean energy resources, such as solar PV, at a residential level. Furthermore, the smart house energy management system can maximize other benefits associated with house DERs and appliances for the good of utility and customer. All these functions are performed without inconvenience the customer and without overloading the distribution transformer, which elongates the service lifetime of the equipment.

The operation of the smart house energy management system requires an advanced house infrastructure. This advanced infrastructure continuously monitors the operation of the house and provides smart control functionality of the house controllable devices in such a way that the distribution transformer is not overloaded, thus avoiding unnecessary loss of service lifetime. At the same time, this advanced house infrastructure provides smart load management services to the utility. The major key components of the infrastructure are: physically based models of important components of the house, house DSE, and advanced house optimization model. Measurements gathered from various house energy resources and loads, distribution circuits, distribution transformer, switches, and other are collected by metering devices and sent to the house DSE to perform state estimation. The final result is a reliable real-time model of the house that is used by the smart house energy management system to perform optimization. Note that, the smart house energy management system can manage a commercial building as well, if the system components are appropriately sized.

Key components of the infrastructure were developed. Advanced house optimization model was developed for two different objective functions: 1) minimization of customer's total energy cost and 2) providing control of the house peak load. The optimization model includes the physical and operational system constraints, which ensure full customer convenience. The electrothermal model of the house, which is part of the optimization model, is constructed from house components such as center-tap distribution transformer, house air-conditioned spaces, house DERs, and house important appliances. These house important components were physically modeled with object oriented approach. This helped unifying the format of various house devices,



applications, and associated controls. Therefore, house system expansion with new loads can be handled easily. Quadratic integration method was implemented to convert models with differential equations into algebraic. All these models (in algebraic form) were then unified in a standard syntax, named SCAQCF format. House DSE was formulated to provide real-time model of the house before executing the optimization. The optimization model is MIQCP and solved after relaxation.  $\lambda$ -formulation technique was implemented to approximate all quadratic terms in the house optimization model. Also, MPC with receding horizon was implemented to optimally compute the house future control variables that optimize the house states trajectory.

Demonstrative case studies are provided to show transformer model characteristics and house operation under different conditions. Several case studies were developed to simulate a center-tap transformer. One study was developed to characterize the transformer model temperature signals rise time. For different transformer ratings, temperature waveforms rise time was found between 15-20 minutes. This amount of time is plenty for the smart house energy management system to provide transformer load management. Another case study was developed to compute the transformer LOIL. When the transformer load was peaked to 1.2 pu, the LOIL at that hour was estimated to be 0.004%. On the other hand, transformer LOIL was 0.029% when the peak load was 1.4 pu. This concludes that when the transformer load increase, transformer insulation deteriorates faster. Therefore, with better transformer load management, transformer service lifetime can be extended. Several demonstrative examples are presented for the house components. To show the response of the house components models during different environmental and loading conditions, house components models were

simulated for two days, July 1<sup>st</sup> and July 29<sup>th</sup> 2012. Another case study was developed to simulate the house operation when the house wall insulation was improved. When the house wall insulation was improved, the ambient temperature impact on the temperature inside the house was reduced. Therefore, the house air conditioner was found to work less frequently.

Two demonstrative case studies are presented to show proof of concept of the smart house energy management system. In both cases, the house has all models that were developed in this research including center-tap transformer, dishwasher, air conditioner, refrigerator, battery storages, and other. In both cases, three devices were controllable. These were dishwasher, EV battery, and house battery. First, the house operation was presented without a smart house energy management system. In this case, the transformer peak load was 12.4 kW and the transformer hot spot peak temperature was 127 °C. Both the load and temperature are above transformer permissible limits. The smart house energy management system was demonstrated on a house with two different objective functions: 1) minimization of the customer's total energy cost and 2) peak load control. The management system controls the house in a smart way that benefits both the utility and customer and works without inconvenience to the customer and without overloading/overheating the distribution transformer beyond permissible limits.

For the first objective function, the smart house energy management system shifted the dishwasher starting time from 5:00 pm to 7:20 pm, worked for 100 minutes, and was already finished by the deadline at 9:00 pm. Further, the smart house energy management system controlled EV and house batteries charging/discharging intelligently to achieve the minimum energy cost. EV was also fully charged by the deadline time at

6:00 am, which was set by the customer. Moreover, the transformer new peak load was 9.69 kW and the transformer new peak for the hot spot temperature was 90.8 °C.

To provide services to the utility, with an agreement with the customer, a second objective function was considered, which is to control the house peak load. In this case, the smart house energy management system moved the starting time of the dishwasher from 5:00 pm to 6:10 pm, worked for 100 minutes, and was already finished by the deadline at 9:00 pm. In addition, the smart house energy management system intelligently rescheduled charging/discharging of both EV and house batteries to levelize the transformer load. EV was also fully charged by the deadline time at 6:00 am, which was set by the customer. In this case, the transformer new peak load was 9.9 kW and the transformer new peak for the hot spot temperature was 103 °C.

## **10.2 Contributions**

This research provides the following contributions: 1) the development of an advanced house infrastructure that can provide real-time management and control of all components that are connected to a house, 2) the new formulation of the house energy management system optimization model in a way that benefits both the utility and customer, without inconvenience to the customer and without overloading or overheating the distribution transformer, 3) the development of physically based and detailed electrothermal model of a center-tap distribution transformer, and 4) the development of physically based and detailed electrothermal/electrical models of various house energy resources and controllable/non-controllable appliances including energy storage batteries, dishwasher, refrigerator, and air conditioner.

### 10.3 Future Research Directions

In this research, a smart house energy management system that provides real-time management and control of a house without inconvenient to the customer was developed. Several research extensions in every part of the house energy management system can be considered. Additional considerations that are a direct follow up to this current work could be to demonstrate the house management system with different environmental and loading conditions. This work was not done in this current research.

Several house appliances were modeled. However, some other important appliances were not modeled in detail such as washer, dryer, and water heater. Water heater usually consumes high energy. Therefore, developing an electrothermal model for it could improve the house system performance. Other appliances, such as washer, dryer, and range can be also modeled in detail, which were ignored in this current research.

The smart house energy management system can perform several functions. However, in this current research only two objective functions were implemented. A possible extension is to implement other objective functions such as maximization of reactive power support and system loss minimization.

The formulation of the house optimization model assumed that the only controllable components in the house are: dishwasher, EV battery, and house battery bank. Further, house appliances, such as air conditioner, washer, dryer, and water heater, can be considered controllable. Considering these appliances to be controllable by the smart house energy management system could lead to better optimization results, i.e. better saving and better load levelization.

The physical system under consideration in this research was one house that is fed by one distribution transformer. Another potential research direction is to let the smart house energy management system provides management and control for more than one house fed by one center-tap transformer. This extra consideration would give the management system extra controllable components that could lead to extra benefits.

Finally, the application of using the real-time model of the house, which is the outcome of the house DSE, is not limited to only optimization. Other advanced applications can be also implemented such as setting-less protection of the entire house. further, the real time model of the house can be synthesized with other house models that have the same time tag by an upper level management system, for example a distribution energy management system, to perform higher level applications such as optimizing the operation of the entire distribution feeder.

## Appendix A Object Oriented Modeling

### Appendix A.1 Mathematical Model in the Standard Form

The quadratized model of a device can have any combination of a differential equation part, linear part, and quadratic part. The differential equations involved the model can be cast in the following equations format

$$A_1 \begin{bmatrix} i(t) \\ 0 \end{bmatrix} + A_2 \frac{d}{dt} \begin{bmatrix} i(t) \\ 0 \end{bmatrix} = B_1 x(t) + B_2 \frac{dx(t)}{dt}, \quad (\text{A.1})$$

whereas the algebraic equations are cast in the below form

$$\begin{bmatrix} i(t) \\ 0 \end{bmatrix} = B_3 x(t) + \begin{bmatrix} x(t)^T F_{eq1} x(t) \\ x(t)^T F_{eq2} x(t) \\ \vdots \end{bmatrix} + K_{eq}, \quad (\text{A.2})$$

where

$$\begin{bmatrix} i(t) \\ 0 \end{bmatrix} = \begin{bmatrix} i_1(t) \\ i_2(t) \\ \vdots \\ 0 \\ 0 \\ \vdots \end{bmatrix}, \quad x(t) = \begin{bmatrix} x_1(t) \\ x_2(t) \\ \vdots \\ x_n(t) \end{bmatrix}$$

$i(t)$ : Vector defining the through variable of the model.

$x(t)$ : Vector defining the external and internal states of the model.

$n$ : Number of internal and external state variables

#### Differential equations:

$A_I$ : Identity matrix defining the linear part of the through variables with appropriate dimension.

$A_2$ : Matrix defining the coefficients of the differential part of the through variables with appropriate dimension.

$B_1$ : Matrix defining the linear part with appropriate dimension.

$B_2$ : Matrix defining the coefficients of the differential part with appropriate dimension.

**Algebraic equations:**

$B_3$ : Matrix defining the linear part with appropriate dimension.

$F_{eq}$ : Matrix defining the quadratic part with appropriate dimension.

$K_{eq}$ : Vector defining the constant part.

**Appendix A.2 Quadratic Integration Method**

The differential equations of the quadratized model that is cast in the form of (A.1) have to be integrated yielding to algebraic equations. The method used to perform the numerical integration is called Quadratic Integration. Simply, this method performs the integration over three points  $x(t-h)$ ,  $x(t_m)$ , and  $x(t)$  that defines a quadratic function in the interval  $[t-h, t]$ . Thus, when the function is integrated over time interval  $[t-h, t]$ , it yields

$$\begin{aligned} A_1 \left[ \frac{h}{6} i(t-h) + \frac{2h}{3} i(t_m) + \frac{h}{6} i(t) \right] + A_2 [i(t) - i(t-h)] \\ = B_1 \left[ \frac{h}{6} x(t-h) + \frac{2h}{3} x(t_m) + \frac{h}{6} x(t) \right] + B_2 [x(t) - x(t-h)] \end{aligned}$$

And when it is integrated over time interval  $[t-h, t_m]$ , it produces

$$\begin{aligned}
& A_1 \left[ \frac{5h}{24} i(t-h) + \frac{h}{3} i(t_m) - \frac{h}{24} i(t) \right] + A_2 [i(t_m) - i(t-h)] \\
& = B_1 \left[ \frac{5h}{24} x(t-h) + \frac{h}{3} x(t_m) - \frac{h}{24} x(t) \right] + B_2 [x(t_m) - x(t-h)]
\end{aligned}$$

Thus, by expressing the above two equations in one compact form, it yields

$$\begin{aligned}
& \begin{bmatrix} \frac{h}{6}A_1 + A_2 & 0 & \frac{2h}{3}A_1 & 0 \\ 0 & 0 & 0 & 0 \\ -\frac{h}{24}A_1 & 0 & \frac{h}{3}A_1 + A_2 & 0 \\ 0 & 0 & 0 & 0 \end{bmatrix} \begin{bmatrix} i(t) \\ 0 \\ i(t_m) \\ 0 \end{bmatrix} \\
& = \begin{bmatrix} \frac{h}{6}B_1 + B_2 & \frac{2h}{3}B_1 \\ -\frac{h}{24}B_1 & \frac{h}{3}B_1 + B_2 \end{bmatrix} \begin{bmatrix} x(t) \\ x(t_m) \end{bmatrix} - \begin{bmatrix} B_2 - \frac{h}{6}B_1 \\ B_2 - \frac{5h}{24}B_1 \end{bmatrix} [x(t-h)] \quad (\text{A.3}) \\
& - \begin{bmatrix} \frac{h}{6}A_1 - A_2 & 0 \\ 0 & 0 \\ \frac{5h}{24}A_1 - A_2 & 0 \\ 0 & 0 \end{bmatrix} \begin{bmatrix} i(t-h) \\ 0 \end{bmatrix},
\end{aligned}$$

By assigning the following:

$$D = \begin{bmatrix} \frac{h}{6}A_1 + A_2 & 0 & \frac{2h}{3}A_1 & 0 \\ 0 & 0 & 0 & 0 \\ -\frac{h}{24}A_1 & 0 & \frac{h}{3}A_1 + A_2 & 0 \\ 0 & 0 & 0 & 0 \end{bmatrix}$$

Since  $A_1$  is the identity matrix, sized according to the number of through variables in (A.1), and  $A_2$  can be assumed to be zero,  $E$  is the pseudo-inverse of  $D$ , which is given by



$$E = \begin{bmatrix} \frac{4}{h}I & 0 & -\frac{8}{h}I & 0 \\ 0 & I & 0 & 0 \\ \frac{1}{2h}I & 0 & \frac{2}{h}I & 0 \\ 0 & 0 & 0 & I \end{bmatrix}$$

Let:

$$F_1 = \begin{bmatrix} \frac{h}{6}B_1 + B_2 & \frac{2h}{3}B_1 \\ -\frac{h}{24}B_1 & \frac{h}{3}B_1 + B_2 \end{bmatrix}$$

$$F_2 = \begin{bmatrix} B_2 - \frac{h}{6}B_1 \\ B_2 - \frac{5h}{24}B_1 \end{bmatrix}$$

$$F_3 = \begin{bmatrix} \frac{h}{6}I & 0 \\ 0 & 0 \\ \frac{5h}{24}I & 0 \\ 0 & 0 \end{bmatrix}$$

Thus, the final form after the integration is performed can be written as the following

$$\begin{bmatrix} i(t) \\ 0 \\ i(t_m) \\ 0 \end{bmatrix} = E F_1 \begin{bmatrix} x(t) \\ x(t_m) \end{bmatrix} - b_{eq}, \quad (\text{A.4})$$

where

$$b_{eq} = E F_2[x(t-h)] + E F_3 \begin{bmatrix} i(t-h) \\ 0 \end{bmatrix}$$

### Appendix A.3 Final Form of AQCF and SCAQCF

Both forms shown in (A.2) and (A.4) are expressed in one matrix form as the following

$$\begin{bmatrix} i(t) \\ 0 \\ i(t_m) \\ 0 \end{bmatrix} = Y_{eq} \begin{bmatrix} x(t) \\ x(t_m) \end{bmatrix} + \begin{bmatrix} x(t)^T F_{eq1} x(t) \\ x(t)^T F_{eq2} x(t) \\ \vdots \\ x(t_m)^T F_{eq1} x(t_m) \\ x(t_m)^T F_{eq2} x(t_m) \\ \vdots \end{bmatrix} - b_{eq}, \quad (\text{A.5})$$

$$b_{eq} = \begin{bmatrix} b_1(t-h) \\ b_2(t-h) \end{bmatrix} = N_{eq} [x(t-h)] + M_{eq} \begin{bmatrix} i(t-h) \\ 0 \end{bmatrix} + K_{eq}, \quad (\text{A.6})$$

$$Y_{eq} = E F_1 + \begin{bmatrix} B_3 & 0 \\ 0 & B_3 \end{bmatrix}, \quad (\text{A.7})$$

$$N_{eq} = E F_2, \quad (\text{A.8})$$

$$M_{eq} = E F_3, \quad (\text{A.9})$$

where

$Y_{eq}$ : Matrix defining the linear part of the model.

$N_{eq}$ : Matrix defining the contribution from the previous time step states.

$M_{eq}$ : Matrix defining the contribution of the previous time step through variables.

$K_{eq}$ : Vector defining the constant part of the model.

### ***Appendix A.3.1 Matrices and Vectors Dimensions***

Assume that there are  $n$  state variables with  $n$  equations. Also, assume that there are  $m$  equations are differential equations for the through variables and  $(n-m)$  are algebraic equations. Therefore, the dimension of the matrices and vectors defining the AQCF is given by the below table:

$\begin{bmatrix} i(t) \\ 0 \end{bmatrix}$	(n by 1)	$x(t)$	(n by 1)	$D$	(2n by 2n)
$\begin{bmatrix} i(t_m) \\ 0 \end{bmatrix}$	(n by 1)	$x(t_m)$	(n by 1)	$Y_{eq}$	(2n by 2n)

$\begin{bmatrix} i(t-h) \\ 0 \end{bmatrix}$	(n by 1)	$x(t-h)$	(n by 1)	$N_{eq}$	(2n by n)
$B_1, B_2, B_3$	(n by n)	$E$	(2n by 2n)	$M_{eq}$	(2n by n)
$A_1$	$I(m \text{ by } m)$	$F_1$	(2n by 2n)	$K_{eq}$	(2n by 1)
		$F_2$	(2n by n)	$b_{eq}$	(2n by 1)
		$F_3$	(2n by n)	$F_{eq1}, F_{eq2}$	(n by n)

### Appendix A.3.2 Network Synthesis

At each node of the system, the connectivity constraints obtained from Kirchhoff's current law is applied. The solution of the network is then achieved at time  $t$  and  $t_m$ . To accomplish this, the set of internal device equations are appended yielding to the following expression

$$\sum_k A^k i^k(t) = 0, \quad (\text{A.10})$$

$$\sum_k A^k i^k(t_m) = 0, \quad (\text{A.11})$$

where

$i^k(t)$  is the device current injection from device  $k$  at time  $t$ .

$i^k(t_m)$  is the device current injection from device  $k$  at time  $t_m$ .

$A^k$  is the incident matrix given by

$$A_{ij}^k = \begin{cases} 1, & \text{if node } j \text{ of device } k \text{ is connected to node } i \\ 0, & \text{otherwise} \end{cases}$$

Similarly, the terminal voltage for each device  $v^k(t)$  is related to the constructed nodal voltage vector  $v(t)$ . This can be mathematically expressed by

$$v^k(t) = A^k I v(t), \quad (\text{A.12})$$

where

$I$ : a 2 by 2 identity matrix.

The device currents in the system of equations expressed by the final AQCF in (A.5) are eliminated with the use of equation (A.10) and (A.11). The resulted set of equations is only in terms of the external and internal state variables. Thus, the set of equations can be expressed by the following format

$$g(x(t), x(t_m)) = Y_{eq} \begin{bmatrix} x(t) \\ x(t_m) \end{bmatrix} + \begin{bmatrix} x(t)^T F_{eq1} x(t) \\ x(t)^T F_{eq2} x(t) \\ \vdots \\ x(t_m)^T F_{eq1} x(t_m) \\ x(t_m)^T F_{eq2} x(t_m) \\ \vdots \end{bmatrix} - b_{eq} = 0.0 \quad (\text{A.13})$$

### **Appendix A.3.3 Network Solver**

The system of equations represented by (A.13) is solved using Newton's method. This method is particularly chosen because it is ideally suited for the solution of quadratic equations. Specifically, the solution is given by the following expression

$$\begin{bmatrix} x^{v+1}(t) \\ x^{v+1}(t_m) \end{bmatrix} = \begin{bmatrix} x^v(t) \\ x^v(t_m) \end{bmatrix} - J_g^{-1} \left[ Y_{eq} \begin{bmatrix} x^v(t) \\ x^v(t_m) \end{bmatrix} + \begin{bmatrix} (x^v(t))^T F_{eq1} x^v(t) \\ (x^v(t))^T F_{eq2} x^v(t) \\ \vdots \\ (x^v(t_m))^T F_{eq1} x^v(t_m) \\ (x^v(t_m))^T F_{eq2} x^v(t_m) \\ \vdots \end{bmatrix} - b_{eq} \right], \quad (\text{A.14})$$

where  $v$  is the iteration step number,  $b_{eq}$  is the contribution from the previous time step given by (A.6) and  $J_g$  is the Jacobian matrix of equation (A.14). Particularly, the Jacobian matrix takes the following form

$$J_g = Y_{eq} + \begin{bmatrix} (x^v(t))^T (F_{eq1} + F_{eq1}^T) \\ (x^v(t))^T (F_{eq2} + F_{eq2}^T) \\ \vdots \\ (x^v(t_m))^T (F_{eq1} + F_{eq1}^T) \\ (x^v(t_m))^T (F_{eq2} + F_{eq2}^T) \\ \vdots \end{bmatrix}. \quad (\text{A.15})$$

Note that the SCAQCF form of the model can be easily deduced from the AQCF form.

#### **Appendix A.3.4 Quadratic and Trapezoidal Integration Case Study**

The RLC circuit that was used in the simulation is shown in Figure 79. Circuit parameters are tabulated in Table 23. The results of the simulation of the capacitor voltage and inductor current are shown in Figure 80 and Figure 81, respectively. The absolute error of the circuit inductor current for the trapezoidal and quadratic integration methods, compared to the analytical solution is shown in Figure 82. The vertical axis is logarithmic scale. In this particular case, the quadratic integration method is found to be almost three orders of magnitude more accurate than the trapezoidal method.

**Table 23. RLC circuit parameters.**

$R = 1 \Omega$	$L = 10 \text{ mH}$	$C = 20 \mu\text{F}$
Simulation time = 0.1 sec	Time step (h) = 1 $\mu\text{sec}$	$V=110\sqrt{2}\sin(120\pi t)$

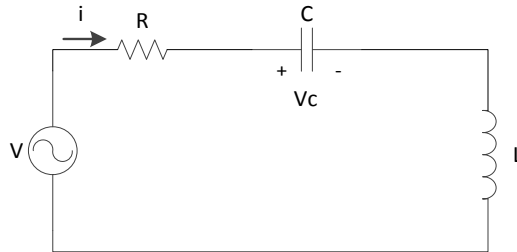


**Figure 79. Series RLC circuit.**

Time domain model of the circuit

$$\frac{dv_c(t)}{dt} = \frac{1}{C}i(t), \quad (\text{A.16})$$

$$\frac{di(t)}{dt} = -\frac{1}{L}v_c(t) - \frac{R}{L}i(t) + \frac{1}{L}(10\sqrt{3}\sin(120\pi t)). \quad (\text{A.17})$$

The time domain equations are formulated in the standard format and then quadratized as necessary as the following

$$0.0 = \frac{dv_c(t)}{dt} - \frac{1}{C}i(t), \quad (\text{A.18})$$

$$0.0 = \frac{di(t)}{dt} - x_1(t), \quad (\text{A.19})$$

$$0.0 = x_1(t) + \frac{1}{L}v_c(t) + \frac{R}{L}i(t) - \frac{1}{L}(110\sqrt{2}\sin(120\pi t)). \quad (\text{A.20})$$

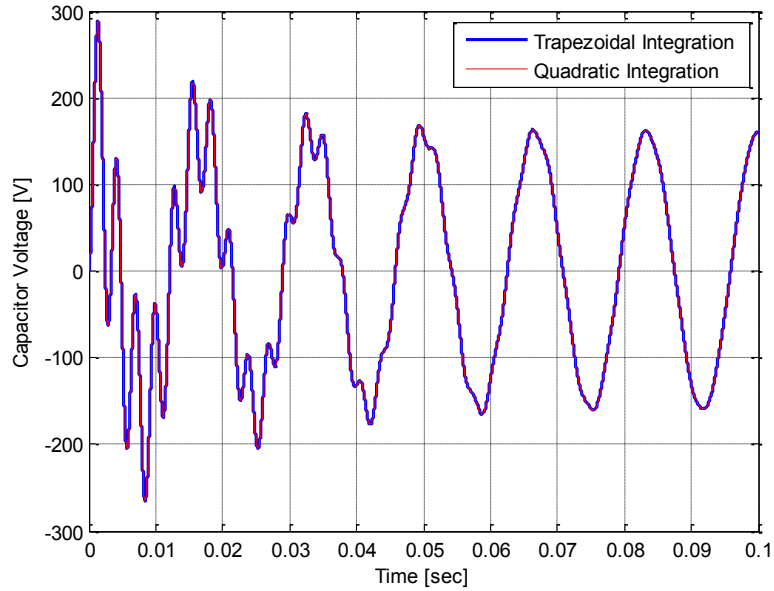
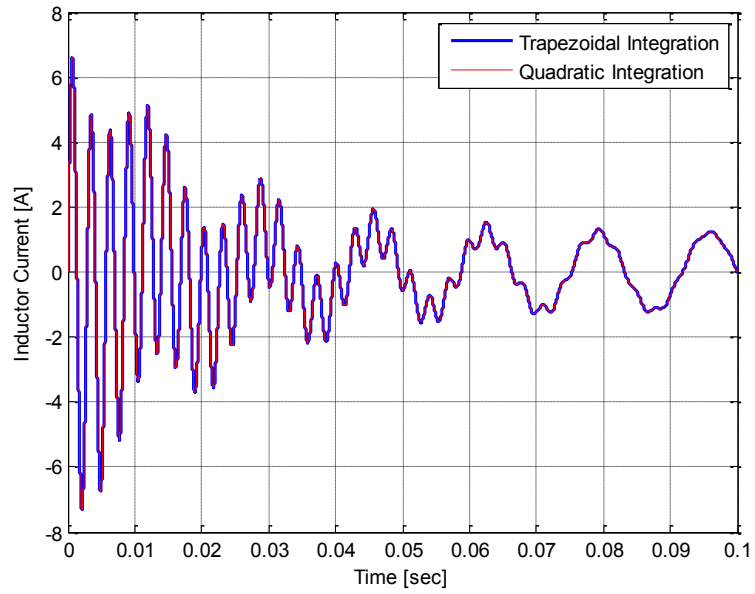
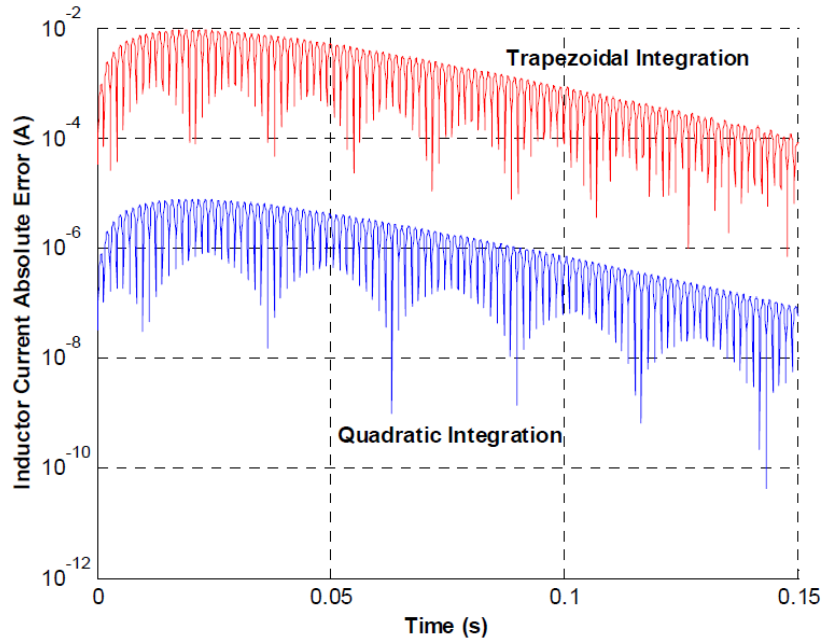


Figure 80. Capacitor voltage waveform.



**Figure 81. Inductor current waveform.**



**Figure 82. Absolute error of the inductor current between the analytic solution and trapezoidal and quadratic integration methods [108].**

## *Appendix B Single Phase Center-Tap Transformer Model*

### **Appendix B.1 Mathematical Model**

The mathematical model of the distribution transformer is presented in this appendix. First, the electrical model is discussed, and then the thermal model is provided. It should be noted that the model of the transformer is in the quasi-dynamic domain.

#### *Appendix B.1.1 Electrical Model*

Model equations of a single phase center-tap distribution transformer are given by the following equations

$$\tilde{I}_1 = Y_1 \tilde{V}_1 - Y_1 \tilde{V}_2 - Y_1 \tilde{E} \quad (\text{B.1})$$

$$\tilde{I}_2 = -\tilde{I}_1 \quad (\text{B.2})$$

$$\tilde{I}_{L1} = Y_2 \tilde{V}_{L1} - Y_2 \tilde{V}_{NN} - \frac{t}{2} Y_2 \tilde{E} \quad (\text{B.3})$$

$$\tilde{I}_{NN} = -(\tilde{I}_{L1} + \tilde{I}_{L2}) \quad (\text{B.4})$$

$$\tilde{I}_{L2} = -Y_2 \tilde{V}_{NN} + Y_2 \tilde{V}_{L2} + \frac{t}{2} Y_2 \tilde{E} \quad (\text{B.5})$$

$$0.0 = -Y_1 \tilde{V}_1 + Y_1 \tilde{V}_2 - \frac{t}{2} Y_2 \tilde{V}_{L1} + \frac{t}{2} Y_2 \tilde{V}_{L2} + (Y_m + Y_1 + \frac{t^2}{2} Y_2) \tilde{E} \quad (\text{B.6})$$

#### *Appendix B.1.2 Thermal Model*

The model equations of the thermal model of a single phase center-tap transformer are given by the following set of equations



$$\begin{aligned}
\dot{q}_{caseT} = & C_{TOT} \frac{d}{dt} (\theta_{CaseT} - \theta_{TOT}) + C_{CaseT} \frac{d}{dt} (\theta_{CaseT} - \theta_{amb}) \\
& + G_{h1-CaseT} (\theta_{CaseT} - \theta_{h1}) + G_{h2-CaseT} (\theta_{CaseT} - \theta_{h2}) \\
& + G_{h3-CaseT} (\theta_{CaseT} - \theta_{h3}) + G_{L11-CaseT} (\theta_{CaseT} - \theta_{L11}) \\
& + G_{L12-CaseT} (\theta_{CaseT} - \theta_{L12}) + G_{L13-CaseT} (\theta_{CaseT} - \theta_{L13}) \\
& + G_{L21-CaseT} (\theta_{CaseT} - \theta_{L21}) + G_{L22-CaseT} (\theta_{CaseT} - \theta_{L22}) \\
& + G_{L23-CaseT} (\theta_{CaseT} - \theta_{L23}) + G_{CT-CaseT} (\theta_{CaseT} - \theta_{CT}) \\
& + G_{CB-CaseT} (\theta_{CaseT} - \theta_{CB}) + G_{CR-CaseT} (\theta_{CaseT} - \theta_{CR}) \\
& + G_{CL-CaseT} (\theta_{CaseT} - \theta_{CL}) + G_{TOT-CaseT} (\theta_{CaseT} - \theta_{TOT}) \\
& + G_{BOT-CaseT} (\theta_{CaseT} - \theta_{BOT}) + G_{ROT-CaseT} (\theta_{CaseT} - \theta_{ROT}) \\
& + G_{LOT-CaseT} (\theta_{CaseT} - \theta_{LOT}) + G_{CaseT-CaseB} (\theta_{CaseT} - \theta_{CaseB}) \\
& + G_{CaseT-CaseR} (\theta_{CaseT} - \theta_{CaseR}) + G_{CaseT-CaseL} (\theta_{CaseT} - \theta_{CaseL}) \\
& + G_{CaseT-amb} (\theta_{CaseT} - \theta_{amb})
\end{aligned} \tag{B.7}$$

$$\begin{aligned}
\dot{q}_{caseB} = & C_{TOB} \frac{d}{dt} (\theta_{CaseB} - \theta_{BOT}) + C_{CaseB} \frac{d}{dt} (\theta_{CaseB} - \theta_{amb}) \\
& + G_{h1-CaseB} (\theta_{CaseB} - \theta_{h1}) + G_{h2-CaseB} (\theta_{CaseB} - \theta_{h2}) \\
& + G_{h3-CaseB} (\theta_{CaseB} - \theta_{h3}) + G_{L11-CaseB} (\theta_{CaseB} - \theta_{L11}) \\
& + G_{L12-CaseB} (\theta_{CaseB} - \theta_{L12}) + G_{L13-CaseB} (\theta_{CaseB} - \theta_{L13}) \\
& + G_{L21-CaseB} (\theta_{CaseB} - \theta_{L21}) + G_{L22-CaseB} (\theta_{CaseB} - \theta_{L22}) \\
& + G_{L23-CaseB} (\theta_{CaseB} - \theta_{L23}) + G_{CT-CaseB} (\theta_{CaseB} - \theta_{CT}) \\
& + G_{CB-CaseB} (\theta_{CaseB} - \theta_{CB}) + G_{CR-CaseB} (\theta_{CaseB} - \theta_{CR}) \\
& + G_{CL-CaseB} (\theta_{CaseB} - \theta_{CL}) + G_{TOT-CaseB} (\theta_{CaseB} - \theta_{TOT}) \\
& + G_{BOT-CaseB} (\theta_{CaseB} - \theta_{BOT}) + G_{ROT-CaseB} (\theta_{CaseB} - \theta_{ROT}) \\
& + G_{LOT-CaseB} (\theta_{CaseB} - \theta_{LOT}) + G_{CaseT-CaseB} (\theta_{CaseB} - \theta_{CaseT}) \\
& + G_{CaseB-CaseR} (\theta_{CaseB} - \theta_{CaseR}) + G_{CaseB-CaseL} (\theta_{CaseB} - \theta_{CaseL}) \\
& + G_{CaseB-amb} (\theta_{CaseB} - \theta_{amb})
\end{aligned} \tag{B.8}$$

$$\begin{aligned}
\dot{\theta}_{caseR} = & C_{ROT} \frac{d}{dt} (\theta_{CaseR} - \theta_{ROT}) + C_{CaseR} \frac{d}{dt} (\theta_{CaseR} - \theta_{amb}) \\
& + G_{h1-CaseR} (\theta_{CaseR} - \theta_{h1}) + G_{h2-CaseR} (\theta_{CaseR} - \theta_{h2}) \\
& + G_{h3-CaseR} (\theta_{CaseR} - \theta_{h3}) + G_{L11-CaseR} (\theta_{CaseR} - \theta_{L11}) \\
& + G_{L12-CaseR} (\theta_{CaseR} - \theta_{L12}) + G_{L13-CaseR} (\theta_{CaseR} - \theta_{L13}) \\
& + G_{L21-CaseR} (\theta_{CaseR} - \theta_{L21}) + G_{L22-CaseR} (\theta_{CaseR} - \theta_{L22}) \\
& + G_{L23-CaseR} (\theta_{CaseR} - \theta_{L23}) + G_{CT-CaseR} (\theta_{CaseR} - \theta_{CT}) \\
& + G_{CB-CaseR} (\theta_{CaseR} - \theta_{CB}) + G_{CR-CaseR} (\theta_{CaseR} - \theta_{CR}) \\
& + G_{CL-CaseR} (\theta_{CaseR} - \theta_{CL}) + G_{TOT-CaseR} (\theta_{CaseR} - \theta_{TOT}) \\
& + G_{BOT-CaseR} (\theta_{CaseR} - \theta_{BOT}) + G_{ROT-CaseR} (\theta_{CaseR} - \theta_{ROT}) \\
& + G_{LOT-CaseR} (\theta_{CaseR} - \theta_{LOT}) + G_{CaseT-CaseR} (\theta_{CaseR} - \theta_{CaseT}) \\
& + G_{CaseB-CaseR} (\theta_{CaseR} - \theta_{CaseB}) + G_{CaseR-CaseL} (\theta_{CaseR} - \theta_{CaseL}) \\
& + G_{CaseR-amb} (\theta_{CaseR} - \theta_{amb})
\end{aligned} \tag{B.9}$$

$$\begin{aligned}
\dot{\theta}_{caseL} = & C_{LOT} \frac{d}{dt} (\theta_{CaseL} - \theta_{LOT}) + C_{CaseL} \frac{d}{dt} (\theta_{CaseL} - \theta_{amb}) \\
& + G_{h1-CaseL} (\theta_{CaseL} - \theta_{h1}) + G_{h2-CaseL} (\theta_{CaseL} - \theta_{h2}) \\
& + G_{h3-CaseL} (\theta_{CaseL} - \theta_{h3}) + G_{L11-CaseL} (\theta_{CaseL} - \theta_{L11}) \\
& + G_{L12-CaseL} (\theta_{CaseL} - \theta_{L12}) + G_{L13-CaseL} (\theta_{CaseL} - \theta_{L13}) \\
& + G_{L21-CaseL} (\theta_{CaseL} - \theta_{L21}) + G_{L22-CaseL} (\theta_{CaseL} - \theta_{L22}) \\
& + G_{L23-CaseL} (\theta_{CaseL} - \theta_{L23}) + G_{CT-CaseL} (\theta_{CaseL} - \theta_{CT}) \\
& + G_{CB-CaseL} (\theta_{CaseL} - \theta_{CB}) + G_{CR-CaseL} (\theta_{CaseL} - \theta_{CR}) \\
& + G_{CL-CaseL} (\theta_{CaseL} - \theta_{CL}) + G_{TOT-CaseL} (\theta_{CaseL} - \theta_{TOT}) \\
& + G_{BOT-CaseL} (\theta_{CaseL} - \theta_{BOT}) + G_{ROT-CaseL} (\theta_{CaseL} - \theta_{ROT}) \\
& + G_{LOT-CaseL} (\theta_{CaseL} - \theta_{LOT}) + G_{CaseT-CaseL} (\theta_{CaseL} - \theta_{CaseT}) \\
& + G_{CaseB-CaseL} (\theta_{CaseL} - \theta_{CaseB}) + G_{CaseR-CaseL} (\theta_{CaseL} - \theta_{CaseR}) \\
& + G_{CaseL-amb} (\theta_{CaseL} - \theta_{amb})
\end{aligned} \tag{B.10}$$

$$\begin{aligned}
\dot{q}_{amb} = & C_{CaseT} \frac{d}{dt} (\theta_{amb} - \theta_{CaseT}) + C_{CaseB} \frac{d}{dt} (\theta_{amb} - \theta_{CaseB}) \\
& + C_{CaseR} \frac{d}{dt} (\theta_{amb} - \theta_{CaseR}) + C_{CaseL} \frac{d}{dt} (\theta_{amb} - \theta_{CaseL}) + \dot{Q}_{h1} \\
& + \dot{Q}_{h2} + \dot{Q}_{h3} + \dot{Q}_{L11} + \dot{Q}_{L12} + \dot{Q}_{L13} + \dot{Q}_{L21} + \dot{Q}_{L22} + \dot{Q}_{L23} + \dot{Q}_{CT} \\
& + \dot{Q}_{CB} + \dot{Q}_{CR} + \dot{Q}_{CL} + G_{CaseT-amb} (\theta_{amb} - \theta_{CaseT}) \\
& + G_{CaseB-amb} (\theta_{amb} - \theta_{CaseB}) + G_{CaseR-amb} (\theta_{amb} - \theta_{CaseR}) \\
& + G_{CaseL-amb} (\theta_{amb} - \theta_{CaseL})
\end{aligned} \tag{B.11}$$

$$\begin{aligned}
\dot{Q}_{h1} = & C_{h1} \frac{d}{dt} (\theta_{h1} - \theta_{CT}) + G_{h1-h2} (\theta_{h1} - \theta_{h2}) + G_{h1-h3} (\theta_{h1} - \theta_{h3}) + G_{h1-L11} (\theta_{h1} \\
& - \theta_{L11}) + G_{h1-L12} (\theta_{h1} - \theta_{L12}) + G_{h1-L13} (\theta_{h1} - \theta_{L13}) \\
& + G_{h1-L21} (\theta_{h1} - \theta_{L21}) + G_{h1-L22} (\theta_{h1} - \theta_{L22}) + G_{h1-L23} (\theta_{h1} \\
& - \theta_{L23}) + G_{h1-CT} (\theta_{h1} - \theta_{CT}) + G_{h1-CB} (\theta_{h1} - \theta_{CB}) + G_{h1-CR} (\theta_{h1} \\
& - \theta_{CR}) + G_{h1-CL} (\theta_{h1} - \theta_{CL}) + G_{h1-TOT} (\theta_{h1} - \theta_{TOT}) + G_{h1-BOT} (\theta_{h1} \\
& - \theta_{BOT}) + G_{h1-ROT} (\theta_{h1} - \theta_{ROT}) + G_{h1-LOT} (\theta_{h1} - \theta_{LOT}) \\
& + G_{h1-CaseT} (\theta_{h1} - \theta_{CaseT}) + G_{h1-CaseB} (\theta_{h1} - \theta_{CaseB}) \\
& + G_{h1-CaseR} (\theta_{h1} - \theta_{CaseR}) + G_{h1-CaseL} (\theta_{h1} - \theta_{CaseL})
\end{aligned} \tag{B.12}$$

$$\begin{aligned}
\dot{Q}_{h2} = & C_{h2} \frac{d}{dt} (\theta_{h2} - \theta_{CL}) + G_{h1-h2} (\theta_{h2} - \theta_{h1}) + G_{h2-h3} (\theta_{h2} - \theta_{h3}) + G_{h2-L11} (\theta_{h2} \\
& - \theta_{L11}) + G_{h2-L12} (\theta_{h2} - \theta_{L12}) + G_{h2-L13} (\theta_{h2} - \theta_{L13}) \\
& + G_{h2-L21} (\theta_{h2} - \theta_{L21}) + G_{h2-L22} (\theta_{h2} - \theta_{L22}) + G_{h2-L23} (\theta_{h2} \\
& - \theta_{L23}) + G_{h2-CT} (\theta_{h2} - \theta_{CT}) + G_{h2-CB} (\theta_{h2} - \theta_{CB}) + G_{h2-CR} (\theta_{h2} \\
& - \theta_{CR}) + G_{h2-CL} (\theta_{h2} - \theta_{CL}) + G_{h2-TOT} (\theta_{h2} - \theta_{TOT}) + G_{h2-BOT} (\theta_{h2} \\
& - \theta_{BOT}) + G_{h2-ROT} (\theta_{h2} - \theta_{ROT}) + G_{h2-LOT} (\theta_{h2} - \theta_{LOT}) \\
& + G_{h2-CaseT} (\theta_{h2} - \theta_{CaseT}) + G_{h2-CaseB} (\theta_{h2} - \theta_{CaseB}) \\
& + G_{h2-CaseR} (\theta_{h2} - \theta_{CaseR}) + G_{h2-CaseL} (\theta_{h2} - \theta_{CaseL})
\end{aligned} \tag{B.13}$$

$$\begin{aligned}
\dot{Q}_{h3} = & C_{h3} \frac{d}{dt} (\theta_{h3} - \theta_{CB}) + G_{h1-h3} (\theta_{h3} - \theta_{h1}) + G_{h2-h3} (\theta_{h3} - \theta_{h2}) + G_{h3-L11} (\theta_{h3} \\
& - \theta_{L11}) + G_{h3-L12} (\theta_{h3} - \theta_{L12}) + G_{h3-L13} (\theta_{h3} - \theta_{L13}) \\
& + G_{h3-L21} (\theta_{h3} - \theta_{L21}) + G_{h3-L22} (\theta_{h3} - \theta_{L22}) + G_{h3-L23} (\theta_{h3} \\
& - \theta_{L23}) + G_{h3-CT} (\theta_{h3} - \theta_{CT}) + G_{h3-CB} (\theta_{h3} - \theta_{CB}) + G_{h3-CR} (\theta_{h3} \\
& - \theta_{CR}) + G_{h3-CL} (\theta_{h3} - \theta_{CL}) + G_{h3-TOT} (\theta_{h3} - \theta_{TOT}) + G_{h3-BOT} (\theta_{h3} \\
& - \theta_{BOT}) + G_{h3-ROT} (\theta_{h3} - \theta_{ROT}) + G_{h3-LOT} (\theta_{h3} - \theta_{LOT}) \\
& + G_{h3-CaseT} (\theta_{h3} - \theta_{CaseT}) + G_{h3-CaseB} (\theta_{h3} - \theta_{CaseB}) \\
& + G_{h3-CaseR} (\theta_{h3} - \theta_{CaseR}) + G_{h3-CaseL} (\theta_{h3} - \theta_{CaseL})
\end{aligned} \tag{B.14}$$

$$\begin{aligned}
\dot{Q}_{L11} = & C_{L11} \frac{d}{dt} (\theta_{L11} - \theta_{CT}) + G_{h1-L11} (\theta_{L11} - \theta_{h1}) + G_{h2-L11} (\theta_{L11} - \theta_{h2}) \\
& + G_{h3-L11} (\theta_{L11} - \theta_{h3}) + G_{L11-L12} (\theta_{L11} - \theta_{L12}) \\
& + G_{L11-L13} (\theta_{L11} - \theta_{L13}) + G_{L11-L21} (\theta_{L11} - \theta_{L21}) \\
& + G_{L11-L22} (\theta_{L11} - \theta_{L22}) + G_{L11-L23} (\theta_{L11} - \theta_{L23}) \\
& + G_{L11-CT} (\theta_{L11} - \theta_{CT}) + G_{L11-CB} (\theta_{L11} - \theta_{CB}) \\
& + G_{L11-CR} (\theta_{L11} - \theta_{CR}) + G_{L11-CL} (\theta_{L11} - \theta_{CL}) \\
& + G_{L11-TOT} (\theta_{L11} - \theta_{TOT}) + G_{L11-BOT} (\theta_{L11} - \theta_{BOT}) \\
& + G_{L11-ROT} (\theta_{L11} - \theta_{ROT}) + G_{L11-LOT} (\theta_{L11} - \theta_{LOT}) \\
& + G_{L11-CaseT} (\theta_{L11} - \theta_{CaseT}) + G_{L11-CaseB} (\theta_{L11} - \theta_{CaseB}) \\
& + G_{L11-CaseR} (\theta_{L11} - \theta_{CaseR}) + G_{L11-CaseL} (\theta_{L11} - \theta_{CaseL})
\end{aligned} \tag{B.15}$$

$$\begin{aligned}
\dot{Q}_{L12} = C_{L12} \frac{d}{dt} & (\theta_{L12} - \theta_{CR}) + G_{h1-L12}(\theta_{L12} - \theta_{h1}) + G_{h2-L12}(\theta_{L12} - \theta_{h2}) \\
& + G_{h3-L12}(\theta_{L12} - \theta_{h3}) + G_{L11-L12}(\theta_{L12} - \theta_{L11}) \\
& + G_{L12-L13}(\theta_{L12} - \theta_{L13}) + G_{L12-L21}(\theta_{L12} - \theta_{L21}) \\
& + G_{L12-L22}(\theta_{L12} - \theta_{L22}) + G_{L12-L23}(\theta_{L12} - \theta_{L23}) \\
& + G_{L12-CT}(\theta_{L12} - \theta_{CT}) + G_{L12-CB}(\theta_{L12} - \theta_{CB}) \\
& + G_{L12-CR}(\theta_{L12} - \theta_{CR}) + G_{L12-CL}(\theta_{L12} - \theta_{CL}) \\
& + G_{L12-TOT}(\theta_{L12} - \theta_{TOT}) + G_{L12-BOT}(\theta_{L12} - \theta_{BOT}) \\
& + G_{L12-ROT}(\theta_{L12} - \theta_{ROT}) + G_{L12-LOT}(\theta_{L12} - \theta_{LOT}) \\
& + G_{L12-CaseT}(\theta_{L12} - \theta_{CaseT}) + G_{L12-CaseB}(\theta_{L12} - \theta_{CaseB}) \\
& + G_{L12-CaseR}(\theta_{L12} - \theta_{CaseR}) + G_{L12-CaseL}(\theta_{L12} - \theta_{CaseL})
\end{aligned} \tag{B.16}$$

$$\begin{aligned}
\dot{Q}_{L13} = C_{L13} \frac{d}{dt} & (\theta_{L13} - \theta_{CR}) + G_{h1-L13}(\theta_{L13} - \theta_{h1}) + G_{h2-L13}(\theta_{L13} - \theta_{h2}) \\
& + G_{h3-L13}(\theta_{L13} - \theta_{h3}) + G_{L11-L13}(\theta_{L13} - \theta_{L11}) \\
& + G_{L12-L13}(\theta_{L13} - \theta_{L12}) + G_{L13-L21}(\theta_{L13} - \theta_{L21}) \\
& + G_{L13-L22}(\theta_{L13} - \theta_{L22}) + G_{L13-L23}(\theta_{L13} - \theta_{L23}) \\
& + G_{L13-CT}(\theta_{L13} - \theta_{CT}) + G_{L13-CB}(\theta_{L13} - \theta_{CB}) \\
& + G_{L13-CR}(\theta_{L13} - \theta_{CR}) + G_{L13-CL}(\theta_{L13} - \theta_{CL}) \\
& + G_{L13-TOT}(\theta_{L13} - \theta_{TOT}) + G_{L13-BOT}(\theta_{L13} - \theta_{BOT}) \\
& + G_{L13-ROT}(\theta_{L13} - \theta_{ROT}) + G_{L13-LOT}(\theta_{L13} - \theta_{LOT}) \\
& + G_{L13-CaseT}(\theta_{L13} - \theta_{CaseT}) + G_{L13-CaseB}(\theta_{L13} - \theta_{CaseB}) \\
& + G_{L13-CaseR}(\theta_{L13} - \theta_{CaseR}) + G_{L13-CaseL}(\theta_{L13} - \theta_{CaseL})
\end{aligned} \tag{B.17}$$

$$\begin{aligned}
\dot{Q}_{L21} = C_{L21} \frac{d}{dt} & (\theta_{L21} - \theta_{CR}) + G_{h1-L21}(\theta_{L21} - \theta_{h1}) + G_{h2-L21}(\theta_{L21} - \theta_{h2}) \\
& + G_{h3-L21}(\theta_{L21} - \theta_{h3}) + G_{L11-L21}(\theta_{L21} - \theta_{L11}) \\
& + G_{L12-L21}(\theta_{L21} - \theta_{L12}) + G_{L13-L21}(\theta_{L21} - \theta_{L13}) \\
& + G_{L21-L22}(\theta_{L21} - \theta_{L22}) + G_{L21-L23}(\theta_{L21} - \theta_{L23}) \\
& + G_{L21-CT}(\theta_{L21} - \theta_{CT}) + G_{L21-CB}(\theta_{L21} - \theta_{CB}) \\
& + G_{L21-CR}(\theta_{L21} - \theta_{CR}) + G_{L21-CL}(\theta_{L21} - \theta_{CL}) \\
& + G_{L21-TOT}(\theta_{L21} - \theta_{TOT}) + G_{L21-BOT}(\theta_{L21} - \theta_{BOT}) \\
& + G_{L21-ROT}(\theta_{L21} - \theta_{ROT}) + G_{L21-LOT}(\theta_{L21} - \theta_{LOT}) \\
& + G_{L21-CaseT}(\theta_{L21} - \theta_{CaseT}) + G_{L21-CaseB}(\theta_{L21} - \theta_{CaseB}) \\
& + G_{L21-CaseR}(\theta_{L21} - \theta_{CaseR}) + G_{L21-CaseL}(\theta_{L21} - \theta_{CaseL})
\end{aligned} \tag{B.18}$$

$$\begin{aligned}
\dot{Q}_{L22} = C_{L22} \frac{d}{dt} & (\theta_{L22} - \theta_{CR}) + G_{h1-L22}(\theta_{L22} - \theta_{h1}) + G_{h2-L22}(\theta_{L22} - \theta_{h2}) \\
& + G_{h3-L22}(\theta_{L22} - \theta_{h3}) + G_{L11-L22}(\theta_{L22} - \theta_{L11}) \\
& + G_{L12-L22}(\theta_{L22} - \theta_{L12}) + G_{L13-L22}(\theta_{L22} - \theta_{L13}) \\
& + G_{L21-L22}(\theta_{L22} - \theta_{L21}) + G_{L22-L23}(\theta_{L22} - \theta_{L23}) \\
& + G_{L22-CT}(\theta_{L22} - \theta_{CT}) + G_{L22-CB}(\theta_{L22} - \theta_{CB}) \\
& + G_{L22-CR}(\theta_{L22} - \theta_{CR}) + G_{L22-CL}(\theta_{L22} - \theta_{CL}) \\
& + G_{L22-TOT}(\theta_{L22} - \theta_{TOT}) + G_{L22-BOT}(\theta_{L22} - \theta_{BOT}) \\
& + G_{L22-ROT}(\theta_{L22} - \theta_{ROT}) + G_{L22-LOT}(\theta_{L22} - \theta_{LOT}) \\
& + G_{L22-CaseT}(\theta_{L22} - \theta_{CaseT}) + G_{L22-CaseB}(\theta_{L22} - \theta_{CaseB}) \\
& + G_{L22-CaseR}(\theta_{L22} - \theta_{CaseR}) + G_{L22-CaseL}(\theta_{L22} - \theta_{CaseL})
\end{aligned} \tag{B.19}$$

$$\begin{aligned}
\dot{Q}_{L23} = & C_{L23} \frac{d}{dt} (\theta_{L23} - \theta_{CB}) + G_{h1-L23} (\theta_{L23} - \theta_{h1}) + G_{h2-L23} (\theta_{L23} - \theta_{h2}) \\
& + G_{h3-L23} (\theta_{L23} - \theta_{h3}) + G_{L11-L23} (\theta_{L23} - \theta_{L11}) \\
& + G_{L12-L23} (\theta_{L23} - \theta_{L12}) + G_{L13-L23} (\theta_{L23} - \theta_{L13}) \\
& + G_{L21-L23} (\theta_{L23} - \theta_{L21}) + G_{L22-L23} (\theta_{L23} - \theta_{L22}) \\
& + G_{L23-CT} (\theta_{L23} - \theta_{CT}) + G_{L23-CB} (\theta_{L23} - \theta_{CB}) \\
& + G_{L23-CR} (\theta_{L23} - \theta_{CR}) + G_{L23-CL} (\theta_{L23} - \theta_{CL}) \\
& + G_{L23-TOT} (\theta_{L23} - \theta_{TOT}) + G_{L23-BOT} (\theta_{L23} - \theta_{BOT}) \\
& + G_{L23-ROT} (\theta_{L23} - \theta_{ROT}) + G_{L23-LOT} (\theta_{L23} - \theta_{LOT}) \\
& + G_{L23-CaseT} (\theta_{L23} - \theta_{CaseT}) + G_{L23-CaseB} (\theta_{L23} - \theta_{CaseB}) \\
& + G_{L23-CaseR} (\theta_{L23} - \theta_{CaseR}) + G_{L23-CaseL} (\theta_{L23} - \theta_{CaseL})
\end{aligned} \tag{B.20}$$

$$\begin{aligned}
\dot{Q}_{CT} = & C_{h1} \frac{d}{dt} (\theta_{CT} - \theta_{h1}) + C_{L11} \frac{d}{dt} (\theta_{CT} - \theta_{L11}) + C_{CT} \frac{d}{dt} (\theta_{CT} - \theta_{TOT}) \\
& + G_{h1-CT} (\theta_{CT} - \theta_{h1}) + G_{h2-CT} (\theta_{CT} - \theta_{h2}) + G_{h3-CT} (\theta_{CT} - \theta_{h3}) \\
& + G_{L11-CT} (\theta_{CT} - \theta_{L11}) + G_{L12-CT} (\theta_{CT} - \theta_{L12}) \\
& + G_{L13-CT} (\theta_{CT} - \theta_{L13}) + G_{L21-CT} (\theta_{CT} - \theta_{L21}) \\
& + G_{L22-CT} (\theta_{CT} - \theta_{L22}) + G_{L23-CT} (\theta_{CT} - \theta_{L23}) + G_{CT-CB} (\theta_{CT} - \theta_{CB}) \\
& + G_{CT-CR} (\theta_{CT} - \theta_{CR}) + G_{CT-CL} (\theta_{CT} - \theta_{CL}) + G_{CT-TOT} (\theta_{CT} - \theta_{TOT}) \\
& + G_{CT-BOT} (\theta_{CT} - \theta_{BOT}) + G_{CT-ROT} (\theta_{CT} - \theta_{ROT}) \\
& + G_{CT-LOT} (\theta_{CT} - \theta_{LOT}) + G_{CT-CaseT} (\theta_{CT} - \theta_{CaseT}) \\
& + G_{CT-CaseB} (\theta_{CT} - \theta_{CaseB}) + G_{CT-CaseR} (\theta_{CT} - \theta_{CaseR}) \\
& + G_{CT-CaseL} (\theta_{CT} - \theta_{CaseL})
\end{aligned} \tag{B.21}$$

$$\begin{aligned}
\dot{Q}_{CB} = & C_{h3} \frac{d}{dt} (\theta_{CB} - \theta_{h3}) + C_{L23} \frac{d}{dt} (\theta_{CB} - \theta_{L23}) + C_{CB} \frac{d}{dt} (\theta_{CB} - \theta_{BOT}) \\
& + G_{h1-CB} (\theta_{CB} - \theta_{h1}) + G_{h2-CB} (\theta_{CB} - \theta_{h2}) + G_{h3-CB} (\theta_{CB} - \theta_{h3}) \\
& + G_{L11-CB} (\theta_{CB} - \theta_{L11}) + G_{L12-CB} (\theta_{CB} - \theta_{L12}) \\
& + G_{L13-CB} (\theta_{CB} - \theta_{L13}) + G_{L21-CB} (\theta_{CB} - \theta_{L21}) \\
& + G_{L22-CB} (\theta_{CB} - \theta_{L22}) + G_{L23-CB} (\theta_{CB} - \theta_{L23}) + G_{CT-CB} (\theta_{CB} - \theta_{CT}) \\
& + G_{CB-CR} (\theta_{CB} - \theta_{CR}) + G_{CB-CL} (\theta_{CB} - \theta_{CL}) + G_{CB-TOT} (\theta_{CB} - \theta_{TOT}) \\
& + G_{CB-BOT} (\theta_{CB} - \theta_{BOT}) + G_{CB-ROT} (\theta_{CB} - \theta_{ROT}) \\
& + G_{CB-LOT} (\theta_{CB} - \theta_{LOT}) + G_{CB-caseT} (\theta_{CB} - \theta_{caseT}) \\
& + G_{CB-caseB} (\theta_{CB} - \theta_{caseB}) + G_{CB-caseR} (\theta_{CB} - \theta_{caseR}) \\
& + G_{CB-caseL} (\theta_{CB} - \theta_{caseL})
\end{aligned} \tag{B.22}$$

$$\begin{aligned}
\dot{Q}_{CR} = & C_{L12} \frac{d}{dt} (\theta_{CR} - \theta_{L12}) + C_{L13} \frac{d}{dt} (\theta_{CR} - \theta_{L13}) + C_{L21} \frac{d}{dt} (\theta_{CR} - \theta_{L21}) \\
& + C_{L22} \frac{d}{dt} (\theta_{CR} - \theta_{L22}) + C_{CR} \frac{d}{dt} (\theta_{CR} - \theta_{ROT}) + G_{h1-CR} (\theta_{CR} - \theta_{h1}) \\
& + G_{h2-CR} (\theta_{CR} - \theta_{h2}) + G_{h3-CR} (\theta_{CR} - \theta_{h3}) + G_{L11-CR} (\theta_{CR} - \theta_{L11}) \\
& + G_{L12-CR} (\theta_{CR} - \theta_{L12}) + G_{L13-CR} (\theta_{CR} - \theta_{L13}) \\
& + G_{L21-CR} (\theta_{CR} - \theta_{L21}) + G_{L22-CR} (\theta_{CR} - \theta_{L22}) \\
& + G_{L23-CR} (\theta_{CR} - \theta_{L23}) + G_{CT-CR} (\theta_{CR} - \theta_{CT}) + G_{CB-CR} (\theta_{CR} - \theta_{CB}) \\
& + G_{CR-CL} (\theta_{CR} - \theta_{CL}) + G_{CR-TOT} (\theta_{CR} - \theta_{TOT}) \\
& + G_{CR-BOT} (\theta_{CR} - \theta_{BOT}) + G_{CR-ROT} (\theta_{CR} - \theta_{ROT}) \\
& + G_{CR-LOT} (\theta_{CR} - \theta_{LOT}) + G_{CR-caseT} (\theta_{CR} - \theta_{caseT}) \\
& + G_{CR-caseB} (\theta_{CR} - \theta_{caseB}) + G_{CR-caseR} (\theta_{CR} - \theta_{caseR}) \\
& + G_{CR-caseL} (\theta_{CR} - \theta_{caseL})
\end{aligned} \tag{B.23}$$



$$\begin{aligned}
\dot{Q}_{CL} = & C_{h2} \frac{d}{dt} (\theta_{CL} - \theta_{h2}) + C_{CL} \frac{d}{dt} (\theta_{CL} - \theta_{LOT}) + G_{h1-CL} (\theta_{CL} - \theta_{h1}) \\
& + G_{h2-CL} (\theta_{CL} - \theta_{h2}) + G_{h3-CL} (\theta_{CL} - \theta_{h3}) + G_{L11-CL} (\theta_{CL} - \theta_{L11}) \\
& + G_{L12-CL} (\theta_{CL} - \theta_{L12}) + G_{L13-CL} (\theta_{CL} - \theta_{L13}) \\
& + G_{L21-CL} (\theta_{CL} - \theta_{L21}) + G_{L22-CL} (\theta_{CL} - \theta_{L22}) \\
& + G_{L23-CL} (\theta_{CL} - \theta_{L23}) + G_{CT-CL} (\theta_{CL} - \theta_{CT}) + G_{CB-CL} (\theta_{CL} - \theta_{CB}) \\
& + G_{CR-CL} (\theta_{CL} - \theta_{CR}) + G_{CL-TOT} (\theta_{CL} - \theta_{TOT}) \\
& + G_{CL-BOT} (\theta_{CL} - \theta_{BOT}) + G_{CL-ROT} (\theta_{CL} - \theta_{ROT}) \\
& + G_{CL-LOT} (\theta_{CL} - \theta_{LOT}) + G_{CL-caseT} (\theta_{CL} - \theta_{caseT}) \\
& + G_{CL-caseB} (\theta_{CL} - \theta_{caseB}) + G_{CL-caseR} (\theta_{CL} - \theta_{caseR}) \\
& + G_{CL-caseL} (\theta_{CL} - \theta_{caseL})
\end{aligned} \tag{B.24}$$

$$\begin{aligned}
0.0 = & C_{CT} \frac{d}{dt} (\theta_{TOT} - \theta_{CT}) + C_{TOT} \frac{d}{dt} (\theta_{TOT} - \theta_{caseT}) + G_{h1-TOT} (\theta_{TOT} - \theta_{h1}) \\
& + G_{h2-TOT} (\theta_{TOT} - \theta_{h2}) + G_{h3-TOT} (\theta_{TOT} - \theta_{h3}) \\
& + G_{L11-TOT} (\theta_{TOT} - \theta_{L11}) + G_{L12-TOT} (\theta_{TOT} - \theta_{L12}) \\
& + G_{L13-TOT} (\theta_{TOT} - \theta_{L13}) + G_{L21-TOT} (\theta_{TOT} - \theta_{L21}) \\
& + G_{L22-TOT} (\theta_{TOT} - \theta_{L22}) + G_{L23-TOT} (\theta_{TOT} - \theta_{L23}) \\
& + G_{CT-TOT} (\theta_{TOT} - \theta_{CT}) + G_{CB-TOT} (\theta_{TOT} - \theta_{CB}) \\
& + G_{CR-TOT} (\theta_{TOT} - \theta_{CR}) + G_{CL-TOT} (\theta_{TOT} - \theta_{CL}) \\
& + G_{TOT-BOT} (\theta_{TOT} - \theta_{BOT}) + G_{TOT-ROT} (\theta_{TOT} - \theta_{ROT}) \\
& + G_{TOT-LOT} (\theta_{TOT} - \theta_{LOT}) + G_{TOT-caseT} (\theta_{TOT} - \theta_{caseT}) \\
& + G_{TOT-caseB} (\theta_{TOT} - \theta_{caseB}) + G_{TOT-caseR} (\theta_{TOT} - \theta_{caseR}) \\
& + G_{TOT-caseL} (\theta_{TOT} - \theta_{caseL})
\end{aligned} \tag{B.25}$$

$$\begin{aligned}
0.0 = & C_{CB} \frac{d}{dt} (\theta_{BOT} - \theta_{CB}) + C_{BOT} \frac{d}{dt} (\theta_{BOT} - \theta_{CaseB}) + G_{h1-BOT} (\theta_{BOT} - \theta_{h1}) \\
& + G_{h2-BOT} (\theta_{BOT} - \theta_{h2}) + G_{h3-BOT} (\theta_{BOT} - \theta_{h3}) \\
& + G_{L11-BOT} (\theta_{BOT} - \theta_{L11}) + G_{L12-BOT} (\theta_{BOT} - \theta_{L12}) \\
& + G_{L13-BOT} (\theta_{BOT} - \theta_{L13}) + G_{L21-BOT} (\theta_{BOT} - \theta_{L21}) \\
& + G_{L22-BOT} (\theta_{BOT} - \theta_{L22}) + G_{L23-BOT} (\theta_{BOT} - \theta_{L23}) \\
& + G_{CT-BOT} (\theta_{BOT} - \theta_{CT}) + G_{CB-BOT} (\theta_{BOT} - \theta_{CB}) \\
& + G_{CR-BOT} (\theta_{BOT} - \theta_{CR}) + G_{CL-BOT} (\theta_{BOT} - \theta_{CL}) \\
& + G_{TOT-BOT} (\theta_{BOT} - \theta_{TOT}) + G_{BOT-ROT} (\theta_{BOT} - \theta_{ROT}) \\
& + G_{BOT-LOT} (\theta_{BOT} - \theta_{LOT}) + G_{BOT-CaseT} (\theta_{BOT} - \theta_{CaseT}) \\
& + G_{BOT-CaseB} (\theta_{BOT} - \theta_{CaseB}) + G_{BOT-CaseR} (\theta_{BOT} - \theta_{CaseR}) \\
& + G_{BOT-CaseL} (\theta_{BOT} - \theta_{CaseL})
\end{aligned} \tag{B.26}$$

$$\begin{aligned}
0.0 = & C_{L21} \frac{d}{dt} (\theta_{ROT} - \theta_{CR}) + C_{ROT} \frac{d}{dt} (\theta_{ROT} - \theta_{CaseR}) + G_{h1-ROT} (\theta_{ROT} - \theta_{h1}) \\
& + G_{h2-ROT} (\theta_{ROT} - \theta_{h2}) + G_{h3-ROT} (\theta_{ROT} - \theta_{h3}) \\
& + G_{L11-ROT} (\theta_{ROT} - \theta_{L11}) + G_{L12-ROT} (\theta_{ROT} - \theta_{L12}) \\
& + G_{L13-ROT} (\theta_{ROT} - \theta_{L13}) + G_{L21-ROT} (\theta_{ROT} - \theta_{L21}) \\
& + G_{L22-ROT} (\theta_{ROT} - \theta_{L22}) + G_{L23-ROT} (\theta_{ROT} - \theta_{L23}) \\
& + G_{CT-ROT} (\theta_{ROT} - \theta_{CT}) + G_{CB-ROT} (\theta_{ROT} - \theta_{CB}) \\
& + G_{CR-ROT} (\theta_{ROT} - \theta_{CR}) + G_{CL-ROT} (\theta_{ROT} - \theta_{CL}) \\
& + G_{TOT-ROT} (\theta_{ROT} - \theta_{TOT}) + G_{BOT-ROT} (\theta_{ROT} - \theta_{BOT}) \\
& + G_{ROT-LOT} (\theta_{ROT} - \theta_{LOT}) + G_{ROT-CaseT} (\theta_{ROT} - \theta_{CaseT}) \\
& + G_{ROT-CaseB} (\theta_{ROT} - \theta_{CaseB}) + G_{ROT-CaseR} (\theta_{ROT} - \theta_{CaseR}) \\
& + G_{ROT-CaseL} (\theta_{ROT} - \theta_{CaseL})
\end{aligned} \tag{B.27}$$

$$\begin{aligned}
0.0 = & C_{CL} \frac{d}{dt} (\theta_{LOT} - \theta_{CL}) + C_{LOT} \frac{d}{dt} (\theta_{LOT} - \theta_{CaseL}) + G_{h1-LOT} (\theta_{LOT} - \theta_{h1}) \\
& + G_{h2-LOT} (\theta_{LOT} - \theta_{h2}) + G_{h3-LOT} (\theta_{LOT} - \theta_{h3}) \\
& + G_{L11-LOT} (\theta_{LOT} - \theta_{L11}) + G_{L12-LOT} (\theta_{LOT} - \theta_{L12}) \\
& + G_{L13-LOT} (\theta_{LOT} - \theta_{L13}) + G_{L21-LOT} (\theta_{LOT} - \theta_{L21}) \\
& + G_{L22-LOT} (\theta_{LOT} - \theta_{L22}) + G_{L23-LOT} (\theta_{LOT} - \theta_{L23}) \\
& + G_{CT-LOT} (\theta_{LOT} - \theta_{CT}) + G_{CB-LOT} (\theta_{LOT} - \theta_{CB}) \\
& + G_{CR-LOT} (\theta_{LOT} - \theta_{CR}) + G_{CL-LOT} (\theta_{LOT} - \theta_{CL}) \\
& + G_{TOT-LOT} (\theta_{LOT} - \theta_{TOT}) + G_{BOT-LOT} (\theta_{LOT} - \theta_{BOT}) \\
& + G_{ROT-LOT} (\theta_{LOT} - \theta_{ROT}) + G_{LOT-CaseT} (\theta_{LOT} - \theta_{CaseT}) \\
& + G_{LOT-CaseB} (\theta_{LOT} - \theta_{CaseB}) + G_{LOT-CaseR} (\theta_{LOT} - \theta_{CaseR}) \\
& + G_{LOT-CaseL} (\theta_{LOT} - \theta_{CaseL})
\end{aligned} \tag{B.28}$$

Equations (B.1)-(B.28) cast into a compact matrix form as follows

$$\begin{bmatrix} I \\ 0 \end{bmatrix} = Y_{eq} \begin{bmatrix} V \\ Y \end{bmatrix} + K_{eq} \tag{B.29}$$

, where

$$I = [\tilde{I}_1 \quad \tilde{I}_2 \quad \tilde{I}_{L1} \quad \tilde{I}_{NN} \quad \tilde{I}_{L2} \quad \dot{q}_{CaseT} \quad \dot{q}_{CaseB} \quad \dot{q}_{CaseR} \quad \dot{q}_{CaseL} \quad \dot{q}_{amb}]^T,$$

$$V = [\tilde{V}_1 \quad \tilde{V}_2 \quad \tilde{V}_{L1} \quad \tilde{V}_{NN} \quad \tilde{V}_{L2} \quad \theta_{CaseT} \quad \theta_{CaseB} \quad \theta_{CaseR} \quad \theta_{CaseL} \quad \theta_{amb}]^T$$

$$Y = [\tilde{E} \quad \theta_{h1} \quad \theta_{h2} \quad \theta_{h3} \quad \theta_{L11} \quad \theta_{L12} \quad \theta_{L13} \quad \theta_{L21} \quad \theta_{L22} \quad \theta_{L23} \quad \theta_{CT} \quad \theta_{CB} \quad \theta_{CR} \\ \theta_{CL} \quad \theta_{TOT} \quad \theta_{BOT} \quad \theta_{ROT} \quad \theta_{LOT}]^T$$

$Y_{eq}$ : Matrix defining the linear part of the model.

$K_{eq}$ : Vector containing the constant part of the model.

Note that there 28 states with 28 equations are identified.

## Appendix B.2 Model Thermal Conductances

To compute the thermal conductance, a percentage of each one is assumed based on the below tables Table 24-Table 44.

**Table 24. Transformer  $T_{h1}$  conductances.**

$T_{h1}$ Conductances	(%) of $G_{h1}$
$G_{h1\_h2}$	20
$G_{h1\_h3}$	9
$G_{h1\_L11}$	6
$G_{h1\_L12}$	5
$G_{h1\_L13}$	4
$G_{h1\_L21}$	3
$G_{h1\_L22}$	2
$G_{h1\_L23}$	1
$G_{h1\_CT}$	7
$G_{h1\_CB}$	5
$G_{h1\_CR}$	3
$G_{h1\_CL}$	10
$G_{h1\_TOT}$	3.5
$G_{h1\_BOT}$	2.5
$G_{h1\_ROT}$	1
$G_{h1\_LOT}$	8
$G_{h1\_CaseT}$	2.5
$G_{h1\_CaseB}$	1.5

$G_{h1\_CaseR}$	1
$G_{h1\_CaseL}$	5

**Table 25. Transformer  $T_{h2}$  conductances.**

<b><math>T_{h2}</math> Conductances</b>	<b>(%) of <math>G_{h2}</math></b>
$G_{h2\_h3}$	20
$G_{h2\_L11}$	3
$G_{h2\_L12}$	3.5
$G_{h2\_L13}$	3.5
$G_{h2\_L21}$	3
$G_{h2\_L22}$	3.5
$G_{h2\_L23}$	3.5
$G_{h2\_CT}$	5.5
$G_{h2\_CB}$	5.5
$G_{h2\_CR}$	2
$G_{h2\_CL}$	10
$G_{h2\_TOT}$	1
$G_{h2\_BOT}$	1
$G_{h2\_ROT}$	0.8
$G_{h2\_LOT}$	8
$G_{h2\_CaseT}$	0.5
$G_{h2\_CaseB}$	0.5
$G_{h2\_CaseR}$	0.2
$G_{h2\_CaseL}$	5

**Table 26. Transformer  $T_{h3}$  conductances.**

<b><math>T_{h3}</math> Conductances</b>	<b>(%) of <math>G_{h3}</math></b>
$G_{h3\_L11}$	1
$G_{h3\_L12}$	2
$G_{h3\_L13}$	3
$G_{h3\_L21}$	4
$G_{h3\_L22}$	5
$G_{h3\_L23}$	6
$G_{h3\_CT}$	5
$G_{h3\_CB}$	7
$G_{h3\_CR}$	3
$G_{h3\_CL}$	10
$G_{h3\_TOT}$	2.5
$G_{h3\_BOT}$	3.5
$G_{h3\_ROT}$	1
$G_{h3\_LOT}$	8
$G_{h3\_CaseT}$	1.5
$G_{h3\_CaseB}$	2.5
$G_{h3\_CaseR}$	1
$G_{h3\_CaseL}$	5

**Table 27. Transformer  $T_{L11}$  conductances.**

<b><math>T_{L11}</math> Conductances</b>	<b>(%) of <math>G_{L11}</math></b>
$G_{L11\_L12}$	15
$G_{L11\_L13}$	12

$G_{L11\_L21}$	9
$G_{L11\_L22}$	6
$G_{L11\_L23}$	3
$G_{L11\_CT}$	6
$G_{L11\_CB}$	4
$G_{L11\_CR}$	7
$G_{L11\_CL}$	3
$G_{L11\_TOT}$	5
$G_{L11\_BOT}$	3
$G_{L11\_ROT}$	5.5
$G_{L11\_LOT}$	1
$G_{L11\_CaseT}$	3
$G_{L11\_CaseB}$	2
$G_{L11\_CaseR}$	5
$G_{L11\_CaseL}$	0.5

**Table 28. Transformer  $T_{L12}$  conductances.**

$T_{L12}$ Conductances	(%) of $G_{L12}$
$G_{L12\_L13}$	15
$G_{L12\_L21}$	12
$G_{L12\_L22}$	9
$G_{L12\_L23}$	6
$G_{L12\_CT}$	4.5
$G_{L12\_CB}$	3.5

$G_{L12\_CR}$	6
$G_{L12\_CL}$	2.5
$G_{L12\_TOT}$	3
$G_{L12\_BOT}$	2
$G_{L12\_ROT}$	3.5
$G_{L12\_LOT}$	1
$G_{L12\_CaseT}$	2
$G_{L12\_CaseB}$	1
$G_{L12\_CaseR}$	3
$G_{L12\_CaseL}$	0.5

**Table 29. Transformer  $T_{L13}$  conductances.**

<b><math>T_{L13}</math> Conductances</b>	<b>(%) of <math>G_{L13}</math></b>
$G_{L13\_L21}$	15
$G_{L13\_L22}$	12
$G_{L13\_L23}$	9
$G_{L13\_CT}$	3.5
$G_{L13\_CB}$	3
$G_{L13\_CR}$	4
$G_{L13\_CL}$	1
$G_{L13\_TOT}$	3
$G_{L13\_BOT}$	2.5
$G_{L13\_ROT}$	3.5
$G_{L13\_LOT}$	0.8



$G_{L13\_CaseT}$	2
$G_{L13\_CaseB}$	1
$G_{L13\_CaseR}$	2
$G_{L13\_CaseL}$	0.2

**Table 30. Transformer  $T_{L21}$  conductances.**

<b><math>T_{L21}</math> Conductances</b>	<b>(%) of <math>G_{L21}</math></b>
$G_{L21\_L22}$	15
$G_{L21\_L23}$	12
$G_{L21\_CT}$	3
$G_{L21\_CB}$	3.5
$G_{L21\_CR}$	4
$G_{L21\_CL}$	1
$G_{L21\_TOT}$	2.5
$G_{L21\_BOT}$	3
$G_{L21\_ROT}$	3.5
$G_{L21\_LOT}$	0.8
$G_{L21\_CaseT}$	1
$G_{L21\_CaseB}$	2
$G_{L21\_CaseR}$	2.5
$G_{L21\_CaseL}$	0.2

**Table 31. Transformer  $T_{L22}$  conductances.**

<b><math>T_{L22}</math> Conductances</b>	<b>(%) of <math>G_{L22}</math></b>
$G_{L22\_L23}$	15

$G_{L22\_CT}$	3.5
$G_{L22\_CB}$	4.5
$G_{L22\_CR}$	6
$G_{L22\_CL}$	2.5
$G_{L22\_TOT}$	2
$G_{L22\_BOT}$	3
$G_{L22\_ROT}$	3.5
$G_{L22\_LOT}$	1
$G_{L22\_CaseT}$	1
$G_{L22\_CaseB}$	2
$G_{L22\_CaseR}$	3
$G_{L22\_CaseL}$	0.5

**Table 32. Transformer  $T_{L23}$  conductances.**

$T_{L23}$ Conductances	(%) of $G_{L23}$
$G_{L23\_CT}$	4
$G_{L23\_CB}$	6
$G_{L23\_CR}$	7
$G_{L23\_CL}$	3
$G_{L23\_TOT}$	3
$G_{L23\_BOT}$	5
$G_{L23\_ROT}$	5.5
$G_{L23\_LOT}$	1
$G_{L23\_CaseT}$	2

$G_{L23\_CaseB}$	3
$G_{L23\_CaseR}$	4.8
$G_{L23\_CaseL}$	0.2

**Table 33. Transformer  $T_{CT}$  conductances.**

<b><math>T_{CT}</math> Conductances</b>	<b>(%) of <math>G_{CT}</math></b>
$G_{CT\_CB}$	7
$G_{CT\_CR}$	10
$G_{CT\_CL}$	10
$G_{CT\_TOT}$	8
$G_{CT\_BOT}$	2
$G_{CT\_ROT}$	5
$G_{CT\_LOT}$	5
$G_{CT\_CaseT}$	5
$G_{CT\_CaseB}$	1
$G_{CT\_CaseR}$	2.5
$G_{CT\_CaseL}$	2.5

**Table 34. Transformer  $T_{CB}$  conductances.**

<b><math>T_{CB}</math> Conductances</b>	<b>(%) of <math>G_{CB}</math></b>
$G_{CB\_CR}$	10
$G_{CB\_CL}$	10
$G_{CB\_TOT}$	2
$G_{CB\_BOT}$	8
$G_{CB\_ROT}$	5

$G_{CB\_LOT}$	5
$G_{CB\_CaseT}$	1
$G_{CB\_CaseB}$	5
$G_{CB\_CaseR}$	2.5
$G_{CB\_CaseL}$	2.5

**Table 35. Transformer  $T_{CR}$  conductances.**

<b><math>T_{CR}</math> Conductances</b>	<b>(%) of <math>G_{CR}</math></b>
$G_{CR\_CL}$	7
$G_{CR\_TOT}$	4
$G_{CR\_BOT}$	4
$G_{CR\_ROT}$	12.9
$G_{CR\_LOT}$	1
$G_{CR\_CaseT}$	2
$G_{CR\_CaseB}$	2
$G_{CR\_CaseR}$	5
$G_{CR\_CaseL}$	0.1

**Table 36. Transformer  $T_{CL}$  conductances.**

<b><math>T_{CL}</math> Conductances</b>	<b>(%) of <math>G_{CL}</math></b>
$G_{CL\_TOT}$	4
$G_{CL\_BOT}$	4
$G_{CL\_ROT}$	2
$G_{CL\_LOT}$	12.9
$G_{CL\_CaseT}$	1.25

$G_{CL\_CaseB}$	1.25
$G_{CL\_CaseR}$	0.1
$G_{CL\_CaseL}$	4.5

**Table 37. Transformer  $T_{TOT}$  conductances.**

$T_{TOT}$ Conductances	(%) of $G_{TOT}$
$G_{TOT\_BOT}$	5
$G_{TOT\_ROT}$	10
$G_{TOT\_LOT}$	10
$G_{TOT\_CaseT}$	15
$G_{TOT\_CaseB}$	2
$G_{TOT\_CaseR}$	7.25
$G_{TOT\_CaseL}$	7.25

**Table 38. Transformer  $T_{BOT}$  conductances.**

$T_{BOT}$ Conductances	(%) of $G_{BOT}$
$G_{BOT\_ROT}$	10
$G_{BOT\_LOT}$	10
$G_{BOT\_CaseT}$	2
$G_{BOT\_CaseB}$	15
$G_{BOT\_CaseR}$	7.25
$G_{BOT\_CaseL}$	7.25

**Table 39. Transformer  $T_{ROT}$  conductances.**

$T_{ROT}$ Conductances	(%) of $G_{ROT}$
$G_{ROT\_LOT}$	4

$G_{ROT\_CaseT}$	6
$G_{ROT\_CaseB}$	6
$G_{ROT\_CaseR}$	10
$G_{ROT\_CaseL}$	1.3

**Table 40. Transformer  $T_{LOT}$  conductances.**

<b><math>T_{LOT}</math> Conductances</b>	<b>(%) of <math>G_{LOT}</math></b>
$G_{LOT\_CaseT}$	5.75
$G_{LOT\_CaseB}$	5.75
$G_{LOT\_CaseR}$	1
$G_{LOT\_CaseL}$	10

**Table 41. Transformer  $T_{CaseT}$  conductances.**

<b><math>T_{CaseT}</math> Conductances</b>	<b>(%) of <math>G_{CaseT}</math></b>
$G_{CaseT\_CaseB}$	3
$G_{CaseT\_CaseR}$	8
$G_{CaseT\_CaseL}$	8
$G_{CaseT\_amb}$	27.5

**Table 42. Transformer  $T_{CaseB}$  conductances.**

<b><math>T_{CaseB}</math> Conductances</b>	<b>(%) of <math>G_{CaseB}</math></b>
$G_{CaseB\_CaseR}$	8
$G_{CaseB\_CaseL}$	8
$G_{CaseB\_amb}$	27.5

**Table 43. Transformer  $T_{CaseR}$  conductances.**

<b><math>T_{CaseR}</math> Conductances</b>	<b>(%) of <math>G_{CaseR}</math></b>
--	--------------------------------------

$G_{CaseR\_CaseL}$	4
$G_{CaseR\_amb}$	21.9

**Table 44. Transformer  $T_{CaseL}$  conductances.**

$T_{CaseL}$ Conductances	(%) of $G_{CaseL}$
$G_{CaseL\_amb}$	27.5

### *Appendix C Thermal Model of a House*

The mathematical model of the single story house with two bedrooms and two bathrooms is given by the following equations

$$\dot{q}_{Bed1} = C_{Bed1} \frac{d}{dt} (T_{Bed1} - T_{Bed1-l}) + G_{Bed1} (T_{Bed1} - T_{Bed1-l}) \quad (C.1)$$

$$\dot{q}_{Bed2} = C_{Bed2} \frac{d}{dt} (T_{Bed2} - T_{Bed2-l}) + G_{Bed2} (T_{Bed2} - T_{Bed2-l}) \quad (C.2)$$

$$\dot{q}_{Bath1} = C_{Bath1} \frac{d}{dt} (T_{Bath1} - T_{Bath1-l}) + G_{Bath1} (T_{Bath1} - T_{Bath1-l}) \quad (C.3)$$

$$\dot{q}_{Bath2} = C_{Bath2} \frac{d}{dt} (T_{Bath2} - T_{Bath2-l}) + G_{Bath2} (T_{Bath2} - T_{Bath2-l}) \quad (C.4)$$

$$\dot{q}_K = C_K \frac{d}{dt} (T_K - T_{K-l}) + G_K (T_K - T_{K-l}) \quad (C.5)$$

$$\dot{q}_L = C_L \frac{d}{dt} (T_L - T_{L-l}) + G_L (T_L - T_{L-l}) \quad (C.6)$$

$$\begin{aligned} \dot{q}_E = & C_{Bed1l} \frac{d}{dt} (T_E - T_{Bed1-l}) + C_{Bath2l} \frac{d}{dt} (T_E - T_{Bath2-l}) + C_E \frac{d}{dt} (T_E \\ & - T_{amb}) + G_{Bed1lE} (T_E - T_{Bed1-l}) + G_{Bed2lE} (T_E - T_{Bed2-l}) \\ & + G_{Bath2lE} (T_E - T_{Bath2-l}) + G_{EN} (T_E - T_N) + G_{ETop} (T_E - T_{Top}) \\ & + G_{ES} (T_E - T_S) + G_{EAmb} (T_E - T_{amb}) \end{aligned} \quad (C.7)$$

$$\begin{aligned} \dot{q}_N = & C_{Bath1l} \frac{d}{dt} (T_N - T_{Bath1-l}) + C_N \frac{d}{dt} (T_N - T_{amb}) \\ & + G_{Bed1lN} (T_N - T_{Bed1-l}) + G_{Bath1lN} (T_N - T_{Bath1-l}) \\ & + G_{LiN} (T_N - T_{L-l}) + G_{EN} (T_N - T_E) + G_{NW} (T_N - T_W) \\ & + G_{NTop} (T_N - T_{Top}) + G_{NAmb} (T_N - T_{amb}) \end{aligned} \quad (C.8)$$



$$\begin{aligned}
\dot{q}_W = & C_{LI} \frac{d}{dt} (T_W - T_{L-I}) + C_W \frac{d}{dt} (T_W - T_{amb}) + G_{LIW} (T_W - T_{L-I}) \\
& + G_{WS} (T_W - T_S) + G_{NW} (T_W - T_N) + G_{WTop} (T_W - T_{Top}) \\
& + G_{WAmb} (T_W - T_{amb})
\end{aligned} \tag{C.9}$$

$$\begin{aligned}
\dot{q}_S = & C_{Bed2I} \frac{d}{dt} (T_S - T_{Bed2-I}) + C_S \frac{d}{dt} (T_S - T_{amb}) + G_{Bed2IS} (T_S - T_{Bed2-I}) \\
& + G_{LIS} (T_S - T_{L-I}) + G_{ES} (T_S - T_E) + G_{WS} (T_S - T_W) \\
& + G_{STOP} (T_S - T_{Top}) + G_{SAmb} (T_S - T_{amb})
\end{aligned} \tag{C.10}$$

$$\begin{aligned}
\dot{q}_{Top} = & C_{KI} \frac{d}{dt} (T_{Top} - T_{K-I}) + C_{Top} \frac{d}{dt} (T_{Top} - T_{amb}) \\
& + G_{Bed1ITop} (T_{Top} - T_{Bed1-I}) + G_{Bed2ITop} (T_{Top} - T_{Bed2-I}) \\
& + G_{Bath1ITop} (T_{Top} - T_{Bath1-I}) + G_{Bath2ITop} (T_{Top} - T_{Bath2-I}) \\
& + G_{KITop} (T_{Top} - T_{K-I}) + G_{LITop} (T_{Top} - T_{L-I}) \\
& + G_{ETop} (T_{Top} - T_E) + G_{WTop} (T_{Top} - T_W) + G_{NTop} (T_{Top} - T_N) \\
& + G_{STop} (T_{Top} - T_S) + G_{TopAmb} (T_{Top} - T_{amb})
\end{aligned} \tag{C.11}$$

$$\begin{aligned}
\dot{q}_{amb} = & C_E \frac{d}{dt} (T_{amb} - T_E) + C_N \frac{d}{dt} (T_{amb} - T_N) + C_W \frac{d}{dt} (T_{amb} - T_W) \\
& + C_S \frac{d}{dt} (T_{amb} - T_S) + C_{Top} \frac{d}{dt} (T_{amb} - T_{Top}) \\
& + G_{EAmb} (T_{amb} - T_E) + G_{NAmb} (T_{amb} - T_N) \\
& + G_{SAmb} (T_{amb} - T_S) + G_{WAmb} (T_{amb} - T_W) \\
& + G_{TopAmb} (T_{amb} - T_{Top})
\end{aligned} \tag{C.12}$$

$$\begin{aligned}
0.0 = & C_{Bed1} \frac{d}{dt} (T_{Bed1-I} - T_{Bed1}) + C_{Bed1I} \frac{d}{dt} (T_{Bed1-I} - T_E) \\
& + G_{Bed1} (T_{Bed1-I} - T_{Bed1}) + G_{Bed1IE} (T_{Bed1-I} - T_E) \\
& + G_{Bed1IN} (T_{Bed1-I} - T_N) + G_{Bed1ITop} (T_{Bed1-I} - T_{Top}) \\
& + G_{Bed1IBath1I} (T_{Bed1-I} - T_{Bath1-I}) \\
& + G_{Bed1IBath2I} (T_{Bed1-I} - T_{Bath2-I}) + G_{Bed1IKI} (T_{Bed1-I} - T_{K-I}) \\
& + G_{Bed1ILI} (T_{Bed1-I} - T_{L-I})
\end{aligned} \tag{C.13}$$

$$\begin{aligned}
0.0 = & C_{Bed2} \frac{d}{dt} (T_{Bed2-I} - T_{Bed2}) + C_{Bed2I} \frac{d}{dt} (T_{Bed2-I} - T_S) \\
& + G_{Bed2} (T_{Bed2-I} - T_{Bed2}) + G_{Bed2IE} (T_{Bed2-I} - T_E) \\
& + G_{Bed2IS} (T_{Bed2-I} - T_S) + G_{Bed2ITop} (T_{Bed2-I} - T_{Top}) \\
& + G_{Bed2IBath2I} (T_{Bed2-I} - T_{Bath2-I}) + G_{Bed2ILI} (T_{Bed2-I} - T_{L-I})
\end{aligned} \tag{C.14}$$

$$\begin{aligned}
0.0 = & C_{Bath1} \frac{d}{dt} (T_{Bath1-I} - T_{Bath1}) + C_{Bath1I} \frac{d}{dt} (T_{Bath1-I} - T_N) \\
& + G_{Bath1} (T_{Bath1-I} - T_{Bath1}) + G_{Bath1IN} (T_{Bath1-I} - T_N) \\
& + G_{Bath1ITop} (T_{Bath1-I} - T_{Top}) \\
& + G_{Bed1IBath1I} (T_{Bath1-I} - T_{Bed1-I}) \\
& + G_{Bath1IKI} (T_{Bath1-I} - T_{K-I}) + G_{Bath1ILI} (T_{Bath1-I} - T_{L-I})
\end{aligned} \tag{C.15}$$

$$\begin{aligned}
0.0 = & C_{Bath2} \frac{d}{dt} (T_{Bath2-I} - T_{Bath2}) + C_{Bath2I} \frac{d}{dt} (T_{Bath2-I} - T_E) \\
& + G_{Bath2} (T_{Bath2-I} - T_{Bath2}) + G_{Bath2IE} (T_{Bath2-I} - T_E) \\
& + G_{Bath2ITop} (T_{Bath2-I} - T_{Top}) \\
& + G_{Bed1IBath2I} (T_{Bath2-I} - T_{Bed1-I}) \\
& + G_{Bed2IBath2I} (T_{Bath2-I} - T_{Bed2-I}) \\
& + G_{Bath2ILI} (T_{Bath2-I} - T_{L-I})
\end{aligned} \tag{C.16}$$

$$\begin{aligned}
0.0 = & C_K \frac{d}{dt} (T_{K-I} - T_K) + C_{KI} \frac{d}{dt} (T_{K-I} - T_{Top}) + G_K (T_{K-I} - T_K) \\
& + G_{KITop} (T_{K-I} - T_{Top}) + G_{Bed1IKI} (T_{K-I} - T_{Bed1-I}) \\
& + G_{Bath1IKI} (T_{K-I} - T_{Bath1-I}) + G_{KILI} (T_{K-I} - T_{L-I})
\end{aligned} \tag{C.17}$$

$$\begin{aligned}
0.0 = & C_L \frac{d}{dt} (T_{L-I} - T_L) + C_{LI} \frac{d}{dt} (T_{L-I} - T_W) + G_L (T_{L-I} - T_L) \\
& + G_{LIS} (T_{L-I} - T_S) + G_{LIW} (T_{L-I} - T_W) + G_{LIN} (T_{L-I} - T_N) \\
& + G_{LITop} (T_{L-I} - T_{Top}) + G_{Bed1ILI} (T_{L-I} - T_{Bed1-I}) \\
& + G_{Bed2ILI} (T_{L-I} - T_{Bed2-I}) + G_{Bath1ILI} (T_{L-I} - T_{Bath1-I}) \\
& + G_{Bath2ILI} (T_{L-I} - T_{Bath2-I}) + G_{KILI} (T_{L-I} - T_{K-I})
\end{aligned} \tag{C.18}$$

Equations (C.1)-(C.18) can be cast into a compact matrix form as follows

$$\begin{bmatrix} I \\ 0 \end{bmatrix} = Y_{eq} \begin{bmatrix} V \\ Y \end{bmatrix} + K_{eq} \tag{C.19}$$

, where

$$I = [\dot{q}_{Bed1} \quad \dot{q}_{Bed2} \quad \dot{q}_{Bath1} \quad \dot{q}_{Bath2} \quad \dot{q}_K \quad \dot{q}_L \quad \dot{q}_E \quad \dot{q}_N \quad \dot{q}_W \quad \dot{q}_S \quad \dot{q}_{Top} \quad \dot{q}_{amb}]^T$$

$$V = [T_{Bed1} \quad T_{Bed2} \quad T_{Bath1} \quad T_{Bath2} \quad T_K \quad T_L \quad T_E \quad T_N \quad T_W \quad T_S \quad T_{Top} \quad T_{amb}]^T$$

$$Y = [T_{Bed1-I} \quad T_{Bed2-I} \quad T_{Bath1-I} \quad T_{Bath2-I} \quad T_{K-I} \quad T_{L-I}]^T$$

$Y_{eq}$ : Matrix defining the linear part.

$K_{eq}$ : Vector containing the constant part of the model.

Note that there 30 states with 30 equations are identified.

To compute the thermal conductance, a percentage of each one is assumed based on the below tables Table 45-Table 55.

**Table 45. House  $T_{bed11}$  conductances.**

<b><math>T_{bed11}</math> Conductances</b>	<b>(%) of <math>G_{bed11}</math></b>
$G_{Bed11E}$	12.5
$G_{Bed11N}$	12.5
$G_{Bed11Top}$	7.5
$G_{Bed11Bath11}$	20
$G_{Bed11Bath21}$	20
$G_{Bed11KI}$	20
$G_{Bed11LI}$	20

**Table 46. House  $T_{bed21}$  conductances.**

<b><math>T_{bed21}</math> Conductances</b>	<b>(%) of <math>G_{bed21}</math></b>
$G_{Bed21E}$	12.5
$G_{Bed21S}$	12.5
$G_{Bed21Top}$	7.5
$G_{Bed21Bath21}$	20
$G_{Bed21LI}$	20

**Table 47. House  $T_{bath11}$  conductances.**

<b><math>T_{bath11}</math> Conductances</b>	<b>(%) of <math>G_{bath11}</math></b>
$G_{bath11N}$	12.5
$G_{bath11Top}$	7.5
$G_{bath11KI}$	20
$G_{bath11LI}$	20

**Table 48. House  $T_{bath2I}$  conductances.**

<b><math>T_{bath2I}</math> Conductances</b>	<b>(%) of <math>G_{bath2I}</math></b>
$G_{bath2IE}$	12.5
$G_{bath2ITop}$	7.5
$G_{bath2ILI}$	20

**Table 49. House  $T_{KI}$  conductances.**

<b><math>T_{LI2}</math> Conductances</b>	<b>(%) of <math>G_{LI2}</math></b>
$G_{KITop}$	7.5
$G_{KILI}$	20

**Table 50. House  $T_{LI}$  conductances.**

<b><math>T_{LI}</math> Conductances</b>	<b>(%) of <math>G_{LI}</math></b>
$G_{LIS}$	12.5
$G_{LIW}$	12.5
$G_{LIN}$	12.5
$G_{LITop}$	7.5

**Table 51. House  $T_E$  conductances.**

<b><math>T_E</math> Conductances</b>	<b>(%) of <math>G_E</math></b>
$G_{EN}$	20
$G_{ETop}$	20
$G_{ES}$	20
$G_{EAMB}$	27.5

**Table 52. House  $T_N$  conductances.**

<b><math>T_N</math> Conductances</b>	<b>(%) of <math>G_N</math></b>
$G_{NW}$	20
$G_{NTop}$	20
$G_{NAMB}$	27.5

**Table 53. House  $T_W$  conductances.**

<b><math>T_W</math> Conductances</b>	<b>(%) of <math>G_W</math></b>
$G_{WS}$	20
$G_{WTop}$	20
$G_{WAMB}$	27.5

**Table 54. House  $T_S$  conductances.**

<b><math>T_S</math> Conductances</b>	<b>(%) of <math>G_S</math></b>
$G_{STop}$	20
$G_{SAMB}$	27.5

**Table 55. House  $T_{Top}$  conductances.**

<b><math>T_{Top}</math> Conductances</b>	<b>(%) of <math>G_{Top}</math></b>
$G_{TopAmb}$	27.5

## Appendix D Electrothermal Air-Conditioner Model

The mathematical model of the electrothermal air conditioner is given by the following equations

$$\tilde{I}_1 = \left( \frac{P_{HVAC} + jQ_{HVAC}}{\tilde{V}_1 - \tilde{V}_2} \right)^* (1 - u_1)u_2 \quad (D.1)$$

$$\tilde{I}_2 = - \left( \frac{P_{HVAC} + jQ_{HVAC}}{\tilde{V}_1 - \tilde{V}_2} \right)^* (1 - u_1)u_2 \quad (D.2)$$

$$0.0 = 0.0 u_2 \quad (D.3)$$

$$\dot{q}_{Bed1} = G_S(\tilde{T}_{Bed1} - \tilde{T}_{Amb}) - K_1 \dot{Q}_{hvac} \quad (D.4)$$

$$\dot{q}_{Bed2} = G_S(\tilde{T}_{Bed2} - \tilde{T}_{Amb}) - K_2 \dot{Q}_{hvac} \quad (D.5)$$

$$\dot{q}_{Bath1} = G_S(\tilde{T}_{Bath1} - \tilde{T}_{Amb}) - K_3 \dot{Q}_{hvac} \quad (D.6)$$

$$\dot{q}_{Bath2} = G_S(\tilde{T}_{Bath2} - \tilde{T}_{Amb}) - K_4 \dot{Q}_{hvac} \quad (D.7)$$

$$\dot{q}_K = G_S(\tilde{T}_K - \tilde{T}_{Amb}) - K_5 \dot{Q}_{hvac} \quad (D.8)$$

$$\dot{q}_L = G_S(\tilde{T}_L - \tilde{T}_{Amb}) - K_6 \dot{Q}_{hvac} \quad (D.9)$$

$$\begin{aligned} \dot{q}_{Amb} = & -G_S(\tilde{T}_{Bed1} + \tilde{T}_{Bed2} + \tilde{T}_{Bath1} + \tilde{T}_{Bath2} + \tilde{T}_K + \tilde{T}_L - 6\tilde{T}_{Amb}) + (K_1 \\ & + K_2 + K_3 + K_4 + K_5 + K_6)\dot{Q}_{hvac} \end{aligned} \quad (D.10)$$

$$P_{HVAC} = \frac{k_{factor} \dot{Q}_{hvac} m}{COP} (1 - u_1)u_2 \quad (D.11)$$

$$Q_{HVAC} = \tan(\cos^{-1}(pf)) P_{HVAC} \quad (D.12)$$

$$\dot{Q}_{hvac} = \frac{BR}{m} (1 - u_1) u_2 \quad (D.13)$$

$$BR = BR_0 \left( 1.4892 - 0.0052 \left( \left( \frac{9}{5} a\tilde{T}_{Amb} \right) + 32 \right) \right) \quad (D.14)$$

$$m = 1.1 + \frac{m_l}{1 + \exp(4 - 0.1\rho)} \quad (D.15)$$

$$COP = \frac{COP_{nom}}{-0.01364 + 0.01067 \left( \left( \frac{9}{5} a \tilde{T}_{Amb} \right) + 32 \right)} \quad (D.16)$$

Equations (D.1)-(D.16) cast into a compact matrix form as follows

$$\begin{bmatrix} I \\ 0 \end{bmatrix} = Y_{eq} \begin{bmatrix} V \\ Y \end{bmatrix} + [V \quad Y] F_{eq} \begin{bmatrix} V \\ Y \end{bmatrix} + K_{eq} \quad (D.17)$$

, where

$$I = [\tilde{I}_1 \quad \tilde{I}_2 \quad 0.0 \quad \dot{q}_{Bed1} \quad \dot{q}_{Bed2} \quad \dot{q}_{Bath1} \quad \dot{q}_{Bath2} \quad \dot{q}_K \quad \dot{q}_L \quad \dot{q}_{Amb}]^T,$$

$$V = [\tilde{V}_1 \quad \tilde{V}_2 \quad u_2 \quad \tilde{T}_{Bed1} \quad \tilde{T}_{Bed2} \quad \tilde{T}_{Bath1} \quad \tilde{T}_{Bath2} \quad \tilde{T}_K \quad \tilde{T}_L \quad \tilde{T}_{Amb}]^T$$

$$Y = [P_{HVAC} \quad Q_{HVAC} \quad \dot{Q}_{hvac} \quad BR \quad m \quad COP]^T$$

$Y_{eq}$ : Matrix defining the linear part.

$F_{eq}$ : Nonlinear and differential parts of the model.

$K_{eq}$ : Vector containing the constant part of the model.

$P_{HVAC}$ : Air conditioner active power consumption in [MW].

$Q_{HVAC}$ : Air conditioner reactive power consumption in [MVar].

$V_{rated}$ : Rated voltage rms of air conditioner in [V].

$Eff$ : The air conditioner electrical efficiency.

$pf$ : Power factor of the device.

$G_s$ : Heat source internal thermal conductance, added for numerical stability purpose in [MBtu/k°C h].

$\dot{Q}_{hvac}$ : Heat rate generated by the air conditioner in [MBtu/h].



$q_{bed1}, \dots, q_L$ : Heat rate through variables in [MBtu/h].

$T_{Bed1}, \dots, T_L$ : Temperature across states variables in [k °C].

$k_{factor}$ : a conversion factor (1 MW ~ 3.414 MBtu/h).

$BR_o$ : Nominal Btu rating of the air conditioner system (at 35 °C) in [MBtu/h].

$m$ : Fraction of the cooling load [unit-less].

$COP_o$ : Nominal cooling coefficient of performance (at 35 °C) [unit-less].

$\rho$ : Outside relative humidity [%].

$K_1, \dots, K_6$ : Constant based on the house layout of ducts.

$a$ : scale factor equals 1000.

$u_1$ : Air conditioner On/Off power service given by

$$u_1 = \begin{cases} 0, & \text{Power ON} \\ 1, & \text{Power OFF} \end{cases}$$

$u_2$ : Air conditioner operation control signal

$$u_2 = \begin{cases} 0, & \text{A/C OFF} \\ 1, & \text{A/C ON} \end{cases}$$

## Appendix E Electrothermal Refrigerator Model

The mathematical model of the electrothermal refrigerator with six temperature spots is given by the following equations

$$\tilde{I}_1 = \left( \frac{P_f + jQ_f}{\tilde{V}_1 - \tilde{V}_2} \right)^* (1 - u_1)u_2 \quad (\text{E.1})$$

$$\tilde{I}_2 = - \left( \frac{P_f + jQ_f}{\tilde{V}_1 - \tilde{V}_2} \right)^* (1 - u_1)u_2 \quad (\text{E.2})$$

$$\begin{aligned} \dot{q}_1 = & C_{frew} \frac{d}{dt} (T_{K1}(t) - T_{frew}(t)) + C_{fzew} \frac{d}{dt} (T_{K1}(t) - T_{fzew}(t)) \\ & + G_{frew-k} (T_{K1}(t) - T_{frew}(t)) + G_{fzew-k} (T_{K1}(t) - T_{fzew}(t)) \end{aligned} \quad (\text{E.3})$$

$$\dot{q}_2 = G_s (T_{K2}(t) - T_{fr}(t)) + G_s (T_{K2}(t) - T_{fz}(t)) + k_1 \dot{Q}_r + k_2 \dot{Q}_r \quad (\text{E.4})$$

$$P_f (1 - u_1)u_2 = k_{factor} \frac{-\dot{Q}_r}{COP} \quad (\text{E.5})$$

$$\begin{aligned} 0.0 = & C_{fr} \frac{d}{dt} (T_{fr}(t) - T_{friw}(t)) + G_{fr} (T_{fr}(t) - T_{friw}(t)) \\ & + G_s (T_{fr}(t) - T_{K2}(t)) - k_1 \dot{Q}_r \end{aligned} \quad (\text{E.6})$$

$$\begin{aligned} 0.0 = & C_{fr} \frac{d}{dt} (T_{friw}(t) - T_{fr}(t)) + C_{friw} \frac{d}{dt} (T_{friw}(t) - T_{frew}(t)) \\ & + G_{fr} (T_{friw}(t) - T_{fr}(t)) + G_{friw-fziw} (T_{friw}(t) - T_{fziw}(t)) \\ & + G_{friw-frew} (T_{friw}(t) - T_{frew}(t)) \end{aligned} \quad (\text{E.7})$$

$$\begin{aligned}
0.0 = & C_{friw} \frac{d}{dt} (T_{frew}(t) - T_{friw}(t)) + C_{frew} \frac{d}{dt} (T_{frew}(t) - T_{K1}(t)) \\
& + G_{friw-frew} (T_{frew}(t) - T_{friw}(t)) \\
& + G_{frew-fzew} (T_{frew}(t) - T_{fzew}(t)) \\
& + G_{frew-K} (T_{frew}(t) - T_{K1}(t))
\end{aligned} \tag{E.8}$$

$$\begin{aligned}
0.0 = & C_{fz} \frac{d}{dt} (T_{fz}(t) - T_{fziw}(t)) + G_{fz} (T_{fz}(t) - T_{fziw}(t)) \\
& + G_s (T_{fz}(t) - T_{K2}(t)) - k_2 \dot{Q}_r
\end{aligned} \tag{E.9}$$

$$\begin{aligned}
0.0 = & C_{fz} \frac{d}{dt} (T_{fziw}(t) - T_{fz}(t)) + C_{fziw} \frac{d}{dt} (T_{fziw}(t) - T_{fzew}(t)) \\
& + G_{fz} (T_{fziw}(t) - T_{fz}(t)) + G_{friw-fziw} (T_{fziw}(t) - T_{friw}(t)) \\
& + G_{fziw-fzew} (T_{fziw}(t) - T_{fzew}(t))
\end{aligned} \tag{E.10}$$

$$\begin{aligned}
0.0 = & C_{fziw} \frac{d}{dt} (T_{fzew}(t) - T_{fziw}(t)) + C_{fzew} \frac{d}{dt} (T_{fzew}(t) - T_{K1}(t)) \\
& + G_{fziw-fzew} (T_{fzew}(t) - T_{fziw}(t)) \\
& + G_{frew-fzew} (T_{fzew}(t) - T_{frew}(t)) \\
& + G_{fzew-K} (T_{frew}(t) - T_{K1}(t))
\end{aligned} \tag{E.11}$$

Equations (E.1)-(E.11) are cast into a compact matrix form as follows:

$$\begin{bmatrix} I \\ 0 \end{bmatrix} = Y_{eq} \begin{bmatrix} V \\ Y \end{bmatrix} + [V \quad Y] F_{eq} \begin{bmatrix} V \\ Y \end{bmatrix} + K_{eq} \tag{E.12}$$

, where

$$I = [\tilde{I}_1 \quad \tilde{I}_2 \quad \dot{q}_1 \quad \dot{q}_2]^T,$$

$$V = [\tilde{V}_1 \quad \tilde{V}_2 \quad T_{K1}(t) \quad T_{K2}(t)]^T$$

$$Y = [T_{fr}(t) \quad T_{friw}(t) \quad T_{frew}(t) \quad T_{fz}(t) \quad T_{fziw}(t) \quad T_{fzew}(t) \quad \dot{Q}_r]^T$$

$I$ : Through variables of the model.

$V$ : Across external states variables of the model.

$Y$ : Internal states variables of the model.

$Y_{eq}$ : Matrix defining the linear part of the model.

$F_{eq}$ : Nonlinear and differential parts of the model.

$K_{eq}$ : Vector containing the constant part of the model.

$P_f$ : Maximum active power consumption of the refrigerator in [MW] computed as the following,

$$P_f = P_{rated} Eff$$

$Q_f$ : Maximum reactive power consumption of the refrigerator [MVar] computed as the following,

$$Q_f = P_f \tan(\cos^{-1}(pf))$$

$u_1$ : Refrigerator On/Off status (main service of operation).

$$u_1 = \begin{cases} 0, & \text{Power ON} \\ 1, & \text{Power OFF} \end{cases}$$

$u_2$ : Refrigerator temperature control.

$$u_2 = \begin{cases} 0, & \text{Refrigerator OFF} \\ 1, & \text{Refrigerator ON} \end{cases}$$

$k_{factor}$ : A conversion factor (1 MW ~ 3.414 MBtu/h)

$P_{rated}$ : Rated power of the refrigerator in [W].

$V_{rated}$ : Rated voltage rms of the refrigerator in [V].

$Eff$ : The refrigerator electrical efficiency. A value of 0.8 is typical for a refrigerator.

$pf$ : Power factor of the device. A value of 0.9 is typical for a refrigerator.

$COP$ : Coefficient of performance. A value of 3.5 is typical for a refrigerator.

$k_1$  and  $k_2$ : Constant depends on the refrigerator manufacture design. Typical values are 0.6 and 0.4 respectively.

$\dot{Q}_r$ : Heat flow rate of the refrigerator [MBtu/h].

$\dot{q}_1$ : Heat flow through variable 1 [MBtu/h].

$\dot{q}_2$ : Heat flow through variable 2 [MBtu/h].

$T_{fr}$ : Fresh food compartment temperature spot in [k°C].

$T_{fz}$ : Freezer compartment temperature spot in [k°C].

$T_{friw}$ : Internal wall of the fresh food compartment temperature spot in [k°C].

$T_{frew}$ : External wall of the fresh food compartment temperature spot in [k°C].

$T_{fziw}$ : Internal wall of the freezer compartment temperature spot in [k°C].

$T_{fzew}$ : External wall of the freezer compartment temperature spot in [k°C].

$T_{k1}$ : Across external state variable kitchen terminal 1 temperature spot in [k°C].

$T_{k2}$ : Across external state variable kitchen terminal 2 temperature spot in [k°C].

$G_{fr}$ : Thermal conductance between the fresh food compartment mass and the fresh food compartment internal wall in [MBtu/k°C h].

$G_{fz}$ : Thermal conductance between the freezer compartment mass and the freezer compartment internal wall in [MBtu/k<sup>o</sup>C h].

$G_{friw-fziw}$ : Thermal conductance between the fresh food compartment internal wall and the freezer compartment internal wall mass in [MBtu/k<sup>o</sup>C h].

$G_{friw-frew}$ : Thermal conductance of the fresh food compartment wall in [MBtu/k<sup>o</sup>C h].

$G_{fziw-fzew}$ : Thermal conductance of the freezer compartment wall in [MBtu/k<sup>o</sup>C h].

$G_{frew-fzew}$ : Thermal conductance of the fresh food and freezer compartments external walls in [MBtu/k<sup>o</sup>C h].

$G_{frew-K}$ : Thermal conductance between the fresh food compartment external wall and the Kitchen air mass in [MBtu/k<sup>o</sup>C h].

$G_{fzew-K}$ : Thermal conductance between the freezer compartment external wall and the Kitchen air mass in [MBtu/k<sup>o</sup>C h].

$G_s$ : Thermal conductance of the heat source in [MBtu/k<sup>o</sup>C h].

$C_{fr}$ : The sum of the heat capacity of every element inside the fresh food compartment in [MBtu/k<sup>o</sup>C].

$C_{friw}$ : Heat capacity of internal door mass in the fresh food compartment in [MBtu/k<sup>o</sup>C].

$C_{frew}$ : Heat capacity of external door mass in the fresh food compartment in [MBtu/k<sup>o</sup>C].

$C_{fz}$ : The sum of the heat capacity of every element inside the freezer compartment in [MBtu/k<sup>o</sup>C].

$C_{fziw}$ : Heat capacity of internal door mass in the freezer compartment in [MBtu/k<sup>o</sup>C].

$C_{fzew}$ : Heat capacity of external door mass in the freezer compartment in [MBtu/k<sup>o</sup>C].

$Vol_{fr}$ : Fresh Food Compartment Capacity in [ft<sup>3</sup>].

$Vol_{fz}$ : Freezer Compartment Capacity in [ft<sup>3</sup>].

$\theta_{sei}$ : Refrigerator desired internal temperature in [k°C]. Typical value is 1-5 °C.

$\theta_{dead-band}$ : Temperature control dead-band in [k°C]. Typically, it is 1-2 °C.

It should be noted that  $C_{fr}(t)$  is the sum of each element heat capacity, including cool air, inside the fresh food compartment at every time  $t$ . It is mathematically expressed as the following:

$$C_{fr}(t) = \Delta C_{fr0}(t) + \Delta C_{fr1}(t) + \Delta C_{fr2}(t) + \dots + \Delta C_{fri}(t)$$

, where

$\Delta C_{fr0}(t)$ : Thermal capacitance of element 0 in the fresh food compartment at time  $t$  [MBtu/k°C].

$\Delta C_{fr1}(t)$ : Thermal capacitance of element 1 in the fresh food compartment at time  $t$  [MBtu/k°C].

$\Delta C_{fr2}(t)$ : Thermal capacitance of element 2 in the fresh food compartment at time  $t$  [MBtu/k°C].

$\Delta C_{fri}(t)$ : Thermal capacitance of element  $i$  in the fresh food compartment at time  $t$  [MBtu/k°C].

$i$ : The total number of elements inside the fresh food compartment.

Also,  $C_{fz}(t)$  is the sum of each element heat capacity, including cold air, inside the freezer compartment at every time  $t$ . It is mathematically expressed as the following:

$$C_{fz}(t) = \Delta C_{fz0}(t) + \Delta C_{fz1}(t) + \Delta C_{fz2}(t) + \dots + \Delta C_{fzj}(t)$$

, where

$\Delta C_{fz0}(t)$ : Thermal capacitance of element 0 in the freezer compartment at time  $t$   
[MBtu/k°C].

$\Delta C_{fz1}(t)$ : Thermal capacitance of element 1 in the freezer compartment at time  $t$   
[MBtu/k°C].

$\Delta C_{fz2}(t)$ : Thermal capacitance of element 2 in the freezer compartment at time  $t$   
[MBtu/k°C].

$\Delta C_{fzj}(t)$ : Thermal capacitance of element  $j$  in the freezer compartment at time  $t$   
[MBtu/k°C].

$j$ : The total number of elements inside the fresh food compartment.

Note that data regarding both refrigerator and freezer elements are specified in the csv file found in the device folder. This file contains the following information,

- Time when the event takes place enter the form (hh:mm:ss)
- Door openings for both fresh food and freezer compartments.
- Mass in (kg) for every element inside both the fresh food and freezer compartments.



## *Appendix F Dishwasher Mathematical Model*

The mathematical model of the dishwasher is given by the following equations

$$\tilde{I}_1 = \left( \frac{P_{dw} + jQ_{dw}}{\tilde{V}_1 - \tilde{V}_2} \right)^* (1 - u_1)u_2u_3z_t \quad (\text{F.1})$$

$$\tilde{I}_2 = - \left( \frac{P_{dw} + jQ_{dw}}{\tilde{V}_1 - \tilde{V}_2} \right)^* (1 - u_1)u_2u_3z_t \quad (\text{F.2})$$

, where:

$P_{dw}$ : Maximum active power consumption of the dishwasher in [W] computed as the following,

$$P_{dw} = P_{rated}Eff$$

$Q_{dw}$ : Maximum reactive power consumption of the dishwasher [VAr] computed as the following,

$$Q_{dw} = P_{dw} \tan(\cos^{-1}(pf))$$

$u_1$ : Dishwasher On/Off status (main service of operation),

$$u_1 = \begin{cases} 0 & , \text{Dishwasher Power On} \\ 1 & , \text{Dishwasher Power Off} \end{cases}$$

$u_2$ : Dishwasher load level variable. It is specified according to the chosen input load level as given in Table 9.

$u_3$ : Power consumption at each stage of the cycle. During every cycle,  $u_3$  will change according to the stage. Every stage of the simulation is determined based on the progress of the simulation time inside the cycle. So,  $u_3$  can be evaluated as the following,

$$u_3 = 0.25[U(t - t_{0_i}) - U(t - t_{0_i} - 0.1t_c)]$$

$$\begin{aligned}
& +[U(t - t_{0_i} - 0.1t_c) - U(t - t_{0_i} - 0.35t_c)] \\
& +0.25[U(t - t_{0_i} - 0.35t_c) - U(t - t_{0_i} - 0.65t_c)] \\
& +[U(t - t_{0_i} - 0.65t_c) - U(t - t_{0_i} - 0.9t_c)] \\
& +0.25[U(t - t_{0_i} - 0.9t_c) - U(t - t_{0_i} - t_c)]
\end{aligned}$$

$z_i$ : a unit step function defined by

$$z_t = U(t - t_{0_i}) - U(t - t_{0_i} - t_c)$$

$P_{rated}$ : Rated power of the dishwasher in [W].

$V_{rated}$ : Rated voltage in root mean square value of the dishwasher in [V].

$Eff$ : The dishwasher efficiency. A value of 0.8 is typical for a dishwasher.

$pf$ : Power factor of the device. A value of 0.9 is typical for a dishwasher.

$t_c$ : Duration time for one full cycle of the dishwasher in [min].

$t_{0_i}$ : The time at  $i$  when the dishwasher is turned on in this form [hh:mm:ss]. For multiple operations, the duration time of full cycle should be taken into account.

The model then is cast into a compact matrix form as follows

$$\begin{bmatrix} I \\ 0 \end{bmatrix} = Y_{eq}V + K_{eq} \quad (F.3)$$

, where

$$I = [\tilde{I}_1 \quad \tilde{I}_2]^T,$$

$$V = [\tilde{V}_1 \quad \tilde{V}_2]^T$$

$I$ : Through variables of the model.

$V$ : Across external states variables of the model.

$Y_{eq}$ : Matrix defining the linear part of the model.

$K_{eq}$ : Vector containing the constant part of the model.

## Appendix G Variable Load Model

The mathematical model of the variable load is given by the following equations

$$\tilde{I}_1 = \left( \frac{P_L(t) + jQ_L(t)}{\tilde{V}_1 - \tilde{V}_2} \right)^* \quad (\text{G.1})$$

$$\tilde{I}_2 = - \left( \frac{P_L(t) + jQ_L(t)}{\tilde{V}_1 - \tilde{V}_2} \right)^* \quad (\text{G.2})$$

, where:

$P_L(t)$ : Load active power consumption at time  $t$  in [MW].

$Q_L(t)$ : Load reactive power consumption of the dishwasher [MVar] computed as the following,

The model then is cast into a compact matrix form as follows

$$\begin{bmatrix} I \\ 0 \end{bmatrix} = Y_{eq}V + K_{eq} \quad (\text{G.3})$$

, where

$$I = [\tilde{I}_1 \quad \tilde{I}_2]^T,$$

$$V = [\tilde{V}_1 \quad \tilde{V}_2]^T$$

$I$ : Through variables of the model.

$V$ : Across external states variables of the model.

$Y_{eq}$ : Matrix defining the linear part of the model.

$K_{eq}$ : Vector containing the constant part of the model.

## *Appendix H Solar Cell Mathematical Model*

The mathematical model used for the solar cell is represented by the following equations

$$I = I_{pv} - I_0 \left[ \exp\left(\frac{V + IR_s}{V_t a}\right) - 1 \right] - \frac{V + IR_s}{R_p} \quad (\text{H.1})$$

$$I_{pv} = (I_{pv_n} + K_I \Delta T) \frac{S}{S_n} \quad (\text{H.2})$$

$$I_0 = (I_{sc_n} + K_I \Delta T) / \left[ \exp\left(\frac{(V_{oc_n} + K_V \Delta T)}{a V_t}\right) - 1 \right] \quad (\text{H.3})$$

$$I_{pv_n} = \frac{R_p + R_s}{R_p} I_{sc_n} \quad (\text{H.4})$$

$$V_t = \frac{N_s k T}{q} \quad (\text{H.5})$$

$$\Delta T = T - T_n \quad (\text{H.6})$$

, where

$I$ : the array output current [A]

$V$ : the array output voltage [V]

$I_{pv}$ : Light generated current [A]

$I_{pv,n}$ : Light generated current at the nominal condition [A]

$I_0$ : the reverse saturation or the leakage current of the diode [A]

$R_s$ : the equivalent series resistance of the array [ $\Omega$ ]

$R_p$ : the equivalent parallel resistance of the array [ $\Omega$ ]

$I_{sc,n}$ : Short circuit current provided by the data sheet [A]

$V_{oc,n}$ : Open circuit voltage provided by the data sheet [V]

$S$ : Current solar irradiance [ $\text{W}/\text{m}^2$ ]

$S_n$ : Nominal solar irradiance =  $1000[\text{W}/\text{m}^2]$

$T$ : Weather temperature [K]

$T_n$ : Nominal temperature =  $273.15$  [K]

$V_t$ : the equivalent thermal voltage of the array [V]

$N_s$ : the number of cells in series provided by the data sheet

$a$ : Diode constant  $1 \leq a \leq 1.5$

$K_I$ : Short circuit current temperature coefficient provided by the data sheet

$K_V$ : Open circuit voltage temperature coefficient provided by the data sheet

$k$ : Boltzmann constant =  $1.3806503 \times 10^{-23}$  [J/K]

$q$ : the electron charge =  $1.60217646 \times 10^{-19}$  [C]

## Appendix I Electrothermal Lead-Acid Battery

The lead acid electrical circuit is shown in Figure 83.

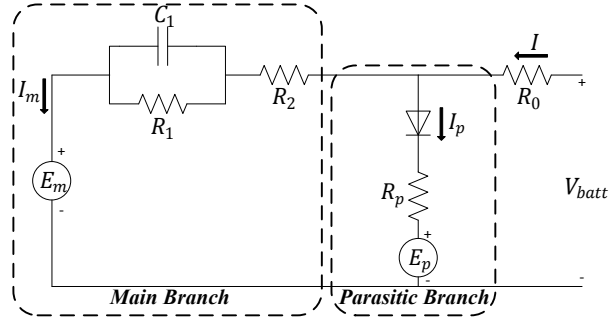


Figure 83. Equivalent lead acid electric circuit model.

### Appendix I.1 Mathematical Model

#### Main Branch

The main branch voltage is a function of the state of charge and the electrolyte temperature and given by

$$E_m = E_{m0} - K_E(273 + \theta)(1 - SOC) \quad (I.1)$$

, where

$E_m$ : Open circuit voltage in [V]

$E_{m0}$ : Open circuit voltage when the battery is full of charge in [V]

$T$ : Electrolyte temperature in [ $^{\circ}$ C]

$SOC$ : State of charge

$K_E$ : Constant in [V/ $^{\circ}$ C]

The main branch resistance and capacitance are given by

$$R_1 = -R_{10} \ln(DOC) \quad (I.2)$$

$$C_1 = \tau_1/R_1 \quad (I.3)$$

, where

$R_1$ : the main branch resistance in [ $\Omega$ ]

$C_1$ : the main branch capacitance in [F]

$R_{10}$ : Constant in [ $\Omega$ ]

$DOC$ : Battery depth of charge

$\tau_1$ : the main branch time constant in [sec]

The main branch second resistance is given by

$$R_2 = R_{20} \exp[A_{21}(1 - SOC)] / (1 + \exp(A_{22}I_m/I^*)) \quad (I.4)$$

, where

$R_2$ : is the main branch second resistance in [ $\Omega$ ]

$R_{20}$ : Constant in [ $\Omega$ ]

$A_{21}$ : Constant

$A_{22}$ : Constant

$I_m$ : The main branch current in [A]

$I^*$ : Battery nominal current in [A]

The terminal resistance of the battery is given by

$$R_0 = R_{00}[1 + A_0(1 - SOC)] \quad (I.5)$$

, where



$R_0$ : the resistance in [ $\Omega$ ]

$R_{00}$ : Constant in [ $\Omega$ ] and equals to the value of  $R_0$  the battery is full of charge

$A_0$ : Constant

### **Parasitic Branch**

The behavior of the parasitic branch is strongly non-linear. However, the value of the current flowing in the branch, which is a function of the parasitic branch voltage, can be computed by the Tafel gassing – current relationship which is given by

$$I_p = V_p G_p \quad (I.6)$$

, where  $G_p$  is

$$G_p = G_{p0} \exp \left[ \frac{V_p}{V_{p0}} + A_p \left( 1 - \frac{T}{T_f} \right) \right] \quad (I.7)$$

, and thus  $R_p$  is

$$R_p = (V_p - E_p) / I_p \quad (I.8)$$

, where

$I_p$ : the current flowing in the parasitic branch in [A]

$V_p$ : The parasitic branch voltage in [V]

$G_{p0}$ : Constant in [S]

$V_{p0}$ : Constant in [V]

$A_p$ : Constant

$T_f$ : Electrolyte freezing temperature in [ $^{\circ}$ C]

## Charge and Battery Capacity

The extracted charge at  $t$  is given by

$$Q_e(t) = Q_{init} + \int_0^t -I_m(\tau) d\tau \quad (I.9)$$

The averaged current can be computed by

$$I_{ave} = I_m / (\tau_1 s + 1) \quad (I.10)$$

The capacity of the battery, which is a function of the battery current  $I$  and the electrolyte temperature, is given by the following

$$C(I, T) = \frac{K_c C_{0^*} \left(1 - \frac{T}{T_f}\right)^\xi}{1 + (K_c - 1) \left(\frac{I}{I^*}\right)^\delta} \quad (I.11)$$

, where

$Q_e$ : the extracted charge in [As] and  $Q_{init}$  is the initial extracted charge in [As]

$\tau$ : The integration time variable

$t$ : the simulation time in [sec]

$K_c$ : a constant

$C_{0^*}$ : no load capacity at 0[°C] in [Ah]

$\xi$  and  $\delta$ : constant

The state of charge and the depth of charge are given by the following equations

$$SOC = 1 - Q_e / C(0, T) \quad (I.12)$$

$$DOC = 1 - Q_e / C(I_{ave}, T) \quad (I.13)$$

## **Thermal Model**

$$\frac{dT}{dt} = 1/C_{th} \left[ P_s - \frac{T - T_a}{R_{th}} \right] \quad (I.14)$$

, where

$C_{th}$ : Thermal capacitance in [Wh/°C]

$R_{th}$ : Thermal resistance in [°C/W]

$P_s$ : The heat power loss in the parasitic branch in [W]

$T_a$ : Ambient temperature or the surrounding temperature in [°C]

## **Appendix I.2 Charging Mode**

The mathematical model of the lead acid battery in the charging mode is given by the following compact equations

$$I_1 = G_0(V_1 - V_x) \quad (I.15)$$

$$I_2 = -G_0(V_1 - V_x) \quad (I.16)$$

$$0.0 = G_p[(V_x - V_2) - E_p] + I_m - G_0(V_1 - V_x) \quad (I.17)$$

$$0.0 = I_m - G_1(V_y - V_z) - C_1 \frac{d}{dt}(V_y - V_z) \quad (I.18)$$

$$0.0 = I_m - G_2(V_x - V_y) \quad (I.19)$$

$$0.0 = (V_z - V_2) - E_{m0} + K_E(273 + T)(1 - SOC) \quad (I.20)$$

$$0.0 = C_1 - \tau_1 G_1 \quad (I.21)$$

$$0.0 = R_0 - R_{00}[1 + A_0(1 - SOC)] \quad (I.22)$$

$$0.0 = I_m + \frac{dQ_e(t)}{dt} \quad (I.23)$$

$$0.0 = SOC C(0, T) - C(0, T) + Q_e \quad (I.24)$$

$$0.0 = DOC C(I_{ave}, T) - C(I_{ave}, T) + Q_e \quad (I.25)$$

$$0.0 = \frac{dT}{dt} - \frac{1}{C_{th}} \left[ P_s - \frac{T - T_a}{R_{th}} \right] \quad (I.26)$$

$$0.0 = R_0 G_0 - 1 \quad (I.27)$$

$$0.0 = R_1 G_1 - 1 \quad (I.28)$$

$$0.0 = R_2 G_2 - 1 \quad (I.29)$$

$$0.0 = C(0, T) - K_c C_{0^*} \left( 1 - \frac{T}{T_f} \right)^\xi \quad (I.30)$$

$$0.0 = C(I_{avg}, T) - \frac{K_c C_{0^*} \left( 1 - \frac{T}{T_f} \right)^\xi}{1 + (K_c - 1) \left( \frac{I_{avg}}{I^*} \right)^\delta} \quad (I.31)$$

$$0.0 = C(I_1, T) - \frac{K_c C_{0^*} \left( 1 - \frac{T}{T_f} \right)^\xi}{1 + (K_c - 1) \left( \frac{I_1}{I^*} \right)^\delta} \quad (I.32)$$

$$0.0 = R_2 - R_{20} \exp[A_{21}(1 - SOC)] / \left[ 1 + \exp\left(\frac{A_{22} I_m}{I^*}\right) \right] \quad (I.33)$$

$$0.0 = G_p - G_{p0} \exp \left[ \left( \frac{V_x - V_2}{V_{p0}} \right) + A_p \left( 1 - \frac{T}{T_f} \right) \right] \quad (I.34)$$

$$0.0 = I_{avg} - \left[ \frac{I_m \exp\left(-\frac{t}{\tau_1}\right)}{\tau_1} \right] \quad (I.35)$$

$$0.0 = R_1 + R_{10} \ln(DOC) \quad (I.36)$$

$$0.0 = P_s - G_p [(V_x - V_2) - E_p]^2 \quad (I.37)$$

For simplicity, equations (I.15)-(I.37) can be cast into a compact matrix form as follows

$$\begin{bmatrix} I \\ 0 \end{bmatrix} = A \begin{bmatrix} V \\ Y \end{bmatrix} + N + C \quad (I.38)$$

, where

$$I = [I_1 \quad I_2]^T,$$

$$V = [V_1 \quad V_2]^T$$

$$Y = [V_x \quad V_y \quad V_z \quad R_0 \quad R_1 \quad R_2 \quad G_0 \quad G_1 \quad G_2 \quad G_p \quad C_1 \quad T \quad SOC \quad DOC \quad I_m \quad P_s$$

$$Q_e \quad I_{avg} \quad C(0, T) \quad C(I_{avg}, T) \quad C(I_1, T)]^T$$

### Appendix I.3 Discharging Mode

The mathematical model of the lead acid battery in the discharging mode is given by the following compact equations

$$I_1 = G_0(V_1 - V_x) \quad (I.39)$$

$$I_2 = -G_0(V_1 - V_x) \quad (I.40)$$

$$0.0 = I_m - G_0(V_1 - V_x) \quad (I.41)$$

$$0.0 = I_m - G_1(V_x - V_z) - C_1 \frac{d}{dt}(V_x - V_z) \quad (I.42)$$

$$0.0 = (V_z - V_2) - E_{m0} + K_E(273 + \theta)(1 - SOC) \quad (I.43)$$

$$0.0 = C_1 - \tau_1 G_1 \quad (I.44)$$

$$0.0 = R_0 - R_{00}[1 + A_0(1 - SOC)] \quad (I.45)$$

$$0.0 = I_m + \frac{d Q_e(t)}{dt} \quad (I.46)$$

$$0.0 = SOC C(0, \theta) - C(0, \theta) + Q_e \quad (I.47)$$

$$0.0 = DOC C(I_{ave}, \theta) - C(I_{ave}, \theta) + Q_e \quad (I.48)$$

$$0.0 = \frac{d\theta}{dt} - \frac{1}{C_\theta} \left[ 0 - \frac{\theta - \theta_a}{R_\theta} \right] \quad (I.49)$$

$$0.0 = R_0 G_0 - 1 \quad (I.50)$$

$$0.0 = R_1 G_1 - 1 \quad (I.51)$$

$$0.0 = C(0, \theta) - K_c C_{0^*} \left(1 - \frac{\theta}{\theta_f}\right)^\xi \quad (I.52)$$

$$0.0 = C(I_{avg}, \theta) - \frac{K_c C_{0^*} \left(1 - \frac{\theta}{\theta_f}\right)^\xi}{1 + (K_c - 1) \left(\frac{I_{avg}}{I^*}\right)^\delta} \quad (I.53)$$

$$0.0 = C(I_1, \theta) - \frac{K_c C_{0^*} \left(1 - \frac{\theta}{\theta_f}\right)^\xi}{1 + (K_c - 1) \left(\frac{I_1}{I^*}\right)^\delta} \quad (I.54)$$

$$0.0 = I_{avg} - \left[ \frac{I_m \exp\left(-\frac{t}{\tau_1}\right)}{\tau_1} \right] \quad (I.55)$$

$$0.0 = R_1 + R_{10} \ln(DOC) \quad (I.56)$$

For simplicity, equations (I.39)-(I.56) can be cast into a compact matrix form as follows

$$\begin{bmatrix} I \\ 0 \end{bmatrix} = A \begin{bmatrix} V \\ Y \end{bmatrix} + N + C \quad (I.57)$$

Where:

$$I = [I_1 \quad I_2]^T,$$

$$V = [V_1 \quad V_2]^T$$

$$Y = [V_x \quad V_z \quad R_0 \quad R_1 \quad G_0 \quad G_1 \quad C_1 \quad \theta \quad SOC \quad DOC \quad I_m \quad Q_e \quad I_{avg}$$

$$C(0, \theta) \quad C(I_{avg}, \theta) \quad C(I_1, \theta)]^T$$

## Appendix J Electric Vehicle Model

### Appendix J.1 Lithium Ion Battery Mathematical Model

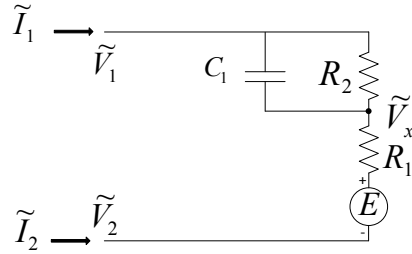


**Figure 84. Equivalent electrical circuit of lithium ion battery.**

In this section, the battery model is reformulated according to the standard device format that is as the following

$$\tilde{I}_1 = \tilde{x}_1 \quad (\text{J.1})$$

$$\tilde{I}_2 = -\tilde{x}_1 \quad (\text{J.2})$$

, where  $x_1$  is given by

$$0.0 = -\tilde{x}_1 + G_2(\tilde{V}_1 - \tilde{V}_x) + j\omega C_1(\tilde{V}_1 - \tilde{V}_x) \quad (\text{J.3})$$

$$0.0 = \tilde{E} - (\tilde{V}_1 - \tilde{V}_2) + (R_1 + R_2)\tilde{x}_1 \quad (\text{J.4})$$

$$0.0 = -\tilde{V}_1 + \tilde{V}_2 + c_0 + c_1 SOD(t) + c_2 SOD^2(t) + c_3 SOD^3(t) + \Delta E(\theta(t)) \quad (\text{J.5})$$

, and the coefficients are listed in Table 56 below

**Table 56. Terminal voltage polynomial coefficients.**

$c_0 = 4.121$	$c_1 = -1.624$	$c_2 = 3.587$	$c_3 = -3.581$
---------------	----------------	---------------	----------------

$$0.0 = \frac{d}{dt} SOD(t) - \frac{1}{Q_r} \alpha(\tilde{I}_1) \beta(\theta(t)) \tilde{x}_1 \quad (\text{J.6})$$

$$0.0 = -m c_p \frac{d\theta(t)}{dt} + P_s(t) - h_c A(\theta(t) - \theta_a) \quad (\text{J.7})$$

, where  $P_s(t)$  is the electric power loss and given by

$$0.0 = P_s(t) - \tilde{x}_1^2 R_1 - G_2(\tilde{V}_1 - \tilde{V}_x)^2 \quad (\text{J.8})$$

The other three fitted to the 2<sup>nd</sup> degree polynomials are

$$\alpha(\tilde{I}_1) = a_0 + a_1 \tilde{x}_1 + a_2 \tilde{x}_1^2 \quad (\text{J.9})$$

$$\beta(\theta(t)) = b_0 + b_1 \theta(t) + b_2 \theta^2(t) \quad (\text{J.10})$$

$$\Delta E(\theta(t)) = d_0 + d_1 \theta(t) + d_2 \theta^2(t) \quad (\text{J.11})$$

where the values of the coefficients are given in the below table

**Table 57. Polynomials coefficients.**

$a_2 = -0.006647$	$a_1 = 0.05215$	$a_0 = 0.9559$
$b_2 = 2.139 \times 10^{-6}$	$b_1 = -0.001835$	$b_0 = 1.052$
$d_2 = -4.935 \times 10^{-5}$	$d_1 = 0.01097$	$d_0 = -0.1793$

The compact form is

$$\tilde{I}_1 = \tilde{x}_1 \quad (\text{J.12})$$

$$\tilde{I}_2 = -\tilde{x}_1 \quad (\text{J.13})$$

$$0.0 = \tilde{E} - (\tilde{V}_1 - \tilde{V}_2) + (R_1 + R_2)\tilde{x}_1 \quad (\text{J.14})$$

$$0.0 = -\tilde{V}_1 + \tilde{V}_2 + c_0 + c_1 SOD + c_2 SOD^2 + c_3 SOD^3 + \Delta E(\theta) \quad (\text{J.15})$$

$$0.0 = -\tilde{x}_1 + G_2(\tilde{V}_1 - \tilde{V}_x) + j\omega C_1(\tilde{V}_1 - \tilde{V}_x) \quad (\text{J.16})$$

$$0.0 = P_s - \tilde{I}_1^2 R_1 - G_2(\tilde{V}_1 - \tilde{V}_x)^2 \quad (\text{J.17})$$

$$0.0 = SOC - 1 + SOD \quad (\text{J.18})$$

$$0.0 = -\alpha(\tilde{x}_1) + a_0 + a_1 \tilde{x}_1 + a_2 \tilde{x}_1^2 \quad (\text{J.19})$$



$$0.0 = -\beta(\theta) + b_0 + b_1\theta + b_2\theta^2 \quad (\text{J.20})$$

$$0.0 = -\Delta E(\theta) + d_0 + d_1\theta + d_2\theta^2 \quad (\text{J.21})$$

For simplicity, equations (J.12)-(J.21) can be cast into a compact matrix form as follows

$$\begin{bmatrix} I \\ 0 \end{bmatrix} = A \begin{bmatrix} V \\ Y \end{bmatrix} + N + C \quad (\text{J.22})$$

, where

$$I = [\tilde{I}_1 \quad \tilde{I}_2]^T,$$

$$V = [\tilde{V}_1 \quad \tilde{V}_2]^T$$

$$Y = [\tilde{V}_x \quad \tilde{E} \quad \tilde{x}_1 \quad SOD \quad P_s \quad \alpha(\tilde{I}_1) \quad \beta(\theta) \quad \Delta E(\theta)]^T$$

*A*: Matrix defining the linear part.

*N*: Nonlinear and differential parts of the model.

*C*: Vector containing the constant part of the model.

## *Appendix K Averaged Model of DC-DC Boost Converter*

The averaged model of the dc-dc boost converter has three different control schemes, dc voltage control, real power control, and maximum power point tracking control. The compact model of each one of them is listed in separate section. First, the model of the averaged dc-dc boost converter with dc voltage control in compact form is presented.

### Appendix K.1 DC Voltage Control

The mathematical model of the dc-dc boost converter with dc voltage control is given by the following equations

$$\tilde{I}_1 = (G_1 - jB)(\tilde{V}_1 - \tilde{V}_x) \quad (\text{K.1})$$

$$\tilde{I}_2 = -(G_1 - jB)(\tilde{V}_1 - \tilde{V}_x) \quad (\text{K.2})$$

$$\tilde{I}_3 = G_2(\tilde{V}_3 - \tilde{V}_y) \quad (\text{K.3})$$

$$\tilde{I}_4 = -G_2(\tilde{V}_3 - \tilde{V}_y) \quad (\text{K.4})$$

$$0.0 = (\tilde{V}_x - \tilde{V}_2) - (1 - D)(\tilde{V}_y - \tilde{V}_4) \quad (\text{K.5})$$

$$0.0 = \tilde{I}_1(1 - D) + \tilde{I}_3 \quad (\text{K.6})$$

Controller 1: Voltage control

$$0.0 = -V_{dc\ ref} + \tilde{V}_y - \tilde{V}_4 \quad (\text{K.7})$$

For simplicity, equations (K.1)-(K.7) can be cast into a compact matrix form as follows

$$\begin{bmatrix} I \\ 0 \end{bmatrix} = A \begin{bmatrix} V \\ Y \end{bmatrix} + N + C \quad (\text{K.8})$$

, where

$$I = [\tilde{I}_1 \quad \tilde{I}_2]^T,$$

$$V = [\tilde{V}_1 \quad \tilde{V}_2 \quad \tilde{V}_3 \quad \tilde{V}_4]^T$$

$$Y = [\tilde{V}_x \quad \tilde{V}_y \quad D]^T$$

*A*: Matrix defining the linear part.

*N*: Nonlinear and differential parts of the model.

*C*: Vector containing the constant part of the model.

Note that there 7 states with 7 equations are identified.

## Appendix K.2 Real Power Control

The mathematical model of the dc-dc boost converter with real power control is given by the following equations

$$\tilde{I}_1 = (G_1 - jB)(\tilde{V}_1 - \tilde{V}_x) \quad (\text{K.9})$$

$$\tilde{I}_2 = -(G_1 - jB)(\tilde{V}_1 - \tilde{V}_x) \quad (\text{K.10})$$

$$\tilde{I}_3 = G_2(\tilde{V}_3 - \tilde{V}_y) \quad (\text{K.11})$$

$$\tilde{I}_4 = -G_2(\tilde{V}_3 - \tilde{V}_y) \quad (\text{K.12})$$

$$0.0 = (\tilde{V}_x - \tilde{V}_2) - (1 - D)(\tilde{V}_y - \tilde{V}_4) \quad (\text{K.13})$$

$$0.0 = \tilde{I}_1(1 - D) + \tilde{I}_3 \quad (\text{K.14})$$

Controller 2: Real power control

$$0.0 = -P_{ref} + \tilde{I}_1(\tilde{V}_1 - \tilde{V}_2) - \frac{\tilde{I}_1^2}{G}, \quad (\text{K.15})$$

$$OR \quad 0.0 = -P_{ref} + \tilde{I}_1(\tilde{V}_x - \tilde{V}_2)$$

For simplicity, equations (K.9)-(K.15) can be cast into a compact matrix form as follows

$$\begin{bmatrix} I \\ 0 \end{bmatrix} = A \begin{bmatrix} V \\ Y \end{bmatrix} + N + C \quad (\text{K.16})$$

, where

$$I = [\tilde{I}_1 \quad \tilde{I}_2]^T,$$

$$V = [\tilde{V}_1 \quad \tilde{V}_2 \quad \tilde{V}_3 \quad \tilde{V}_4]^T$$

$$Y = [\tilde{V}_x \quad \tilde{V}_y \quad D]^T$$

*A*: Matrix defining the linear part.

*N*: Nonlinear and differential parts of the model.

*C*: Vector containing the constant part of the model.

Note that there 7 states with 7 equations are identified.

### Appendix K.3 Maximum Power Point Tracking (MPPT) Control

The mathematical model of the dc-dc boost converter with MPPT control is given by the following equations

$$\tilde{I}_1 = (G_1 - jB)(\tilde{V}_1 - \tilde{V}_x) \quad (\text{K.17})$$

$$\tilde{I}_2 = -(G_1 - jB)(\tilde{V}_1 - \tilde{V}_x) \quad (\text{K.18})$$

$$\tilde{I}_3 = G_2(\tilde{V}_3 - \tilde{V}_y) \quad (\text{K.19})$$

$$\tilde{I}_4 = -G_2(\tilde{V}_3 - \tilde{V}_y) \quad (\text{K.20})$$

$$0.0 = (\tilde{V}_x - \tilde{V}_2) - (1 - D)(\tilde{V}_y - \tilde{V}_4) \quad (\text{K.21})$$

$$0.0 = \tilde{I}_1(1 - D) + \tilde{I}_3 \quad (\text{K.22})$$

For simplicity, equations (K.17)-(K.22) can be cast into a compact matrix form as follows

$$\begin{bmatrix} I \\ 0 \end{bmatrix} = A \begin{bmatrix} V \\ Y \end{bmatrix} + N + C \quad (\text{K.23})$$

, where

$$I = [\tilde{I}_1 \quad \tilde{I}_2]^T,$$

$$V = [\tilde{V}_1 \quad \tilde{V}_2 \quad \tilde{V}_3 \quad \tilde{V}_4]^T$$

$$Y = [\tilde{V}_x \quad \tilde{V}_y]^T$$

*A*: Matrix defining the linear part.

*N*: Nonlinear and differential parts of the model.

*C*: Vector containing the constant part of the model.

Note that there 6 states with 6 equations are identified.

## **Appendix L Averaged Full Bridge Model of DC-AC Inverter**

The averaged model of a single phase full bridge dc-ac inverter with two different control schemes, voltage-reactive power (VQ) control and active-reactive power (PQ) control is developed. The compact model of each one of them is listed in separate section. First, the model of the averaged dc-ac inverter with VQ control in compact form is presented.

### Appendix L.1 VQ Control

The mathematical model of the dc-ac inverter with VQ control is given by the following equations

$$\tilde{I}_1 = G_{dc}(\tilde{V}_1 - \tilde{V}_x) \quad (\text{L.1})$$

$$\tilde{I}_2 = -G_{dc}(\tilde{V}_1 - \tilde{V}_x) \quad (\text{L.2})$$

$$\tilde{I}_3 = (G_{dc} - jB_{ac})(\tilde{V}_3 - \tilde{V}_y) \quad (\text{L.3})$$

$$\tilde{I}_4 = -(G_{dc} - jB_{ac})(\tilde{V}_3 - \tilde{V}_y) \quad (\text{L.4})$$

$$0.0 = |\tilde{V}_y| - |\tilde{V}_4| - \sqrt{2} m(\tilde{V}_x - \tilde{V}_2) \quad (\text{L.5})$$

$$0.0 = \tilde{I}_1 + m\tilde{I}_3 \quad (\text{L.6})$$

$$\text{OR } 0.0 = \tilde{I}_1(\tilde{V}_x - \tilde{V}_2) + \text{Re}\{\tilde{I}_3^*(\tilde{V}_y - \tilde{V}_4)\}$$

$$0.0 = -V_{dc \text{ ref}} + \tilde{V}_x - \tilde{V}_2 \quad (\text{L.7})$$

$$0.0 = Q_{ref} + \text{Im}\{\tilde{I}_3^*(\tilde{V}_y - \tilde{V}_4)\} \quad (\text{L.8})$$

For simplicity, equations (L.1)-(L.8) can be cast into a compact matrix form as follows

$$\begin{bmatrix} I \\ 0 \end{bmatrix} = Y_{eq} \begin{bmatrix} V \\ Y \end{bmatrix} + [V \quad Y] F_{eq} \begin{bmatrix} V \\ Y \end{bmatrix} + K_{eq} \quad (\text{L.9})$$

, where

$$I = [\tilde{I}_1 \quad \tilde{I}_2 \quad \tilde{I}_3 \quad \tilde{I}_4]^T,$$

$$V = [\tilde{V}_1 \quad \tilde{V}_2 \quad \tilde{V}_3 \quad \tilde{V}_4]^T$$

$$Y = [\tilde{V}_x \quad \tilde{V}_y \quad m]^T$$

$Y_{eq}$ : Matrix defining the linear part.

$F_{eq}$ : Nonlinear and differential parts of the model.

$K_{eq}$ : Vector containing the constant part of the model.

Note that there 7 states with 7 equations are identified.

## Appendix L.2 PQ Control

The mathematical model of the dc-ac inverter with PQ control is given by the following equations

$$\tilde{I}_1 = G_{dc}(\tilde{V}_1 - \tilde{V}_x) \quad (\text{L.10})$$

$$\tilde{I}_2 = -G_{dc}(\tilde{V}_1 - \tilde{V}_x) \quad (\text{L.11})$$

$$\tilde{I}_3 = (G_{dc} - jB_{ac})(\tilde{V}_3 - \tilde{V}_y) \quad (\text{L.12})$$

$$\tilde{I}_4 = -(G_{dc} - jB_{ac})(\tilde{V}_3 - \tilde{V}_y) \quad (\text{L.13})$$

$$0.0 = |\tilde{V}_y| - |\tilde{V}_4| - \sqrt{2} m(\tilde{V}_x - \tilde{V}_2) \quad (\text{L.14})$$

$$0.0 = \tilde{I}_1 + m\tilde{I}_3 \quad (\text{L.15})$$

$$\text{OR } 0.0 = \tilde{I}_1(\tilde{V}_x - \tilde{V}_2) + \text{Re}\{\tilde{I}_3^*(\tilde{V}_y - \tilde{V}_4)\}$$

$$0.0 = P_{ref} + \text{Re}\{\tilde{I}_3^*(\tilde{V}_y - \tilde{V}_4)\} \quad (\text{L.16})$$

$$0.0 = Q_{ref} + \text{Im}\{\tilde{I}_3^*(\tilde{V}_y - \tilde{V}_4)\} \quad (\text{L.17})$$

For simplicity, equations (L.10)-(L.17) can be cast into a compact matrix form as follows

$$\begin{bmatrix} I \\ 0 \end{bmatrix} = Y_{eq} \begin{bmatrix} V \\ Y \end{bmatrix} + [V \quad Y] F_{eq} \begin{bmatrix} V \\ Y \end{bmatrix} + K_{eq} \quad (\text{L.18})$$

, where

$$I = [\tilde{I}_1 \quad \tilde{I}_2 \quad \tilde{I}_3 \quad \tilde{I}_4]^T,$$

$$V = [\tilde{V}_1 \quad \tilde{V}_2 \quad \tilde{V}_3 \quad \tilde{V}_4]^T$$

$$Y = [\tilde{V}_x \quad \tilde{V}_y \quad m]^T$$

$Y_{eq}$ : Matrix defining the linear part.

$F_{eq}$ : Nonlinear and differential parts of the model.

$K_{eq}$ : Vector containing the constant part of the model.

Note that there 7 states with 7 equations are identified.



## *Appendix M Averaged Model of DC-DC Buck-Boost Converter*

The averaged model of the dc-dc buck-boost converter has two different control schemes, dc voltage control and real power control. The compact model of each one of them is listed in separate section. First, the model of the averaged dc-dc boost converter with dc voltage control in compact form is presented.

### Appendix M.1 DC Voltage Control

The mathematical model of the averaged dc-dc buck-boost converter is given in the following compact form

$$\tilde{I}_1 = (G_1 - jB)(\tilde{V}_1 - \tilde{V}_x) \quad (\text{M.1})$$

$$\tilde{I}_2 = -(G_1 - jB)(\tilde{V}_1 - \tilde{V}_x) \quad (\text{M.2})$$

$$\tilde{I}_3 = G_2(\tilde{V}_3 - \tilde{V}_y) \quad (\text{M.3})$$

$$\tilde{I}_4 = -G_2(\tilde{V}_3 - \tilde{V}_y) \quad (\text{M.4})$$

$$0.0 = (\tilde{V}_x - \tilde{V}_2) - \frac{1-D}{D}(\tilde{V}_y - \tilde{V}_4) \quad (\text{M.5})$$

$$0.0 = \frac{\tilde{I}_1(1-D)}{D} + \tilde{I}_3 \quad (\text{M.6})$$

$$0.0 = -V_{dc\ ref} + \tilde{V}_y - \tilde{V}_4 \quad (\text{M.7})$$

For simplicity, equations (M.1)-(M.7) can be cast into a compact matrix form as follows

$$\begin{bmatrix} I \\ 0 \end{bmatrix} = A \begin{bmatrix} V \\ Y \end{bmatrix} + N + C \quad (\text{M.8})$$

, where

$$I = [\tilde{I}_1 \quad \tilde{I}_2]^T,$$

$$V = [\tilde{V}_1 \quad \tilde{V}_2 \quad \tilde{V}_3 \quad \tilde{V}_4]^T$$

$$Y = [\tilde{V}_x \quad \tilde{V}_y \quad D]^T$$

*A*: Matrix defining the linear part.

*N*: Nonlinear and differential parts of the model.

*C*: Vector containing the constant part of the model.

## Appendix M.2 Real Power Control

The mathematical model of the averaged dc-dc buck-boost converter is given in the following compact form

$$\tilde{I}_1 = (G_1 - jB)(\tilde{V}_1 - \tilde{V}_x) \quad (\text{M.9})$$

$$\tilde{I}_2 = -(G_1 - jB)(\tilde{V}_1 - \tilde{V}_x) \quad (\text{M.10})$$

$$\tilde{I}_3 = G_2(\tilde{V}_3 - \tilde{V}_y) \quad (\text{M.11})$$

$$\tilde{I}_4 = -G_2(\tilde{V}_3 - \tilde{V}_y) \quad (\text{M.12})$$

$$0.0 = (\tilde{V}_x - \tilde{V}_2) - \frac{1-D}{D}(\tilde{V}_y - \tilde{V}_4) \quad (\text{M.13})$$

$$0.0 = \frac{\tilde{I}_1(1-D)}{D} + \tilde{I}_3 \quad (\text{M.14})$$

$$0.0 = -P_{ref} + \tilde{I}_1(\tilde{V}_1 - \tilde{V}_2) - \frac{\tilde{I}_1^2}{G}, \quad (\text{M.15})$$

$$\text{OR } 0.0 = -P_{ref} + \tilde{I}_1(\tilde{V}_x - \tilde{V}_2)$$

For simplicity, equations (M.9)-(M.15) can be cast into a compact matrix form as follows

$$\begin{bmatrix} I \\ 0 \end{bmatrix} = A \begin{bmatrix} V \\ Y \end{bmatrix} + N + C \quad (\text{M.16})$$

, where

$$I = [\tilde{I}_1 \quad \tilde{I}_2]^T,$$

$$V = [\tilde{V}_1 \quad \tilde{V}_2 \quad \tilde{V}_3 \quad \tilde{V}_4]^T$$

$$Y = [\tilde{V}_x \quad \tilde{V}_y \quad D]^T$$

*A*: Matrix defining the linear part.

*N*: Nonlinear and differential parts of the model.

*C*: Vector containing the constant part of the model.

## Appendix N Ambient Temperature Model

This appendix presents the mathematical model equations in the frequency domain in a compact form for the ambient temperature. The ambient temperature is modeled as heat source behind a thermal resistance.

The model equation is given by

$$\dot{q}_1 = G_{th}(\tilde{T}_1 - T_{amb}) \quad (\text{N.1})$$

, where

$\dot{q}_1$ : heat flow rate in [MBTU/h]

$T_i$ : Temperature in [k°C]

$G_{th}$ : Thermal conductance in [MBTU/h k°C]

$T_{amb}$ : Ambient temperature input by the user in [°C] and converted internally to [k°C]

After separating the real and imaginary part

$$\dot{q}_{1r} = G_{th}(T_{1r} - T_{amb}) \quad (\text{N.2})$$

$$\dot{q}_{1i} = G_{th}T_{1i} \quad (\text{N.3})$$

Equations (N.2)-(N.3) cast into a compact matrix form as follows

$$I = Y_{eq}V + K_{eq} \quad (\text{N.4})$$

Where,

$$I = [\dot{q}_{1r} \quad \dot{q}_{1i}]^T,$$

$$V = [T_{1r} \quad T_{1i}]^T$$

$$Y_{eq} = \begin{bmatrix} G_{th} & 0 \\ 0 & G_{th} \end{bmatrix},$$

$$K_{eq} = \begin{bmatrix} -T_{amb} \\ 0 \end{bmatrix}$$

## Appendix O Thermostat Model

This appendix presents the thermostat mathematical model equations in the frequency domain and in a compact form.

The model equation is given by

$$0.0 = 0.0\tilde{T}_1 \quad (\text{O.1})$$

$$\dot{q}_1 = \tilde{T}_2 - u_1 \quad (\text{O.2})$$

where

$q_I$ : heat flow rate in [MBTU/h]

$T_1, T_2$ : Temperature terminals in [k°C]

$u_I$ : Air conditioner control signal

After separating the real and imaginary part

$$0.0 = 0.0T_{1r} \quad (\text{O.3})$$

$$0.0 = 0.0T_{1i} \quad (\text{O.4})$$

$$\dot{q}_{1r} = T_{2r} - u_1 \quad (\text{O.5})$$

$$\dot{q}_{1i} = T_{2i} \quad (\text{O.6})$$

Equations (O.3)-(O.6) cast into a compact matrix form as follows

$$I = Y_{eq}V + K_{eq} \quad (\text{O.7})$$

where

$$I = [0.0 \quad 0.0 \quad \dot{q}_{1r} \quad \dot{q}_{1i}]^T,$$

$$V = [T_{1r} \quad T_{1i} \quad T_{2r} \quad T_{2i}]^T$$

$$Y_{eq} = \begin{bmatrix} 0 & 0 & 0 & 0 \\ 0 & 0 & 0 & 0 \\ 0 & 0 & 1 & 0 \\ 0 & 0 & 0 & 1 \end{bmatrix},$$

$$K_{eq} = \begin{bmatrix} 0 \\ 0 \\ -u_1 \\ 0 \end{bmatrix}$$

$$u_1 = \begin{cases} 0, & T_{1r} < T_{set} + T_d \\ 1, & T_{1r} \geq T_{set} + T_d \end{cases}$$

, and  $T_{set}$  is the setting temperature and  $T_d$  is the thermostat deadband temperature.

## REFERENCES

- [1] "Energy Independence and Security Act of 2007," *The 110th Congress of the United States, Title XIII*, December 2007.
- [2] P. P. Sarah Jackson, Doug Hurley, and Tim Woolf, "Forecasting Distributed Generation Resources in New England," Synapse Energy Economics Inc., June 2013.
- [3] "Modeling Distributed Generation in the Buildings Sectors," US Energy Information Administration, August 2013.
- [4] T. Hubert and S. Grijalva, "Realizing Smart Grid Benefits Requires Energy Optimization Algorithms at the Residential Level," *IEEE PES Innovative Smart Grid Technologies (ISGT)*, pp. 1 - 8, 2011.
- [5] B. V. Lundin. (2014, August 12). *Pike Research: Smart appliances a \$26.1B market by 2019*. Available: <http://www.fierceenergy.com/story/pike-research-smart-appliances-261b-market-2019/2011-04-14>
- [6] "McKinsey on Smart Grid: Can the smart grid live up to its expectations?," McKinsey, Summer 2010.
- [7] "A National Assessment of Demand Response Potential," Federal Energy Regulatory Commission, June 2009.
- [8] H. Pezeshki and P. Wolfs, "Impact of High PV Penetration on Distribution Transformer Life Time," in *IEEE Power and Energy Society General Meeting (PES)*, 2013, pp. 1-5.
- [9] "The Future of the Electric Grid," MIT, 2011.
- [10] *"Electric Vehicles - The Benefits and Barriers"*: InTech, September 2011.
- [11] Stanton W. Hadley and A. A. Tsvetkova, "Potential impacts of plug-in hybrid electric vehicles on regional power generation," *The Electricity Journal*, vol. 22, pp. 56-68, December 2009.
- [12] "State of the Electric Utility," Utility Dive, 2015.
- [13] "DSTAR's Transformer Cost Analysis Software Enhances Utility Decision Process," GE, 2004.
- [14] A. Thomas, M. Shincovich, S. Ryan, D. Korn, and J. Shugars, "Replacing Distribution Transformers A Hidden Opportunity for Energy Savings " presented at the *ACEEE Summer Study on Energy Efficiency in Buildings*, 2002.
- [15] W. El-Khattam and M. M. A. Salama, "Distributed generation technologies, definitions and benefits," *Electric Power Systems Research*, vol. 71, pp. 119-128, October 2004.
- [16] S. S. Venkata, A. Pahwa, R. E. Brown, and R. D. Christie, "What Future Distribution Engineers Need to Learn," *IEEE Transactions on Power Systems*, vol. 19, pp. 17-23, 2004.
- [17] "The Potential Benefits of Distributed Generation and Rate-Related Issues that May Impede Their Expansion," US Department of Energy, February 2007.
- [18] P. Chiradeja, "Benefit of Distributed Generation: A Line Loss Reduction Analysis," in *IEEE/PES Transmission and Distribution Conference & Exhibition: Asia and Pacific*, Dalian, China, 2005.
- [19] "Benefits of Electric Vehicles A National Perspective," US Department of Energy Solar Decathlon, 2011.



- [20] M. Falahi, H.-M. Chou, M. Ehsani, L. Xie, and K. L. Butler-Purpy, "Potential Power Quality Benefits of Electric Vehicles," *IEEE Transactions on Sustainable Energy*, vol. 4, pp. 1016-1023, 2013.
- [21] A. Shortt and M. O'Malley, "Quantifying the long-term power system benefits of electric vehicles," in *IEEE PES Innovative Smart Grid Technologies (ISGT)*, 2012, pp. 1-6.
- [22] T. P. Dirienzo, N. A. Krishnan, Srijia, and J. R. Santos, "Effects of smart appliances on residential consumption patterns," in *Systems and Information Engineering Design Symposium (SIEDS)*, 2014, pp. 188-192.
- [23] J. C. Fuller and G. B. Parker, "Modeling of GE Appliances: Cost Benefit Study of Smart Appliances in Wholesale Energy, Frequency Regulation, and Spinning Reserve Markets," Pacific Northwest National Laboratory, 2012.
- [24] A. P. Sakis Meliopoulos, Cokkinides, G. , Thomas Overbye, Jerome Meisel, "Power System Level Impacts of Plug-In Hybrid Vehicles," Power Systems Engineering Research Center, September 2012.
- [25] S. G. M. Therien, "Distributed Generation- Issues Concerning a Changing Power Grid Paradigm," Master of Science Electrical Engineering, California Polytechnic State University, 2010.
- [26] C. A. Roe, "Power System Impacts of Plug-In Hybrid Electric Vehicles," Master of Science, School of Electrical and Computer Engineering, Georgia Institute of Technology, August 2009.
- [27] "Impact of Distributed Resources on Distribution Relay Protection " Power System Relay Committee of The IEEE Power Engineering Society prepared by working group D3, August 2004.
- [28] A. F. Sarabia, "Impact of distributed generation on distribution system," Degree of Master Graduate, Faculty of Engineering, Science and Medicine, Aalborg University, Aalborg, Denmark, June 2011.
- [29] F. M. Uriarte and R. E. Hebner, "Impact of Residential Photovoltaic Generation and Electric Vehicles on Distribution Transformers," Center of Electromechanics of The University of Texas at Austin, April 2013.
- [30] H. C. Ureh, "Impacts of Plug-In Electric Vehicle on Residential Electric Distribution System using Stochastic and Sensitivity Approach," Master of Science, Electrical Engineering, California Polytechnic State University, 2011.
- [31] P. S. Moses, M. A. S. Masoum, and S. Hajforoosh, "Overloading of distribution transformers in smart grid due to uncoordinated charging of plug-In electric vehicles," in *IEEE PES Innovative Smart Grid Technologies (ISGT)*, 2012, pp. 1-6.
- [32] Amir S. Masoum, Ahmed Abu-Siada, and S. Islam, "Impact of Uncoordinated and Coordinated Charging of Plug-In Electric Vehicles on Substation Transformer in Smart Grid with Charging Stations " in *IEEE PES Innovative Smart Grid Technologies Asia (ISGT)*, 2011, pp. 1-7.
- [33] M. A. S. Masoum, P. S. Moses, and S. Hajforoosh, "Distribution Transformer Stress in Smart Grid with Coordinated Charging of Plug-In Electric Vehicles " in *IEEE PES Innovative Smart Grid Technologies (ISGT)*, 2012, pp. 1-8.
- [34] A. S. Masoum, S. Deilami, P. S. Moses, M. A. S. Masoum, and A. Abu-Siada, "Smart load management of plug-in electric vehicles in distribution and

- residential networks with charging stations for peak shaving and loss minimisation considering voltage regulation," *IET Generation, Transmission & Distribution*, vol. 5, pp. 877-888, 2011.
- [35] S. Shafiee, M. Fotuhi-Firuzabad, and M. Rastegar, "Investigating the Impacts of Plug-in Hybrid Electric Vehicles on Power Distribution Systems," *IEEE Transactions on Smart Grid*, vol. 4, pp. 1351-1360 2013.
- [36] L. Trovao and H. M. Jorge, "Power Demand Impacts of the Charging of Electric Vehicles on the Power Distribution Network in a Residential Area " in *3rd International Youth Conference on Energetics (IYCE)*, 2011.
- [37] P. Papadopoulos, S. Skarvelis-Kazakos, I. Grau, B. Awad, L. M. Cipcigan, and N. Jenkins, "Impact of Residential Charging of Electric Vehicles on Distribution Networks, a Probabilistic Approach " in *45th International Universities Power Engineering Conference (UPEC)*, 2010, pp. 1-5.
- [38] T. J. Geiles and S. Islam, "Impact of PEV Charging and Rooftop PV Penetration on Distribution Transformer Life," in *IEEE Power and Energy Society General Meeting (PES)*, 2013, pp. 1-5.
- [39] E. Veldman, M. Gibescu, H. Slootweg, and W. L. Kling, "Impact of Electrification of Residential Heating on Loading of Distribution Networks " in *IEEE Trondheim PowerTech*, 2011, pp. 1-7.
- [40] A. Safdarian, M. Fotuhi-Firuzabad, and M. Lehtonen, "Benefits of Demand Response on Operation of Distribution Networks: A Case Study " *IEEE Systems Journal*, vol. PP, pp. 1-9, 2014.
- [41] Z. Wang, R. Paranjape, A. Sadanand, and Z. Chen, "Residential Demand Response: an Overview of Recent Simulation and Modeling Applications," in *26th Annual IEEE Canadian Conference on Electrical and Computer Engineering (CCECE)*, 2013, pp. 1-6.
- [42] (2014, August 13, 2014). *Federal Energy Regulatory Commission Top Three Initiatives*. Available: <https://www.ferc.gov/about/top-initiatives.asp>
- [43] N. Zhang, L. F. Ochoa, and D. S. Kirschen, "Investigating the Impact of Demand Side Management on Residential Customers," in *2nd IEEE PES International Conference and Exhibition on Innovative Smart Grid Technologies (ISGT Europe)*, 2011, pp. 1-6.
- [44] K. P. Schneider, J. C. Fuller, and D. P. Chassin, "Analysis of Distribution Level Residential Demand Response," in *IEEE/PES Power Systems Conference and Exposition (PSCE)*, 2011, pp. 1-6.
- [45] M. H. Albadi and E. F. El-Saadany, "Demand Response in Electricity Markets: An Overview," in *IEEE Power Engineering Society General Meeting*, 2007, pp. 1-5.
- [46] K. P. Wacks, "Utility Load Management Using Home Automation," *IEEE Transactions on Consumer Electronics*, vol. 37, pp. 168-174, 1991.
- [47] G. C. Heffner and C. A. Goldman, "Demand Responsive Programs - An Emerging Resource for Competitive Electricity Markets?," University of California Berkeley, California, August 2001.
- [48] "Pacific Northwest GridWise Testbed Demonstration Projects; Part 1. Olympic Peninsula Project," Pacific Northwest National Laborator - US Department of Energy, October 2007.

- [49] D. P. Chassin, D. J. Hammerstrom, and J. G. DeSteese, "The Pacific Northwest Demand Response Market Demonstration " in *IEEE Power and Energy Society General Meeting - Conversion and Delivery of Electrical Energy in the 21st Century*, 2008, pp. 1-6.
- [50] F. Rahimi and A. Ipakchi, "Demand Response as a Market Resource Under the Smart Grid Paradigm," *IEEE Transactions on Smart Grid* vol. 1, pp. 82-88, 2010.
- [51] D. S. Kirschen, "Demand-Side View of Electricity Markets," *IEEE Transactions on Power Systems*, vol. 18, pp. 520-527, 2003 2003.
- [52] L. Mardira, T. K. Saha, and M. Eghbal, "Investigating impacts of battery energy storage systems on electricity demand profile," in *Australasian Universities Power Engineering Conference (AUPEC)*, 2014, pp. 1-5.
- [53] O. Lavrova, F. Cheng, S. Abdollahy, H. Barsun, A. Mammoli, D. Dreisigmayer, *et al.*, "Analysis of battery storage utilization for load shifting and peak smoothing on a distribution feeder in New Mexico," in *IEEE PES Innovative Smart Grid Technologies (ISGT)*, 2012, pp. 1-6.
- [54] "Advanced Metering Infrastructure (AMI)/Home Area Network (HAN) Economic Benefits Analysis for Utilities," Electric Power Research Institute (EPRI), Decemeber 2009.
- [55] N. Ruiz, I. Cobelo, and J. Oyarzabal, "A direct load control model for virtual power plant management," *IEEE Transactions on Power Systems*, vol. 24, pp. 959-966, 2009.
- [56] K.-H. Ng and G. B. Sheble, "Direct load control-A profit-based load management using linear programming," *IEEE Transactions on Power Systems*, vol. 13, pp. 688-694, 1998.
- [57] A. Gomes, C. H. Antunes, and A. G. Martins, "A multiple objective approach to direct load control using an interactive evolutionary algorithm," *IEEE Transactions on Power Systems*, vol. 22, pp. 1004-1011, 2007.
- [58] N. Lu, "An Evaluation of the HVAC Load Potential for Providing Load Balancing Service," *IEEE Transactions on Smart Grid*, vol. 3, pp. 1263-1270, September 2012.
- [59] S. Abras, S. Pesty, S. Ploix, and M. Jacomino, " An anticipation mechanism for power management in a smart home using multi-agent systems," in *3rd International Conference on Information and Communication Technologies: From Theory to Applications*, 2008, pp. 1-6.
- [60] A.-H. Mohsenian-Rad, V. W. S. Wong, J. Jatskevich, R. Schober, and A. Leon-Garcia, "Optimal and Autonomous Incentive-based Energy Consumption Scheduling Algorithm for Smart Grid," in *Innovative Smart Grid Technologies (ISGT)*, 2010, pp. 1-6.
- [61] A.-H. Mohsenian-Rad, V. W. S. Wong, J. Jatskevich, R. Schober, and A. Leon-Garcia, "Autonomous Demand-Side Management Based on Game-Theoretic Energy Consumption Scheduling for the Future Smart Grid," *IEEE Transactions on Smart Grid*, vol. 1, pp. 320-331, 2010.
- [62] Y. Suhara, T. Nakabe, G. Mine, and H. Nishi, "Distributed Demand Side Management System for Home Energy Management," in *36th Annual Conference on IEEE Industrial Electronics Society*, 2010, pp. 2430-2435

- [63] D. J. Shahgoshtasbi, M. , "Modified Intelligent Energy Management system in a smart house," *World Automation Congress (WAC)*, pp. 1-6, 2012.
- [64] D. Shahgoshtasbi and M. Jamshidi, "Energy efficiency in a smart house with an intelligent Neuro-Fuzzy lookup table," *6th International Conference on System of Systems Engineering (SoSE)*, pp. 288-292, 2011.
- [65] M. A. A. Pedrasa, T. D. Spooner, and I. F. MacGill, "Coordinated scheduling of residential distributed energy resources to optimize smart home energy services," *IEEE Transactions on Smart Grid*, vol. 1, pp. 134-143, 2010.
- [66] N. Gudi, L. Wang, V. Devabhaktuni, and S. S. S. R. Depuru, "Demand response simulation implementing heuristic optimization for home energy management," in *North American Power Symposium (NAPS)*, 2010, pp. 1-6.
- [67] A. A. Moholkar, "Computer Aided Home Energy Management System," Master of Science in Electrical Engineering, Dept. Computer Science and Electrical Engineering West Virginia University, 2005.
- [68] C. H. Antunes, A. Gomes, and A. G. Martins, "A two-phase decision support approach for the selection of load control actions," in *IEEE International Engineering Management Conference*, 2008, pp. 1-6.
- [69] T. Ikegami, Y. Iwafune, and K. Ogimoto, "Optimum Operation Scheduling Model of Domestic Electric Appliances for Balancing Power Supply and Demand," *International Conference on Power System Technology (POWERCON)*, pp. 1-8, 2010.
- [70] A. Esser, A. Kamper, M. Franke, D. Möst, and O. Rentz, "Scheduling of Electrical Household Appliances with Price Signals," *Operations Research Proceedings*, pp. 253-258, 2006.
- [71] H. Tischer and G. Verbic, "Towards a smart home energy management system - A dynamic programming approach," *IEEE PES Innovative Smart Grid Technologies Asia (ISGT)*, pp. 1-7, 2011.
- [72] T.-H. Chang, M. Alizadeh, and A. Scaglione, "Coordinated Home Energy Management for Real-Time Power Balancing," *IEEE Power and Energy Society General Meeting*, pp. 1-8, 2012.
- [73] T.-H. Chang, M. Alizadeh, and A. Scaglione, "Real-Time Power Balancing Via Decentralized Coordinated Home Energy Scheduling," *IEEE Transactions on Smart Grid*, vol. 4, pp. 1490-1504, 2013.
- [74] D. O'Neill, M. Levorato, A. Goldsmith, and U. Mitra, "Residential Demand Response Using Reinforcement Learning," in *First IEEE International Conference on Smart Grid Communications (SmartGridComm)*, 2010, pp. 409-414.
- [75] D. Ren, H. Li, and Y. Ji, "Home energy management system for the residential load control based on the price prediction," *IEEE Online Conference on Green Communications (GreenCom)*, pp. 1-6, 2011.
- [76] M. Pipattanasomporn, M. Kuzlu, and S. Rahman, "An algorithm for intelligent home energy management and demand response analysis," *IEEE Transactions on Smart Grid*, vol. 3, pp. 2166-2173, 2012.
- [77] Y. Ozturk, D. Senthilkumar, S. Kumar, and G. Lee, "An Intelligent Home Energy Management System to Improve Demand Response," *IEEE Transactions on Smart Grid*, vol. 4, pp. 694-701, 2013.

- [78] M. C. Bozchalui, S. A. Hashmi, H. Hassen, C. A. Canizares, and K. Bhattacharya, "Optimal Operation of Residential Energy Hubs in Smart Grids," *IEEE Transaction on Smart Grid*, vol. 3, pp. 1755-1766, 2012.
- [79] A. Molderink, V. Bakker, M. G. C. Bosman, J. L. Hurink, and G. J. M. Smit, "Domestic energy management methodology for optimizing efficiency in Smart Grids," in *IEEE Bucharest PowerTech*, 2009, pp. 1-7.
- [80] A. Molderink, V. Bakker, M. G. C. Bosman, J. L. Hurink, and G. J. M. Smit, "Management and Control of Domestic Smart Grid Technology," *IEEE Transactions on Smart Grid*, vol. 1, pp. 109-119, 2010.
- [81] H.-C. Jo, S. Kim, and S.-K. Joo, "Smart Heating and Air Conditioning Scheduling Method Incorporating Customer Convenience for Home Energy Management System," *IEEE Transactions on Consumer Electronics*, vol. 59, pp. 316-322, 2013.
- [82] A. G. Thomas, P. Jahangiri, D. Wu, C. Cai, H. Zhao, D. C. Aliprantis, *et al.*, "Intelligent Residential Air-Conditioning System With Smart-Grid Functionality," *IEEE Transactions on Smart Grid*, vol. 3, pp. 2240-2251, 2012.
- [83] F. Shariatzadeh and A. K. Srivastava, "Look-ahead Control Approach for Thermostatic Electric Load in Distribution System," *North American Power Symposium*, September 2013.
- [84] H. Yamauchi, M. Miyagi, K. Uchida, A. Yona, and T. Senjyu, "Advanced Smart House with An Electric Vehicle," *International Conference on Renewable Energy Research and Applications (ICRERA)*, pp. 1-6, 2012.
- [85] I. Hazyuk, C. Ghiaus, and D. Penhouet, "Optimal temperature control of intermittently heated buildings using Model Predictive Control: Part I - Building modeling," *Building and Environment*, vol. 51, pp. 379-387, May 2012.
- [86] D. Wang, C.C. Federspiel, and F. Rubinstein, "Modeling occupancy in single person offices," *Energy and Buildings*, vol. 37, pp. 121-126, 2005.
- [87] H. G. L. Holmer, and K. Parsons, "Personal factors in thermal comfort assessment: clothing properties and metabolic heat production," *Energy and Buildings*, vol. 34, pp. 581-591, July 2002.
- [88] H. Park, M. Ruellan, N. Martaj, R. Bennacer, and E. Monmasson, "Generic Thermal Model of Electric Appliances Integrated in Low Energy Building," in *38th Annual Conference on IEEE Industrial Electronics Society - IECON*, 2012, pp. 3318-3323.
- [89] H. Park, M. Ruellan, A. Bouvet, E. Monmasson, and R. Bennacer, "Thermal Parameter Identification of Simplified Building Model with Electric Appliance," in *11th International Conference on Electrical Power Quality and Utilisation (EPQU)*, 2011, pp. 1-6.
- [90] E. Bompard, E. Carpaneto, G. Chicco, and R. Napoli, "Analysis and modelling of thermostatically-controlled loads," in *8th Mediterranean Electrotechnical Conference*, 1996, pp. 730-734.
- [91] G. T. Costanzo, F. Sossan, M. Marinelli, P. Bacher, and H. Madsen, "Grey-box Modeling for System Identification of Household Refrigerators: a Step Toward Smart Appliances," in *4th International Youth Conference on Energy (IYCE)*, 2013, pp. 1-5.

- [92] B. Tashtoush, M. Molhim, and M. Al-Rousan, "Dynamic model of an HVAC system for control analysis," *Energy*, vol. 30, pp. 1729-1745, July 2005.
- [93] S. Kawachi, H. Hagiwara, and J. Baba, "Modeling and Simulation of Heat Pump Air Conditioning Unit Intending Energy Capacity Reduction of Energy Storage System in Microgrid," *Proceedings of the 2011-14th European Conference on Power Electronics and Applications (EPE 2011)*, pp. 1-9, August 2011.
- [94] Z. Taylor and S. Katipamula, "GridLAB-D Technical Support Document Residential End-Use Module Version 1\_0 " July, 2008.
- [95] A. P. S. Meliopoulos, "Power System Quality Class Notes," ed. Georgia Institute of Technology.
- [96] IEEE, "IEEE Guide for Loading Mineral-Oil Immersed Transformers," in *IEEE Std C57.91-2011 (Revision of IEEE Std C57.91-1995) - Redline* ed, 2012, pp. 1-172.
- [97] D. Susa, M. Lehtonen, and H. Nordman, "Dynamic Thermal Modelling of Power Transformers," *IEEE Transactions on Power Delivery*, vol. 20, pp. 197-204, 2005.
- [98] D. Susa and M. Lehtonen, "Dynamic thermal modeling of power transformers: further Development-part I," *IEEE Transactions on Power Delivery*, vol. 21, pp. 1961-1970, 2006.
- [99] D. Susa and M. Lehtonen, "Dynamic thermal modeling of power transformers: further Development-part II," *IEEE Transactions on Power Delivery*, vol. 21, pp. 1971-1980, 2006.
- [100] G. Swift, T. S. Molinski, and W. Lehn, "A fundamental approach to transformer thermal modeling. I. Theory and equivalent circuit," *IEEE Transactions on Power Delivery*, vol. 16, pp. 171-175, 2001.
- [101] G. Swift, T. S. Molinski, R. Bray, and R. Menzies, "A Fundamental Approach to Transformer Thermal Modeling Part II Field Verification," *IEEE Transactions on Power Delivery*, vol. 16, pp. 176-180, 2001.
- [102] H. Xiaofeng, Z. Lijun, W. Guangning, and D. Qingquan, "Simulation Models of Transformer Hot-spot Temperature," *IEEE 10th International Conference on the Properties and Applications of Dielectric Materials (ICPADM)*, pp. 1-4, 2012.
- [103] W. H. Tang, Q. H. Wu, and Z. J. Richardson, "A Simplified Transformer Thermal Model Based on Thermal-Electric Analogy," *IEEE Transactions on Power Delivery*, vol. 19, pp. 1112-1119, 2004.
- [104] A. P. S. Sakis Meliopoulos, George Cokkinides, Renke Huang, Evangelos Farantatos, Sungyun Choi, Yonghee Lee, *et al.*, "Smart Grid Technologies for Autonomous Operation and Control," *IEEE Transactions on Smart Grid*, vol. 2, pp. 1-10, March 2011.
- [105] A. P. S. Meliopoulos, G. J. Cokkinides, and G. Stefopoulos, "Symbolic Integration of Dynamical Systems by Collocation Methods," in *IEEE PES Power Systems Conference and Exposition*, 2006, pp. 362 - 367.
- [106] G. K. Stefopoulos, G. J. Cokkinides, and A. P. S. Meliopoulos, "Quadratized Model of Nonlinear Saturable-Core Inductor for Time-Domain Simulation," *IEEE Power & Energy Society General Meeting*, pp. 1 - 8, 2009.

- [107] G. K. Stefopoulos and A. P. S. Meliopoulos, "Quadratized Three-Phase Induction Motor Model for Steady-State and Dynamic Analysis," *38th North American Power Symposium*, pp. 65 - 75, 2006.
- [108] A. P. Meliopoulos, G. J. Cokkinides, and G. K. Stefopoulos, "Quadratic Integration Method," *International Conference on Power Systems Transients (IPST'05)*, 2005.
- [109] Y. Cho, G. J. Cokkinides, and A. P. Meliopoulos, "Advanced time domain method for remote wind farms with LFAC transmission systems: Power transfer and harmonics," *North American Power Symposium (NAPS)*, pp. 1-6, 2012.
- [110] A. S. Meliopoulos, G. Cokkinides, and R. James, "Transformer Diagnostic System for Loss of Life and Coil Integrity," in *Proceedings of the 1998 Georgia Tech Fault and Disturbance Analysis Conference*, 1998, pp. 4-5.
- [111] ANSI/IEEE, "IEEE Guide for Loading Mineral-Oil-Immersed Overhead and Pad-Mounted Distribution Transformers Rated 500 kVa and Less With 65 Degrees C Or 55 Degrees C Average Winding Rise," in *ANSI/IEEE Std C57.91-1981*, ed, 1981.
- [112] C. Strock and R. Koral, *handbook of air conditioning heating and ventilating*. New York: Industrial Press, 1965.
- [113] *2006 ASHRAE handbook - Refrigeration*: American Society of Heating - Refrigerating and Air-Conditioning Engineers, 2006.
- [114] David E. Hoak, D. S. Parker, and A. H. Hermelink, "How Energy Efficient are Modern Dishwashers? ," in *American Council for an Energy Efficient Economy*, Washington DC, 2008.
- [115] C. Natascha, "Energy and Water Consumption Testing of a Conventional Dishwasher and an Adaptive Control Dishwasher," in *Proceedings of the International Appliance Technology Conference*, 1997.
- [116] M. G. Villalva, J. R. Gazoli, and E. R. Filho, "Comprehensive approach to modeling and simulation of Photovoltaic Arrays," *IEEE Transaction on Power Electronics*, pp. 1198-1208, 2009.
- [117] M. Ceraolo, "New Dynamical Models of Lead–Acid Batteries," *IEEE Transactions on Power Systems*, vol. 15, 2000.
- [118] R. A. Jackey, "A Simple, Effective Lead-Acid Battery Modeling Process for Electrical System Component Selection," 2007.
- [119] S Barsali and M. Ceraolo, "Dynamical models of lead-acid batteries: implementation issues," *IEEE Transactions on Energy Conversion*, vol. 17, pp. 16-23, 2002.
- [120] Lijun Gao, Shengyi Liu, and R. A. Dougal, "Dynamic Lithium-Ion Battery Model for System Simulation," *IEEE Transaction on Components and Packaging Technologies*, vol. 25, September 2002.
- [121] T. Eswam and P. L. Chapman, "Comparison of Photovoltaic Array Maximum Power Point Tracking Techniques," *IEEE Transaction at the Energy Conversion*, vol. 22, pp. 439 - 449, 2007.
- [122] A. P. S. Meliopoulos, G. J. Cokkinides, F. Galvan, B. Fardanesh, and P. Myrda, "Distributed state estimator – Advances and demonstration,," *Proceedings of the 41st Annual Hawaii International Conference on System Sciences*, p. 163, 2008.

- [123] A. P. S. Meliopoulos, G. J. Cokkinides, F. Galvan, B. Fardanesh, and P. Myrda, "Advances in the SuperCalibrator Concept – Practical Implementations," *40th Annual Hawaii International Conference on System Sciences, (HICSS)*, p. 118, 2007.
- [124] S. Mohagheghi, R. H. Alaileh, G. J. Cokkinides, and A. P. S. Meliopoulos, "Distributed state estimation based on the SuperCalibrator concept – Laboratory Implementation," *iREP Symposium on Bulk Power System Dynamics and Control* pp. 1-9, 2007.
- [125] A. P. S. Meliopoulos, G. J. Cokkinides, C. Hedrington, and T. L. Conrad, "The SuperCalibrator – A Fully Distributed State Estimator," *IEEE Power and Energy Society General Meeting*, pp. 1-8, 2010.
- [126] H. P. Williams, *Model Building in Mathematical Programming*: Wiley, 2013.
- [127] J. Bisschop, *AIMMS Optimization Modeling*: Paragon Decision Technology, 2012.
- [128] L. Wang, *Model Predictive Control System Design and Implementation Using MATLAB*: Springer, 2010.
- [129] L. Grüne and J. Pannek, *Nonlinear Model Predictive Control: Theory and Algorithms*: Springer, 2011.
- [130] *Single Phase Center Tap Transformer Datasheet* [ABB]. Available: <http://alturl.com/g45p4>
- [131] *Single Phase Center Tap Transformer Datasheet* [Coopre Power Systems]. Available: <http://alturl.com/e93ib>
- [132] *Gurobi Optimization, Inc.* Available: <http://www.gurobi.com/>